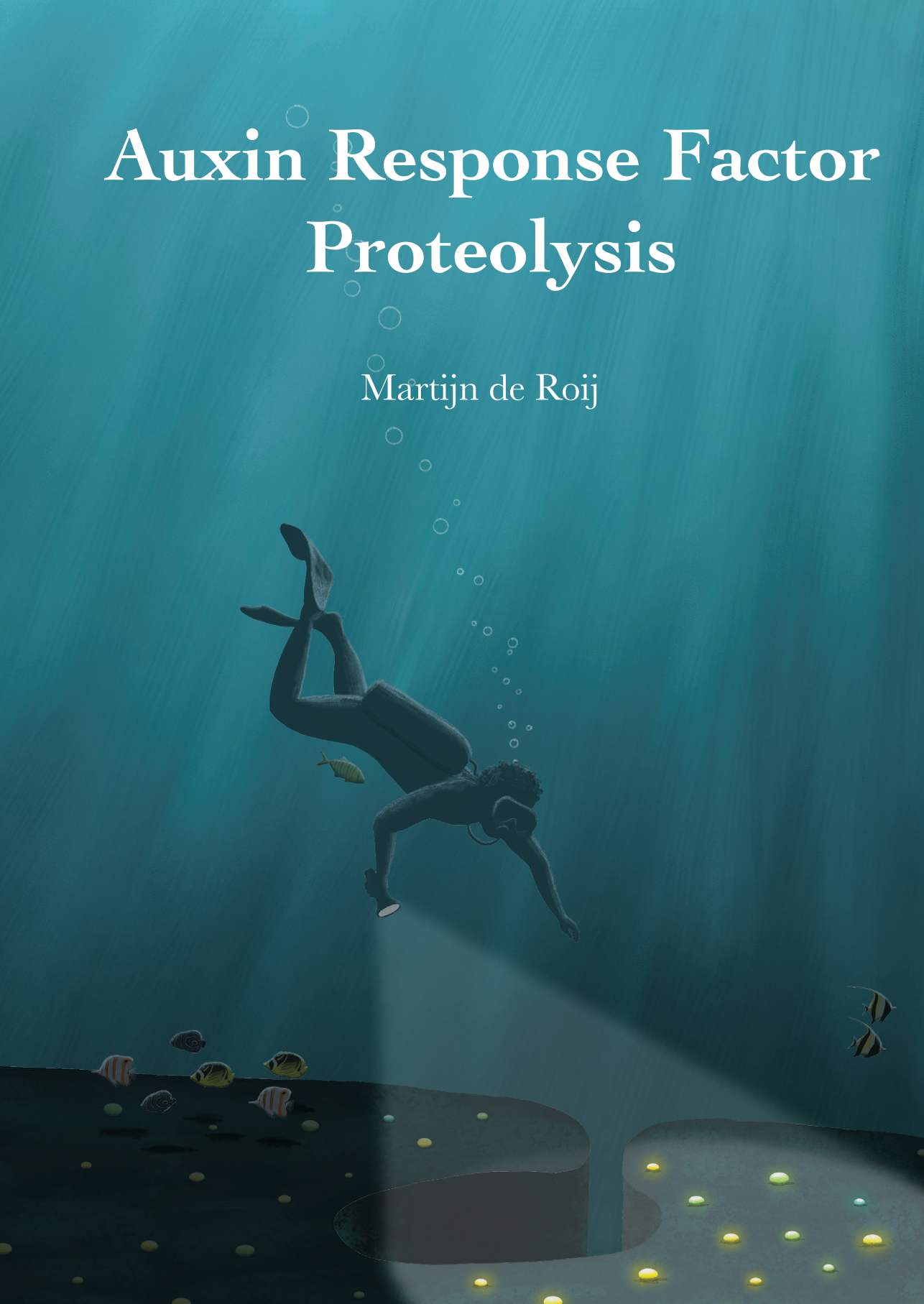
Auxin Response Factor Proteolysis

Martijn de Roij



Propositions

1. Forward genetic screens are fundamentally constrained by the need for a well-defined and unambiguous phenotypic readout. (this thesis)
2. Identification of additional proteins involved in Auxin Response Factor degradation will greatly improve our understanding of the evolution of the auxin response system. (this thesis)
3. Without a well-defined global population control policy, reversing climate change and environmental degradation will be unsuccessful.
4. Access to time, support, and data are stronger determinants of PhD obtainment than a candidate's talent.
5. A mandatory community-based or military conscription greatly strengthens societal cohesion.
6. A strictly enforced ban on smartphone and social media use by children under sixteen is a powerful way to combat the mental health crisis.

Propositions belonging to the thesis entitled:

"Auxin Response Factor Proteolysis"

Martijn de Roij

Wageningen, 2 September 2026

Auxin Response Factor Proteolysis

Martijn de Roij

Thesis committee

Promotor

Prof. Dr Dolf Weijers

Professor of Biochemistry

Wageningen University & Research

Co-promotor

Dr Jan Willem Borst

Assistant professor in Biochemistry

Wageningen University & Research

Other members

Prof. Dr Teva Vernoux, Centre national de la recherche scientifique & École normale supérieure, Lyon, FR

Prof. Dr Ronald Pierik, Wageningen University & Research

Dr Annis Richardson, University of Edinburgh, UK

Dr Charlotte Gommers, Wageningen University & Research

This research was conducted under the auspices of the Graduate School Experimental Plant Sciences

Auxin Response Factor Proteolysis

Martijn de Roij

Thesis

submitted in fulfilment of the requirements for the degree of doctor
at Wageningen University
by the authority of the Rector Magnificus,
Prof. Dr C. Kroeze,
in the presence of the
Thesis Committee appointed by the Academic Board
to be defended in public
on Wednesday 2 September 2026
at 3:30 p.m. in the Omnia Auditorium

Martijn de Roij

Auxin Response Factor Proteolysis

272 pages

PhD thesis, Wageningen University, Wageningen, the Netherlands (2026)

With references, with summaries in English and Dutch

ISBN: 978-94-6534-524-6

DOI: 10.18174/681862

Table of contents

Chapter 1 General Introduction and thesis outline 7

Chapter 2 Protein degradation in auxin response 23

Chapter 3 Quantitative analysis of the nuclear auxin signaling pathway in *Marchantia polymorpha* 49

Chapter 4 ARF degradation defines a deeply conserved step in auxin response 93

Chapter 5 Diversification of functional requirements for proteolysis of Auxin Response Factors 119

Chapter 6 A forward genetic screen for mutants defective in Auxin Response Factor degradation 177

Chapter 7 Mapping the MpARF2 proximal interactome identifies putative degradation regulators 211

Chapter 8 General Discussion 237

Appendices

Summary (English) 256

Summary (Dutch) 259

Authorship statement 263

Acknowledgments 265

About the author 270

List of publications 271



Chapter 1

General Introduction and thesis outline

Authors

Martijn de Roij[1]

Affiliations

[1] Laboratory of Biochemistry, Wageningen University, Stippeneng 4, 6708WE Wageningen, the Netherlands

Green pioneering requires developmental engineering

When reflecting on the origin of life on Earth, attention is often drawn to major evolutionary transitions that enabled life on land. You might imagine a bubbling primordial soup or a prehistoric animal slowly developing limbs and crawling out of the sea onto land. These are compelling images, but a great deal still had to occur before conditions on land became suitable to support animal life. In ancient times, roughly the early Proterozoic era, Earth was an inhospitable place. The atmosphere contained very little oxygen, harmful UV radiation reached the surface unhindered due to the lack of a protective ozone layer, and the rocky substrate was barren (Fig. 1)[1-3]. These conditions rendered the terrestrial habitat largely unsuitable for complex lifeforms.

This began to change roughly 500 million years ago when a charophyte algal ancestor left their (semi)aquatic environment and slowly moved onto land (Fig. 1)[4-9]. The descendants then gave rise to a group of non-vascular plants we now call the bryophytes (formed by mosses, liverworts, and hornworts) as well as the lineage comprising the tracheophytes (lycophytes, pterophytes, gymnosperms and angiosperms; Fig. 1)[4,6,7]. Together, the bryophytes and tracheophytes form the embryophyte clade (Fig. 1)[4,6,7]. This gradual conquering of the terrestrial environment by the early embryophytes resulted in fundamental climatic and environmental changes[1,10]. Atmospheric CO_2 was captured and converted into oxygen through photosynthesis, this contributed to the formation of a protective ozone layer, and plants eroded the rocky substrate and created more suitable soils for other plants (and later animals)[1,10-12]. These biological and geochemical revolutions can be viewed as some of the most profound events in the history of Earth.

As the conditions on land were so unhospitable, the first embryophytes had to conquer unprecedented challenges[1]. To overcome the severe stress factors found in their new environment, major innovations in development and body plan organization were required[7]. Plants had to evolve strategies to combat desiccation, withstand the force of gravity, reproduce outside of the water, and find novel ways to acquire nutrients (Fig. 1)[13-16]. Meeting all these challenges necessitated an increasingly complex, multicellular body plan, and in turn, formation of such a body plan required novel regulatory systems capable of coordinating growth, cellular patterning and differentiation[7,17].

Molecular control of plant development

Unlike many multicellular organisms, plants do not follow a rigid, predetermined body plan[18]. Instead, plant development is characterized by an extraordinary degree of plasticity[17,19,20]. Throughout the plant life cycle, new organs can be continuously generated, and growth patterns can be reprogrammed to respond to changes in environmental cues such as light, temperature, water availability, and nutrient accessibility[17,19,20]. In fact, genetically identical individuals belonging to the same plant species can adopt a strikingly different morphology when exposed to different environmental conditions[20]. This plasticity places a strong demand on developmental regulation[20]. At the cellular level, pattern formation, organ initiation and cell fate decisions must be accurately coordinated across space and time. On top of this, these processes need to remain responsive to changes in the environment.

Understanding how plants integrate such diverse inputs into developmental programming is a fundamental goal of plant science. Over the last decades, research on developmental control has revealed a core set of regulatory signals that consistently govern multiple aspects of plant development, among which the signaling molecule auxin stands out as the most prevalent[7,21,22]. Auxin has an essential role in nearly every aspect of plant development, from embryogenesis and organ formation to tropic growth responses, regeneration and environmental adaptation[21-24]. Acting across multiple spatial and temporal scales of the plant lifecycle, auxin is widely regarded as a central coordinator of plant development[24,25].

The name auxin derives from the Greek "*auxein*", meaning "to grow", reflecting its early association with growth promotion. However, auxin is far more than a simple stimulator of growth. It functions as a positional signal, a regulator of tissue patterning and a potent modulator of transcriptional responses and networks. How a seemingly simple, singular, molecule can orchestrate and influence such a wide array of developmental processes remains one of the most enduring and fascinating questions in the field of biology to this day.

The discovery of auxin

The existence of a mobile growth-controlling substance in plants was already hypothesized by Charles and Francis Darwin in the nineteenth century, long before auxin was officially identified[26]. In their book *The Power of Movement in Plants*, they showed that

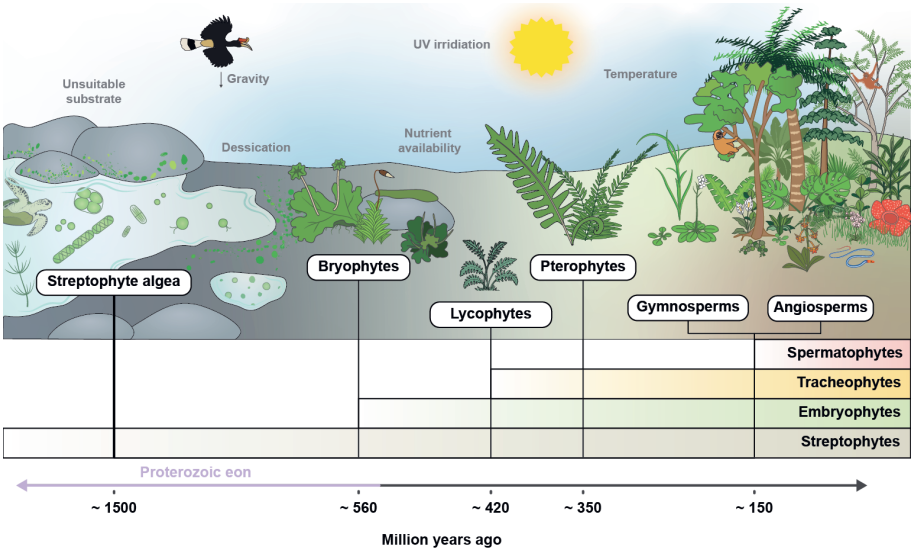


Fig. 1 | Schematic overview of plant evolution and terrestrialization. Illustration summarizing the evolutionary history of plants, depicting the emergence of major plant clades along a geological timescale (million years ago), and their phylogenetic relationship. The transition from aquatic streptophyte algae to fully terrestrial plants is shown from left to right. Early land plant ancestors originated from aquatic environments. During terrestrialization, plants encountered novel stressors, such as an unsuitable substrate, frequent desiccation, increased UV irradiation, temperature fluctuations, heterogenous nutrient availability and gravity. Major stressors associated with a terrestrial environment are shown in grey.

perception of light occurred at the tip of blades of grass, whereas the consequential growth response occurred in the tissues below[26]. From this they inferred that a transmissible signal was sent from the site of perception to the site of response. The Darwins hereby laid the conceptual groundwork for the discovery of auxin as a signal, but the nature of this signal as a chemical, transportable entity, was not uncovered until later. This discovery can be attributed to the Dutch scientist Frits Went, who was the first to officially document isolating auxin as a substance, and demonstrating its activity in the twentieth century[27]. This was later followed by the chemical identification of auxin in the 1930s by Kögl et al.[28] They identified Indole-3-Acetic Acid (IAA) as the principal, naturally occurring auxin (Fig. 2a)[28]. From these early works, it was clear that auxin was a mobile signaling molecule which had an influence on plant development, but how auxin exerted its influence at the molecular and biochemical level long remained enigmatic.

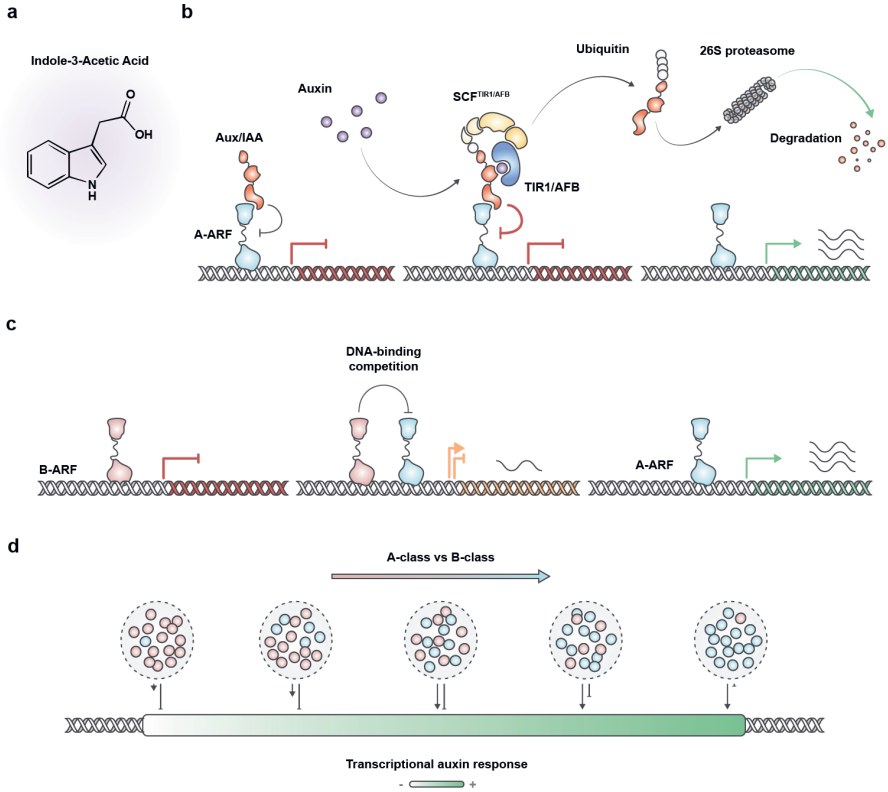


Fig. 2 | Molecular mechanisms underlying auxin perception and signaling in land plants.
a. The chemical structure of Indole-3-Acetic acid (IAA), the principal, naturally occurring, auxin and a crucial regulator of plant development. **b.** The canonical Nuclear Auxin signaling Pathway (NAP). In the absence of auxin, Aux/IAA inhibitors interact with the activating A-class ARFs, which can bind to auxin-responsive promoter elements. Aux/IAA-ARF interaction will lead to transcriptional repression. At increased intracellular levels, auxin acts as a molecular glue which promotes the interaction between Aux/IAAs and the $SCF^{TIR1/AFB}$ E3 ubiquitin ligase complex. Subsequently, $SCF^{TIR1/AFB}$ ubiquitylates the Aux/IAA substrate, leading to its degradation by the 26S proteasome. This will release A-class ARFs from repression and enable transcriptional activation of auxin-responsive genes. **c.** Transcriptional regulation through A -and B-class ARF DNA-binding competition. B-ARFs act as transcriptional repressors and compete for binding the same DNA cis-regulatory elements as the A-ARF transcriptional activators. The relative intranuclear abundance and DNA-binding kinetics of each ARF defines the transcriptional outcome at auxin-responsive loci. **d.** Simplified illustration of the graded auxin responses emerging from distinct ARF network compositions. Changes in the stoichiometry of A -and B-class ARFs within the nucleus generate a unique transcriptional output, ranging from repression and a dampened auxin response to activation and a strong auxin response.

Molecular mechanisms of auxin signaling

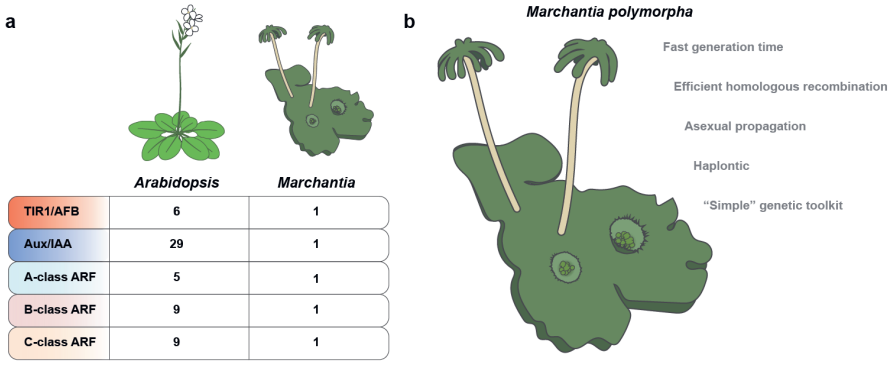
Despite early identification and recognition of auxin's importance, the underlying molecular mechanisms remained elusive

for decades afterwards. This changed dramatically in the 1990's and early 2000's when genetic studies revolutionized the plant biology field by identifying and characterizing a transcriptional auxin signaling module comprised of a set of core proteins (reviewed in **Chapter 2**[29]). These works formed a highly robust foundation for the field of plant science and inspired many successive revolutionary biochemical studies[29]. In short, nuclear auxin signaling involves three major protein families: the AUXIN RESPONSE FACTORS (ARFs), TRANSPORT INHIBITOR RESPONSE1/AUXIN SIGNALING F-BOX (TIR1/AFBs), and auxin/indole-3-acetic acid proteins (Aux/IAAs)[24,30]. In land plants, canonical ARF proteins are DNA-binding transcription factors which regulate the transcriptional response to auxin[31]. Land plant ARFs represent three distinct subfamilies, A, B, and C-class ARFs, with distinct functional properties (Fig. 2b, c)[31-33]. A-class ARFs function as auxin-dependent transcriptional activators of auxin-responsive genes (Fig. 2b)[24,31]. This auxin dependency comes from their ability to interact with the transcriptionally inhibitory Aux/IAAs, which are degraded by the 26S proteasome following auxin-induced interaction with the SKP-CULLIN-F-BOX$^{TIR1/AFB}$ ($SCF^{TIR1/AFB}$) complex (Fig. 2b)[34]. Aux/IAA degradation allows A-class ARFs to activate transcription of their target genes (Fig. 2b)[24,31]. These same genes are repressed by B-class ARFs[24,31]. B-ARF repression is auxin independent as these mostly do not interact with Aux/IAAs[35], but occurs because A -and B-ARFs compete in a stoichiometry-dependent way for DNA-binding at promoter elements of auxin-responsive genes.(Fig. 2c, d)[36-38]. Biochemical and genetic studies have identified C-class ARFs as unconnected to the canonical, transcriptional auxin response, regulating different genes[24,31,36]. However, recent findings have shown that A, B, -and C-ARFs in *Arabidopsis* can bind similar *cis*-elements in an interclade specific manner[39].

Together, these proteins form the Nuclear Auxin Pathway (NAP), a model that has remained almost unchanged for the better half of two decades (Fig. 2c, d)[30]. However, recent discoveries, as explored in this thesis, indicate that additional processes influence auxin signaling, requiring an update of the classical NAP model.

The need for tractable genetic systems to study the NAP

During embryophyte evolution, repeated genome duplications have dramatically expanded gene family sizes[40-42]. The popular model angiosperm (a clade of tracheophytes which bear flowers and fruits) *Arabidopsis thaliana* reflects this, as its genome encodes sub-



	Arabidopsis	Marchantia
TIR1/AFB	6	1
Aux/IAA	29	1
A-class ARF	5	1
B-class ARF	9	1
C-class ARF	9	1

Fig. 3 | *Marchantia polymorpha* as a plant model for molecular biology. **a.** Schematic representation of differences between *Arabidopsis thaliana* (left) and *Marchantia polymorpha* (right) in the size and complexity of auxin response protein gene families. This table summarizes the number of auxin signaling components encoded by the genomes of each species. Highlighted is the expanded complexity of the auxin signaling toolkit in *Arabidopsis* when compared to *Marchantia*, which possesses the minimal number of genes per gene family. **b.** Illustration of a female (Tak-2) plant of the thalloid liverwort *Marchantia polymorpha*. Emphasized here are its relatively simple morphology and properties making it suitable for molecular biology (in grey). Together, the panels illustrate why *Marchantia* serves as a powerful plant model system.

stantially enlarged NAP gene families (Fig. 1; Fig. 3a)[32]. For example, the genome of *Arabidopsis* encodes 23 different ARFs, 5 A-ARFs, 15 B-ARFs, and 3 C-ARFs (Fig. 3a)[32,33]. This expansion is the result of successive gene duplications, followed by sub -and neofunctionalization[32]. As a result, these ARFs can acquire novel functions, but may also show functional overlap with each other[39,43-49]. While this redundancy allows for increased signaling flexibility and complexity, it also complicates genetic analysis and obscures fundamental principles which drive auxin-mediated transcriptional control. Therefore, important questions about how ARF activity is controlled are difficult to answer using angiosperm plant models.

Retracing the trajectory of embryophyte evolution offers powerful, comparative frameworks to deal with these challenges (Fig. 1). For example, the liverwort *Marchantia polymorpha* has emerged as a particularly attractive model system (Fig. 1)[50]. The genome of *Marchantia* retains core hormonal and developmental pathways, while largely lacking the genetic redundancy characteristic of angiosperms[36,50-54]. All major NAP proteins are encoded by the *Marchantia* genome, with the minimal gene family sizes: 1 TIR/AFB, 1 Aux/IAA, 1 A-class ARF, 1 B-class ARF, and 1 C-class ARF (Fig. 3a)[32,36,54]. Addi-

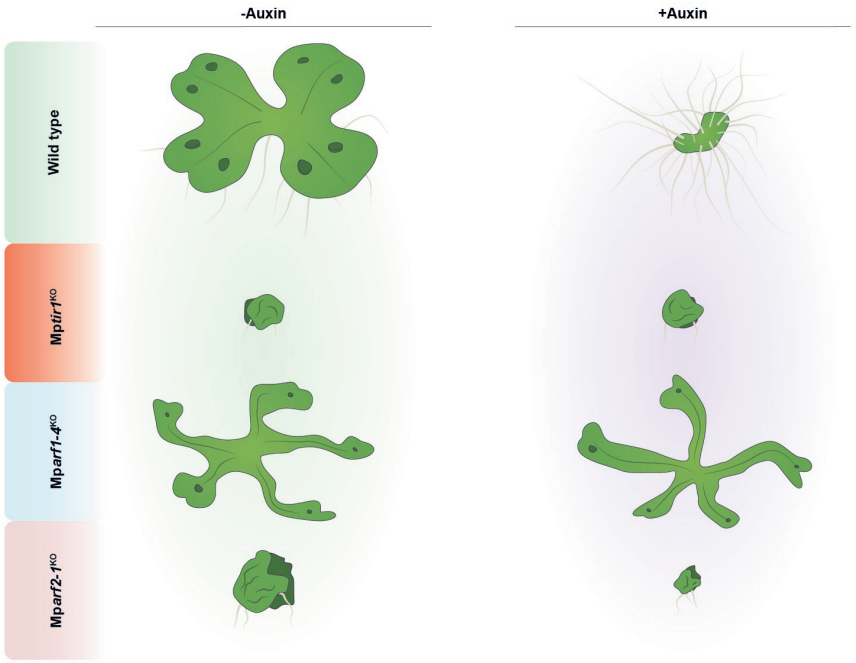


Fig. 4 | *Marchantia polymorpha* auxin signaling mutant(s).
Schematic approximation of morphologies of wild type (WT) *Marchantia* plants, and the Mp*tir1*^{KO}, Mp*arf1-4*^{KO}, and Mp*arf2-1*^{KO} mutants, both in normal growth conditions and after treatment with exogenous auxin. Illustrations are based on Ref.[52,58,59]. The Mp*tir1*^{KO} mutant has severe problems with cellular differentiation and does not develop normal organs[58]. Furthermore, whereas WT shows a very strong response to exogenous auxin, Mp*tir1*^{KO} fails to respond, illustrating the profound effect of auxin perception and signaling on *Marchantia* development[58]. The Mp*arf1-4*^{KO} mutant typically has epinastic growth defects and is auxin insensitive[52], whereas the Mp*arf2-1*^{KO} mutant, similar to Mp*tir1*^{KO}, has severe problems in differentiation and is auxin hypersensitive[59].

tionally, the *Marchantia* genome holds a bryo -and lycophyte specific non-canonical ARF (ncARF), which lacks the DBD[32,54].

This streamlined auxin signaling architecture, together with other properties such as efficient homologous recombination, fast generation times, and a dominant, gametophytic, haploid life stage, make *Marchantia* uniquely tractable for identifying and dissecting fundamental regulatory mechanisms (Fig. 3b)[50,55,56]. Moreover, auxin plays a central and conserved role in growth, differentiation and development in *Marchantia*[53,57]. Illustrating this, when the single Mp*tir1* auxin receptor is knocked out, *Marchantia* plants fail to produce organs and do not show the characteristic, severe, morphological response to exogenous auxin (Fig. 4)[58]. Knockout of the sole activa-

tor A-class Mp*ARF1* reduces auxin sensitivity[52], whereas knockout of the B-class repressor Mp*ARF2* increases auxin sensitivity (Fig. 4)[59].

ARF proteolysis

The transcriptional output of auxin signaling is strongly influenced by the relative abundance of different ARF proteins within a cell (Fig. 2d)[60]. The competition between activating A-ARFs and repressing B-ARFs is defined by their stoichiometry[36,37,60]. Precise and dynamic control of this stoichiometry is therefore essential for developmental regulation. Recent observations, including those presented in this thesis (**Chapter 3**, **4**, and **5**), support this dynamic regulation as ARFs themselves are subject to degradation by the 26S proteasome[61-63]. This challenges the traditional, more static, view of ARFs, and implies that these signaling components should be viewed from a dynamic and quantitative perspective (Fig. 2c, d)[60]. Understanding how ARF proteolysis and stability are controlled, which molecular mechanisms are involved, how these evolved, and how significant these are during development are essential questions to be addressed for a more complete understanding of auxin signaling.

Scope of the thesis

By exploiting the genetic toolkit and pivotal evolutionary position of *Marchantia* as a model system, I will delve into the phenomenon of ARF degradation. In this thesis I uncover essential proteolytic mechanisms controlling ARF proteostasis, explore their developmental and biological relevance, and trace their evolutionary origins. The work presented in this thesis establishes ARF degradation as a hitherto underappreciated, fundamental component of auxin-regulated plant development.

In **Chapter 2** I establish the conceptual framework for this thesis. It reviews the historical development of the field of auxin biology and the intimate connection between auxin, the NAP and cellular proteolytic systems. I first address the initial identification and characterization of the auxin signaling machinery in the late 20th and early 21st centuries. Next, I assess evidence of molecular mechanism that regulate degradation in the NAP and its applicability in non-plant systems. Finally, I survey known molecular mechanisms regulating proteolysis within the NAP, including parallels in non-plant systems, and evaluate the limited and fragmentary evidence bearing on ARF degradation thereby defining unresolved questions surrounding this topic.

In **Chapter 3** we develop and deploy experimental tools in *Marchantia* to examine the *in vivo* behavior of auxin signaling components. We generate homologous recombination-based (HR) knockin lines to fluorescently label auxin response proteins expressed from native loci. This enables us to accurately resolve the spatial and quantitative aspects of auxin response protein accumulation, thereby laying the groundwork for subsequent functional and mechanistic studies in this thesis.

In **Chapter 4** I focus on the molecular basis and evolutionary conservation of ARF degradation in *Marchantia*. Focusing on the B-class MpARF2, this chapter explores sequence features within this protein, candidate to mediating proteolytic turnover. I study the functional importance of these features and investigate them from within a comparative evolutionary context to trace their evolutionary origins.

In **Chapter 5** I build on chapter 4 and address the developmental consequences of perturbing ARF proteostasis. By experimentally altering ARF stability, inducible expression of stable ARF variants, and mutant complementation analysis, this chapter investigates the requirements of ARF degradation for development and

genetic regulation.

In **Chapter 6** and **Chapter 7** I seek to uncover the molecular machinery responsible for ARF degradation. In Chapter 6 I use the bryophyte *Physcomitrium patens* as a model for a forward-genetic mutagenesis screen in which I identify mutants that display increased stability of the MpARF2 paralog, PpARFb2. I map mutations occurring in these mutants to uncover genetic components regulating PpARFb2 degradation. Chapter 7 complements this approach, as here I employ a TurboID-based reverse-genetic strategy to identify candidate proteins associated with unstable ARFs and investigate their potential regulatory roles.

Finally, in **Chapter 8** I compile an overview of the major findings presented in this thesis and integrate them within the broader scientific context of auxin and plant biology. I speculate on the role, mechanism and evolution of ARF degradation. I supplement this synthesis with a discussion of outstanding research questions and future scientific directions to further understand ARF proteostasis through degradation, and its role in plant biology.

References

1 Boyce, C. K. & Lee, J.-E. Plant Evolution and Climate Over Geological Timescales. *Annual Review of Earth and Planetary Sciences* **45**, 61–87 (2017). https://doi.org/10.1146/annurev-earth-063016-015629

2 Shear, W. A. The early development of terrestrial ecosystems. *Nature* **351**, 6 (1991).

3 Gerrienne, P., Servais, T. & Vecoli, M. Plant evolution and terrestrialization during Palaeozoic times—The phylogenetic context. *Review of Palaeobotany and Palynology* **227**, 4–18 (2016). https://doi.org/10.1016/j.revpalbo.2016.01.004

4 McCourt, R. M., Delwiche, C. F. & Karol, K. G. Charophyte algae and land plant origins. *Trends in Ecology & Evolution* **19**, 661–666 (2004). https://doi.org/10.1016/j.tree.2004.09.013

5 Harholt, J., Moestrup, O. & Ulvskov, P. Why Plants Were Terrestrial from the Beginning. *Trends Plant Sci* **21**, 96–101 (2016). https://doi.org/10.1016/j.tplants.2015.11.010

6 Donoghue, P. C. J., Harrison, C. J., Paps, J. & Schneider, H. The evolutionary emergence of land plants. *Curr Biol* **31**, R1281–R1298 (2021). https://doi.org/10.1016/j.cub.2021.07.038

7 de Vries, J. & Archibald, J. M. Plant evolution: landmarks on the path to terrestrial life. *New Phytol* **217**, 1428–1434 (2018). https://doi.org/10.1111/nph.14975

8 Wellman, C. H., Osterloff, P. L. & Mohiuddin, U. Fragments of the earliest land plants. *Nature* **425**, 3 (2003). https://doi.org/https://doi.org/10.1038/nature01884

9 Heckman, D. S. *et al.* Molecular Evidence for the Early Colonization of Land by Fungi and Plants. *Science* **293**, 4 (2001). https://doi.org/DOI: 10.1126/science.1061457

10 Lenton, T. M. *et al.* Earliest land plants created modern levels of atmospheric oxygen. *Proc Natl Acad Sci U S A* **113**, 5 (2016). https://doi.org/10.1073/pnas.1604787113Downloaded

11 Knauth, L. P. & Kennedy, M. J. The late Precambrian greening of the Earth. *Nature* **460**, 728–732 (2009). https://doi.org/10.1038/nature08213

12 McMahon, W. J. & Davies, N. S. Evolution of alluvial mudrock forced by early land plants. *Science* **359**, 2 (2018). https://doi.org/DOI: 10.1126/science.aan4660

13 Maberly, S. C. The fitness of the environments of air and water for photosynthesis, growth, reproduction and dispersal of photoautotrophs: An evolutionary and biogeochemical perspective. *Aquatic Botany* **118**, 4–13 (2014). https://doi.org/10.1016/j.aquabot.2014.06.014

14 Maberly, S. C. & Gontero, B. Ecological imperatives for aquatic CO2-concentrating mechanisms. *J Exp Bot* **68**, 3797–3814 (2017). https://doi.org/10.1093/jxb/erx201

15 Karsten, U. & Holzinger, A. Green algae in alpine biological soil crust communities: acclimation strategies against ultraviolet radiation and dehydration. *Biodivers Conserv* **23**, 1845–1858 (2014). https://doi.org/10.1007/s10531-014-0653-2

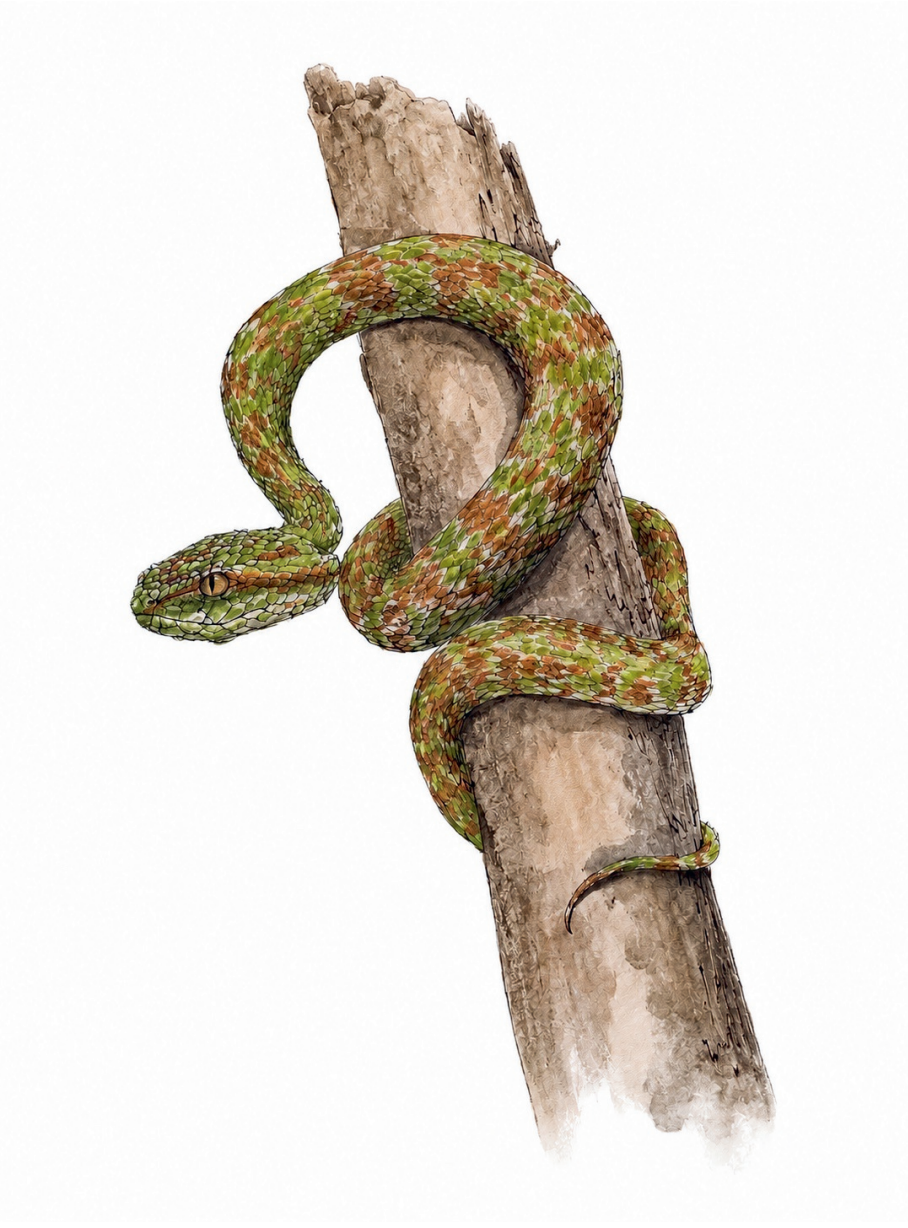
16 Herburger, K. & Holzinger, A. Localization and Quantification of Callose in the Streptophyte Green Algae Zygnema and Klebsormidium: Correlation with Desiccation Tolerance. *Plant Cell Physiol* **56**, 2259–2270 (2015). https://doi.org/10.1093/pcp/pcv139

17 Graham, L. E., Cook, M. E. & Busse, J. S. The origin of plants: Body plan changes

contributing to a major evolutionary radiation. *Proc Natl Acad Sci* **97**, 5 (2000).
18 Kiss, J. Z. Up, down, and all around: How plants sense and respondto environmental stimuli. *Proc Natl Acad Sci U S A* **103**, 11 (2006). https://doi.org/doi10.1073pnas.0510471102
19 de Jong, M. & Leyser, O. Developmental plasticity in plants. *Cold Spring Harb Symp Quant Biol* **77**, 63–73 (2012). https://doi.org/10.1101/sqb.2012.77.014720
20 Abley, K., Locke, J. C. & Leyser, H. M. Developmental mechanisms underlying variable, invariant and plastic phenotypes. *Ann Bot* **117**, 733–748 (2016). https://doi.org/10.1093/aob/mcw016
21 Mockaitis, K. & Estelle, M. Auxin receptors and plant development: a new signaling paradigm. *Annu Rev Cell Dev Biol* **24**, 55–80 (2008). https://doi.org/10.1146/annurev.cellbio.23.090506.123214
22 Durbak, A., Yao, H. & McSteen, P. Hormone signaling in plant development. *Curr Opin Plant Biol* **15**, 92–96 (2012). https://doi.org/10.1016/j.pbi.2011.12.004
23 Weijers, D., Nemhauser, J. L. & Zhenbiao, Y. Auxin: small molecule, big impact *J Exp Bot* **69**, 3 (2018). https://doi.org/https://doi.org/10.1093/jxb/erx463
24 Weijers, D. & Wagner, D. Transcriptional Responses to the Auxin Hormone. *Annu Rev Plant Biol* **67**, 539–574 (2016). https://doi.org/10.1146/annurev-arplant-043015-112122
25 Sauer, M., Robert, S. & Kleine-Vehn, J. Auxin: simply complicated. *J Exp Bot* **64**, 2565–2577 (2013). https://doi.org/10.1093/jxb/ert139
26 Darwin, C. & Darwin, F. *The power of movement in plants*. (John Murray, 1880).
27 Went, F. W. & Thimman, K. V. *Phytohormones*. (MacMillan, 1937).
28 Kögl, F., Erxleben, H. & Haagen-Smit, A. J. Über die Isolierung der Auxine a und b aus pflanzlichen Materialien. 9. Mitteilung über pflanzliche Wachstumsstoffe. *Physiologische Chemie* **228**, 8 (1934).
29 de Roij, M., Borst, J. W. & Weijers, D. Protein degradation in auxin response. *Plant Cell* (2024). https://doi.org/10.1093/plcell/koae125
30 Vanneste, S., Pei, Y. & Friml, J. Mechanisms of auxin action in plant growth and development. *Nat Rev Mol Cell Biol* (2025). https://doi.org/10.1038/s41580-025-00851-2
31 Roosjen, M., Paque, S. & Weijers, D. Auxin Response Factors: output control in auxin biology. *J Exp Bot* **69**, 179–188 (2018). https://doi.org/10.1093/jxb/erx237
32 Mutte, S. K. *et al.* Origin and evolution of the nuclear auxin response system. *Elife* **7** (2018). https://doi.org/10.7554/eLife.33399
33 Cance, C., Martin-Arevalillo, R., Boubekeur, K. & Dumas, R. Auxin response factors are keys to the many auxin doors. *New Phytol* **235**, 402–419 (2022). https://doi.org/10.1111/nph.18159
34 Leyser, O. Auxin Signaling. *Plant Physiol* **176**, 465–479 (2018). https://doi.org/10.1104/pp.17.00765
35 Vernoux, T. *et al.* The auxin signalling network translates dynamic input into robust patterning at the shoot apex. *Mol Syst Biol* **7**, 508 (2011). https://doi.org/10.1038/msb.2011.39
36 Kato, H. *et al.* Design principles of a minimal auxin response system. *Nat Plants* **6**, 473–482 (2020). https://doi.org/10.1038/s41477-020-0662-y
37 Lavy, M. & Estelle, M. Mechanisms of auxin signaling. *Development* **143**, 3226–3229 (2016). https://doi.org/10.1242/dev.131870
38 Rienstra, J., Carrillo-Carrasco, V. P., de Roij, M., Hernandez-Garcia, J. & Weijers, D. A conserved ARF-DNA interface underlies auxin-triggered transcriptional

response. *Proc Natl Acad Sci U S A* **122**, e2501915122 (2025). https://doi.org/10.1073/pnas.2501915122
39 Martin-Arevalillo, R. *et al.* Synthetic deconvolution of an auxin-dependent transcriptional code. *Cell* **188**, 2872–2889 e2824 (2025). https://doi.org/10.1016/j.cell.2025.03.028
40 Iohannes, S. D. & Jackson, D. Tackling redundancy: genetic mechanisms underlying paralog compensation in plants. *New Phytol* **240**, 1381–1389 (2023). https://doi.org/10.1111/nph.19267
41 Cusack, S. A. *et al.* Predictive Models of Genetic Redundancy in Arabidopsis thaliana. *Mol Biol Evol* **38**, 3397–3414 (2021). https://doi.org/10.1093/molbev/msab111
42 Panchy, N., Lehti-Shiu, M. & Shiu, S. H. Evolution of Gene Duplication in Plants. *Plant Physiol* **171**, 2294–2316 (2016). https://doi.org/10.1104/pp.16.00523
43 Okushima, Y. *et al.* Functional Genomic Analysis of the AUXIN RESPONSE FACTOR Gene Family Members in Arabidopsis thaliana: Unique and Overlapping Functions of ARF7 and ARF19 *The Plant Cell* **17**, 19 (2005). https://doi.org/https://doi.org/10.1105/tpc.104.028316
44 Berleth, T. & Jurgens, G. The role of the monopteros gene in organising the basal body region of the Arabidopsis embryo *Development* **118**, 12 (1993). https://doi.org/https://doi.org/10.1016/0168-9525(93)90246-E
45 Nagpal, P. *et al.* Auxin response factors ARF6 and ARF8 promote jasmonic acid production and flower maturation. *Development* **132**, 4107–4118 (2005). https://doi.org/10.1242/dev.01955
46 Tabata, R. *et al.* Arabidopsis AUXIN RESPONSE FACTOR6 and 8 Regulate Jasmonic Acid Biosynthesis and Floral Organ Development via Repression of Class 1 KNOX Genes. *Plant and Cell Physiology* **51**, 11 (2010). https://doi.org/https://doi.org/10.1093/pcp/pcp176
47 Wu, M. F., Tian, Q. & Reed, J. W. Arabidopsis microRNA167 controls patterns of ARF6 and ARF8 expression, and regulates both female and male reproduction. *Development* **133**, 4211–4218 (2006). https://doi.org/10.1242/dev.02602
48 Okushima, Y., Fukaki, H., Onoda, M., Theologis, A. & Tasaka, M. ARF7 and ARF19 regulate lateral root formation via direct activation of LBD/ASL genes in Arabidopsis. *Plant Cell* **19**, 118–130 (2007). https://doi.org/10.1105/tpc.106.047761
49 Wilmoth, J. C. *et al.* NPH4/ARF7 and ARF19 promote leaf expansion and auxin-induced lateral root formation. *Plant J* **43**, 118–130 (2005). https://doi.org/10.1111/j.1365-313X.2005.02432.x
50 Bowman, J. L. *et al.* The renaissance and enlightenment of Marchantia as a model system. *Plant Cell* **34**, 3512–3542 (2022). https://doi.org/10.1093/plcell/koac219
51 Flores-Sandoval, E., Eklund, D. M. & Bowman, J. L. A Simple Auxin Transcriptional Response System Regulates Multiple Morphogenetic Processes in the Liverwort Marchantia polymorpha. *PLoS Genet* **11**, e1005207 (2015). https://doi.org/10.1371/journal.pgen.1005207
52 Kato, H. *et al.* The Roles of the Sole Activator-Type Auxin Response Factor in Pattern Formation of Marchantia polymorpha. *Plant Cell Physiol* **58**, 1642–1651 (2017). https://doi.org/10.1093/pcp/pcx095
53 Eklund, D. M. *et al.* Auxin Produced by the Indole-3-Pyruvic Acid Pathway Regulates Development and Gemmae Dormancy in the Liverwort Marchantia polymorpha. *Plant Cell* **27**, 1650–1669 (2015). https://doi.org/10.1105/tpc.15.00065
54 Bowman, J. L. *et al.* Insights into Land Plant Evolution Garnered from the

Marchantia polymorpha Genome. *Cell* **171**, 287–304 e215 (2017). https://doi.org/10.1016/j.cell.2017.09.030
55 Shimamura, M. Marchantia polymorpha: Taxonomy, Phylogeny and Morphology of a Model System. *Plant Cell Physiol* **57**, 230–256 (2016). https://doi.org/10.1093/pcp/pcv192
56 Ishizaki, K., Nishihama, R., Yamato, K. T. & Kohchi, T. Molecular Genetic Tools and Techniques for Marchantia polymorpha Research. *Plant Cell Physiol* **57**, 262–270 (2016). https://doi.org/10.1093/pcp/pcv097
57 Kato, H. *et al.* Auxin-Mediated Transcriptional System with a Minimal Set of Components Is Critical for Morphogenesis through the Life Cycle in Marchantia polymorpha. *PLoS Genet* **11**, e1005084 (2015). https://doi.org/10.1371/journal.pgen.1005084
58 Suzuki, H., Kato, H., Iwano, M., Nishihama, R. & Kohchi, T. Auxin signaling is essential for organogenesis but not for cell survival in the liverwort Marchantia polymorpha. *Plant Cell* **35**, 1058–1075 (2023). https://doi.org/10.1093/plcell/koac367
59 Flores-Sandoval, E. *et al.* The B-class auxin response factor MpARF2 is essential for meristem organization in free-living plant gametophytes. *Curr Biol* (2025). https://doi.org/10.1016/j.cub.2025.11.015
60 Das, S., Weijers, D. & Borst, J. W. Auxin Response by the Numbers. *Trends Plant Sci* **26**, 442–451 (2021). https://doi.org/10.1016/j.tplants.2020.12.017
61 de Roij, M., Hernandez Garcia, J., Das, S., Borst, J. W. & Weijers, D. ARF degradation defines a deeply conserved step in auxin response. *Nat Plants* **11**, 717–724 (2025). https://doi.org/10.1038/s41477-025-01975-1
62 Prigge, M. J. *et al.* Comparative mutant analyses reveal a novel mechanism of ARF regulation in land plants. *Nat Plants* **11**, 821–835 (2025). https://doi.org/10.1038/s41477-025-01973-3
63 de Roij, M. *et al.* Diversification of functional requirements for proteolysis of auxin response factors. *Nature Communications* (2026). https://doi.org/10.1038/s41467-026-70440-0



Chapter 2

Protein degradation in auxin response

Authors

Martijn de Roij[1], Jan Willem Borst[1] & Dolf Weijers[1,*]

Affiliations

[1] Laboratory of Biochemistry, Wageningen University, Stippeneng 4, 6708WE Wageningen, the Netherlands

* Corresponding author: dolf.weijers@wur.nl

This chapter has been published as:

de Roij, M., Borst, J. W. & Weijers, D. Protein degradation in auxin response. *The Plant Cell* (2024).

https://doi.org/10.1093/plcell/koae125

Abstract

The signaling molecule auxin sits at the nexus of plant biology and coordinates essentially all growth and developmental processes in plants. Auxin molecules are transported throughout plant tissues and are capable of evoking highly specific physiological responses in plant cells by inducing various molecular pathways. In many of these pathways, proteolysis plays a crucial role for correct physiological responses. This review provides a chronology of the discovery and characterization of the auxin receptor, which is a fascinating example of separate research trajectories ultimately converging on the discovery of a core auxin signaling hub which relies on degradation of a family of transcriptional inhibitor proteins – the Aux/IAAs. Beyond describing the "classical" proteolysis-driven auxin response system, we explore more recent examples of the interconnection of proteolytic systems, which target a range of other auxin signaling proteins, and auxin response. By highlighting these emerging concepts, we provide potential future directions to further investigate the role of protein degradation within the framework of auxin response.

Introduction

The signaling molecule auxin holds tremendous significance in orchestrating plant growth and development[1,2]. Following its synthesis, auxin is transported to cells both at short and long distances, where it elicits a specific response by initiating a signaling cascade[1,3]. To ensure appropriate auxin responses, signal transduction is subject to multi-layered control mechanisms that rely on a precisely tuned proteome[2,3]. Therefore, control of the abundance, activity, and localization of proteins that participate in auxin response necessitates accurate regulation. This occurs through modulation of protein synthesis by altering transcription rates[4], by post-transcriptional regulation[5] and post-translational modifications[6,7], as well as through selective removal of proteins from the proteome via active degradation[8,9]. Key switches in molecular signaling events triggered by auxin, and their proper homeostasis, require rapid and well-timed degradation of specific auxin response proteins[2,3]. These degradation events are deeply intertwined with auxin signaling and are facilitated by proteolytic systems which, when disrupted, generally result in aberrant accumulation patterns of auxin signaling effectors often with severe consequences for plant development[2].

In this review, we provide an overview of the fundamental role of proteolytic processes within the context of auxin response. Because the stepwise discovery of the nuclear auxin response mechanism from genetic, biochemical, and molecular biological data over several decades is a beautiful example of how biological principles unfold, we start with an overview of the identification of the auxin receptor which mediates gene expression. Much attention in connecting auxin response to protein degradation has focused on the Aux/IAA proteins. We extend the exploration of proteolysis in auxin response by highlighting emerging roles of protein degradation of other effectors within the auxin signaling pathway.

Identification of a core ubiquitin ligase in auxin response

Pioneering scientific work conducted in the late 19th and early 20th century led to the discovery of auxins, with indole-3-acetic acid (IAA) representing the major naturally occurring auxin[10-12]. These signaling molecules elicit specific plant growth responses, and their identification gave rise to the field of auxin research. Decades of efforts towards elucidating the role of auxin in plant biology resulted in the recognition of auxins as crucial coordinators of virtually all aspects of plant development[1,2]. In parallel to studies that charac-

terized the physiological roles that auxin plays, a key finding was that auxin can trigger profound changes in gene expression[13-16].

The pursuit of the mechanisms underlying auxin action has followed multiple parallel tracks that eventually converged. A prominent track was the genetic analysis of auxin function. Mutagenesis genetic screens based on resistance of *Arabidopsis thaliana* seedlings to a high concentration of the synthetic auxin 2,4-Dichlorophenoxyacetic acid (2,4D), or to the auxin transport inhibitor *N*-1-naphthylphthalamic acid (NPA), led to the isolation of loci that are required for auxin response (Fig. 1). The first genes isolated this way were *AUXIN-RESISTANT1* (*AXR1)* and *TRANSPORT INHIBITOR RESISTANT1* (*TIR1)*, which directly pointed to the involvement of the Ubiquitin-Proteasome System (UPS) in auxin response (Fig. 1; Fig. 2a)[17-19]. While *AXR1* encodes an enzyme involved in the regulation of ubiquitin ligase activity, *TIR1* encodes an F-box protein, a substrate-binding subunit of E3 ubiquitin ligase complexes (Fig. 2a-b)[19-21]. Indeed, TIR1 was found to interact with the ubiquitin ligase complex subunits Arabidopsis SKP1-like (AtASK) and AtCULLIN1 (AtCUL1), together forming the SCF^{TIR1} complex (Fig. 2d-e)[22]. The *auxin-resistant6* (*axr-6*) mutant carries a mutation in AtCUL1, which affects its interaction with AtASK and results in severe auxin-related phenotypes (Fig. 1)[23,24]. SCF complexes are multi-subunit E3 ubiquitin ligase enzymes capable of recognizing and interacting with substrate proteins, conjugating it with ubiquitin proteins by recruiting E2 ligases and thereby targeting ubiquitylated subst3rates for degradation by the 26S proteasome (Fig. 2a)[25]. The E2 ligase is tethered to SCF^{TIR1} by RING BOX1 (RBX1) which associates with the AtCUL1 subunit (Fig. 2e)[26]. SCF target specificity is conferred by subunits harboring the F-box domain as these often selectively interact with a singular protein or a group of related targets[27]. TIR1 was found to be a member of a small, six-gene clade of F-box proteins which also included AUXIN SIGNALING F-BOX PROTEIN1-5[28,29]. As mutations that disrupted $SCF^{TIR1/AFB}$ assembly, as well as TIR1 overexpression, all interfered with auxin response, it was highly likely that auxin signaling required degradation of a specific protein or group of proteins capable of interacting with TIR1/AFB family members[22].

Identification of auxin-triggered proteolysis substrates

The identification of the elusive substrate proteins for TIR1/AFB also came from genetic screens investigating mutant plants with abnormal development (Fig. 1). Several auxin-resistant mu-

tants were identified with aberrant root and hypocotyl elongation, inhibited lateral root formation, and disturbed tropic responses: *auxin-resistant2* (*axr2*), *auxin-resistant3* (*axr3*), and *short hypocotyl2* (*shy2;* Fig. 1)[30-33]. When underlying genetic defects were identified, it was found that these mutants were all mutated in genes encoding proteins belonging to the same protein family – the AUXIN/INDOLE-3-ACETIC ACID (Aux/IAA) proteins[34-36]. The *Aux/IAA* family received its name from the identification of some of its members as transcripts that are rapidly increased upon auxin treatment[37-39]. Rapid auxin-induced transcription of these genes did not require the synthesis of new protein, indicating that all molecular components required for this upregulation were already present and could quickly respond[39]. A plausible explanation for this phenomenon was the existence of a de-repression mechanism whereby short-lived repressor proteins are quickly removed upon auxin stimulation[4,40].

Canonical Aux/IAA proteins share four conserved domains (numbered I to IV) and most of these proteins are markedly short-lived, with half-lives ranging from minutes to tens of minutes (Fig. 2b)[38,41-45]. The short-lived nature of canonical Aux/IAAs relies on a conserved 13 amino acid "degron" embedded in domain II[45]. This degron is composed of a conserved core GWPP[VIL] motif and is required for proteasome-dependent degradation (Fig. 2b)[45]. Mutations within the degron dramatically increase Aux/IAA protein stability[8,45]. Interestingly, *iaa7/axr2*, *iaa17/axr3*, and *iaa3/shy2* all had hypermorphic gain-of-function mutations which are located within the degron, causing protein stabilization[34-36]. While degron integrity is essential for Aux/IAA degradation, later work revealed that a KR motif between domain I and II and other regions outside of the degron also strongly influence Aux/IAA stability[44,46-49].

Molecular biological assays had meanwhile shown that Aux/IAAs are negative regulators of auxin-dependent gene activation[50]. The mechanism by which they act was revealed by the use of a minimal auxin-regulated promoter and screening for transcription factor binding[51]. This led to the identification of AUXIN RESPONSE FACTOR1 (ARF1), which directly binds to Auxin Responsive Elements (AuxREs) in auxin-induced promoters (Fig. 1b)[51]. ARF proteins are encoded by a multigene family and are discussed in more detail in other reviews[52,53]. Canonical ARFs have a general topology consisting of an amino-terminal DNA-binding domain (DBD), a middle region (MR), and a carboxy-terminal Phox and Bem 1 domain (PB1) (Fig. 2b)[54]. The latter domain mediates direct interaction with Aux/IAA proteins[51,55]. Thus, ARF activity is inhibited by the interaction with Aux/IAAs, whose degradation would relieve inhibition[53,56].

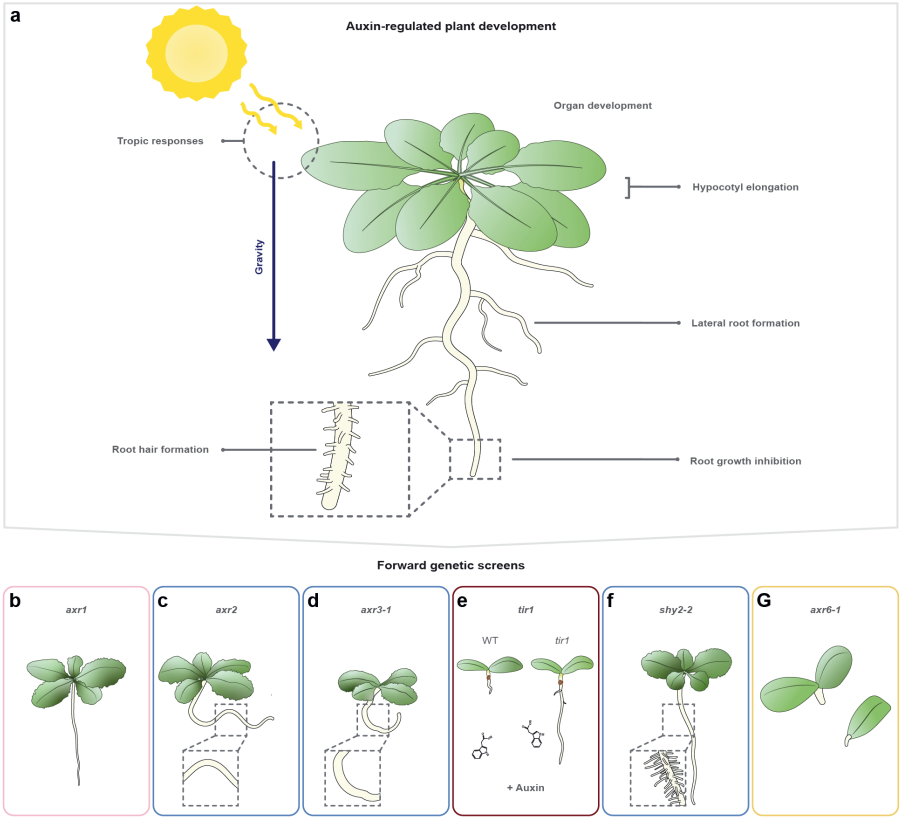


Fig. 1 | Phenotypes in auxin-insensitive mutants.
a. Schematic illustration of auxin-controlled plant developmental processes which were used as read-outs in various genetic screens. **b-g** Examples of mutants identified in genetic screens. Images reproduced from: **b.** Estelle and Somerville, 1987; **c.** Wilson et al., 1990; **d.** Leyser et al., 1996; **e.** Ruegger et al., 1997; **f.** Tian and Reed., 1999; **g.** Hobbie et al., 2000.

These two strands of research were connected when IAA7/AXR2 and IAA17/AXR3 were found to be degraded in response to external application of auxin, which depended on an intact degron, on TIR1, and on the proteasome[57]. In fact, TIR1 directly interacted with domain II of IAA7/AXR2 and IAA17/AXR3 and this interaction was stimulated by auxin (Fig. 2b-e)[57].

Identification of TIR1 as an auxin receptor

Most pieces of the puzzle were now identified, but a crucial piece, the auxin receptor, was still missing. Further characteriza-

tion of the Aux/IAA-SCF^{TIR1} interaction revealed that this interaction remained intact in cell-free environments, and that the site of auxin perception must therefore be soluble[58]. A real breakthrough occurred when two seminal studies demonstrated that TIR1 itself was capable of binding auxin[28,59]. The Aux/IAA-SCF^{TIR1} interaction relied on the presence of auxin and remained auxin-inducible in heterologous systems without additional plant proteins (Fig. 2c-e)[28,59]. It was clear that the TIR1 subunit of SCF^{TIR1} was the auxin receptor, thereby bypassing the need for additional signaling components which grants SCF^{TIR1} its ability to rapidly respond to auxin. The mechanism of auxin signaling was cemented by solving the structure of the AtASK1-TIR1 complex bound to auxin and an IAA7/AXR2 peptide[60]. Auxins extend the TIR1-Aux/IAA protein-interaction interface and thereby stabilize IAA degron binding, this phenomenon was famously described as auxin acting as molecular glue (Fig. 2d-e)[60].

Regulation of SCF$^{TIR1/AFB}$ activity

TIR1/AFBs and Aux/IAAs, as members of protein families, engage in diverse combinatorial interactions influenced by co-expression, binding affinities, and relative concentrations in cells[61,62]. Precise regulation of auxin-responsive gene expression requires degradation of other response proteins in addition to Aux/IAAs. Mutations that untether TIR1 from the SCF complex, lead to increased TIR1 protein accumulation[9]. This is caused by increased stability due to reduced TIR1 turnover by the proteasome. Structural and biochemical analysis indicates that these mutations (E12K and E15K) impede interaction with the SCF backbone AtCUL1[9,63]. This implies that TIR1, when assembled into SCF^{TIR1}, is targeted for autocatalytic degradation (Fig. 2e). Alternatively, TIR1 might be targeted for degradation by an unknown E3 ligase, although this is less likely as experimental data suggests that such an E3 ligase would have to be present in yeast (Fig. 2e)[9]. It is noteworthy that the amino acid residue in AFB1 that corresponds with the E12 position in TIR1 is a lysine (K8), which coincides with the finding that AFB1 does not efficiently assemble into an SCF complex and is concomitantly highly stable[5,9]. This implies that AFB1 is a naturally occurring auxin receptor mutant with a distinct function from the rest of the TIR1/AFB family members[9].

Aside from being a part of an enzymatically active E3-ligase, TIR1/AFBs were recently shown to possess adenylate cyclase (AC) activity[64]. The AC motif is located at the C-terminus of the protein and neighbours the auxin binding pocket in the TIR1/AFB structure

(Fig. 2b). *In silico* docking of ATP onto the TIR1/AFB structure revealed that ATP may be positioned near the Aux/IAA degron which potentially immobilizes ATP. TIR1 AC activity increased when bound to Aux/IAA7 and 17 and it was dependent on the presence of auxin. Mutant tir1 proteins that were AC-deficient were incapable of complementing the *tir1-1 afb2-3* double mutant and were unable to induce transcription of auxin-responsive genes suggesting that this AC activity has an important physiological role. However, it is not yet clear if these mutations in the AC motif also affect Aux/IAA degradation. In order to understand the kinetics of TIR1/AFB Aux/IAA binding in a broader context, TIR1/AFB AC activity and its effects on Aux/IAA recruitment and degradation should be examined. These recent findings however reinvigorated the exploration of a potential role of cAMP as a second messenger in plants, which remains enigmatic and requires further study[65].

Plasticity of the cellular SCF repertoire is ensured through the adaptive exchange model wherein SCF complexes undergo dynamic dis -and reassembly as well as (de)activation[66,67]. This occurs through RELATED TO UBIQUITIN1 (RUB1) modification of CUL1, which activates the SCF, but this is blocked when CUL1 is associated with CULLIN ASSOCIATED AND NEDDYLATION DISSOCIATED1 (CAND1) which dissociates the F-box protein from the SCF complex thereby deactivating it[67-69]. This system is also implicated in auxin-response. First of all, the aforementioned AXR1 and E1 C-TERMINAL-RELATED1 (ECR1), together with RUB-CONJUGATING ENZYME1 (RCE1), modify AtCUL1 with RUB1 (Fig. 2e)[20,70,71]. The COP9 signalosome (CSN) promotes RUB1 cleavage and associates with SCF^{TIR1} components *in vivo*[72,73]. Aberrant RUB1 (de)conjugation of AtCUL1 decreased SCF^{TIR1} activity and auxin response[26,71,72,74,75]. This was also observed for mutants deficient in CAND1 modification of AtCUL1[76-79]. It is important to note that the RUB1 and CAND1 (de) conjugation machinery is a general mechanism for SCF regulation and is not $SCF^{TIR1/AFB}$ nor auxin specific. Nevertheless, the data above show that these mechanisms are important for appropriate auxin responses.

Auxin-inducible degron systems in non-plant systems

Throughout the characterization of the auxin response system, many of its key interactions have been explored in heterologous assays, including in yeast[46,80-82]. In recent years, the entire auxin response system has been ported to yeast, allowing for sys-

tematic analysis of quantitative system properties and specificity[80]. The ability to trigger auxin-dependent degradation of proteins in heterologous systems did not go unnoticed outside of the plant research community, and inspired the development of the auxin-inducible degron (AID) system, which uses the central components in the auxin response system to target any protein for degradation, and thus allows for controlled and fast degradation of proteins of interest in non-plant eukaryotes[83-87]. AID involves the fusion of a target protein to an Aux/IAA degron coupled with heterologous expression of a TIR1/AFB[83-87]. The target protein is rapidly degraded upon treatment with (synthetic) auxins. AID can be used to investigate protein function during specific developmental events, such as cell cycle stages. For example, precisely timed depletion of condensins and cohesins through AID revealed distinct roles for both complexes during specific mitotic phases[88-92]. AID is a versatile customizable tool and further innovative utilization could shed light on various other complicated biological processes in non-plant eukaryotic systems.

Beyond TIR1: Auxin control of protein degradation

After the discovery of TIR1 as an F-box protein mediating auxin response, a second, unrelated F-box protein was reported to be controlled by auxin. S-PHASE KINASE-ASSOCIATED PROTEIN2 (AtSKP2A) is a constituent of a functional SCF^{SKP2A} ubiquitin ligase that targets cell-cycle regulating transcription factors for degradation[93-95]. Notably, AtSKP2A itself is unstable and subject to degradation by the UPS[95]. In the mutant *axr1*, AtSKP2A accumulated, while being less stable in the mutants *axr2* and *axr3*[93,95]. Chemical inhibition of auxin signaling increased AtSKP2A levels whereas treatment with various auxins in a cell-free system destabilized AtSKP2A, suggesting a direct effect of auxin on SKP2A stability[95,96]. Molecular docking simulations revealed a potential auxin binding site and when key residues within this site were mutated, AtSKP2A retained less auxin and was more stable[96]. These findings, combined with the requirement of AtSKP2A to bind auxin in order to interact with one of its substrates, suggest that AtSKP2A regulates cell proliferation as a non-canonical auxin receptor, but this awaits substantiation. It should be noted that, following a series of studies that initially reported the auxin regulation of SKP2A, there has been a paucity of further reports, and it is unclear if and how SKP2A connects to other auxin response components, or to development.

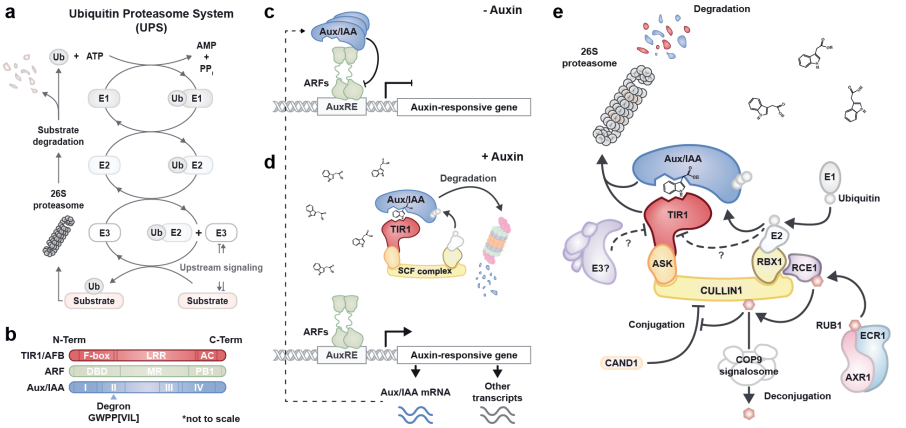


Fig. 2 | Overview of the UPS, domain architecture of auxin response proteins, and the canonical nuclear auxin pathway.
a. Schematic overview of the enzymatic cascade leading to ubiquitylation of a substrate protein, resulting in its recognition and subsequent degradation by the 26S proteasome. Ub, ubiquitin. **b.** General domain composition of canonical TIR1/AFB, ARF, and Aux/IAA proteins. This Fig. is not an alignment and the protein and domain sizes are not to scale. LRR, Leucine-rich Repeat; AC, Adenylate Cyclase; DBD, DNA-binding Domain; MR, Middle Region; PB1, Phox-Bem1. **c-e** Model of auxin signaling through auxin-induced and $SCF^{TIR1/AFB}$-mediated degradation of the Aux/IAA repressors. When auxin levels are low (**c.**), ARFs are repressed by Aux/IAAs but upon removal of the Aux/IAA repressors by auxin-triggered degradation (**d.**), ARF proteins are able to induce transcription of auxin-responsive genes, which includes Aux/IAA encoding genes. **e.** detailed overview of the composition of the $SCF^{TIR1/AFB}$ complex and hypothesized (dashed lines) as well as known (solid lines) regulatory mechanisms which tune $SCF^{TIR1/AFB}$ activity.

In addition to being an end station for ubiquitylated Aux/IAA proteins, the 26S proteasome regulates the abundance of virtually all plant proteins, either directly or indirectly[25]. Beyond its role in promoting specific E3 ligases, auxin was shown to also inhibit the proteolytic activity of the 26S proteasome, leading to a profound global effect on the proteome[97]. Repression of 26S proteasome activity by auxin requires PROTEASOME REGULATOR1 (PTRE1) which, counterintuitively, acts as a stimulant of 26S proteasome activity[97]. Auxin depletes nuclear PTRE1 and causes PTRE1 enrichment at the plasma membrane (Fig. 3)[97]. This sequence of events occurs comparatively slower than the rapid $SCF^{TIR1/AFB}$-mediated Aux/IAA degradation and potentially counteracts the rapid degradation process[97]. It is proposed that PTRE1 and its homologs are components of a feedback loop, ensuring proper homeostasis of the auxin signaling cascade and on the proteome in a more general sense. Furthermore, it is hypothesized that PTRE1 has a direct role in regulating Aux/IAA degradation, as PTRE1 co-immunoprecipitated with an Aux/IAA degron peptide, although this avenue remains to be explored[97].

Degradation of Auxin Response Factors

ARFs are final executors of the canonical auxin signaling pathway, as they modulate the expression of auxin-responsive genes[52,56,98]. It is becoming clear that the spatiotemporal components of ARF abundance, stoichiometry, and interactions are essential parameters driving auxin response[1,61,62,98]. In recent years, evidence is accumulating that tuning the auxin response machinery involves ARF proteostasis. Interestingly, the abundances of multiple ARF proteins have been reported to be regulated by proteolysis. AtARF1 has a half-life of three to four hours[99]. Although AtARF1 degradation was shown to be proteasome-dependent, neither knock-out of AtCUL1 nor exogenous auxin treatment influenced its degradation, therefore AtARF1 is likely routed to the UPS through a path different from the Aux/IAAs[99]. AtARF1 contains a degron in its MR and components required for its degradation likely reside in the nucleus, but these components have not been identified (Fig. 3)[99].

Another ARF, AtARF6, was previously reported to be unstable, with a shorter half-life than AtARF1[100]. Abscisic acid (ABA) and cold treatments promoted proteasome-dependent degradation of AtARF6, showing that hormonal crosstalk and environmental stimuli can affect ARF degradation (Fig. 3)[101]. Proteasome-dependent degradation of AtARF2 was also reportedly enhanced in response to ethylene treatment but was inhibited when etiolated seedlings were exposed to light (Fig. 3)[102]. Likewise, AtARF8 and 17 were observed to be degraded through the proteasome (Fig. 3). In none of these cases is there any insight into the protein domains or motifs (degrons) required for this degradation, or the identity of the ubiquitin ligases responsible for ARF targeting. Nonetheless, ARF degradation appears a prevalent and potentially relevant component in auxin response.

Very recently, a first component in ARF degradation was identified. A mutation in the AUXIN RESPONSE FACTOR F-BOX1 (AFF1) was recovered in a genetic screen for mutants with excessive AtARF7 protein accumulation. AFF1 is a component of an SCF^{AFF1} E3 ubiquitin ligase that recruits AtARF7 and its close paralog AtARF19, causing their proteasomal degradation[103]. Counterintuitively, AtARF7 and 19 displayed lower nuclear, but increased cytoplasmic abundance in root meristem cells of *aff1* mutants, suggesting a regulatory role for AFF1 in driving ARF nucleo-cytoplasmic partitioning (Fig. 3). Cytoplasmic AtARF7 and 19 form biomolecular condensates, a process that is dependent on protein concentrations. Impaired SCF^{AFF1}-mediated degradation might be indirectly responsible for in-

creased AtARF7 and 19 concentrations and condensate formation, although underlying mechanisms have not yet been identified (Fig. 3). The *aff1* mutants have reduced auxin response, signifying that non-nuclear cytoplasmic AtARF7 and 19 are unable to contribute to auxin response even when accumulated to abnormally high levels. AFF1-directed intracellular localization of AtARF7 and 19 occurs in a cell-type-specific manner, most prominent in root meristematic cells. Such ARF degradation may serve to eliminate damaged and unwanted protein yet might also provide an avenue to influence auxin response to react to biological stimuli. In either scenario, there are implied roles for regulatory modules to ensure AFF1 activity and therefore AtARF7 and 19 nuclear accumulation, but these have yet to be identified.

ARF degradation is not exclusive to *Arabidopsis thaliana*, but it has also been reported in other plant species. In apple (*Malus domestica*), the BROAD-COMPLEX, TRAMTRACK, AND BRIC A BRAC and TRANSCRIPTION ADAPTOR PUTATIVE ZINC FINGER (BTB-TAZ) PROTEIN2 (MdBT2) promotes MdARF8 degradation (Fig. 3)[104]. BTB-TAZ proteins form E3 ubiquitin ligases together with CULLIN3 (CUL3) proteins[105]. Interestingly, the MdARF8 interaction partner MdIAA3 also appeared to associate with MdBT2[104]. Overexpression of Md*BT2* increased MdIAA3 abundance and although a transcriptional effect is not ruled out, it is possible that MdBT2 stabilizes MdIAA3 post-transcriptionally since these two proteins were shown to interact[104]. Thus, MdBT2 might affect auxin signaling by regulating MdARF8 and MdIAA3 accumulation, but this requires further experimental verification[104]. Another apple ARF, MdARF5, is part of an ethylene-auxin-mediated transcriptional module that regulates anthocyanin production[106]. MdARF5 ubiquitylation and degradation is regulated by the E3 ligase SEVEN IN ABSENTIA11 (MdSINA11)[106]. A second E3 ligase, SEVEN IN ABSENTIA4 (MdSINA4), acts antagonistically to MdSINA11 and ubiquitylates and destabilizes the latter[106]. NAA treatment induced and reduced Md*SINA4* and Md*SINA11* transcription, respectively, revealing a complex degradation feedback loop to manage MdARF5 turnover (Fig. 3)[106].

Recent preprints provide evidence for ARF degradation by the UPS in monocots and bryophytes as well[107,108]. Comparative analysis of maize (*Zea mays*) and *Physcomitrium patens* mutants identified in genetic screens, revealed a deeply conserved degron in the DBD of ZmARF28 and PpARF1-4, which was also conserved in AtARF2 (Fig. 3)[107]. Mutations in residues part of the degron resulted in ARF stabilization, suppression of auxin response, and strong developmental defects[107]. ZmARF28, PpARF1-4, and AtARF2 are

class-B ARFs, which are considered repressors of auxin-responsive genes, whereas ARFs that fall into class-A are generally viewed as activators of genes[54,109]. Class-B ARF-mediated repression of auxin-responsive genes revolves around a competition model, whereby class-A and B ARFs compete for the same DNA-binding sites[53,110,111]. It is therefore interesting that another preprint shows that *Marchantia polymorpha* MpARF1 and MpARF2 protein levels decline during breakage of dormancy of asexually produced clonal propagules named gemmae (Fig. 3)[108]. Chemical inhibition of the UPS resulted in stable MpARF1 and accumulated MpARF2[108]. MpARF1 and MpARF2 fall into classes A and B, respectively. After the MpARF degradation event, MpARF1 and MpARF2 stoichiometry seemingly changed[108]. Experiments and mathematical modelling showed that MpARF degradation essentially reprograms the auxin response pathway and its transcriptional output[108]. These studies suggest that the stoichiometry of class-A and B ARFs, and consequentially their competition for DNA-binding sites, can be tuned through controlled degradation, but this theory requires further substantiation. Apart from PTM through ubiquitylation, MdARF8 is also subject to SUMOylation, which is the covalent attachment of a SMALL UBIQUITIN-LIKE MODIFIER (SUMO) protein to a substrate protein, thereby altering its functioning[104,112,113]. MdARF8 SUMOylation occurs through the E3 ligase SAP AND MIZ1 (MdSIZ1)[113]. This required SUMO-CONJUGATING ENZYME1 (MdSCE1), which directly interacted with MdARF8, whereas MdSIZ1 did not[113]. MdSIZ1 did enhance SUMO-conjugating activity of MdSCE1, suggesting that both are required for MdARF8 SUMOylation[113]. MdARF8 SUMOylation by MdSIZ1 reduces its susceptibility to degradation by the 26S proteasome, this could be because the SUMO moiety occupies lysine residues that would otherwise be ubiquitylated (Fig. 3). MdARF8-mediated induction of transcription of auxin-responsive genes requires SUMOylation[113]. The necessity of SUMO modification of MdARF8 might rely on the fact that it confers increased protein stability, but it could also regulate activity in an alternative, thus far unknown manner[113]. Alternative consequences of SUMOylation on ARF activity are observed for AtARF7, a class-A ARF that positively regulates auxin-induced lateral root formation[114,115]. Lateral root emergence is strongly and asymmetrically promoted on the side of the root exposed to high water availability compared to the side facing dry conditions. This process is known as hydropatterning[116]. At*ARF7* is expressed throughout the whole root system, however, it is SUMOylated on the dry side of the root when the latter is unilaterally exposed to moisture (Fig. 3)[114]. SUMOylation of AtARF7 reduces its DNA-binding activity and is required for recruitment of the repressor IAA3, thus impairing AtARF7 function

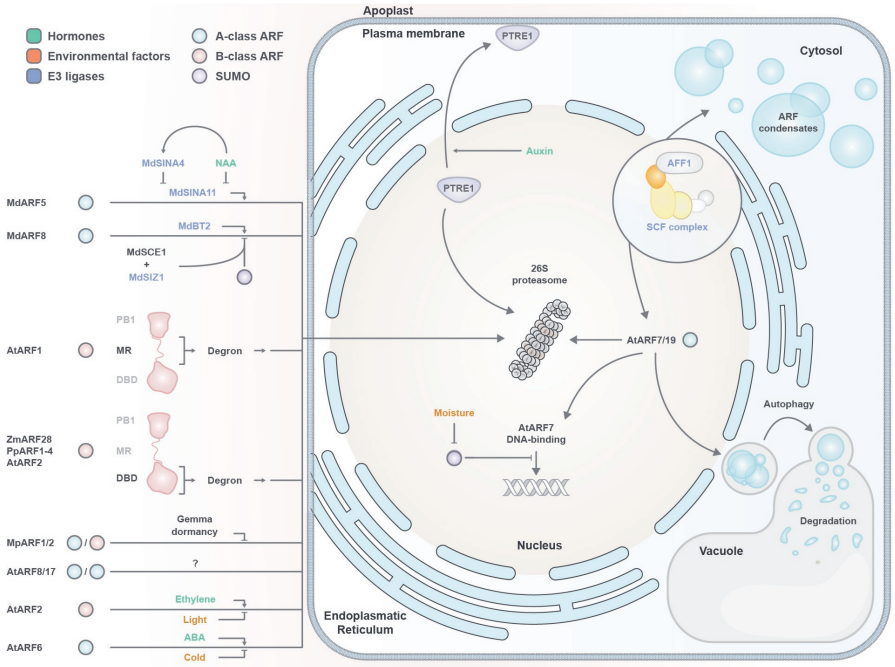


Fig. 3 | Regulation of ARF activity and accumulation via proteolysis and PTRE1-mediated tuning of proteasomal functioning.
Factors influencing degradation are colour coded as indicated in the legend. Abbreviations preceding protein names indicate that these proteins are from the following plant species: At, *Arabidopsis thaliana*; Md, *Malus domesticus*; Zm, *Zea mays*; Pp, *Physcomitrium patens*; Mp, *Marchantia polymorpha*. Color codes correspond to signal -and protein types, see legend in the top left.

as an auxin-induced transcriptional activator (Fig. 3)[114]. Preventing AtARF7 SUMOylation abolished hydropatterning, highlighting the pivotal role of this PTM in modulating ARF activity in response to environmental cues[114].

Lastly, a recent preprint reports on another degradation mechanism for AtARF7 and 19 which involves proteolytic turnover through macroautophagy (Fig. 3)[117]. Macroautophagy describes engulfment of a portion of cytoplasm by a double-membraned autophagosome, which then fuses with the vacuole where its cargo is degraded[118]. Interference with the autophagy machinery led to increased accumulation of AtARF7 in the cytoplasm and reduced auxin response[117]. These findings are similar to observed AtARF7 behavior in *aff1* mutants, although nuclear AtARF7 levels were not assessed[103,118]. Autophagy entails a new mechanism through which nuclear auxin response can be modulated future studies should address this possibility.

Future challenges & Outlook

It should be clear that auxin response is deeply intertwined with various forms of protein degradation, and these are indispensable for plant survival and development. However, large open questions remain. We outline some of the outstanding questions, and directions for their investigation, below.

I. The position of $SCF^{TIR1/AFB}$ at the core of nuclear auxin response was thought to be thoroughly understood, but its recently reported AC activity raises questions regarding other, hitherto undiscovered, functional roles of this complex. Two questions emerge: what roles does cAMP play in plants and is there a connection between AC activity of $SCF^{TIR1/AFB}$ and Aux/IAA degradation rates? An attractive hypothesis is that AC activity influences auxin signaling by modulating ARF activity, either directly through cAMP, or indirectly by e.g. affecting Aux/IAA stability. Evidence for this hypothesis is thus far lacking and would require further testing.

II. $SCF^{TIR1/AFB}$ can be viewed as a central auxin signaling hub and a comprehensive understanding of how $SCF^{TIR1/AFB}$ activity is modulated is therefore essential. While some of these regulatory mechanisms have been observed, such as TIR1 degradation and RUB modification, underlying mechanisms remain elusive and it is unclear if, and in what contexts, these regulatory layers are relevant for the specificity and amplitude of auxin response output.

III. PTRE1 modulates 26S proteasome activity, thus integrating auxin-regulated proteostasis distinct from transcriptional regulation by the typical auxin signaling response. The exact, proteome-wide effects of this remain unclear and will be important to address to determine the relevance of this system. Furthermore, mechanistic data on how PTRE1 governs 26S proteasome activity, and on how PTRE1 itself is regulated, is required. PTRE1 interacts with an Aux/IAA degron peptide, hinting at a more direct role in managing Aux/IAA degradation, which deserves additional attention as PTRE1 might be a component of an auxin signaling feedback loop.

IV. Plants are capable of responding to auxin within very short time frames and these responses largely predate transcriptional feedback, which is relatively slow[98,119]. Pathways underpinning fast auxin responses have recently been identified and are reviewed by others[98,119-121]. Physiological outputs of fast auxin response are for instance membrane depolarization and increased velocity of cytoplasmic streaming, which are likely mediated by rapidly occurring

proteome-wide (de)phosphorylation[120,122]. PTM by (de)phosphorylation can have profound effects on ubiquitin ligase activity, protein stability and turnover, and the UPS[123,124]. It is likely that there is crosstalk between rapid auxin response and the proteolytic machinery, which deserves more attention. Identification of the rapid auxin phospho-response revealed the power of large-scale proteomic approaches, which should be harnessed for future investigations into auxin response.

V. It is evident that qualitative and quantitative nuclear accumulation of ARFs are important parameters, defining which genes will be regulated by auxin and in what way. Dynamic signaling requires timely and selective removal of ARFs from the nucleus by degradation and/or translocation. This facet of auxin biology has remained relatively underexplored until recently. There is mounting evidence for the controlled degradation of ARFs through multiple systems, however, the underlying mechanisms remain ambiguous. To disentangle these, motifs constituting ARF degrons, stability-defining PTMs, and external factors impacting ARF degradation, and its kinetics, need to be identified and thoroughly investigated. A handful of E3 ligases that regulate ARF stability are known, but others must exist, and once identified, these will provide targets for mutagenesis or interaction screens. Furthermore, some environmental conditions and hormonal treatments, have demonstrated the ability to promote or inhibit ARF degradation, but how this occurs remains unknown. Lastly, the recent report of ARFs being degraded through autophagy opens up new opportunities to identify novel mechanisms by which the plant cell can dictate nuclear accumulation of ARFs.

Acknowledgements

We would like to thank Jorge Hernández-García for critically reviewing this manuscript, as well as Sophie Valk and Simon Lindhoud for advice regarding the figures and the anonymous reviewers for their helpful suggestions. This work was supported by the Netherlands Organization for Scientific Research (OCENW.M20.031 to J.W.B.).

References

1 Vanneste, S. & Friml, J. Auxin: a trigger for change in plant development. *Cell* **136**, 1005-1016 (2009). https://doi.org:10.1016/j.cell.2009.03.001

2 Mockaitis, K. & Estelle, M. Auxin receptors and plant development: a new signaling paradigm. *Annu Rev Cell Dev Biol* **24**, 55-80 (2008). https://doi.org:10.1146/annurev.cellbio.23.090506.123214

3 Leyser, O. Auxin Signaling. *Plant Physiol* **176**, 465-479 (2018). https://doi.org:10.1104/pp.17.00765

4 Abel, S. & Theologis, A. Early genes and auxin action. *Plant Physiol* **111**, 9-17 (1996). https://doi.org:10.1104/pp.111.1.9

5 Parry, G. et al. Complex regulation of the TIR1/AFB family of auxin receptors. *Proc Natl Acad Sci* **106**, 22540-22545 (2009). https://doi.org:10.1073/pnas.0911967106

6 Terrile, M. C. et al. Nitric oxide influences auxin signaling through S-nitrosylation of the Arabidopsis TRANSPORT INHIBITOR RESPONSE 1 auxin receptor. *Plant J* **70**, 492-500 (2012). https://doi.org:10.1111/j.1365-313X.2011.04885.x

7 Cho, H. et al. A secreted peptide acts on BIN2-mediated phosphorylation of ARFs to potentiate auxin response during lateral root development. *Nat Cell Biol* **16**, 66-76 (2014). https://doi.org:10.1038/ncb2893

8 Tiwari, S. B., Wang, X. J., Hagen, G. & Guilfoyle, T. J. AUX/IAA proteins are active repressors, and their stability and activity are modulated by auxin. *The Plant Cell* **13**, 2809-2822 (2001). https://doi.org:10.1105/tpc.010289

9 Yu, H. et al. Untethering the TIR1 auxin receptor from the SCF complex increases its stability and inhibits auxin response. *Nat Plants* **1** (2015). https://doi.org:10.1038/nplants.2014.30

10 Went, F. W. & Thimman, K. V. *Phytohormones.* (MacMillan, 1937).

11 Thimann, K. V. & Schneider, C. L. The Relative Activities of Different Auxins. *American Journal of Botany* **26** (1939). https://doi.org:https://doi.org/10.2307/2436468

12 Enders, T. A. & Strader, L. C. Auxin activity: Past, present, and future. *Am J Bot* **102**, 180-196 (2015). https://doi.org:10.3732/ajb.1400285

13 Kaufman, P. & Thimann, K. V. Hormone Action in the Whole Life of Plants. *Bulletin of the Torrey Botanical Club* **105** (1978). https://doi.org:10.2307/2484273

14 Guilfoyle, T. J. & Key, J. L. Auxin-regulated gene expression in higher plants. *Critical Reviews in Plant Sciences* **4**, 247-276 (1986). https://doi.org:10.1080/07352688609382226

15 Key, J. L. Modulation of gene expression by auxin. *Bioessays* **11**, 52-58 (1989). https://doi.org:10.1002/bies.950110204

16 Theologis, A. Rapid Gene Regulation by Auxin. *Annual Review of Plant Physiology* **37**, 407-438 (1986). https://doi.org:https://doi.org/10.1146/annurev.pp.37.060186.002203

17 Estelle, M. A. & Somerville, C. Auxin-resistant mutants of Arabidopsis thaliana with an altered morphology. *Molecular and General Genetics* **206**, 200-206 (1987). https://doi.org:10.1007/bf00333575

18 Ruegger, M. et al. Reduced Naphthylphthalamic Acid Binding in the tir3 Mutant of Arabidopsis Is Associated with a Reduction in Polar Auxin Transport and Diverse Morphological Defects. *The Plant Cell* **9** (1997). https://doi.org:10.2307/3870429

19 Leyser, H. M. et al. Arabidopsis auxin-resistance gene AXR1 encodes a protein related to ubiquitin-activating enzyme E1. *Nature* **364,** 161-164 (1993).

https://doi.org:10.1038/364161a0
20 del Pozo, J. C. & Estelle, M. The Arabidopsis cullin AtCUL1 is modified by the ubiquitin-related protein RUB1. *Proc Natl Acad Sci* **96**, 15342-15347 (1999). https://doi.org:10.1073/pnas.96.26.15342
21 Ruegger, M. et al. The TIR1 protein of Arabidopsis functions in auxin response and is related to human SKP2 and yeast Grr1P. *Current Opinion in Plant Biology* **1**, 198-207 (1998). https://doi.org:10.1016/s1369-5266(98)80055-1
22 Gray, W. M. et al. Identification of an SCF ubiquitin-ligase complex required for auxin response in Arabidopsis thaliana. *Genes Dev* **13**, 1678-1691 (1999). https://doi.org:10.1101/gad.13.13.1678
23 Hobbie, L. et al. The axr6 mutants of Arabidopsis thaliana define a gene involved in auxin response and early development. *Development* **127**, 23-32 (2000). https://doi.org:10.1242/dev.127.1.23
24 Hellmann, H. et al. Arabidopsis AXR6 encodes CUL1 implicating SCF E3 ligases in auxin regulation of embryogenesis. *EMBO J* **22**, 3314-3325 (2003). https://doi.org:10.1093/emboj/cdg335
25 Vierstra, R. D. The ubiquitin-26S proteasome system at the nexus of plant biology. *Nat Rev Mol Cell Biol* **10**, 385-397 (2009). https://doi.org:10.1038/nrm2688
26 Gray, W. M., Hellmann, H., Dharmasiri, S. & Estelle, M. Role of the Arabidopsis RING-H2 protein RBX1 in RUB modification and SCF function. *The Plant Cell* **14**, 2137-2144 (2002). https://doi.org:10.1105/tpc.003178
27 Gagne, J. M., Downes, B. P., Shiu, S. H., Durski, A. M. & Vierstra, R. D. The F-box subunit of the SCF E3 complex is encoded by a diverse superfamily of genes in Arabidopsis. *Proc Natl Acad Sci* **99**, 11519-11524 (2002). https://doi.org:10.1073/pnas.162339999
28 Dharmasiri, N., Dharmasiri, S. & Estelle, M. The F-box protein TIR1 is an auxin receptor. *Nature* **435**, 441-445 (2005). https://doi.org:10.1038/nature03543
29 Dharmasiri, N. et al. Plant development is regulated by a family of auxin receptor F box proteins. *Dev Cell* **9**, 109-119 (2005). https://doi.org:10.1016/j.devcel.2005.05.014
30 Wilson, A. K., Pickett, F. B., Turner, J. C. & Estelle, M. A dominant mutation in Arabidopsis confers resistance to auxin, ethylene and abscisic acid. *Mol Gen Genet* **222**, 377-383 (1990). https://doi.org:10.1007/BF00633843
31 Leyser, H. M., Pickett, F. B., Dharmasiri, S. & Estelle, M. Mutations in the AXR3 gene of Arabidopsis result in altered auxin response including ectopic expression from the SAUR-AC1 promoter. *Plant J* **10**, 403-413 (1996). https://doi.org:10.1046/j.1365-313x.1996.10030403.x
32 Kim, B. C., Soh, M. C., Kang, B. J., Furuya, M. & Nam, H. G. Two dominant photomorphogenic mutations of Arabidopsis thaliana identified as suppressor mutations of hy2. *Plant J* **9**, 441-456 (1996). https://doi.org:10.1046/j.1365-313x.1996.09040441.x
33 Reed, J. W., Elumalai, R. P. & Chory, J. Suppressors of an Arabidopsis thaliana phyB mutation identify genes that control light signaling and hypocotyl elongation. *Genetics* **148**, 1295-1310 (1998). https://doi.org:10.1093/genetics/148.3.1295
34 Nagpal, P. et al. AXR2 encodes a member of the Aux/IAA protein family. *Plant Physiol* **123**, 563-574 (2000). https://doi.org:10.1104/pp.123.2.563
35 Rouse, D., Mackay, P., Stirnberg, P., Estelle, M. & Leyser, O. Changes in auxin response from mutations in an AUX/IAA gene. *Science* **279**, 1371-1373 (1998). https://doi.org:10.1126/science.279.5355.1371

36 Tian, Q. & Reed, J. W. Control of auxin-regulated root development by the Arabidopsis thaliana SHY2/IAA3 gene. *Development* **126**, 711-721 (1999). https://doi.org:10.1242/dev.126.4.711
37 Theologis, A., Huynh, T. V. & Davis, R. W. Rapid induction of specific mRNAs by auxin in pea epicotyl tissue. *J Mol Biol* **183**, 53-68 (1985). https://doi.org:10.1016/0022-2836(85)90280-3
38 Abel, S., Oeller, P. W. & Theologis, A. Early auxin-induced genes encode short-lived nuclear proteins. *Proc Natl Acad Sci* **91**, 326-330 (1994). https://doi.org:10.1073/pnas.91.1.326
39 Abel, S., Nguyen, M. D. & Theologis, A. The PS-IAA4/5-like family of early auxin-inducible mRNAs in Arabidopsis thaliana. *J Mol Biol* **251**, 533-549 (1995). https://doi.org:10.1006/jmbi.1995.0454
40 Ballas, N., Wong, L. M., Ke, M. & Theologis, A. Two auxin-responsive domains interact positively to induce expression of the early indoleacetic acid-inducible gene PS-IAA4/5. *Proc Natl Acad Sci* **92**, 3483-3487 (1995). https://doi.org:10.1073/pnas.92.8.3483
41 Oeller, P. W., Keller, J. A., Parks, J. E., Silbert, J. E. & Theologis, A. Structural characterization of the early indoleacetic acid-inducible genes, PS-IAA4/5 and PS-IAA6, of pea (Pisum sativum L.). *J Mol Biol* **233**, 789-798 (1993). https://doi.org:10.1006/jmbi.1993.1555
42 Worley, C. K. et al. Degradation of Aux/IAA proteins is essential for normal auxin signalling. *Plant J* **21**, 553-562 (2000). https://doi.org:10.1046/j.1365-313x.2000.00703.x
43 Zenser, N., Ellsmore, A., Leasure, C. & Callis, J. Auxin modulates the degradation rate of Aux/IAA proteins. *Proc Natl Acad Sci* **98**, 11795-11800 (2001). https://doi.org:10.1073/pnas.211312798
44 Dreher, K. A., Brown, J., Saw, R. E. & Callis, J. The Arabidopsis Aux/IAA protein family has diversified in degradation and auxin responsiveness. *The Plant Cell* **18**, 699-714 (2006). https://doi.org:10.1105/tpc.105.039172
45 Ramos, J. A., Zenser, N., Leyser, O. & Callis, J. Rapid degradation of auxin/indoleacetic acid proteins requires conserved amino acids of domain II and is proteasome dependent. *The Plant Cell* **13**, 2349-2360 (2001). https://doi.org:10.1105/tpc.010244
46 Calderon Villalobos, L. I. et al. A combinatorial TIR1/AFB-Aux/IAA co-receptor system for differential sensing of auxin. *Nat Chem Biol* **8**, 477-485 (2012). https://doi.org:10.1038/nchembio.926
47 Niemeyer, M. et al. Flexibility of intrinsically disordered degrons in AUX/IAA proteins reinforces auxin co-receptor assemblies. *Nat Commun* **11**, 2277 (2020). https://doi.org:10.1038/s41467-020-16147-2
48 Moss, B. L. et al. Rate Motifs Tune Auxin/Indole-3-Acetic Acid Degradation Dynamics. *Plant Physiol* **169**, 803-813 (2015). https://doi.org:10.1104/pp.15.00587
49 Havens, K. A. et al. A synthetic approach reveals extensive tunability of auxin signaling. *Plant Physiol* **160**, 135-142 (2012). https://doi.org:10.1104/pp.112.202184
50 Ulmasov, T., Murfett, J., Hagen, G. & Guilfoyle, T. J. Aux/IAA proteins repress expression of reporter genes containing natural and highly active synthetic auxin response elements. *The Plant Cell* **9**, 1963-1971 (1997). https://doi.org:10.1105/tpc.9.11.1963
51 Ulmasov, T., Hagen, G. & Guilfoyle, T. J. ARF1, a transcription factor that binds

to auxin response elements. *Science* **276**, 1865-1868 (1997). https://doi.org:10.1126/science.276.5320.1865
52 Cance, C., Martin-Arevalillo, R., Boubekeur, K. & Dumas, R. Auxin response factors are keys to the many auxin doors. *New Phytol* **235**, 402-419 (2022). https://doi.org:10.1111/nph.18159
53 Roosjen, M., Paque, S. & Weijers, D. Auxin Response Factors: output control in auxin biology. *J Exp Bot* **69**, 179-188 (2018). https://doi.org:10.1093/jxb/erx237
54 Finet, C., Berne-Dedieu, A., Scutt, C. P. & Marletaz, F. Evolution of the ARF gene family in land plants: old domains, new tricks. *Mol Biol Evol* **30**, 45-56 (2013). https://doi.org:10.1093/molbev/mss220
55 Kim, J., Harter, K. & Theologis, A. Protein-protein interactions among the Aux/IAA proteins. *Proc Natl Acad Sci* **94**, 11786-11791 (1997). https://doi.org:10.1073/pnas.94.22.11786
56 Weijers, D. & Wagner, D. Transcriptional Responses to the Auxin Hormone. *Annu Rev Plant Biol* **67**, 539-574 (2016). https://doi.org:10.1146/annurev-arplant-043015-112122
57 Gray, W. M., Kepinski, S., Rouse, D., Leyser, O. & Estelle, M. Auxin regulates SCF(TIR1)-dependent degradation of AUX/IAA proteins. *Nature* **414**, 271-276 (2001). https://doi.org:10.1038/35104500
58 Dharmasiri, N., Dharmasiri, S., Jones, A. M. & Estelle, M. Auxin action in a cell-free system. *Curr Biol* **13**, 1418-1422 (2003). https://doi.org:10.1016/s0960-9822(03)00536-0
59 Kepinski, S. & Leyser, O. The Arabidopsis F-box protein TIR1 is an auxin receptor. *Nature* **435**, 446-451 (2005). https://doi.org:10.1038/nature03542
60 Tan, X. et al. Mechanism of auxin perception by the TIR1 ubiquitin ligase. *Nature* **446**, 640-645 (2007). https://doi.org:10.1038/nature05731
61 Das, S., Weijers, D. & Borst, J. W. Auxin Response by the Numbers. *Trends Plant Sci* **26**, 442-451 (2021). https://doi.org:10.1016/j.tplants.2020.12.017
62 Del Bianco, M. & Kepinski, S. Context, specificity, and self-organization in auxin response. *Cold Spring Harb Perspect Biol* **3**, a001578 (2011). https://doi.org:10.1101/cshperspect.a001578
63 Zheng, N. et al. Structure of the Cul1-Rbx1-Skp1-F boxSkp2 SCF ubiquitin ligase complex. *Nature* **416**, 703-709 (2002). https://doi.org:10.1038/416703a
64 Qi, L. et al. Adenylate cyclase activity of TIR1/AFB auxin receptors in plants. *Nature* **611**, 133-138 (2022). https://doi.org:10.1038/s41586-022-05369-7
65 Qi, L. & Friml, J. Tale of cAMP as a second messenger in auxin signaling and beyond. *New Phytol* **240**, 489-495 (2023). https://doi.org:10.1111/nph.19123
66 Liu, X. et al. Cand1-Mediated Adaptive Exchange Mechanism Enables Variation in F-Box Protein Expression. *Mol Cell* **69**, 773-786 e776 (2018). https://doi.org:10.1016/j.molcel.2018.01.038
67 Pierce, N. W. et al. Cand1 promotes assembly of new SCF complexes through dynamic exchange of F box proteins. *Cell* **153**, 206-215 (2013). https://doi.org:10.1016/j.cell.2013.02.024
68 Wu, S. et al. CAND1 controls in vivo dynamics of the cullin 1-RING ubiquitin ligase repertoire. *Nat Commun* **4**, 1642 (2013). https://doi.org:10.1038/ncomms2636
69 Zemla, A. et al. CSN- and CAND1-dependent remodelling of the budding yeast SCF complex. *Nat Commun* **4**, 1641 (2013). https://doi.org:10.1038/ncomms2628

70 del Pozo, J. C., Timpte, C., Tan, S., Callis, J. & Estelle, M. The ubiquitin-related protein RUB1 and auxin response in Arabidopsis. *Science* **280**, 1760-1763 (1998). https://doi.org:10.1126/science.280.5370.1760
71 del Pozo, J. C. et al. AXR1-ECR1-dependent conjugation of RUB1 to the Arabidopsis Cullin AtCUL1 is required for auxin response. *The Plant Cell* **14**, 421-433 (2002). https://doi.org:10.1105/tpc.010282
72 Schwechheimer, C. et al. Interactions of the COP9 signalosome with the E3 ubiquitin ligase SCFTIRI in mediating auxin response. *Science* **292**, 1379-1382 (2001). https://doi.org:10.1126/science.1059776
73 Lyapina, S. et al. Promotion of NEDD-CUL1 conjugate cleavage by COP9 signalosome. *Science* **292**, 1382-1385 (2001). https://doi.org:10.1126/science.1059780
74 Dharmasiri, S., Dharmasiri, N., Hellmann, H. & Estelle, M. The RUB/Nedd8 conjugation pathway is required for early development in Arabidopsis. *EMBO J* **22**, 1762-1770 (2003). https://doi.org:10.1093/emboj/cdg190
75 Woodward, A. W., Ratzel, S. E., Woodward, E. E., Shamoo, Y. & Bartel, B. Mutation of E1-CONJUGATING ENZYME-RELATED1 decreases RELATED TO UBIQUITIN conjugation and alters auxin response and development. *Plant Physiol* **144**, 976-987 (2007). https://doi.org:10.1104/pp.107.100404
76 Gray, W. M., Muskett, P. R., Chuang, H. W. & Parker, J. E. Arabidopsis SGT1b is required for SCF(TIR1)-mediated auxin response. *The Plant Cell* **15**, 1310-1319 (2003). https://doi.org:10.1105/tpc.010884
77 Chuang, H. W., Zhang, W. & Gray, W. M. Arabidopsis ETA2, an apparent ortholog of the human cullin-interacting protein CAND1, is required for auxin responses mediated by the SCF(TIR1) ubiquitin ligase. *The Plant Cell* **16**, 1883-1897 (2004). https://doi.org:10.1105/tpc.021923
78 Cheng, Y., Dai, X. & Zhao, Y. AtCAND1, a HEAT-repeat protein that participates in auxin signaling in Arabidopsis. *Plant Physiol* **135**, 1020-1026 (2004). https://doi.org:10.1104/pp.104.044495
79 Zhang, W. et al. Genetic analysis of CAND1-CUL1 interactions in Arabidopsis supports a role for CAND1-mediated cycling of the SCFTIR1 complex. *Proc Natl Acad Sci* **105**, 8470-8475 (2008). https://doi.org:10.1073/pnas.0804144105
80 Pierre-Jerome, E., Jang, S. S., Havens, K. A., Nemhauser, J. L. & Klavins, E. Recapitulation of the forward nuclear auxin response pathway in yeast. *Proc Natl Acad Sci* **111**, 9407-9412 (2014). https://doi.org:10.1073/pnas.1324147111
81 Shimizu-Mitao, Y. & Kakimoto, T. Auxin sensitivities of all Arabidopsis Aux/IAAs for degradation in the presence of every TIR1/AFB. *Plant Cell Physiol* **55**, 1450-1459 (2014). https://doi.org:10.1093/pcp/pcu077
82 Pierre-Jerome, E., Moss, B. L., Lanctot, A., Hageman, A. & Nemhauser, J. L. Functional analysis of molecular interactions in synthetic auxin response circuits. *Proc Natl Acad Sci* **113**, 11354-11359 (2016). https://doi.org:10.1073/pnas.1604379113
83 Nishimura, K., Fukagawa, T., Takisawa, H., Kakimoto, T. & Kanemaki, M. An auxin-based degron system for the rapid depletion of proteins in nonplant cells. *Nat Methods* **6**, 917-922 (2009). https://doi.org:10.1038/nmeth.1401
84 Nishimura, K. et al. A super-sensitive auxin-inducible degron system with an engineered auxin-TIR1 pair. *Nucleic Acids Res* **48**, e108 (2020). https://doi.org:10.1093/nar/gkaa748
85 Li, S., Prasanna, X., Salo, V. T., Vattulainen, I. & Ikonen, E. An efficient auxin-inducible degron system with low basal degradation in human cells. *Nat Methods*

16, 866-869 (2019). https://doi.org:10.1038/s41592-019-0512-x
86 Yesbolatova, A. et al. The auxin-inducible degron 2 technology provides sharp degradation control in yeast, mammalian cells, and mice. *Nat Commun* **11**, 5701 (2020). https://doi.org:10.1038/s41467-020-19532-z
87 Holland, A. J., Fachinetti, D., Han, J. S. & Cleveland, D. W. Inducible, reversible system for the rapid and complete degradation of proteins in mammalian cells. *Proc Natl Acad Sci* **109**, E3350-3357 (2012). https://doi.org:10.1073/pnas.1216880109
88 Gibcus, J. H. et al. A pathway for mitotic chromosome formation. *Science* **359** (2018). https://doi.org:10.1126/science.aao6135
89 Thiecke, M. J. et al. Cohesin-Dependent and -Independent Mechanisms Mediate Chromosomal Contacts between Promoters and Enhancers. *Cell Rep* **32**, 107929 (2020). https://doi.org:10.1016/j.celrep.2020.107929
90 Rao, S. S. P. et al. Cohesin Loss Eliminates All Loop Domains. *Cell* **171**, 305-320 e324 (2017). https://doi.org:10.1016/j.cell.2017.09.026
91 Rhodes, J. D. P. et al. Cohesin Disrupts Polycomb-Dependent Chromosome Interactions in Embryonic Stem Cells. *Cell Rep* **30**, 820-835 e810 (2020). https://doi.org:10.1016/j.celrep.2019.12.057
92 Wutz, G. et al. Topologically associating domains and chromatin loops depend on cohesin and are regulated by CTCF, WAPL, and PDS5 proteins. *EMBO J* **36**, 3573-3599 (2017). https://doi.org:10.15252/embj.201798004
93 del Pozo, J. C., Boniotti, M. B. & Gutierrez, C. Arabidopsis E2Fc functions in cell division and is degraded by the ubiquitin-SCF(AtSKP2) pathway in response to light. *The Plant Cell* **14**, 3057-3071 (2002). https://doi.org:10.1105/tpc.006791
94 del Pozo, J. C., Diaz-Trivino, S., Cisneros, N. & Gutierrez, C. The balance between cell division and endoreplication depends on E2FC-DPB, transcription factors regulated by the ubiquitin-SCFSKP2A pathway in Arabidopsis. *The Plant Cell* **18**, 2224-2235 (2006). https://doi.org:10.1105/tpc.105.039651
95 Jurado, S. et al. SKP2A, an F-box protein that regulates cell division, is degraded via the ubiquitin pathway. *Plant J* **53**, 828-841 (2008). https://doi.org:10.1111/j.1365-313X.2007.03378.x
96 Jurado, S. et al. The Arabidopsis cell cycle F-box protein SKP2A binds to auxin. *The Plant Cell* **22**, 3891-3904 (2010). https://doi.org:10.1105/tpc.110.078972
97 Yang, B. J. et al. Arabidopsis PROTEASOME REGULATOR1 is required for auxin-mediated suppression of proteasome activity and regulates auxin signalling. *Nat Commun* **7**, 11388 (2016). https://doi.org:10.1038/ncomms11388
98 Caumon, H. & Vernoux, T. A matter of time: auxin signaling dynamics and the regulation of auxin responses during plant development. *J Exp Bot* **74**, 3887-3902 (2023). https://doi.org:10.1093/jxb/erad132
99 Salmon, J., Ramos, J. & Callis, J. Degradation of the auxin response factor ARF1. *Plant J* **54**, 118-128 (2008). https://doi.org:10.1111/j.1365-313X.2007.03396.x
100 Lakehal, A. et al. A Molecular Framework for the Control of Adventitious Rooting by TIR1/AFB2-Aux/IAA-Dependent Auxin Signaling in Arabidopsis. *Mol Plant* **12**, 1499-1514 (2019). https://doi.org:10.1016/j.molp.2019.09.001
101 Li, K., Wang, S., Wu, H. & Wang, H. Protein Levels of Several Arabidopsis Auxin Response Factors Are Regulated by Multiple Factors and ABA Promotes ARF6 Protein Ubiquitination. *Int J Mol Sci* **21** (2020). https://doi.org:10.3390/ijms21249437
102 Li, H., Johnson, P., Stepanova, A., Alonso, J. M. & Ecker, J. R. Convergence of signaling pathways in the control of differential cell growth in Arabidopsis. *Dev*

Cell **7**, 193-204 (2004). https://doi.org:10.1016/j.devcel.2004.07.002
103 Jing, H. et al. Regulation of AUXIN RESPONSE FACTOR condensation and nucleo-cytoplasmic partitioning. *Nat Commun* **13**, 4015 (2022). https://doi.org:10.1038/s41467-022-31628-2
104 Ji, X. L. et al. The BTB protein MdBT2 recruits auxin signaling components to regulate adventitious root formation in apple. *Plant Physiol* **189**, 1005-1020 (2022). https://doi.org:10.1093/plphys/kiac084
105 Gingerich, D. J. et al. Cullins 3a and 3b assemble with members of the broad complex/tramtrack/bric-a-brac (BTB) protein family to form essential ubiquitin-protein ligases (E3s) in Arabidopsis. *J Biol Chem* **280**, 18810-18821 (2005). https://doi.org:10.1074/jbc.M413247200
106 Li, H. L. et al. E3 ubiquitin ligases SINA4 and SINA11 regulate anthocyanin biosynthesis by targeting the IAA29-ARF5-1-ERF3 module in apple. *The Plant Cell* Environ (2023). https://doi.org:10.1111/pce.14709
107 Prigge, M. J. et al. Comparative mutant analyses reveal a novel mechanism of ARF regulation in land plants. *bioRxiv* (2023). https://doi.org:10.1101/2023.11.09.566459
108 Das, S. et al. Selective degradation of ARF monomers controls auxin response in Marchantia. *bioRxiv* (2022). https://doi.org:10.1101/2022.11.04.515187
109 Mutte, S. K. et al. Origin and evolution of the nuclear auxin response system. *Elife* **7**, (2018). https://doi.org:10.7554/eLife.33399
110 Lavy, M. et al. Constitutive auxin response in Physcomitrella reveals complex interactions between Aux/IAA and ARF proteins. *Elife* **5**, (2016). https://doi.org:10.7554/eLife.13325
111 Kato, H. et al. Design principles of a minimal auxin response system. *Nat Plants* **6**, 473-482 (2020). https://doi.org:10.1038/s41477-020-0662-y
112 Johnson, E. S. Protein modification by SUMO. *Annu Rev Biochem* **73**, 355-382 (2004). https://doi.org:10.1146/annurev.biochem.73.011303.074118
113 Zhang, C. L. et al. Apple SUMO E3 ligase MdSIZ1 facilitates SUMOylation of MdARF8 to regulate lateral root formation. *New Phytol* **229**, 2206-2222 (2021). https://doi.org:10.1111/nph.16978
114 Orosa-Puente, B. et al. Root branching toward water involves posttranslational modification of transcription factor ARF7. *Science* **362**, 1407-1410 (2018). https://doi.org:10.1126/science.aau3956
115 Okushima, Y., Fukaki, H., Onoda, M., Theologis, A. & Tasaka, M. ARF7 and ARF19 regulate lateral root formation via direct activation of LBD/ASL genes in Arabidopsis. *The Plant Cell* **19**, 118-130 (2007). https://doi.org:10.1105/tpc.106.047761
116 Robbins, N. E., 2nd & Dinneny, J. R. Growth is required for perception of water availability to pattern root branches in plants. *Proc Natl Acad Sci* **115**, E822-E831 (2018). https://doi.org:10.1073/pnas.1710709115
117 Ebstrup, E., Ansbøl, J., Chevalier, J., Clemmens, P. & Rodriguez, E. NBR1 -mediated selective autophagy of ARF7 modulates root branching *bioRxiv* (2023). https://doi.org:10.1101/2022.08.19.504407
118 Wang, P. et al. Plant Autophagy: An Intricate Process Controlled by Various Signaling Pathways. *Front Plant Sci* **12**, 754982 (2021). https://doi.org:10.3389/fpls.2021.754982
119 Fiedler, L. & Friml, J. Rapid auxin signaling: Unknowns old and new. Curr Opin *Plant Biol* **75**, 102443 (2023). https://doi.org:10.1016/j.pbi.2023.102443
120 Friml, J. et al. ABP1-TMK auxin perception for global phosphorylation and auxin

canalization. *Nature* **609**, 575-581 (2022). https://doi.org:10.1038/s41586-022-05187-x

121 Ang, A. C. H. & Ostergaard, L. Save your TIRs - more to auxin than meets the eye. *New Phytol* **238**, 971-976 (2023). https://doi.org:10.1111/nph.18783

122 Kuhn, A. et al. RAF-like protein kinases mediate a deeply conserved, rapid auxin response. *Cell* **187**, 130-148 e117 (2024). https://doi.org:10.1016/j.cell.2023.11.021

123 Nelson, C. J. & Millar, A. H. Protein turnover in plant biology. *Nat Plants* **1**, 15017 (2015). https://doi.org:10.1038/nplants.2015.17

124 Lee, J. M., Hammaren, H. M., Savitski, M. M. & Baek, S. H. Control of protein stability by post-translational modifications. *Nat Commun* **14**, 201 (2023). https://doi.org:10.1038/s41467-023-35795-8



Chapter 3

Quantitative analysis of the nuclear auxin signaling pathway in *Marchantia polymorpha*

Authors

Shubhajit Das[1,4], Martijn de Roij[1], Simon Bellows[2], Melissa Dipp Alvarez[1], Sumanth Mutte[1], Wouter Kohlen[3], Etienne Farcot[2], Dolf Weijers[1*], Jan Willem Borst[1*]

Affiliations

[1]Laboratory of Biochemistry, Wageningen University and Research, the Netherlands.

[2]School of Mathematical Sciences, University of Nottingham, United Kingdom.

[3]Laboratory of Molecular Biology, Wageningen University and Research, the Netherlands.

[4]Current address: Institute of Science and Technology, Austria

*Corresponding authors dolf.weijers@wur.nl and jan.willem.borst@wur.nl

This chapter has been published as:

Das, S. *et al.* Quantitative imaging reveals the role of MpARF proteasomal degradation during gemma germination. *Plant Commun*, 101039 (2024).

https://doi.org/10.1016/j.xplc.2024.101039

Abstract

The auxin signaling molecule controls a variety of growth and developmental processes in land plants. Auxin regulates gene expression through a nuclear auxin signaling pathway (NAP) consisting of the ubiquitin ligase auxin receptor TIR1/AFB, its Aux/IAA degradation substrate, and DNA-binding ARF transcription factors. Although extensive qualitative understanding of the pathway and its interactions has been obtained, mostly by studying the flowering plant *Arabidopsis thaliana*, it remains unknown how these translate to quantitative system behavior *in vivo*, a problem that is confounded by the large NAP gene families in most species. Here, we used the minimal NAP of the liverwort *Marchantia polymorpha* to quantitatively map NAP protein accumulation and dynamics in vivo through the use of knock-in fluorescent fusion proteins. Beyond revealing the dynamic native accumulation profile of the entire NAP protein network, we discovered that the two central ARFs, MpARF1 and MpARF2, are proteasomally degraded. This auxin-independent degradation tunes ARF protein stoichiometry to favor gene activation, thereby reprogramming auxin response during the developmental progression. Thus, quantitative analysis of the entire NAP has enabled us to identify ARF degradation and the stoichiometries of activator and repressor ARFs as a potential mechanism for controlling gemma germination.

Introduction

The plant signaling molecule auxin triggers a multitude of growth, developmental, and physiological responses across land plants[1,2]. Key to the cellular response is a canonical Nuclear Auxin signaling Pathway (NAP)[3]. Auxin promotes the binding of AUXIN/INDOLE-3-ACETIC ACID (Aux/IAA) repressor proteins to the nuclear auxin receptor TRANSPORT INHIBITOR RESPONSE1/AUXIN SIGNALING F-BOX (TIR1/AFB)[4]. This triggers degradation of Aux/IAA proteins[5] and releases DNA-binding AUXIN RESPONSE FACTORS (ARFs)[6,7] from inhibition (Fig. 1a). In past decades, the NAP has been studied extensively in the angiosperm *Arabidopsis thaliana*[2]. These studies have led to a comprehensive qualitative model of auxin signaling, supported by atomic structures of each component. A key challenge in understanding auxin response is the large size of gene families representing each component in angiosperms[8]. Specifically, it is hard to tell whether any one protein behaves typically or atypically. More recent analysis of the auxin response system in the bryophytes *Physcomitrium patens* (a moss) and *Marchantia polymorpha* (a liverwort) has helped to reduce system complexity and derive common core principles. Phylogenetic analysis has shown that the simple NAP system in Marchantia consists of one ARF in each of the three subclasses (A-class: MpARF1; B-class: MpARF2; C-class: MpARF3), a single Aux/IAA (MpIAA), and a single TIR1 receptor (MpTIR1), in addition to a non-canonical ARF (MpncARF) and a non-canonical Aux/IAA (MpncIAA)[9]. Studies in *Physcomitrium* and *Marchantia* led to the formulation of a model in which the auxin response revolves around antagonistic interactions between A- and B-class ARFs competing for the same DNA-binding sites. While A-ARFs are regulated by auxin and can switch between repression and activation, B-ARFs are auxin-independent repressors[3,10]. Thus, stoichiometry of the A- and B-class ARFs is predicted to determine the output of auxin response. The C-class ARF in Marchantia acts as an auxin-independent transcriptional repressor[11], and the MpncARF, that lacks the DNA-binding domain, positively influences auxin response[9]. However, the mechanisms of C-class ARF DNA binding and MpncARF-driven auxin response remain to be explored.

Despite our deep understanding of the NAP, one key element remains largely unresolved: essentially all *in vivo* findings are built on qualitative data, and the true *in vivo* concentrations and accumulation patterns of NAP components and their relative concentrations or stoichiometries are unknown. As a consequence, it is unclear whether domains of different auxin activities are generated and, if so, through what mechanisms. Likewise, it is nearly impos-

sible to infer dynamics from genetic or *in vitro* biochemical data, which thus leaves many questions unanswered about the temporal aspects of auxin response. Given that any biochemical interaction is determined by both affinity and concentration of, and among, components, it will be essential to map protein patterns *in vivo*. The ability to tag endogenous proteins through homologous-recombination-based gene targeting in bryophytes enables us to visualize the dynamics of proteins at native concentrations, as a first step toward understanding system behavior.

In this study, we generated and characterized fluorescent genomic knockin lines for all *Marchantia* NAP proteins. In addition to resolving spatial and temporal maps of protein accumulation, this enabled us to identify active proteasomal degradation of both MpARF1 and MpARF2. We show that degradation tunes A-/B-ARF stoichiometry to permit normal development and auxin response. Our study provides a unique resource for the quantitative analysis of auxin response in *Marchantia* and reveals proteasomal degradation as a regulatory mechanism for ARFs.

Results

Development of a collection of genomic knockin lines for the *Marchantia* NAP

Essentially all activities and properties underlying protein function are dependent upon protein concentration. Therefore, a quantitative understanding of any biological process requires the monitoring of endogenous protein accumulation patterns, which can be achieved either by immunolabeling—which suffers from difficulties in reproducible quantification across different proteins—or by endogenous tagging. The latter has so far not been feasible in flowering plants because of the extremely low efficiencies of homology-directed gene targeting, but it is realistic in bryophytes. We set out to generate genomic knockin translational fluorescent fusion lines for all components of the NAP in *Marchantia* (Fig. 1b)[12]. We previously generated knockin lines for both MpARF1 and MpARF2, fused to mScarlet-I[10]. We extended this, and using homologous recombination, we knocked in a fluorescent protein (either mNeonGreen or mScarlet-I) at the C-terminus of each auxin signaling protein: MpARF1 (A-class), MpARF2 (B-class), MpARF3 (C-class), MpIAA, MpTIR1, and MpncARF, thus effectively replacing the single endogenous copy with a fluorescently tagged one.

Where analyzed, overexpression and loss of function of these proteins have been shown to cause strong phenotypes[9,10,13-16]. In contrast, all knockin lines displayed macroscopically normal morphologies and responded to externally applied auxin in a manner qualitatively similar to that of the wild type (Supplementary Information Fig. 1). This suggests that all fusion proteins are functional and that none accumulate at levels significantly outside of the normal range. Next, we used confocal microscopy to visualize all auxin signaling proteins in dormant gemmae residing within the gemma cup, and we compared fusions of all NAP components to the same fluorescent protein (mScarlet-I) under identical experimental conditions. All three ARFs localized to nuclei, but their tissue-wide accumulation patterns showed clear differences (Fig. 1c-e) MpARF1-mScarlet-I showed the highest accumulation among all the NAP components and was present in most cell types of the gemma (see explanation of different cell types in Supplementary Information Fig. 1). MpARF2-mScarlet-I accumulation was much weaker and was absent in the region distal of the apical notch where rhizoid initials reside. MpARF3-mScarlet-I (C-class) displayed a weak yet broad accumulation pattern in all cell types. The auxin receptor MpTIR1-mScarlet-I

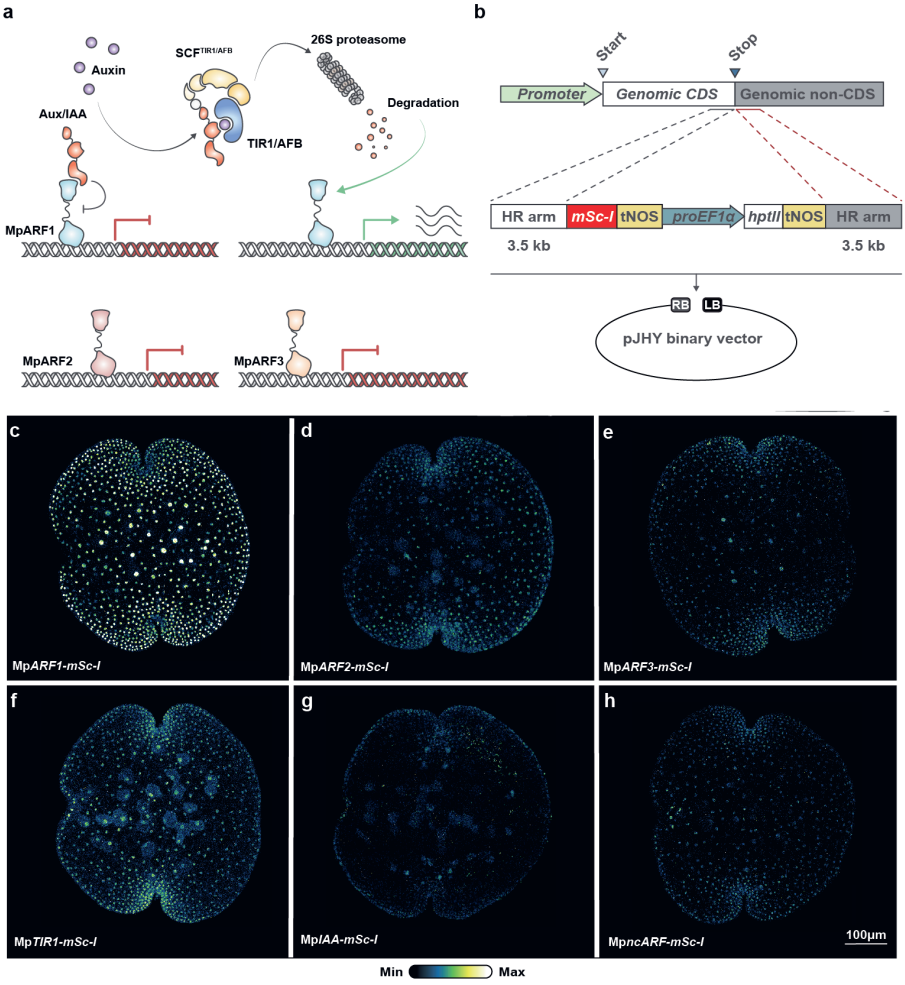


Fig. 1 | Native cellular accumulation patterns of NAP signaling proteins in *Marchantia* gemmae.
a. Schematic diagram of the nuclear auxin signaling pathway in *Marchantia*. In the absence of auxin, Aux/IAA (AUXIN/INDOLE-3-ACETIC ACID) transcriptional inhibitors interact with the A-class MpARF1 (AUXIN RESPONSE FACTOR) to inhibit transcriptional activation. In the presence of auxin, TIR1 (TRANSPORT INHIBITOR RESPONSE 1) interacts with Aux/IAA and targets it for proteasomal degradation, releasing MpARF1 to initiate transcription of auxin-responsive genes. MpARF2 is independent of this regulation, while the regulatory mechanism of MpARF3 is not well characterized. MpARF2 -and 3 act as transcriptional repressors. **b.** Principle of homologous recombination (HR)-mediated genomic knock-in of fluorescent proteins at the C-terminus of a gene of interest. LB, T-DNA left border; RB, T-DNA right border; mSc-1, mScarlet-I; $_{pro}$Mp*EF1α*, ELONGATION FACTOR 1α promoter; tNOS, NOPALINE SYNTHASE terminator; *hptII*, hygromycin phosphotransferase. **c.–h.** Fluorescence patterns reflecting accumulation of core nuclear auxin signaling proteins in dormant gemmae of *Marchantia* knock-in lines expressing mScarlet-I–tagged proteins (mSc-I).

and the non-canonical MpncARF-mScarlet-I showed low, nuclear accumulation, and MpIAA-mScarlet-I was not detected at this stage (Fig. 1f-h). In summary, we established a collection of knockin lines that enabled mapping and quantification of NAP protein accumulation patterns *in vivo*.

Co-receptor-ligand dynamics in the *Marchantia* NAP

We could not detect MpIAA in dormant gemma (Fig. 1g), and therefore we monitored MpIAA accumulation patterns in the first 24 h following gemma germination. The first weak nuclear signals could be detected after 24 h of growth (Fig 2a). It is conceivable that the MpIAA protein is expressed in dormant gemmae but continuously degraded owing to high auxin concentrations. Indeed, treatment of dormant gemmae with the proteasome inhibitor MG132 led to a clear nuclear signal within 2 h (Fig. 2a). By quantifying free IAA concentrations in germinating gemmae, we found a clear decline in the 24 h following germination (Fig. 2b), consistent with IAA-triggered MpIAA degradation at early stages. Pharmacological inhibition of auxin synthesis by combining L-kynurenine and yucasin inhibitors[17,18] led to abundant nuclear MpIAA-mScarlet-I accumulation across gemmae within 2 h (Fig. 2a). These findings suggest that MpTIR1 is active throughout gemma development in mediating IAA-triggered MpIAA degradation. MpTIR1-mScarlet-I was detectable at all stages and showed a gradual increase in protein levels as gemmae grew (Fig. 2c). Thus, as gemmae break dormancy and grow, the auxin response system moves from restrictive to permissive.

The pace of auxin signal relay from TIR1/AFBs to ARFs depends on the degradation rate of Aux/IAA proteins. A quick transcriptional response to auxin, therefore, relies on the rapid degradation of Aux/IAAs[19]. Aux/IAA degradation rates in *Arabidopsis*, where studied, range from 10 min to 1.3 h, and it is unclear what rate reflects the ancestral state within the Aux/IAA family. To determine the *in vivo* MpIAA half-life, we first depleted endogenous auxin with L-kynurenine and Yucasin (Fig. 3a). This led to abundant nuclear accumulation of MpIAA. Gemmae were next treated with 3 µM of the stable, synthetic auxin NAA (1-naphthaleneacetic acid), and MpIAA protein levels were tracked and quantified by time-lapse imaging (Fig. 3b). We detected a clear loss of fluorescence signal and determined the half-life of MpIAA to be 6.5 min (Fig. 3c). To confirm that the signal decline was due to proteasomal degradation, we added MG132 and found that the fluorescence signal remained over the

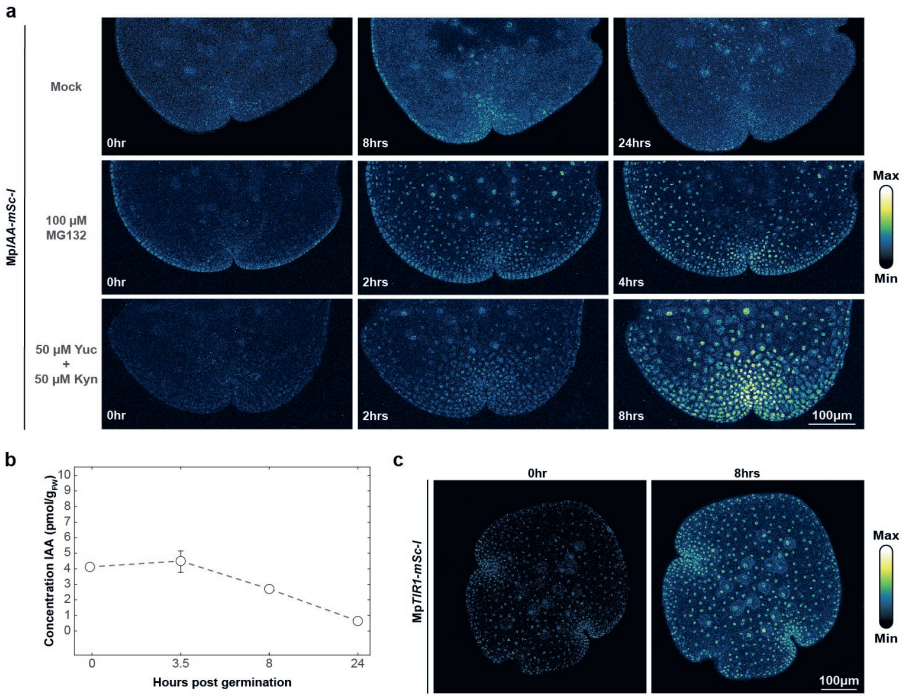


Fig. 2 | Auxin and MpIAA concentrations are dynamic during gemma development.
a. Time-course imaging of Mp*IAA-mSc-I* gemmae treated with Mock, 100 µM of the proteasome inhibitor MG132, or with a combination of the auxin biosynthesis inhibitors 50 µM kynurenine (Kyn) and 50 µM Yucasin (Yuc), as indicated. **b.** LC–MS quantification shows that total IAA levels drop following gemma germination. **c.** Time-course imaging of Mp*TIR1-mSc-I* shows that its accumulation levels gradually increase during gemma germination.

time course (Supplementary Information Fig. 3). Likewise, the signal of MpARF1-mScarlet-I did not decline over the same time with the same imaging settings (Supplementary Information Fig. 4). This demonstrated that the imaging settings used did not induce significant photobleaching. These results suggest that the ancestral condition of the NAP may be characterized by fast Aux/IAA turnover and that the slower degradation rates found in *Arabidopsis* may be a derived property.

Dynamic MpARF protein accumulation

Dynamics in the NAP are ascribed primarily to the degradation of Aux/IAA proteins, whereas TIR1 and ARFs are considered to be more stable factors. Indeed, transcriptional levels of MpARFs were stable following gemma germination (Fig. 4a). To explore the

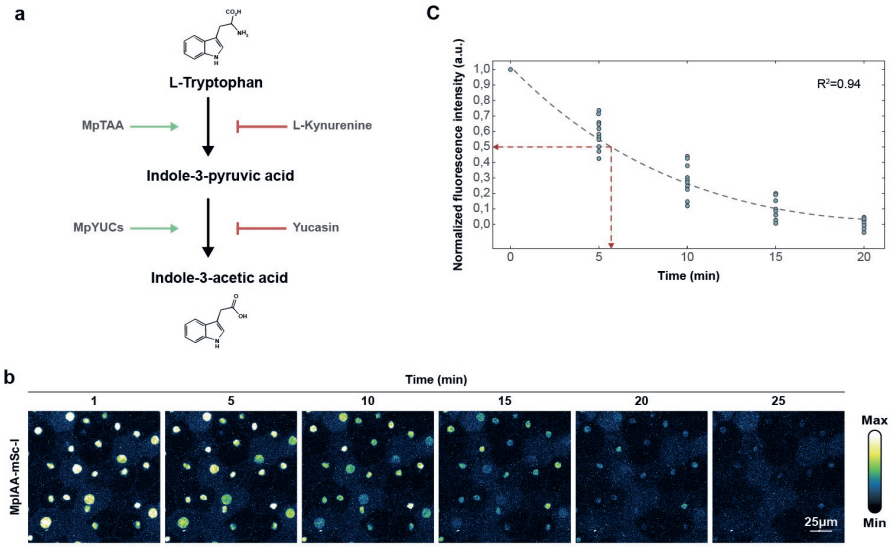


Fig. 3 | Quantification of MpIAA turnover.
a. Auxin biosynthesis via the Indole pyruvic acid pathway is catalyzed by two key enzymes, TRYPTOPHAN AMINOTRANSFERASE OF ARABIDOPSIS (TAA1) and YUCCA (YUC). To lower auxin levels in plant tissues, enzymes can be chemically inhibited by L-Kynurenine and Yucasin, respectively. **b.** Time-lapse confocal imaging on Mp*IAA-mSc-I* gemmae pre-treated with 50 µM L-Kynurenine and 50 µM Yucasin. Upon auxin (3 µM NAA) treatment, fluorescence rapidly decreases due to Mp*IAA-mSc-I* degradation. **c.** Fitting the normalized fluorescence intensity using a one component exponential model results in a predicted MpIAA half-life of 6.5 minutes.

accumulation dynamics of the MpARF proteins, we imaged each ARF during the first 24 h following germination. Remarkably, we found that both MpARF1 and MpARF2 protein levels progressively declined (Fig. 4b,c and Supplementary Information Fig. 5). By contrast, MpARF3 patterns did not change in this time window (Fig. 4d). Given the higher starting levels of MpARF1 in dormant gemmae and the lower MpARF2 concentrations, the former was still detectable after 8 h, whereas the MpARF2 signal declined to undetectable levels (Supplementary Information Fig. 5). Comparable dynamics were found for MpARF1-mNeonGreen and MpARF2-mNeonGreen (Supplementary Information Fig. 5), indicating that signal decline was independent of the fluorescent protein tag.

Given that MpARF transcript levels did not change in the same time window (Fig. 4a), MpARF1 and MpARF2 must be post-transcriptionally controlled by either translational or post-translational regulation. To test the involvement of proteolysis, we treated plants with the proteasome inhibitor MG132 or bortezomib. While MpARF3 was unaffected by the treatments (Fig. 4d,e), the decline of MpARF1

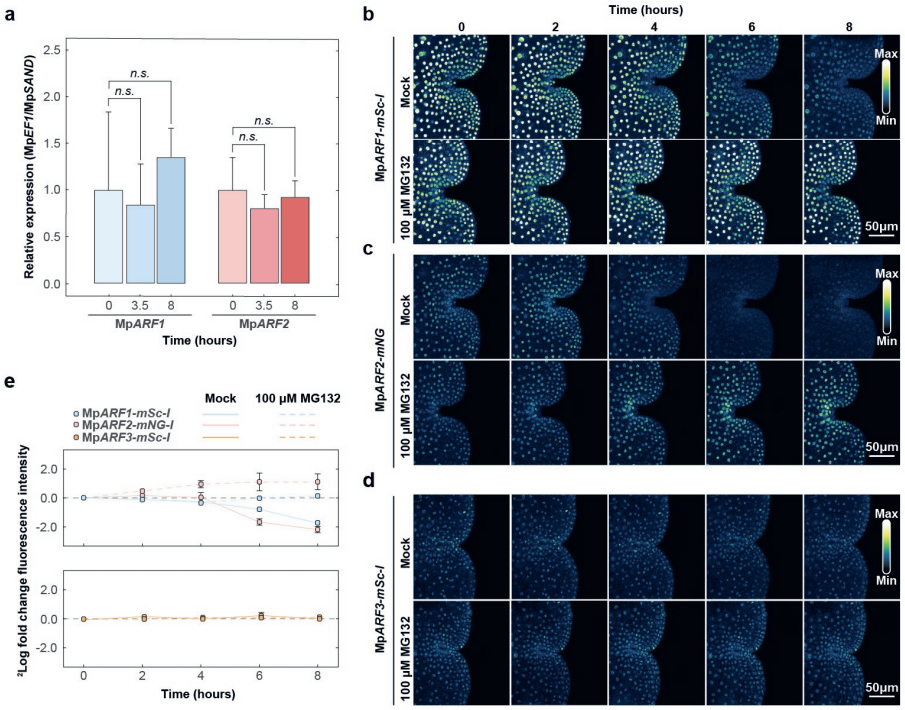


Fig. 4 | MpARF protein accumulation in gemmae is post-translationally regulated by the proteasome.
a. qRT-PCR of Mp*ARF1* -and *2* transcripts shows stable gene transcription levels during gemmae germination. Error bars show the standard deviation. Relative transcription was compared via a student's T-test (P<.05; ns is not significant). **b.-d.** Time-course imaging of MpARF1, MpARF2 and MpARF3 protein fusions to either mNeonGreen (mNG) or mScarlet-I (mSc-I) in germinating gemmae. Plants were either treated with Mock or with 100 µM MG132, as indicated. **e.** Quantification of Mp*ARF1-mSc-I*, Mp*ARF2-mNG* and Mp*ARF3-mSc-I* fluorescence levels relative to their starting values in dormant gemmae.

was prevented by either inhibitor (Fig. 4b,c,e, and Supplementary Information Fig. 6). MpARF2 levels not only stabilized upon treatment with the inhibitors but even increased relative to those of dormant gemmae (Fig. 3b,c,e, and Supplementary Information Fig. 6). This implies that both MpARF1 and MpARF2, but not MpARF3, are proteasomally degraded.

Proteolysis of regulatory proteins, including transcriptional regulators, is often part of feedback control or a point of regulation in signaling pathways. To investigate whether auxin or any other known signaling molecule triggers MpARF degradation during germination, we exogenously treated gemmae for ±16 h with auxin and a range of other plant hormones or inhibitors. Neither auxin nor abscisic

acid, gibberellic acid, or jasmonic acid altered MpARF degradation. Similarly, auxin transport or biosynthesis inhibitors did not affect degradation (Supplementary Information Fig. 7), suggesting that ARF degradation is not controlled by auxin or other tested hormones.

Regulated degradation controls ARF stoichiometry for normal development and auxin response

A key question is what function is served by the regulated degradation of MpARF1 and MpARF2. We previously proposed that auxin responsiveness in *Marchantia* is determined by the stoichiometry of MpARF1 and MpARF2[10]. We therefore explored the possibility that this stoichiometry is actively regulated by proteolysis. Because such stoichiometries may differ among individual cells, it is not possible to derive them by comparing individual knockin lines. To visualize both MpARF1 and MpARF2 quantities in the same tissue and in the same cell, we crossed Mp*ARF1-mScarlet-I* with Mp*ARF2-mNeonGreen* and Mp*ARF1-mNeonGreen* with Mp*ARF2-mScarlet-I* and obtained two double knockin lines. Both double knockins showed ARF accumulation patterns comparable to those of the single MpARF lines (Fig. 4b,c, and Fig. 5a,b). As expected from their individual patterns, MpARF1 and MpARF2 were present in different stoichiometries in different cell types. In nuclei of meristematic apical notch cells, MpARF2 displayed higher accumulation than MpARF1 (Fig. 5a,b,c). In rhizoid initial cells, MpARF2 protein was nearly undetectable, whereas MpARF1 showed clear accumulation (Fig. 5d). In the region separating the apical notch and the rhizoid initial cells, which we refer to here as the transition zone, both MpARFs were present (Fig, 5a,b, and Supplementary Information Fig. 8).

We next determined MpARF1/MpARF2 stoichiometries following gemma germination in an Mp*ARF1-mSc-I* x Mp*ARF2-mNG* double knockin line. For this analysis, we measured relative MpARF1:MpARF2 fluorescence intensities in individual nuclei within four independent gemmae at four time points. Quantification of the MpARF1 and 2 fluorescence intensities in the transition zone showed that the MpARF1:MpARF2 stoichiometry consistently increased during gemmae germination, favoring MpARF1 over MpARF2 (Fig. 5e).

We then asked what the impact of this change in MpARF1:MpARF2 stoichiometry might be, and we first developed a mathematical model of the minimal *Marchantia* NAP and its known interactions

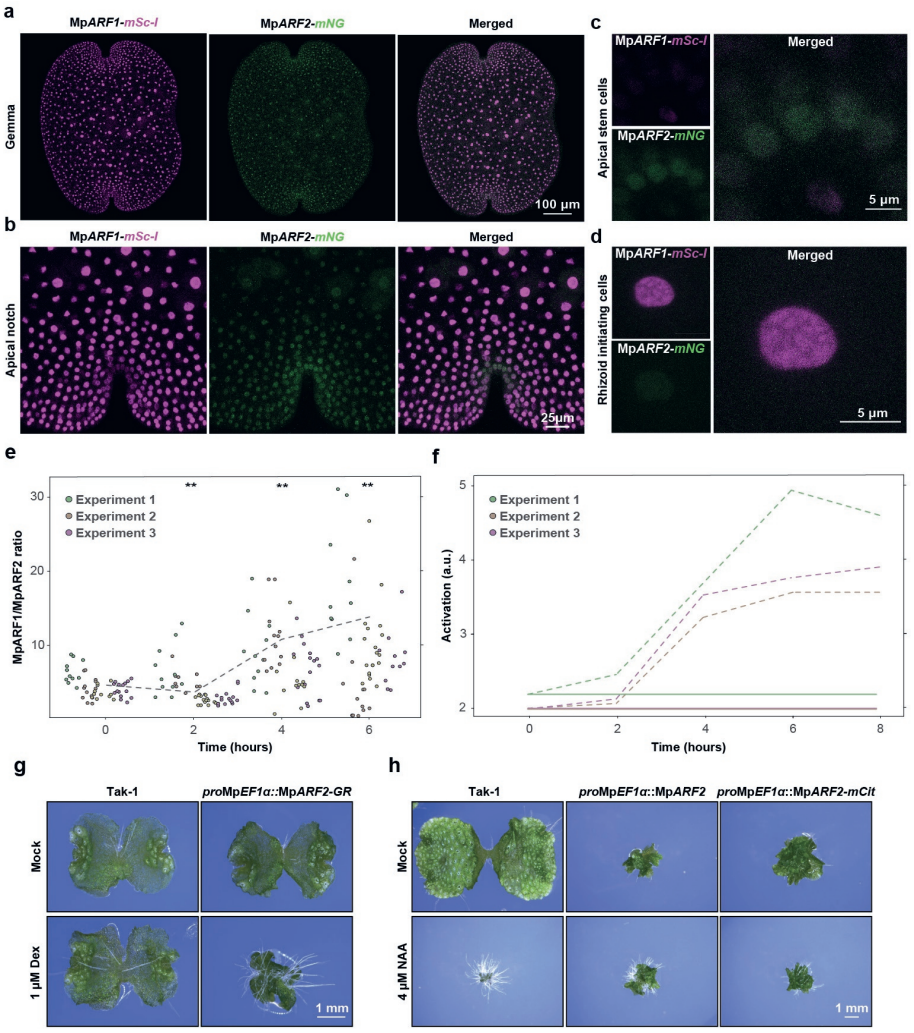


Fig. 5 | Control of growth by regulated MpARF1/MpARF2 stoichiometry.
a. Overview of Mp*ARF1-mSc-I* and Mp*ARF2-mNG* accumulation patterns in dormant gemmae of double knockin lines. **b.-d.** Detail of Mp*ARF1-mSc-I* and Mp*ARF2-mNG* accumulation patterns in the apical notch region, outermost apical notch cells (**c**) and rhizoid initial cells (**d**). **e.** Quantification of MpARF1:MpARF2 stoichiometry in individual nuclei of the double knock-in line (Mp*ARF1-mSc-I* x Mp*ARF2-mNG*) during gemma germination. Colors mark nuclei from different gemmae. ** indicates a statistically significant difference to t=0 h (P<.01) determined by paired student T-test. **f.** Predicted transcription pattern of an auxin inducible gene (a.u. are arbitrary units) during gemma germination. Dashed lines indicate transcription rate in normal condition where MpARFs degrade during gemma germination, as observed, whereas solid lines indicate the putative transcription rate in absence of proteasomal degradation of MpARF2. Lines correspond to predictions modelled in three replicate measurements of MpARF levels. **g.** Phenotypes of wild-type and $_{pro}$Mp*EF1a*::Mp*ARF2-GR* lines treated for 7 days with 1 µM Dexamethasone (Dex) or the Mock control. **h.** Phenotypes of 14-day old wild type (Tak-1) and untagged ($_{pro}$Mp*EF1a*::Mp*ARF2*) or mCitrine-tagged ($_{pro}$Mp*EF1a*::Mp*ARF2-mCit*) constitutive Mp*ARF2* overexpression lines grown on Mock medium or medium containing 4 µM NAA.

(Supplemental File 1). Using a piecewise polynomial function, we fit three independent, experimentally quantified MpARF accumulation profiles into the mathematical model, in which the effect of changing MpARF1 and MpARF2 levels on the outcome of auxin response was modeled as the transcription of a hypothetical ARF-regulated gene. Model simulations predicted that the increased MpARF1:MpARF2 ratio would enhance transcriptional response output (dashed lines, Fig. 5f). Simulated loss of MpARF2 degradation predicted no response output (solid lines, Fig. 5f). Thus, ARF degradation may be required to switch auxin-regulated genes from an inactive to an active transcriptional state by acting on the MpARF1:MpARF2 stoichiometry.

To test the prediction that regulated, low MpARF2 levels are needed for proper auxin sensitivity, we made use of the published Mp*ARF2* inducible overexpression lines[10]. In addition, we generated a new set of stable overexpression lines with and without a C-terminal mCitrine (mCit) fluorescent tag. Induction of MpARF2-GR activity with dexamethasone prevented thallus growth (Fig. 5g)[13,20]. Likewise, 2-week-old stable $_{pro}$Mp*EF1a::*Mp*ARF2* overexpression lines had multiple apical notches, were strongly defective in growth, lacked gemma cups (Supplementary Information Fig. 9), and were completely insensitive to auxin treatment (Fig. 5h and Supplementary Information Fig. 6a,b). The inducible Mp*ARF2-GR* lines had a lower expression of auxin response genes[10]. In addition, in previous reports, overexpression of MpARF1 has been shown to cause auxin hypersensitivity and increased branching rates (see Ref.[10,21]). These results support the prediction that elevated levels of MpARF1 and MpARF2 have opposite effects on auxin sensitivity.

Transcriptional reprogramming in germinating gemmae

The dynamics of NAP components, particularly the shift in ARF stoichiometry following gemma germination, suggest that auxin-regulated genes are dynamically controlled. To test this prediction directly, we performed an RNA-sequencing (RNA-seq) experiment on gemmae collected at 0 h (dormant), 3.5 h, and 8 h of growth. Principal-component analysis (PCA) resulted in a strong clustering of biological replicates and a high variance between different time points (Fig. 6a). This suggests major differences in the transcriptome at different developmental stages and implies massive transcriptional reprogramming early during gemma germination (Fig. 6a). After 3.5 h of gemma growth, we found hundreds of differentially regulated

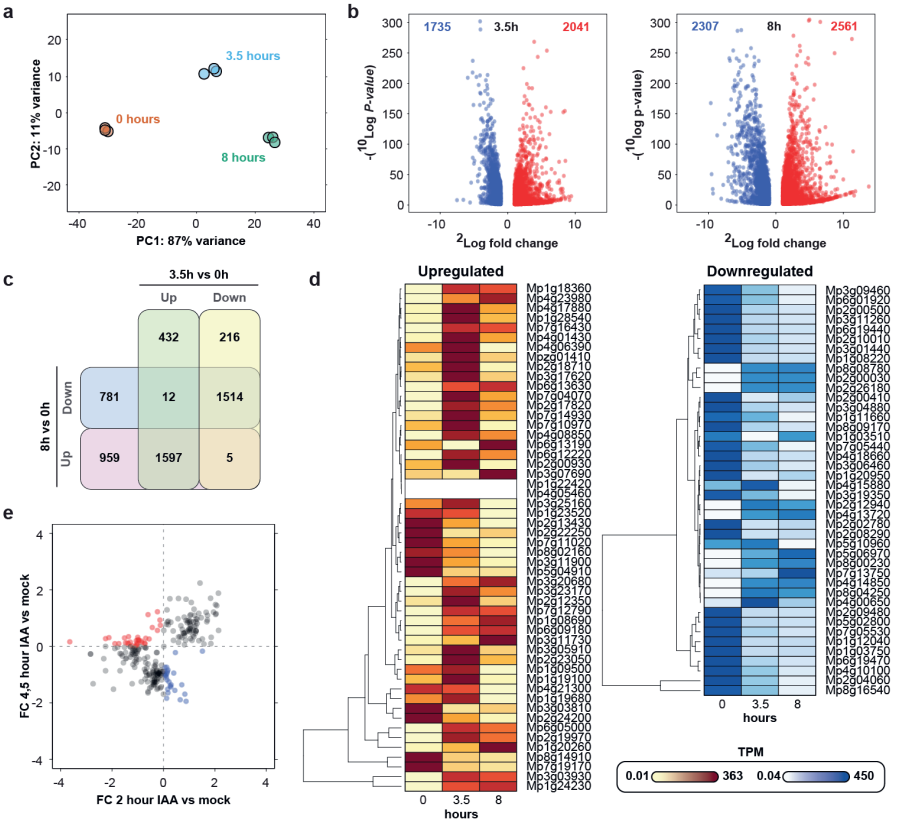


Fig. 6 | Reprogramming of transcriptional auxin response capacity during early gemma development.
a. Principal Component Analysis (PCA) plot of RNA-sequencing transcriptomes of dormant gemmae and gemmae grown in normal ½ strength Garborg's B5 medium for 3.5 and 8 hours, respectively. **b.** Volcano plots show the number of significantly upregulated (red) and downregulated (blue) genes (P_{adj}<.05) at 3,5 and 8 hours, relative to the 0 hour timepoint. **c.** Venn diagram which illustrates the overlap of Differentially Expressed Genes (DEGs) in gemma germinated for 3.5 and 8 hours, when compared to dormant gemmae (0 hours). **d.** Transcriptional dynamics in Transcripts Per Million (TPM) of auxin-responsive genes during gemmae germination. **e.** Plot of ^{2}Log Fold Change (FC) differently regulated genes between 2- and 4.5-hour old gemmae treated with Mock medium or exogenous auxin. Plot shows FC in average TPM counts of all differently regulated genes at the two time points. Commonly regulated genes are marked in black, genes with opposite regulation at 2 and 4.5 hours are indicated in blue and red, respectively.

genes, and this effect was even more pronounced after 8 h (Fig. 6b). There was a large overlap in genes that were either up- or downregulated at 3.5 h and 8 h compared with the 0 h time point (Fig. 6c). However, a substantial fraction of genes was also uniquely regulated at each time point (Fig. 6c). Canonical NAP response proteins showed a limited difference in expression (Supplementary

Information Fig. 10a). We next identified 94 known auxin-regulated genes from available transcriptome data of auxin-treated wildtype plants[9]. and determined their expression levels across the time series. Transcript levels of the majority of auxin-upregulated genes were higher following germination, and likewise, transcript counts of most auxin-downregulated genes were lower in germinated gemmae (Fig. 6d and Supplementary Information Fig. 10b). Thus, as predicted, at a global scale, transcriptional auxin response is elevated upon dormancy release. However, there also seems to be a dampening of auxin-regulated gene expression at 8 h, which suggests that there is additional complexity at this time point that our model does not capture. To directly test the capacity for auxin-regulated gene expression at different times during gemma germination, we harvested gemmae either 1 or 3.5 h after removal from the gemma cup, treated each set separately with 1 µM IAA for 1 h, and then performed RNA-seq analysis. We determined differential expression upon IAA treatment at each time point and plotted the fold change (FC) for each gene at the two time points (Fig. 6e). This analysis showed that among 289 auxin-regulated genes (152 at 1 h and 137 at 3.5 h), 26 showed similar regulation at both time points. Notably, there was no substantial feedback regulation of NAP components, including Mp*IAA* (Supplementary Information Fig. 10c). Of the 26 genes with similar auxin regulation at both time points, a substantial fraction showed a clear difference in amplitude between time points. This result demonstrates that, as time passes after gemma germination, the capacity for auxin-regulated gene expression changes both qualitatively (identity of genes) and quantitatively (amplitude of regulation).

Discussion

We used the simple, minimal auxin response system of *Marchantia* to map protein levels both quantitatively and qualitatively throughout gemma development. To this end, we generated a full set of genomic knockin lines in which fluorescent proteins (two spectrally unique fluorophores) were fused to the C terminus of each auxin signaling protein by homologous recombination. Such an effort would also be possible in *Physcomitrium patens*, given the ease of gene targeting in that species[22], but it would be much more complicated owing to the larger gene families. We do not know of any other plant species that would currently allow such a holistic investigation of the auxin response system. Given their macroscopically normal phenotypes, we believe that these knockins faithfully represent the native spatiotemporal accumulation profile of all nuclear auxin signaling proteins in *Marchantia*.

A noticeable pattern in MpARF spatial expression was the cell-specific difference in ARF quantities. Cell types with either A-class ARF1, B-class ARF2, or both, were observed. Because class A and B ARFs can recognize the same DNA-binding element in *Arabidopsis*, *Physcomitrium*, and *Marchantia*[23,24], the relative concentrations of these two competing MpARFs should determine auxin responsiveness. The contrasting localization maps of MpARF1 and MpARF2 in various cell types satisfy the protein abundance requirements to support an ARF stoichiometry-dependent model of gene regulation (Supplementary Information Fig. 8). The relatively high MpARF1 accumulation observed in rhizoid initial cells points toward an MpARF1-dominated gene activation mode. In the apical cells, we observed the opposite pattern—relatively high MpARF2 abundance, suggesting a gene repression mode. A plausible explanation is that auxin levels are high in stem cells, resulting in the degradation of MpIAA and relieving any auxin-dependent repression. To keep these stem cells transcriptionally silent and possibly to maintain stem cell identity, MpARF2 expression is relatively high. In the transition zone, both MpARF1 and MpARF2 accumulate, suggesting that this region is defined by a competitive ARF-DNA binding mode. MpARF-DNA binding assays and transcriptome analysis at a single-cell resolution would help determine the actual ARF output at cellular resolution.

By following the localization of all NAP components over time, we characterized the dynamics of the MpTIR1 receptor, the MpIAA repressor, and IAA itself, which suggested a progressive transition from a state with high auxin, low receptor, and low MpIAA

to one with low auxin, high receptor, and higher MpIAA. Thus, the capacity for MpIAA-dependent auxin response changes dynamically during development. It could be that the gemma cup itself provides a high-auxin environment, as proposed previously[21], and causes effective Aux/IAA degradation in gemmae. The capacity to respond to auxin depends on both the TIR1–Aux/IAA machinery and the ARF transcription factors[6,7]. As auxin at high concentration is a growth inhibitory signal and is required to keep gemmae dormant inside gemma cups (see Ref.[21]), a reduction in auxin is required to release dormancy and allow gemma growth. As MpARF1:MpARF2 stoichiometry increases post-germination, transcriptional responses are permitted at an auxin concentration that is more favorable for growth. While imaging native MpARF levels, we found a surprising and profound degradation process that changes the ARF landscape during the first hours of gemma germination. Permissive auxin conditions at the early stage are countered by an ARF landscape that is relatively inhibitory. Over time, this ARF landscape shifts to a relatively activating state. The prediction would be that as time progresses, gemmae will become more sensitive to small changes in auxin concentrations, but this prediction remains to be tested.

We observed an elevated auxin response after dormancy release (Fig. 6). By contrast, the quantified endogenous auxin levels were lower after 6 h of growth (Fig. 2d). To explain this contradiction, we must consider the genes that are regulated exclusively by MpARF1 or MpARF2. MpARF1 is an auxin-dependent activator, whereas MpARF2 is an auxin-independent transcriptional repressor. Genes activated by MpARF1 alone are therefore expected to be downregulated when auxin levels are low after germination. Genes repressed by MpARF2 are not expected to change in expression with changes in auxin level, but as the MpARF2 protein is degraded, these genes are expected to be de-repressed. Genes regulated by both MpARF1 and MpARF2 are upregulated as their relative ratio increases, favoring MpARF1 function. In addition, we also observed increased expression of MpTIR1 upon dormancy release, suggesting modulation of the auxin response system at multiple points. Therefore, the transcriptional output is a reflection of not only the auxin level itself but also the relative concentrations of the signaling proteins and their stability at the stage of growth that caused this contradictory response.

We could connect MpARF degradation to an active control of A-/B-ARF stoichiometry. Even in the absence of any treatment, and in static observations, gemmae represent a rich landscape of MpARF1:MpARF2 stoichiometries. From first principles, and support-

ed by mathematical modeling, these sites of varying stoichiometries should translate into areas with different auxin response outputs. Indeed, we see that the cells with the most "activating" stoichiometry are rhizoid initial cells, which are known to be highly sensitive to externally applied auxin[25-27]. Thus, the endogenous MpARF accumulation patterns will likely translate to a corresponding map of auxin sensitivities. Unfortunately, these are hard to map at present owing to the absence of a cellular-resolution reporter for mapping of the auxin response output. Given that stoichiometry manipulation does prevent normal auxin response and development, we do expect that the maps, both in the gemma studied here and beyond, will be an exciting starting point for mapping sites of auxin action.

A key question is how changes in ARF stoichiometry are brought about. In principle, any gene/protein regulatory process can contribute to protein accumulation, and this stoichiometry therefore serves as a central pivot point for the control of auxin output. Although it remains to be seen what transcriptional inputs contribute to diverse MpARF gene expression patterns, we do see that, given unequal starting levels, a relatively generic degradation rate can create large changes in MpARF1:MpARF2 stoichiometry. Identification of components in the degradation mechanism, as well as in (post)transcriptional controls such as the microRNA390–TAS3–ARF pathway[28], will help to resolve the tuning mechanisms.

MpARF1 and MpARF2 are the sole representatives of the A-class and B-class ARFs in *Marchantia*, and both are derived from an inferred algal proto-A-/B-ARF that is likely represented by ARF proteins of streptophyte algae[9]. It is thus plausible that proteolytic degradation is a property inherited from the proto-A-/B-ARF. This raises the question of how widespread this type of regulation is. Several of the 23 *Arabidopsis* ARFs (AtARF1, AtARF6, AtARF7, AtARF17, and AtARF19) have been reported to be proteasomally degraded[29-31]. Neither the degron nor the biological relevance of these degradations is entirely clear, but there is clearly potential for this degradation mechanism to be intimately connected to auxin response.

Methods

Plant growth conditions

M. polymorpha male Takaragaike-1 (Tak-1) and female Takaragaike-2 (Tak-2) plants were used as the wild-type variety. For vegetative propagation, plants were grown on ½ Gamborg B5 media plates in growth chambers with 40 µmol photons m^{-2} s^{-1} continuous white light at 22°C. For sexual reproduction, plants were grown on ½ Gamborg B5 medium supplemented with 1% sucrose and maintained under 40 µmol photons m^{-2} s^{-1} continuous white fluorescent light for 1 month. Plants were then moved into 40 µmol photons m^{-2} s^{-1} continuous white light supplemented with 15 µmol photons m^{-2} s^{-1} far-red light to induce antheridiophore and archegoniophore development. Plants were repeatedly crossed manually to ensure fertilization. Sporangia with mature spores were collected aseptically and used in spore transformation.

Development of genomic knockin translational fusions

Marchantia knockin lines were developed to study native auxin response proteins at endogenous concentrations. A nopaline synthase (NOS) terminator and a fluorescent marker gene (either mScarlet-I or mNeonGreen) were cloned sequentially at the HindIII restriction site of the pJHY-TMp1 binary plasmid to create pJHY-mScarlet-I and pJHY-mNeonGreen vectors. After each cloning step, the HindIII site was regenerated by adding a HindIII site in the forward primer. This enabled subsequent cloning at the 5’ end of the previous insert in the same plasmid. Two 3.5-kb genomic DNA fragments were amplified by PCR and used as homologous arms for recombination. The first genomic DNA fragment contained the 3.5-kb sequence upstream of the stop codon of the gene of interest, and the second fragment was composed of the 3.5-kb sequence downstream of the stop codon. The first fragment was cloned at the HindIII site, and the second fragment was cloned at the AscI site of pJHY-mScarlet-I and pJHY-mNeonGreen. This cloning strategy was used to create homologous recombination constructs for MpARF1, MpARF2, MpARF3, MpTIR1, MpAux/IAA, and MpncARF. Wild-type (Tak-1) spores were transformed by the *Agrobacterium*-mediated transformation protocol described in Ref.[32]. Transformants were selected on ½ Gamborg B5 + 100 mg/L cefotaxime medium with 10 mg/L hygromycin selection. Genomic DNA PCR was used to isolate true knockin lines.

Generation of Mp*ARF2* overexpression lines

To overexpress Mp*ARF2* in *Marchantia*, the Mp*ARF2* coding sequence was amplified and cloned under the Mp*EF1*α promoter. The Mp*ARF2* -CDS was cloned into the published gateway vectors pMpGWB103 and pMpGWB108[33] to generate an unfused and a mCitrine-fluorophore-fused version, respectively. Constructs were transformed in *Marchantia* Tak-1 using *Agrobacterium*-mediated transformation of gemmae. Positive transformants were obtained through hygromycin selection on ½ Gamborg B5 medium plates.

IAA quantification

Total IAA was quantified to estimate the total cellular auxin levels during gemma growth. Gemmae were collected from 4-week-old Tak-1 plants. Tak-1 gemmae were grown on liquid ½ B5 medium, and samples were collected after 0, 3.5, 8, and 24 h of growth. Samples were snap frozen in liquid nitrogen, ground into a fine powder, and weighed. For extraction of IAA, ~150 mg snap-frozen plant material was used per sample. Tissue was ground into a fine powder at −80°C using 3-mm stainless-steel beads at 50 Hz for 2 × 30 s in a TissueLyser LT (Qiagen). Ground samples were extracted with 1 mL cold methanol containing [phenyl $^{13}C_6$]-IAA (0.1 nmol/mL) as an internal standard in a 2 mL Eppendorf tube as described previously[34]. Samples were filtered through a 0.45 µm Minisart SRP4 filter (Sartorius) and measured on the same day. IAA was measured on a Waters Xevo TQ-S tandem quadrupole mass spectrometer.

Auxin sensitivity and physiological analysis of knockins

Knockin lines were tested for their wild-type-like growth, physiology, and auxin sensitivity. Tak-1, Tak-2, and all knockin lines were treated with ½ B5 medium supplemented with either DMSO or 3 µM NAA and grown for 7 days. On the 8th day, plants (n = 10 per genotype) were imaged with a stereomicroscope to compare their physiological responses to auxin (Supplementary Information Fig. 1).

Microscope slide-mount setup for time-course imaging

A microscope slide mount was set up for live imaging of gemmae to precisely track a selected set of cells for temporal protein expression analysis. The mount consisted of a circular aluminium disc with a plastic inset fitted at the center of the disc (Supplemen-

tary Information Fig. 11). Melted ½ B5 medium with or without desired treatments was poured into the cavity of the plastic inset and allowed to solidify. Gemmae were carefully placed on top of the solidified medium and covered with a round coverslip. The bottom of the mount was sealed with parafilm to prevent any evaporation and drying of the medium during time-series imaging. Between two imaging time points in a time-series experiment, the mounts were placed inverted in growth chambers to keep the gemmae exposed to light and allow for normal growth.

Confocal live-cell imaging

All live-cell imaging was performed on a Leica SP8X-SMD confocal microscope equipped with hybrid detectors and a pulsed (40 MHz) white-light laser. mNeonGeen and mScarlet-I were excited with the 506-nm and 561-nm laser lines, respectively. The laser powers were set at 4% output to avoid bleaching of the fluorophores. Fluorescence was detected between 512 and 560 nm (mNeonGreen) and 570 and 620 nm (mScarlet-I) using hybrid detectors in photon counting mode. Z-stack images were acquired using a 20× water immersion objective lens and time-gated detection to suppress chlorophyll autofluorescence. Images were processed using ImageJ software. Maximum-intensity projections of z-stack images were used to quantify total cellular fluorescence in each analyzed nucleus, corrected for background fluorescence. For presentation of the representative images of protein expression patterns, outlines of gemmae were cut in Adobe Photoshop and placed onto a black background. For quantification of images, the background signal was always taken into consideration.

RNA extraction, cDNA synthesis, and qPCR

Total plant RNA was extracted from gemmae collected from gemma cups of 4-week-old Tak-1 and knockin plants and subsequently incubated in liquid ½ B5 medium for 0, 3.5, and 8 hours before freezing in liquid nitrogen. RNA was extracted from ground tissue using the TRIzol reagent and the Qiagen Plant mini-kit. An on-column RNase-free DNase (Qiagen) treatment was performed before final elution. cDNA was synthesized from 1 µg total RNA using the iScript Reverse Transcriptase kit (Bio-Rad). qPCR reactions were carried out using 2× IQ SYBR green (Bio-Rad) on a CFX384 Touch Real-Time PCR detection system (Bio-Rad). Data analysis was performed as described in[35]. The housekeeping genes Mp*E*-

F1a and Mp*SAND* were used for transcript-level normalization.

RNA-seq data analysis

The quality of the raw fastq reads was analyzed in FastQC. Reads were then mapped onto the *M. polymorpha* genome (MpTak1v5.1, accessed through MarpolBase, https://marchantia.info/download/tak1v5.1/) using HISAT2 (v2.2.1)[36] with -dta and -trim5 10 as additional parameters. SAM and BAM files were handled using SAMtools (v1.11)[37]. The raw reads were then counted using FeatureCounts (v2.0.1)[38] with the additional parameters: -t exon; -g gene_id; -Q 30; -p; -primary. The results were imported into R (v3.6.1), and raw count normalization as well as identification of differentially expressed genes (adjusted P_{adj} <.05) were performed using DESeq2[39]. Genes with a total read count of <45 were excluded from the analysis, and genes with an absolute $\log_2$(FC) of >1 and P_{adj}<.05 were deemed differentially expressed. All plots were generated in R (www.r-project.org). Raw RNA-seq reads were deposited in the NCBI Sequence Read Archive under project number PRJNA1019931.

Inducible MpARF2 overexpression

For inducible MpARF2 overexpression, the $_{pro}$Mp*EF1a*::Mp*ARF2-GR* lines were used[10]. Plants (n = 10 per genotype) were treated with either DMSO or 1 µM dexamethasone in B5 medium and imaged after 3 days to look for rhizoid formation as an indicator of gemma germination. Dexamethasone treatment was used to induce the movement of MpARF2-GR from the cytosol to the nucleus.

Mathematical modeling

Provided below is a full description of the auxin signaling model for *Marchantia polymorpha* (Mp), used in the main paper. Note that the prefix Mp is dropped in the following as the model is largely species independent and relies on the general structure of the NAP, with a few *ad hoc* assumptions. Firstly, the model is described, then theoretical properties are discussed before showing numerical simulations. The main underlying assumptions are similar to previous NAP models from literature (see Ref.[40]), with adaptations motivated by the *Marchantia* data presented in this paper. It is known that oligomers involving both ARF and Aux/IAA proteins can form via both a protein-protein domain, DIII-IV (or PB1 since its structure was uncovered)[41] and a DNA binding domain, DBD[23].

Based on this, the model includes populations of proteins and a generic AuxRE-bearing promoter, describing the competition between the different complexes that can be formed from these actors. As the model focuses on the early stages of development, at which Aux/IAA proteins are essentially absent from the system, we do not include Aux/IAA in the models. On the other hand, we consider both ARF1 and ARF2 along with all the complexes they can form, though limiting oligomer sizes to 2. This leads to the possible configurations - and transitions between them – shown in Supplementary Information Fig. 12. The equations are in exact correspondence (using mass action) with the diagram in Supplementary Information Fig. 12.

$$\frac{dA_1}{dt} = -2\alpha_{A_1A_1}A_1A_1 + 2\theta_{D_{A_1A_1}}D_{A_1A_1} - \alpha_{A_1A_2}A_1A_2 + \theta_{A_1A_2}D_{A_1A_2} - \alpha_{GA_1}GA_1$$
$$+\theta_{GA_1}G_{A_1}$$
$$-\alpha_{A_1GA_1}A_1G_{A_1}\theta_{A_1GA_1}G_{A_1A_1} - \alpha_{A_1GA_2}A_1G_{A_2} + \theta_{A_1GA_2}G_{A_1A_2}$$
$$\frac{dA_2}{dt} = -\alpha_{A_1A_2}A_1A_2 + \theta_{A_1A_2}D_{A_1A_2} - 2\alpha_{A_2A_2}A_2A_2 + 2\theta_{A_2A_2}D_{A_2A_2} - \alpha_{A_2GA_1}A_2G_{A_1}$$
$$+\theta_{A_2GA_1}G_{A_1A_2}$$
$$-\alpha_{GA_2}GA_2 + \theta_{GA_2}G_{A_2} - \alpha_{A_2GA_2}G_{A_2}A_2 + \theta_{A_2GA_2}G_{A_2A_2}$$
$$\frac{dD_{A_1A_1}}{dt} = \alpha_{A_1A_1}A_1A_1 - \theta_{D_{A_1A_1}}D_{A_1A_1} - \alpha_{A_1A_1G}D_{A_1A_1}G + \theta_{A_1A_1G}G_{A_1A_1}$$
$$\frac{dD_{A_1A_2}}{dt} = \alpha_{A_1A_2}A_1A_2 - \theta_{A_1A_2}D_{A_1A_2} - \alpha_{A_1A_2G}D_{A_1A_2}G + \theta_{A_1A_2G}G_{A_1A_2}$$
$$\frac{dD_{A_2A_2}}{dt} = \alpha_{A_2A_2}A_2A_2 - \theta_{A_2A_2}D_{A_2A_2} + \theta_{A_2A_2G}G_{A_2A_2} - \alpha_{A_2A_2G}D_{A_2A_2}G$$
$$\frac{dG}{dt} = -\alpha_{GA_1}GA_1 + \theta_{GA_1}G_{A_1} - \alpha_{GA_2}GA_2 + \theta_{GA_2}G_{A_2} - \alpha_{A_1A_1G}D_{A_1A_1}G + \theta_{A_1A_1G}G_{A_1A_1}$$
$$-\alpha_{A_1A_2G}D_{A_1A_2}G + \theta_{A_1A_2G}G_{A_1A_2} - \alpha_{A_2A_2G}D_{A_2A_2}G + \theta_{A_2A_2G}G_{A_2A_2}$$
$$\frac{dG_{A_1}}{dt} = \alpha_{GA_1}GA_1 - \theta_{GA_1}G_{A_1} - \alpha_{A_1GA_1}A_1G_{A_1} + \theta_{A_1GA_1}G_{A_1A_1} - \alpha_{A_2GA_1}A_2G_{A_1}$$
$$+\theta_{A_2GA_1}G_{A_1A_2}$$
$$\frac{dG_{A_2}}{dt} = \alpha_{GA_2}GA_2 - \theta_{GA_2}G_{A_2} - \alpha_{A_1GA_2}A_1G_{A_2} + \theta_{A_1GA_2}G_{A_1A_2} - \alpha_{A_2GA_2}G_{A_2}A_2$$
$$+\theta_{A_2GA_2}G_{A_2A_2}$$
$$\frac{dG_{A_1A_1}}{dt} = \alpha_{A_1GA_1}A_1G_{A_1} - \theta_{A_1GA_1}G_{A_1A_1} + \alpha_{A_1A_1G}D_{A_1A_1}G - \theta_{A_1A_1G}G_{A_1A_1}$$
$$\frac{dG_{A_1A_2}}{dt} = \alpha_{A_2GA_1}A_2G_{A_1} - \theta_{A_2GA_1}G_{A_1A_2} + \alpha_{A_1GA_2}A_1G_{A_2} - \theta_{A_1GA_2}G_{A_1A_2}$$
$$+\alpha_{A_1A_2G}D_{A_1A_2}G - \theta_{A_1A_2G}G_{A_1A_2}$$
$$\frac{dG_{A_2A_2}}{dt} = \alpha_{A_2A_2G}D_{A_2A_2}G - \theta_{A_2A_2G}G_{A_2A_2} + \alpha_{A_2GA_2}G_{A_2}A_2 - \theta_{A_2GA_2}G_{A_2A_2}$$

The notational conventions are as follows:

- A_1 (resp. A_2) denotes the concentration of MpARF1 (resp. MpARF2).
- $D_{XY}, X, Y \in \{A_1, A_2\}$ denotes the concentration of an X:Y dimer, with parameters α, θ for association/dissociation rates as mentioned, and subscripts being hopefully explicit.

- $G, G_{A_1}, G_{A_2}, G_{A_1A_1}, G_{A_1A_2}, G_{A_2A_2}$ denote the proportion, or probabilities, that a generic promoter is free, or bound with one of the possible ARF complexes as denoted in subscript.

To assign values to the constants α_{XY} and θ_{XY}, we use estimates based on literature, in particular Ref.[42]. This paper shows that DBD allows for cooperative binding: dimers are more stably bound to DNA than monomers. To account for this, we use a cooperativity parameter γ, typically ≈ 100. In fact, data from Ref.[42] indicates three orders of magnitude, for equilibrium dissociation constants:

$$K^d_{AA} \approx K^d_{AGA} \ll K^d_{AAG} \ll K^d_{AG}$$

denoting $K^d = \frac{\theta}{\alpha}$ and each occurrence of A being either ARF1 or ARF2. It also appears that the intermediary constant is comparable to the dissociation rate of ARF:ARF dimers. For simplicity, we rely on 4 pairs of association/dissociation constants:

- Kon1/Koff1 define ARF1 homodimerization; their default values are Kon1=1, Koff1 $= 1$.
- Kon2/Koff2 define ARF2 homodimerization; their default values are Kon2=1, Koff2 $= 1$.
- Kon3/Koff3 define ARF1/ARF2 heterodimerization, with defaults Kon3=1, Koff3=1.
- Kon4/Koff4 define ARF/AuxRE binding, supposed to be non-specific amongst ARFs; this defines the smallest order of magnitude above. Accordingly, their default values are Kon4 $= 1$, Koff4 $= 1/\gamma = 0.01$.

All parameters are listed below, following the conventions discussed above:

Parameter	Value	Description
γ	100	Cooperativity coefficient
$\alpha_{A_1A_1}/\theta_{A_1A_1}$	Kon1 / Koff1	Association / dissociation of ARF1 with itself
$\alpha_{A_2A_2}/\theta_{A_2A_2}$	Kon2 / Koff2	Association / dissociation of ARF2 with itself
$\alpha_{A_1A_2}/\theta_{A_1A_2}$	Kon3 / Koff3	Association / dissociation of ARF1 and ARF2
$\alpha_{A_iG} = \alpha_{A_iA_jG} = 2\alpha_{A_iGA_j}$	Kon4	Association of any ARF to a single AuxRE; A_i, A_j denote any of ARF1/ARF2
$\theta_{A_iG} = \gamma\theta_{A_iA_jG} = \gamma^2\theta_{A_iGA_j}$	Koff4	Dissociation of any ARF to a single AuxRE; A_i, A_j denote any of ARF1/ARF2

Model properties

The structure of the model confers some general properties which are true regardless of specific parameters (Supplementary Information Fig. 12). Firstly, since the roles of the two ARFs are perfectly symmetric (whether heterodimers are included or not), one expects an exact balance between ARF1 (resp. ARF1:ARF1) and ARF2 (resp. ARF2:ARF2), unless there are quantitative differences in their binding/unbinding rates. However, even with similar kinetics the balance between Class A and Class B ARFs can be shifted by changes in the amount of available proteins, due to the presence of three conservation relations:

$$
\begin{aligned}
A_1^{\text{tot}} &\doteq A_1 + 2A_{11} + A_{12} + G_{A_1} + 2G_{A_1A_1} + G_{A_1A_2} \\
A_2^{\text{tot}} &= A_2 + A_{12} + 2A_{22} + G_{A_2} + G_{A_1A_2} + 2G_{A_2A_2} \\
G^{\text{tot}} &\doteq G + G_{A_1} + G_{A_2} + G_{A_1A_1} + G_{A_1A_2} + G_{A_2A_2}
\end{aligned}
$$

Intuitively, these mean that the total amounts of each of ARF1, ARF2 and promoters remain unchanged over time. Therefore, they are completely determined by their initial value at time zero. The model describes how this initial amount is reallocated between the different subpopulations represented in Supplementary Information Fig. 12. This has two benefits:

- By systematically using initial conditions with $\left(G, G_{A_1}, G_{A_2}, G_{A_1A_1}, G_{A_1A_2}, G_{A_2A_2}\right) = (1,0,0,0,0,0)$, i.e. a population including only unoccupied promoters, the conservation relation guarantees that $G^{\text{tot}} = 1$ at all times, i.e. that the model describes a probability distribution.
- Since ARFs are conserved we can represent the experimental time series from the main paper as follows: for each experimental time point we use the experimental amounts of ARF1 and ARF2 as initial condition, from which we derive the distribution of all other variables using the model, which will therefore evolve between each time point. This explains why there is no production or degradation of ARFs included in the model equations. The underlying assumption is that the binding events described in the model are much faster than the 2 h period between successive time points. This is justified given the dissociation constants shown e.g. Ref.[42,43] and which are of the order of 1-100 s^{-1}, giving time scales of minutes or shorter.

To describe the 'response' of the system, rather than using arbitrary assumptions to model a transcription rate, we consider the ratio between AuxRE sites occupied by activators and repressors:

$$\text{Response } = \frac{G_{A_1} + G_{A_1A_1} + G_{A_1A_2}}{G + G_{A_2} + G_{A_1A_2} + G_{A_2A_2}}$$

Note that whether A_1A_2 dimers are activators or repressors is unclear, so we include them twice. In fact, there is no clear evidence to date that these heterodimers form at all and in the following we will consider both scenarios with and without their formation.
One notices that the response term shown above is entirely auxin independent, which may seem contradictory. This is a consequence of these two facts:

(1) the above concerns a situation where Aux/IAA proteins have been removed.

(2) the primary effect of auxin on the NAP is to induce the degradation of Aux/IAA, hence suppressing their transcriptional repression as well as their sequestration of ARF proteins. Consequently, in tissues where Aux/IAA have been degraded independently of auxin, it is expected that the effect of auxin itself becomes largely diminished. Including Aux/IAA explicitly in the model would result in a significant increase in complexity, roughly doubling the number of dimers seen in Supplemental Figure S12, and adding many unknown parameters. Given that Aux/IAA is experimentally mostly absent this seems an unnecessary complication.

One may still assess responsiveness to auxin as follows. Even a small amount of Aux/IAA will form dimers with ARF1, which will act as repressors. We denote auxin concentration by x and the population of promoter bound ARF1:Aux/IAA dimers by $G_{A_1 I}(x)$. The repressive effect of dimers means that the transcriptional response should include a new term:

$$R(x) = \frac{G_{A_1} + G_{A_1 A_1} + G_{A_1 A_2}}{G + G_{A_2} + G_{A_1 A_2} + G_{A_2 A_2} + G_{A_1 I}(x)}$$

Since auxin induces Aux/IAA degradation, $G_{A_1 I}(x)$ decreases to 0 as x increases. One simple way to measure sensitivity is then to evaluate the rate of response change with respect to auxin:

$$\frac{dR}{dx}(x) = \frac{-\left(G_{A_1} + G_{A_1 A_1} + G_{A_1 A_2}\right)}{\left(G + G_{A_2} + G_{A_1 A_2} + G_{A_2 A_2} + G_{A_1 I}(x)\right)^2} \cdot \frac{dG_{A_1 I}}{dx}(x)$$

As Aux/IAA is low, it makes sense to consider this rate when $G_{A_1 I}(x) \approx 0$. Also, the term $\frac{dG_{A_1 I}}{dx}(x) < 0$ is indicative of how effective the degradation of Aux/IAA is in response to auxin; with the data available this could only be a speculated figure. Therefore, we have chosen to measure auxin sensitivity as the rate of increase in transcription relative to the rate $\frac{dG_{A_1 I}}{dx}(x)$, in the limit of where $G_{A_1 I} \to 0$. In equation: (Auxin Sensitivity)

$$S = \frac{G_{A_1} + G_{A_1 A_1} + G_{A_1 A_2}}{\left(G + G_{A_2} + G_{A_1 A_2} + G_{A_2 A_2}\right)^2}$$

Numerical simulations (time series)

Time course simulations are run using the well-known ODE solver scipy.integrate.odeint available in Python (v3.9), as well as plotting functions from the matplotlib library. All codes are available and free to use.

As mentioned previously, one uses the five timepoints $\mathrm{t} = 0, 2, 4, 6, 8\ \mathrm{h}$ present in the data. For each, we set an initial condition where ARF1 and ARF2 are directly read from the data, and all other variables are zero except for $G = 1$ (as discussed). We then solve the model using odeint, until nearing equilibrium. The obtained values are used for the corresponding timepoint. Successive timepoints are connected linearly, in absence of information regarding intermediary times. Using this method, the default parameter values lead to the time series shown in Supplementary Information Fig. 13.

As expected, the decrease of ARF monomers over time induces a redistribution of all other variables which results, overall in an increased transcriptional response, relative to a situation where ARF levels are maintained; with the initial ARFs amounts, there is ≈ 2.5 x more activator-bound AuxREs than repressor-bound, and this raises to $\approx 5\mathrm{x}$ as ARFs get degraded. Using the model, different conditions can be simulated to assess their effect on the system's behavior. We include a small number here, but the python script could be used to investigate an endless number or alternative conditions. We restrict to two main aspects:
(1) As mentioned, there is no direct evidence that ARF1:ARF2 dimers form, only the fact that they cannot be ruled out based on protein structure only. We therefore ran simulations where Kon3=0, precluding the formation of heterodimers. Note that with our default assumptions on parameters, the routes $A_1 + A_2 + G \rightarrow G_{A_1} + A_2 \rightarrow G_{A_1A_2}$ are still permitted since their rates are linked to Kon4. For this scenario specifically, we therefore forced Kon4 to 0, but only in terms leading to the formation $G_{A_1A_2}$, still allowing every other AuxRE configurations.
(2) Also mentioned earlier, the symmetry of the reaction network could be broken in favor of ARF1 accumulation if the rates Kon1/Koff1 are distinctly more favorable to dimer formation than the rates Kon2/Koff2. We therefore also considered this scenario, to assess how much this would enhance the response increase seen with default parameters (where all 4 rates are equal).

These alternative conditions are summarized in Supplementary Information Fig. 13. Interestingly, there is little effect on the response resulting from an enhanced ARF1:ARF1 formation. This could be an indication that the repression of ARF seen in the data is a more effective mechanism to generate a transcriptional response. On the other hand, the removal of ARF1:ARF2 heterodimers (highlighted cases in Supplementary Information Fig. 14) systematically leads to an improved response. This is due to the reduced competition between paths of dimer formation. It would be interesting to confirm experimentally whether heterodimers form.

0: Default parameters (identical to Figure 2).	1: no A1:A2 heterodimers	2: Kon1 $= 10$.	3: Koff1 $= 0.1$
4: Kon1=10, Koff1 $= 0.1$.	5: Kon1 $= 10$, no A1:A2 heterodimers	6: Koff1=0.1, no A1:A2 heterodimers	7: Kon1=10, Koff1=0.1, no A1:A2 heterodimers

To conclude, we assessed sensitivity (as defined above) in a similar way to response amplitude. The results, shown in Supplementary Information Fig. 15 are remarkably consistent with those pertaining to response amplitude; quantitative changes in the ARF1 affinities are largely inconsequential, whereas the removal of MpARF1:MpARF2 heterodimer significantly improves sensitivity to auxin.

Funding

This work was supported by the Netherlands Organization for Scientific Research (grant ALWOP.402 and OCENW.M20.031 to J.W.B.) and the Human Frontiers Research Program (grant RGP0015/2022 to D.W.).

Author contributions

Conceptualization, DW, JWB; Investigation, S.D., M.d.R., S.M., M.D.A., W.K; Modelling, E.F., S.B. Writing- original draft S.D., M.d.R, W.K., S.B., E.F., J.W.B., D.W.; Writing-reviewing & editing S.D., J.W.B., D.W. Supervision; J.W.B. and D.W.

Acknowledgements

We are grateful to Iris Nieuwland and Neri van Laar for experimental support.

Supplementary Information

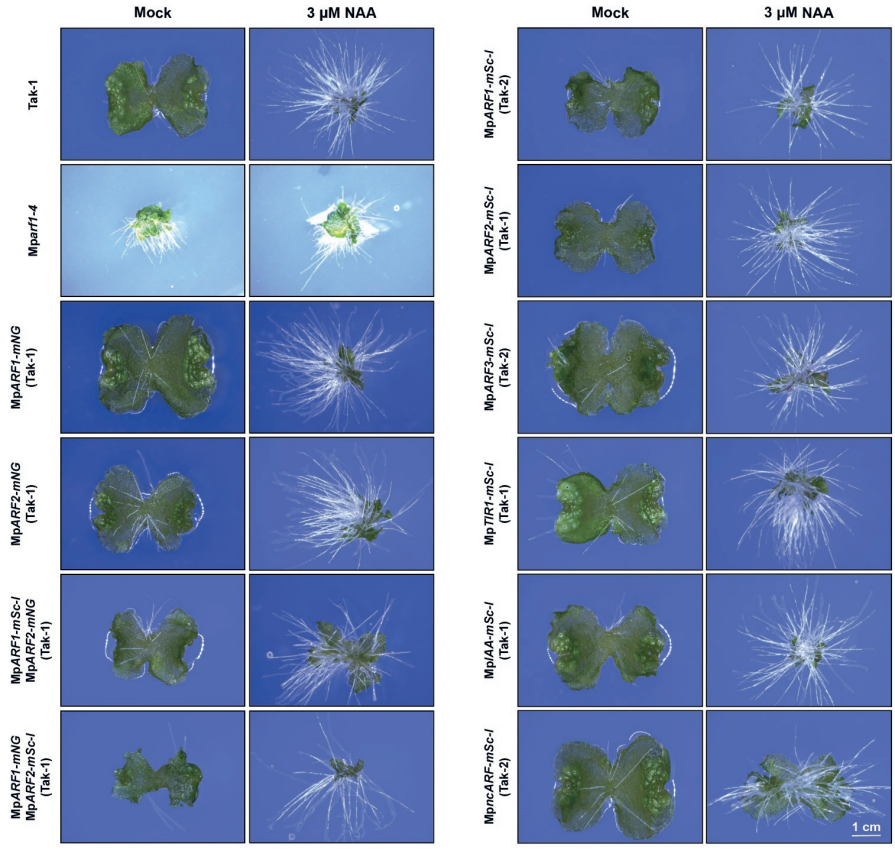


Fig. 1 | Phenotype and auxin response in knock-in lines.
Auxin response assay on all genomic knock-in lines. All knockins were treated with Mock or 3 µM NAA and imaged after 1 week. All knockins show wild type-like auxin response with thallus growth inhibition and ectopic rhizoid formation.

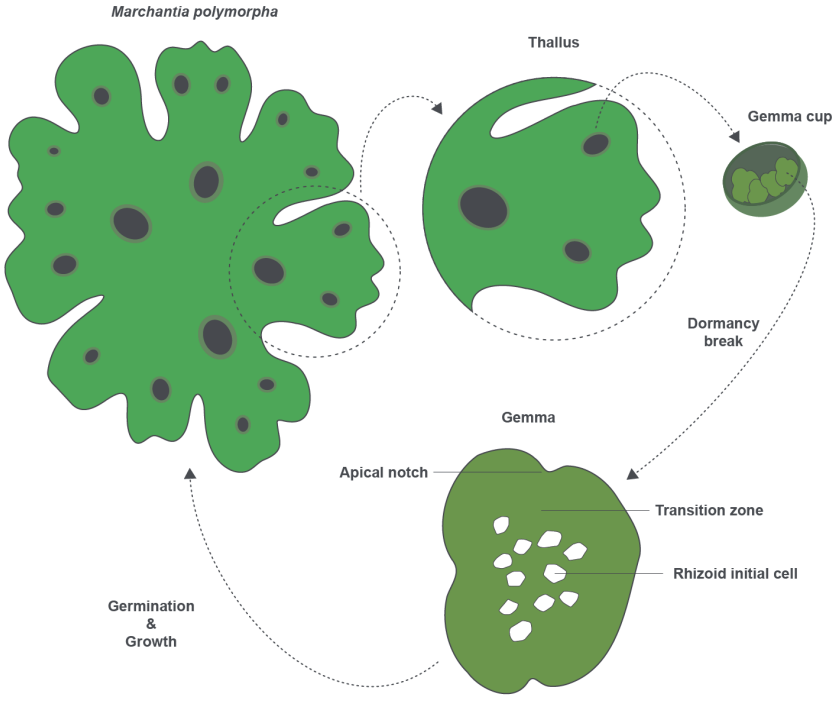


Fig. 2 | Schematic representation of the Marchantia tissues and different cell types within a gemma.

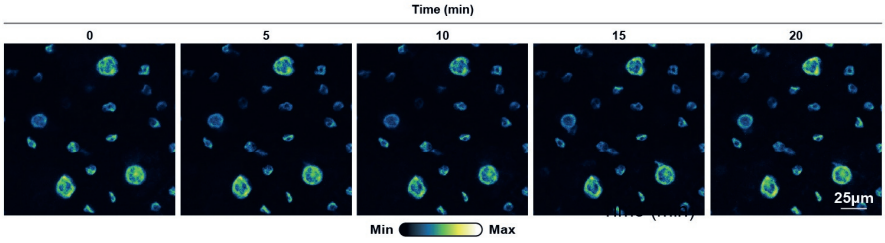


Fig. 3 | Time-lapse imaging on Mp*IAA-mSc-I* gemmae pre-treated with (50 µM) L-Kynurenine and (50 µM) Yucasin.
Upon auxin (1-NAA; 3 µM) treatment, fluorescence rapidly decreases due to MpIAA-mSc-I degradation, whereas the fluorescence remains constant if the sample is mock treated or incubated with the proteasomal inhibitor (100 µM) MG132, shown here.

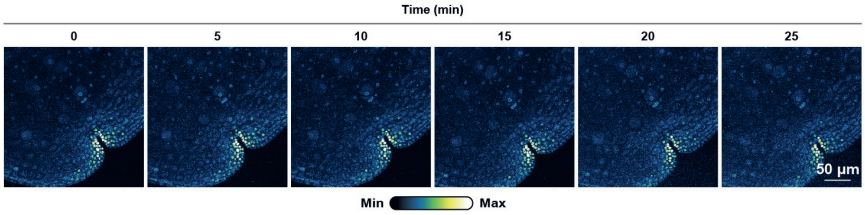


Fig. 4 | Time course of Mp*ARF1-mSc-I*.
Confocal imaging of Mp*ARF1-mSc-I* at the same time points as the Mp*IAA-mSc-I* time course experiment (presented in Main Fig. 3b,c) showing no significant photobleaching of Mp*ARF1-mSc-I*.

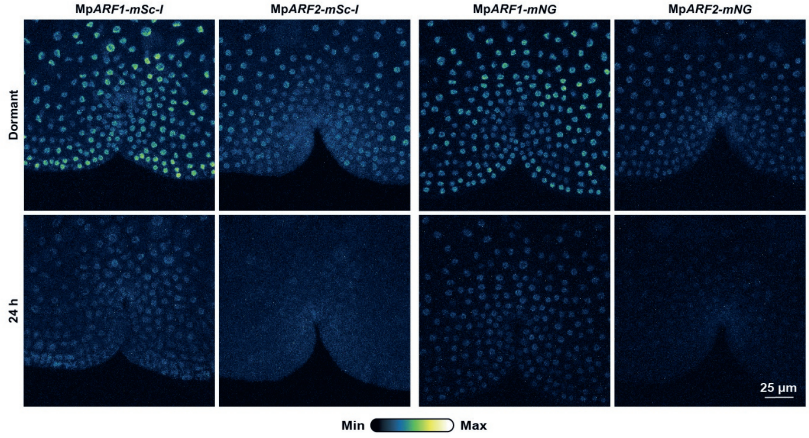


Fig. 5 | MpARF1 and MpARF2 protein accumulation dynamics is independent of the fluorophore tag used.
Time course imaging on MpARF1 and MpARF2 single knock-in lines fused to the mScarlet-I (mSc-I) and mNeonGreen (mNG) fluorescent proteins. Both mNG and mSc-I fusion variants of MpARF1 and MpARF2 show similar fluorescence decline during gemma germination (dormant, top row; 24 h, bottom row).

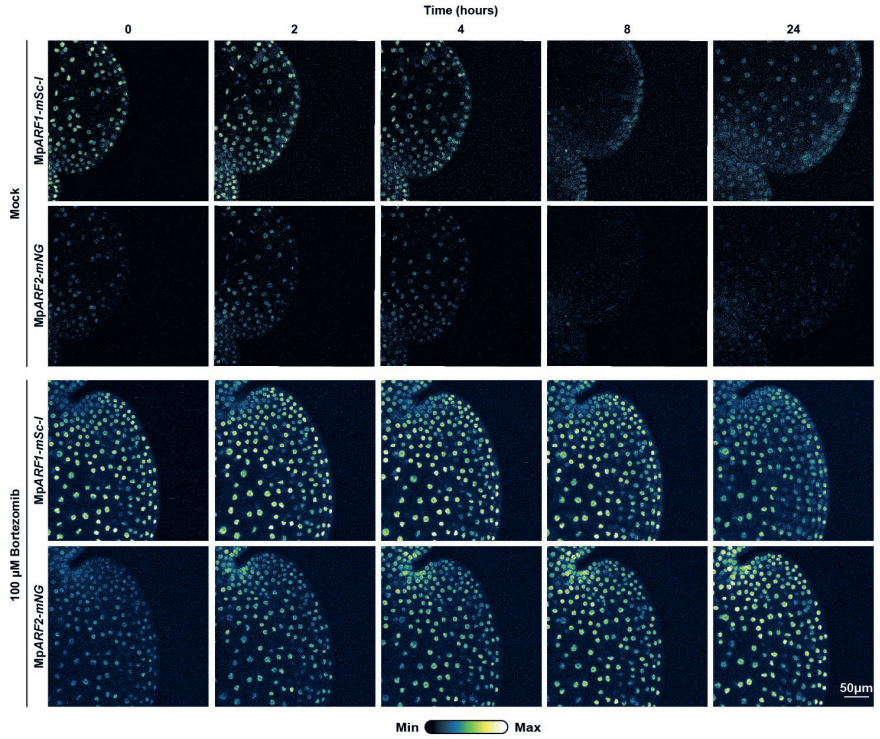


Fig. 6 | Bortezomib prevents MpARF degradation.
Treatment with proteasomal degradation inhibitor Bortezomib also blocks the degradation of MpARF1-mSC-I and MpARF2-mNG.

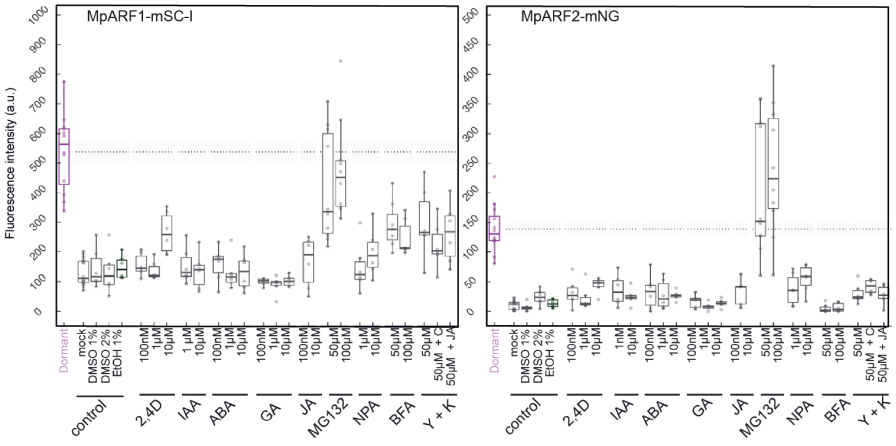


Fig. 7 | Proteasomal degradation of MpARF is independent of auxin and other tested common plant hormones.
Treatment with common plant hormones such as natural (IAA) and synthetic (2,4-D) auxin, abscisic acid (ABA), gibberellic acid (GA), and jasmonic acid (JA), as well as inhibitors of auxin biosynthesis (Yucasin and L-kyneurenine), auxin transport (NPA) and endocytosis (BFA), do not have any effect on MpARF degradation. Only the proteasomal inhibitor (MG132) can block MpARF degradation.

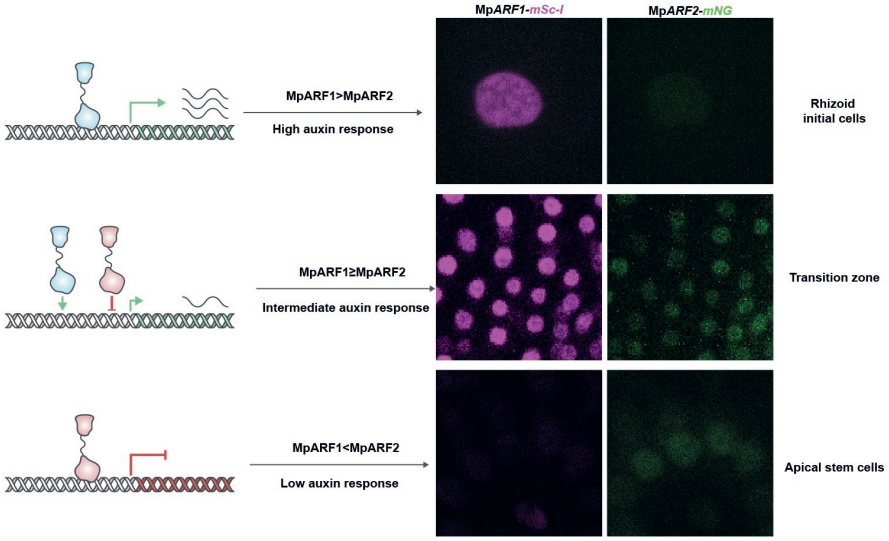


Fig. 8 | Model for how differential MpARF stoichiometry may underpin auxin response output across tissues.
Three possible modes of gene regulation by the relative stoichiometry of class A and class B ARFs, adapted from Kato et. al. 2020[10]. At a relatively higher concentration of MpARF1, DNA binding and gene activation is controlled by MpARF1 in an auxin-dependent manner (top). This mode might be operational in rhizoid initial cells where MpARF2 expression is below detection limit and MpARF1 is abundant. The second mode of gene regulation considers the presence of both A -and B-class MpARFs leading to competition-driven gene regulation (middle) in the transition zone. The third mode describes gene repression by B-class MpARFs, independent of cellular auxin concentrations. Apical meristem cells of gemmae could represent this third mode as these cells have relatively higher MpARF2 levels and no detectable MpARF1 levels.

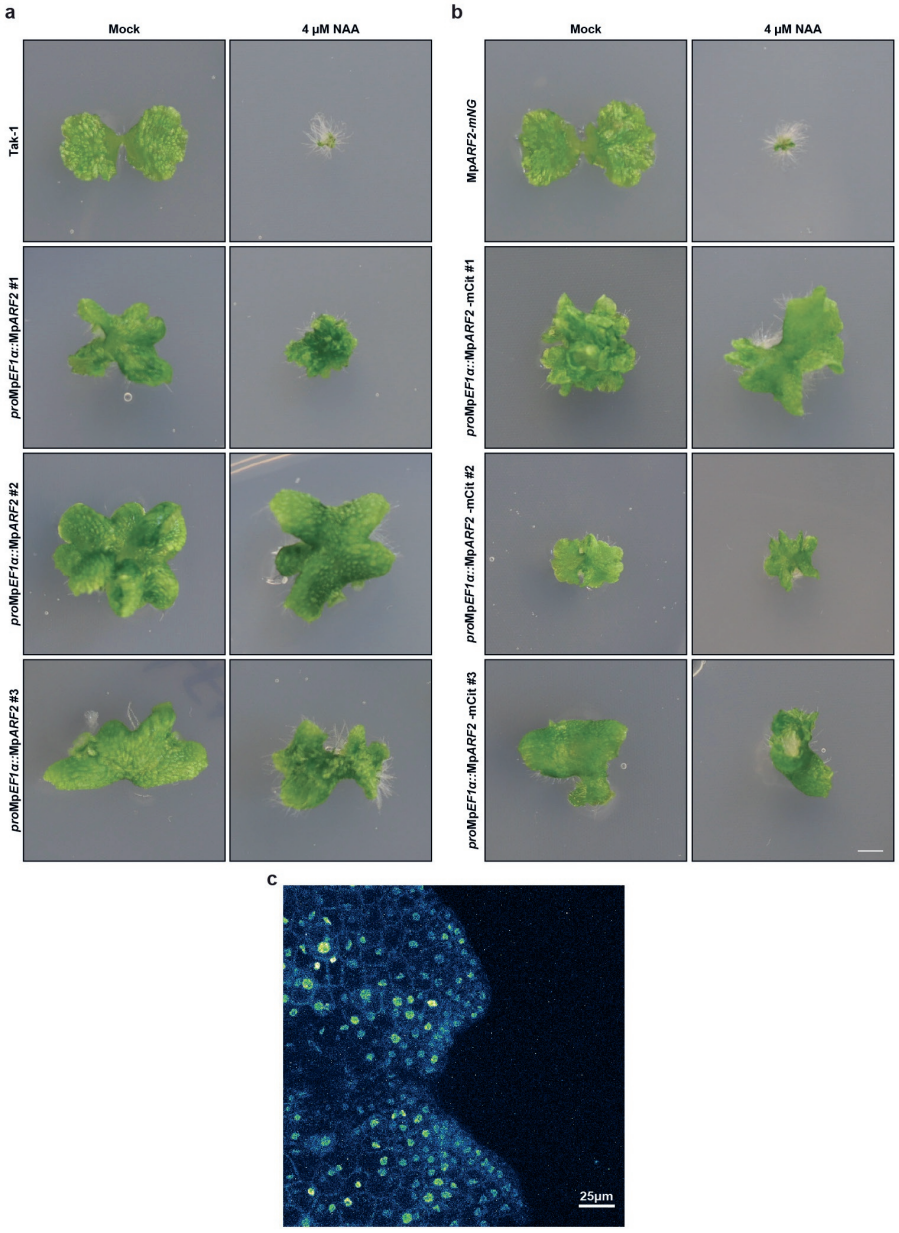


Fig. 9 | Accumulation of MpARF2 leads to an auxin insensitive phenotype. **a.** Growth of three independent $_{pro}$Mp*EF1α*::Mp*ARF2* lines (lines indicated with a hash) on Mock and medium containing 4 µM NAA. Images are of 2-week-old plants. **b.** Growth of three independent $_{pro}$Mp*EF1α*::Mp*ARF2-mCitrine* lines (lines indicated with a hash) on Mock and medium containing 4 µM NAA. Images are of 2-week-old plants. **c.** Expression of MpARF2-mCitrine in $_{pro}$Mp*EF1α*::Mp*ARF2-mCit* #1 assessed through confocal microscopy.

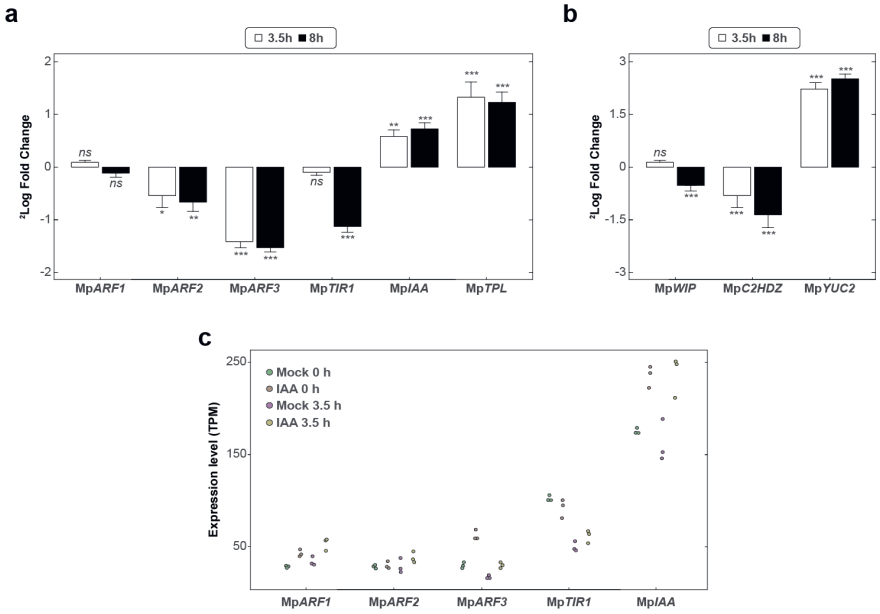


Fig. 10 | Gene expression analysis of auxin response protein encoding genes.
a. & **b.** RNA-seq experiment analyzing gene expression changes (depicted as ^{2}Log Fold Changes relative to dormant gemmae at 0 h). Shown are ^{2}Log FC of auxin response proteins (**a**) and auxin responsive genes (**b**); ns P>*.05*, *P<*.05*, **P<*.01*, ***P<*.001*. **c.** Expression values for Mp*ARF1/2/3*, Mp*TIR1* and Mp*IAA* in Mock -and IAA-treated gemmae at 0 and 3,5 hours after removal from the gemmae cup (Transcripts Per Million, TPM).

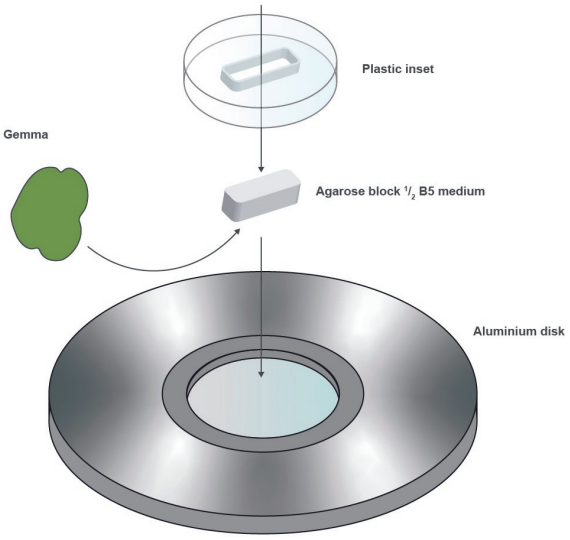


Fig. 11 | Microscope sample mount used to culture and image gemmae.
Basic design of the microscope slide mount, used for time course imaging. B5 media blocks are solidified inside the plastic inset and gemmae are placed on top of the media. The media is supplemented with desired treatment or mock before casting in the inset. A round coverslip is gently placed on top of the gemmae. The plastic inset containing the gemma samples on the media block, is inverted and placed on the aluminium disc and tightened with a screw to prevent movement. Evaporation of water from the media block is prevented by sealing the reverse side of the block with parafilm.

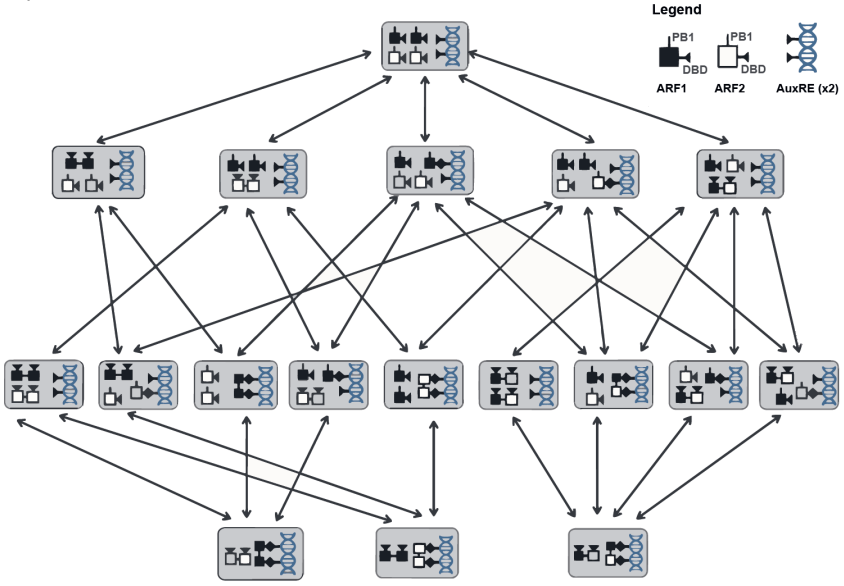


Fig. 12 | Model assumptions and scenarios.
All possible protein/AuxRE complexes included in the model. As one possible scenario, we have ignored all MpARF heterodimers, indicated by the grey box. The equations are in an exact correspondence (using mass action) with the diagram in Supplementary Information Figure 12.

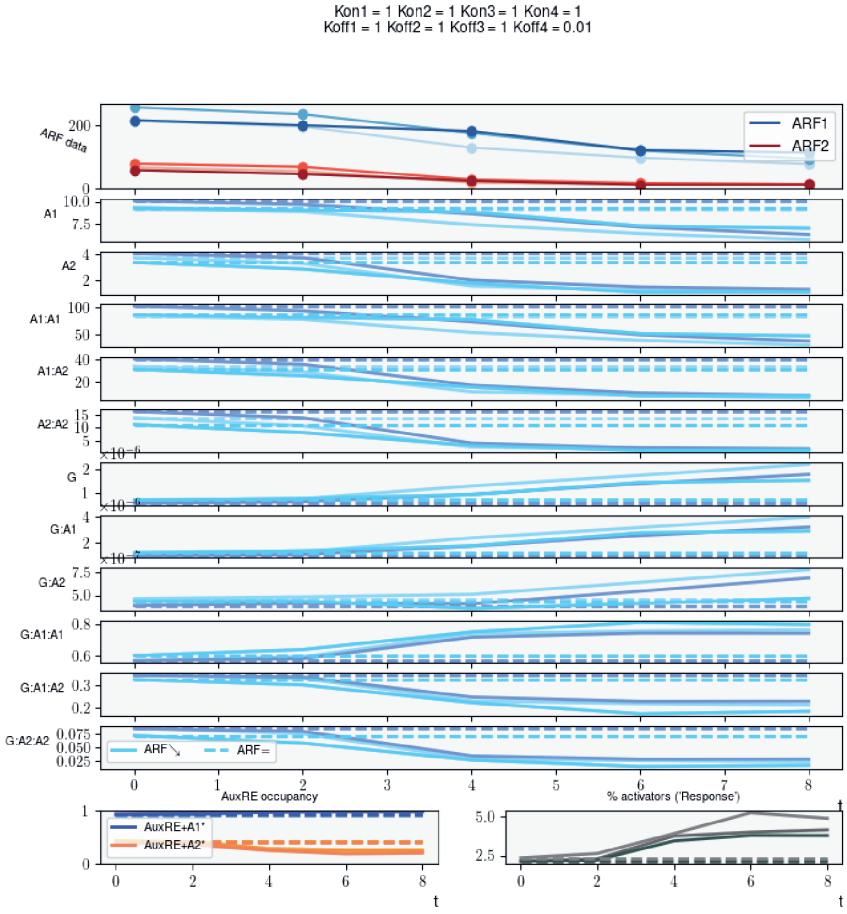


Fig. 13 | Modelling of time-based changes in model parameters.
Time simulation as described in the text, for the default parameter values. Experimental data is included in the first row. For comparison, variables as they would be without any decrease of ARF over time are shown using dashed lines. Shades of similar colors represent the three replicate time series obtained experimentally.

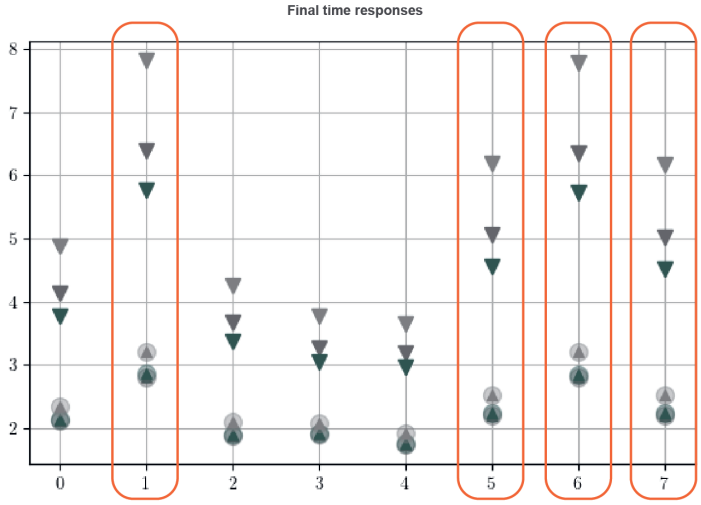


Fig. 14 | Predicted flux in auxin response.
One shade of grey for each of the 3-time courses. The final response value (downwards triangle) compared to its initial value (circle upwards triangle), for a range of conditions along the x -axis, specified as follows (only non-default parameter values are indicated); for x-axis definitions, see the methods section.

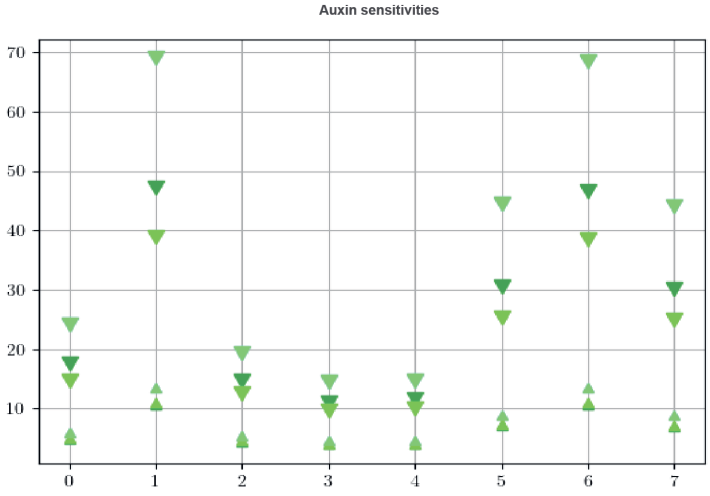


Fig. 15 | Predicted flux in auxin sensitivity.
One shade of green for each of the 3 time courses. The final sensitivity value (downwards triangle) compared to its initial value (upwards triangle), for a range of conditions along the x -axis, identical to Supplementary Figure 14.

References

1 Teale, W. D., Paponov, I. A. & Palme, K. Auxin in action: signalling, transport and the control of plant growth and development. *Nat Rev Mol Cell Biol* **7**, 847–859 (2006). https://doi.org/10.1038/nrm2020

2 Vanneste, S. & Friml, J. Auxin: a trigger for change in plant development. *Cell* **136**, 1005–1016 (2009). https://doi.org/10.1016/j.cell.2009.03.001

3 Lavy, M. & Estelle, M. Mechanisms of auxin signaling. *Development* **143**, 3226–3229 (2016). https://doi.org/10.1242/dev.131870

4 Tan, X. *et al.* Mechanism of auxin perception by the TIR1 ubiquitin ligase. *Nature* **446**, 640–645 (2007). https://doi.org/10.1038/nature05731

5 Gray, W. M., Kepinski, S., Rouse, D., Leyser, O. & Estelle, M. Auxin regulates SCF(TIR1)-dependent degradation of AUX/IAA proteins. *Nature* **414**, 271–276 (2001). https://doi.org/10.1038/35104500

6 Weijers, D. & Wagner, D. Transcriptional Responses to the Auxin Hormone. *Annu Rev Plant Biol* **67**, 539–574 (2016). https://doi.org/10.1146/annurev-arplant-043015-112122

7 Leyser, O. Auxin Signaling. *Plant Physiol* **176**, 465–479 (2018). https://doi.org/10.1104/pp.17.00765

8 Luo, J., Zhou, J. J. & Zhang, J. Z. Aux/IAA Gene Family in Plants: Molecular Structure, Regulation, and Function. *Int J Mol Sci* **19** (2018). https://doi.org/10.3390/ijms19010259

9 Mutte, S. K. *et al.* Origin and evolution of the nuclear auxin response system. *Elife* **7** (2018). https://doi.org/10.7554/eLife.33399

10 Kato, H. *et al.* Design principles of a minimal auxin response system. *Nat Plants* **6**, 473–482 (2020). https://doi.org/10.1038/s41477-020-0662-y

11 Flores-Sandoval, E. *et al.* Class C ARFs evolved before the origin of land plants and antagonize differentiation and developmental transitions in Marchantia polymorpha. *New Phytol* **218**, 1612–1630 (2018). https://doi.org/10.1111/nph.15090

12 Ishizaki, K., Johzuka-Hisatomi, Y., Ishida, S., Iida, S. & Kohchi, T. Homologous recombination-mediated gene targeting in the liverwort Marchantia polymorpha L. *Sci Rep* **3**, 1532 (2013). https://doi.org/10.1038/srep01532

13 Flores-Sandoval, E., Eklund, D. M. & Bowman, J. L. A Simple Auxin Transcriptional Response System Regulates Multiple Morphogenetic Processes in the Liverwort Marchantia polymorpha. *PLoS Genet* **11**, e1005207 (2015). https://doi.org/10.1371/journal.pgen.1005207

14 Kato, H. *et al.* Auxin-Mediated Transcriptional System with a Minimal Set of Components Is Critical for Morphogenesis through the Life Cycle in Marchantia polymorpha. *PLoS Genet* **11**, e1005084 (2015). https://doi.org/10.1371/journal.pgen.1005084

15 Kato, H. *et al.* The Roles of the Sole Activator-Type Auxin Response Factor in Pattern Formation of Marchantia polymorpha. *Plant Cell Physiol* **58**, 1642–1651 (2017). https://doi.org/10.1093/pcp/pcx095

16 Suzuki, H., Kato, H., Iwano, M., Nishihama, R. & Kohchi, T. Auxin signaling is essential for organogenesis but not for cell survival in the liverwort Marchantia polymorpha. *Plant Cell* **35**, 1058–1075 (2023). https://doi.org/10.1093/plcell/koac367

17 Wenrong He *et al.* A Small-Molecule Screen Identifies l-Kynurenine as a Competitive Inhibitor of TAA1/TAR Activity in Ethylene-Directed Auxin Biosynthesis and Root Growth in Arabidopsis *The Plant Cell* **23**, 16 (2011). https://doi.org/

https://doi.org/10.1105/tpc.111.089029
18 Nishimura, T. *et al.* Yucasin is a potent inhibitor of YUCCA, a key enzyme in auxin biosynthesis. *Plant J* **77**, 352–366 (2014). https://doi.org/10.1111/tpj.12399
19 Dreher, K. A., Brown, J., Saw, R. E. & Callis, J. The Arabidopsis Aux/IAA protein family has diversified in degradation and auxin responsiveness. *Plant Cell* **18**, 699–714 (2006). https://doi.org/10.1105/tpc.105.039172
20 Jones , V. A. S. & Dolan, L. The evolution of root hairs and rhizoids. *Ann Bot* **110**, 7 (2012). https://doi.org/https://doi.org/10.1093/aob/mcs136
21 Eklund, D. M. *et al.* Auxin Produced by the Indole-3-Pyruvic Acid Pathway Regulates Development and Gemmae Dormancy in the Liverwort Marchantia polymorpha. *Plant Cell* **27**, 1650–1669 (2015). https://doi.org/10.1105/tpc.15.00065
22 Alison W. Roberts, C. S. D., Michael J. Budziszek Jr., Chessa A. Goss, Virginia Lai Knocking Out the Wall: Protocols for Gene Targeting in Physcomitrella patens. *The Plant Cell Wall*, 17 (2010).
23 Boer, D. R. *et al.* Structural basis for DNA binding specificity by the auxin-dependent ARF transcription factors. *Cell* **156**, 577–589 (2014). https://doi.org/10.1016/j.cell.2013.12.027
24 Freire-Rios, A. *et al.* Architecture of DNA elements mediating ARF transcription factor binding and auxin-responsive gene expression in Arabidopsis. *Proc Natl Acad Sci U S A* **117**, 24557–24566 (2020). https://doi.org/10.1073/pnas.2009554117
25 Sakakibara, K. *et al.* Involvement of auxin and a homeodomain-leucine zipper I gene in rhizoid development of the moss Physcomitrella patens
. *Development* **130**, 11 (2003). https://doi.org/https://doi.org/10.1242/dev.00644
26 Ashton, N. W., Grimsley, N. H. & Cove, D. J. Analysis of gametophytic development in the moss, Physcomitrella patens, using auxin and cytokinin resistant mutants. **114**, 8 (1979). https://doi.org/10.1007/BF00380118
27 Prigge, M. J., Lavy, M., Ashton, N. W. & Estelle, M. Physcomitrella patens auxin-resistant mutants affect conserved elements of an auxin-signaling pathway. *Curr Biol* **20**, 1907–1912 (2010). https://doi.org/10.1016/j.cub.2010.08.050
28 Xia , R., Xu , J. & Meyers, B. C. The Emergence, Evolution, and Diversification of the miR390-TAS3-ARF Pathway in Land Plants *The Plant Cell* **29**, 15 (2017). https://doi.org/https://doi.org/10.1105/tpc.17.00185
29 Salmon, J., Ramos, J. & Callis, J. Degradation of the auxin response factor ARF1. *Plant J* **54**, 118–128 (2008). https://doi.org/10.1111/j.1365-313X.2007.03396.x
30 Lakehal, A. *et al.* A Molecular Framework for the Control of Adventitious Rooting by TIR1/AFB2-Aux/IAA-Dependent Auxin Signaling in Arabidopsis. *Mol Plant* **12**, 1499–1514 (2019). https://doi.org/10.1016/j.molp.2019.09.001
31 Jing, H. *et al.* Regulation of AUXIN RESPONSE FACTOR condensation and nucleo-cytoplasmic partitioning. *Nat Commun* **13**, 4015 (2022). https://doi.org/10.1038/s41467-022-31628-2
32 Kubota, A., Ishizaki, K., Hosaka, M. & Kohchi, T. Efficient Agrobacterium-mediated transformation of the liverwort Marchantia polymorpha using regenerating thalli. *Biosci Biotechnol Biochem* **77**, 167–172 (2013). https://doi.org/10.1271/bbb.120700
33 Ishizaki, K. *et al.* Development of Gateway Binary Vector Series with Four Different Selection Markers for the Liverwort Marchantia polymorpha. *PLoS One* **10**, e0138876 (2015). https://doi.org/10.1371/journal.pone.0138876
34 Ruyter-Spira, C. *et al.* Physiological effects of the synthetic strigolactone analog

GR24 on root system architecture in Arabidopsis: another belowground role for strigolactones? *Plant Physiol* **155**, 721–734 (2011). https://doi.org/10.1104/pp.110.166645

35 Taylor, S. C. *et al.* The Ultimate qPCR Experiment: Producing Publication Quality, Reproducible Data the First Time. *Trends Biotechnol* **37**, 761–774 (2019). https://doi.org/10.1016/j.tibtech.2018.12.002

36 Kim, D., Paggi, J. M., Park, C., Bennett, C. & Salzberg, S. L. Graph-based genome alignment and genotyping with HISAT2 and HISAT-genotype. *Nat Biotechnol* **37**, 907–915 (2019). https://doi.org/10.1038/s41587-019-0201-4

37 Danecek, P. *et al.* Twelve years of SAMtools and BCFtools. *Gigascience* **10** (2021). https://doi.org/10.1093/gigascience/giab008

38 Liao, Y., Smyth, G. K. & Shi, W. featureCounts: an efficient general purpose program for assigning sequence reads to genomic features. *Bioinformatics* **30**, 923–930 (2014). https://doi.org/10.1093/bioinformatics/btt656

39 Love, M. I., Huber, W. & Anders, S. Moderated estimation of fold change and dispersion for RNA-seq data with DESeq2. *Genome Biol* **15**, 550 (2014). https://doi.org/10.1186/s13059-014-0550-8

40 Farcot, E., Lavedrine, C. & Vernoux, T. A modular analysis of the auxin signalling network. *PLoS One* **10**, e0122231 (2015). https://doi.org/10.1371/journal.pone.0122231

41 Nanao, M. H. *et al.* Structural basis for oligomerization of auxin transcriptional regulators. *Nat Commun* **5**, 3617 (2014). https://doi.org/10.1038/ncomms4617

42 Fontana, M. *et al.* Cooperative action of separate interaction domains promotes high-affinity DNA binding of Arabidopsis thaliana ARF transcription factors. *Proc Natl Acad Sci U S A* **120**, e2219916120 (2023). https://doi.org/10.1073/pnas.2219916120

43 Han, X. *et al.* Auxin-callose-mediated plasmodesmal gating is essential for tropic auxin gradient formation and signaling. *Dev Cell* **28**, 132–146 (2014). https://doi.org/10.1016/j.devcel.2013.12.008



Chapter 4

ARF degradation defines a deeply conserved step in auxin response

Authors

Martijn de Roij[1], Jorge Hernández García[1], Shubhajit Das[1,#], Jan Willem Borst[1], Dolf Weijers[1,*]

Affiliations

[1], Laboratory of Biochemistry, Wageningen University, Stippeneng 4, 6708WE Wageningen, the Netherlands

[#] Present address: Institute for Science and Technology Austria, Klosterneuburg, Austria

* Corresponding author: dolf.weijers@wur.nl

This chapter has been published as:

de Roij, M., Hernandez Garcia, J., Das, S., Borst, J. W. & Weijers, D. ARF degradation defines a deeply conserved step in auxin response. *Nature Plants* **11**, 717–724 (2025).

https://doi.org/10.1038/s41477-025-01975-1

Abstract

In land plants, the signaling molecule auxin profoundly controls growth and development, chiefly through a transcriptional response system. Auxin response is mediated by modulating the activity of DNA-binding AUXIN RESPONSE FACTOR (ARF) proteins. The concentrations and stoichiometry of the competing A- and B-class ARFs define cells' capacity for auxin response. In the minimal auxin response system of the liverwort *Marchantia polymorpha*, both A- and B-ARFs are unstable, but the underlying mechanisms, developmental relevance and evolutionary history of this instability are unknown. Here, we identify a minimal motif that is necessary for MpARF2 (B-class) degradation and show that it is critical for development and auxin response. Through comparative analysis and motif swaps among all ARF classes in extant algae and land plants, we infer that emergence of ARF instability most likely occurred in the ancestor of the A -and B-ARF clades and therefore preceded or coincided with the origin of the auxin response system.

Main text

Auxin is a central signaling molecule in plant development[1] and acts chiefly through the activation of Auxin Response Factors (ARFs), a family of DNA-binding transcription factors[2,3]. In land plants, ARFs are phylogenetically divided into three classes (A, B, and C)[4]. A-ARFs are auxin-dependent gene regulators and are antagonized by auxin-independent B-ARFs[5,6]. Based on work in the liverwort *Marchantia polymorpha*, C-ARFs appear detached from auxin response[5]. Given that competition between A- and B-ARFs determines auxin response, their levels and stoichiometry are key parameters defining this response. We recently developed fluorescent knock-in reporters of all auxin response proteins in Marchantia[7], which encodes single copies of each ARF class. We found that both A- (MpARF1) and B-class (MpARF2) ARF proteins are unstable, and that this instability requires the 26S proteasome[7]. Several other ARFs have been reported to be targeted for degradation (reviewed in Ref.[8]), but many questions regarding mechanisms, biological significance, and evolutionary origin of the instability remain.

To address these questions, we first mapped the region in MpARF2 conferring instability. We expressed mNeonGreen (mNG) fluorescently tagged, nuclear-targeted, protein domains from the native Mp*ARF2* promoter (Fig. 1a). While the NLS-mNG control accumulated to high levels, full-length MpARF2 (NLS-FL-mNG) could not be detected (Fig. 1a-b,d) unless the 26S proteasome was inhibited with Bortezomib (Bz; Fig. 1c; Extended Data Fig. 1a-b & 2), as expected. While mNG fusions to the Middle Region (NLS-MR-mNG) or PB1 domains (NLS-PB1-mNG) were stable (Fig. 1a-b,d), the DNA-Binding Domain (NLS-DBD-mNG) alone was sufficient to confer instability (Fig. 1a-b,d); Extended Data Fig. 1c-e). Again, Bz treatment led to protein accumulation (Fig. 1c-d; Extended Data Fig. 1c). Thus, the MpARF2 DBD contains the minimal elements required for instability.

Recently, mutations in the DBD of *Physcomitrium patens* and *Zea mays* (Maize) B-ARFs were shown to inhibit proteasome-dependent degradation. In both cases, mutations map to the same short motif and engineering an equivalent mutation in *Arabidopsis thaliana* AtARF2 also reduced breakdown[9]. It is therefore possible that instability in B-ARFs has a single, common origin in ARF evolution (Fig. 2a). The existence of a single B-ARF in Marchantia enables testing this hypothesis. Indeed, the amino acids required for instability in Physcomitrium and Maize are conserved in MpARF2 (E297, S299, and R300 in MpARF2; Fig. 2b). When mapped onto our ex-

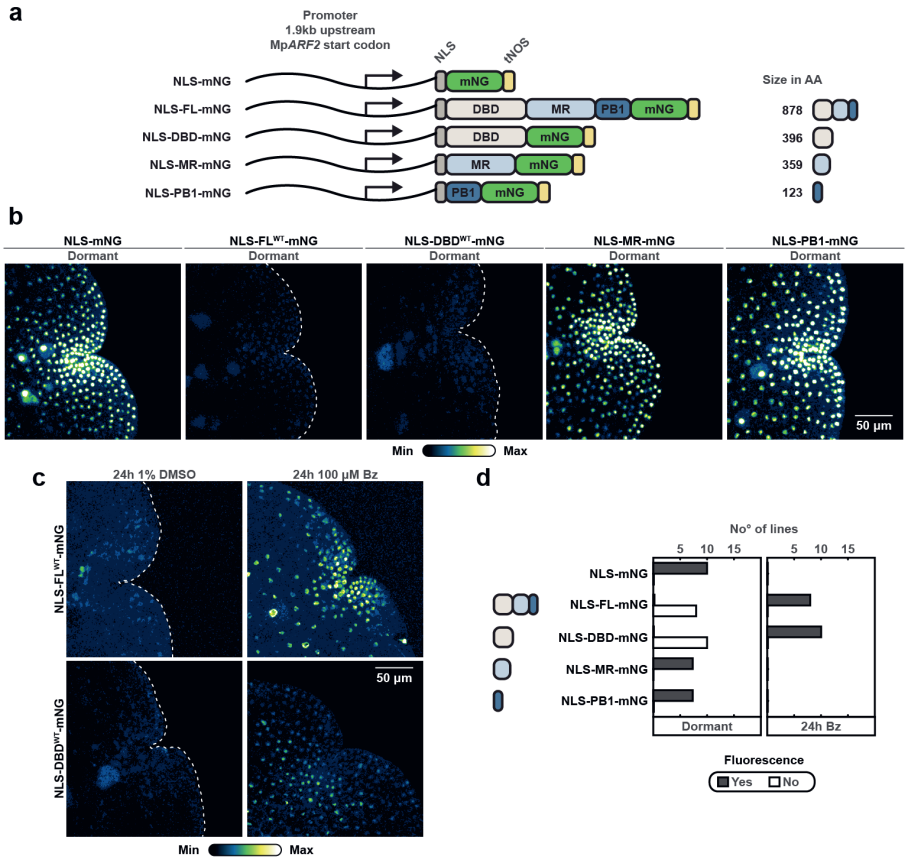


Fig. 1 | The DNA-binding domain confers MpARF2 instability.
a. Schematic overview of translational fusion proteins assessed in subsequent assays. **b.** Confocal images of *M. polymorpha* gemmae, showing expression of fusion proteins outlined in a. **c.** Gemmae were treated with Bz or DMSO and imaged by confocal microscopy, proteins correspond to a. **d.** Quantification of fluorescence patterns shown in b-c in a set of independent transgenic lines. If no fluorescence in dormant gemmea was detected (left panel), plants were treated with Bz and fluorescence was reassessed (right panel)**. c-d** Bz, Bortezomib.

perimentally determined MpARF2 DBD structure[5], we found these to be positioned in an outward facing loop towards the C-terminus of α-helix 6, close to the DBD dimerization interface (Fig. 2b-c). Despite the proximity of the mutations that interfere with degradation in Physcomitrium, Maize, and Arabidopsis B-class ARFs to this interface, Alphafold-based structural models of of the mutations in MpARF2 (Extended Data Fig. 3a-b), suggest that homodimerization may not be affected.

Next we engineered E297K, S299N, and R300Q single mutations, as well as E297K+R300Q (E+R) double mutations in the NLS-DBD-mNG protein and analyzed accumulation and stability (Extend-

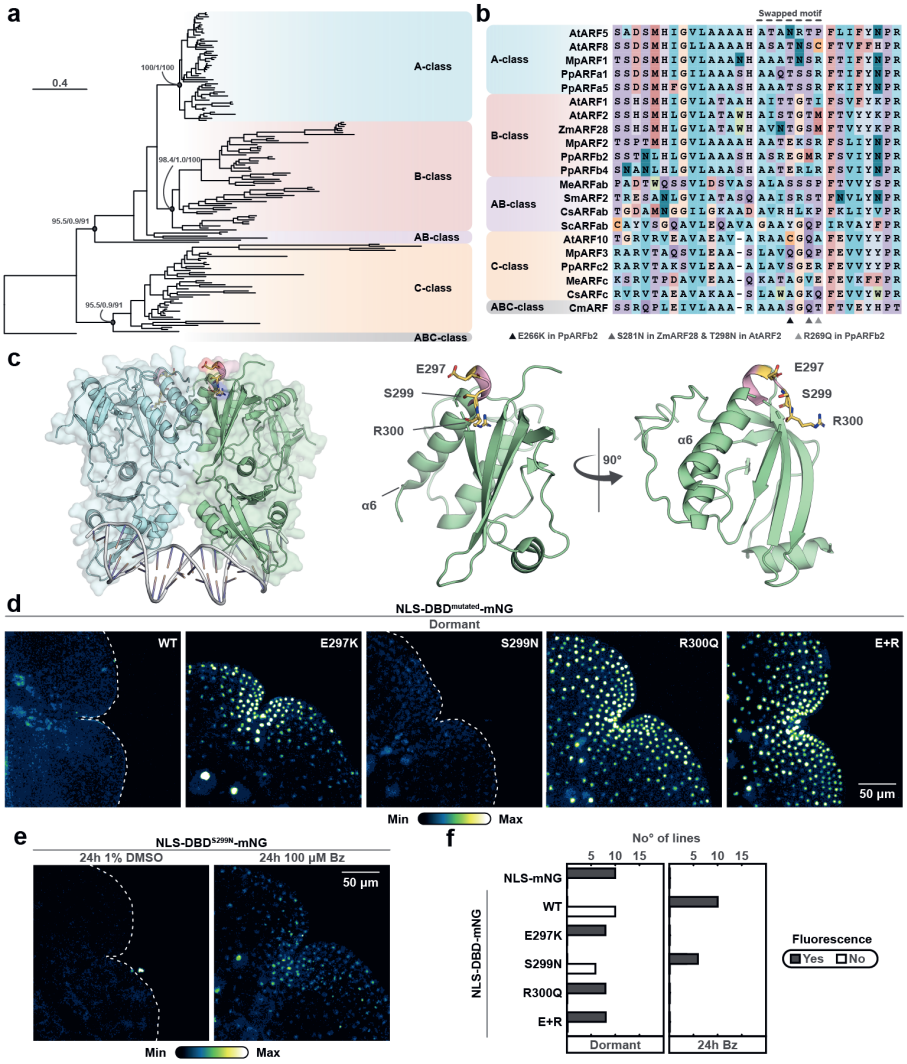


Fig. 2 | Identification of a motif in MpARF2 essential for instability.
a. Phylogenetic relationships between ARFs. Statistical support for major nodes are shown as SH-aLRT branch test/Approximate bayesian test/Ultrafast bootstrap approximation values. **b.** Multiple sequence alignment of ARFs representing the major classes. Putative amino acids responsible for instability (and the swapped motifs) are outlined. **c.** MpARF2 DBD crystal structure with key residues E297, S299, and R300 highlighted and enlarged. **d.** Confocal images of gemmae expressing NLS-DBD-mNG fusions carying outlined mutations. **e.** Gemmae were treated with Bz or DMSO and imaged by confocal microscopy **j.** Similar to Fig. 1d., the same controls were plotted. **e-f** Bz, Bortezomib.

ed Data Fig. 3a). All mutations except S299N led to strong nuclear signal (Fig. 2d-f; Extended Data Fig. 3c-d). In contrast, the S299N mutation did not stabilize the protein (Fig. 2d-f; Extended Data Fig. 3c-d). Thus, B-ARF degradation likely has a single evolutionary ori-

gin, but as discussed in[9], there probably is co-evolution between the ARF and its proteolysis partner.

We deliberately engineered mutations in the DBD, to uncouple degradation and accumulation from potential effects on plant growth and development (Extended Data Fig. 4a-b). It is however unclear what biological relevance MpARF2 degradation has. To address the impact of a lack of MpARF2 degradation on growth, development and auxin response, we engineered the E+R mutation in the full-length fusion protein. As expected, NLS-FL^{E+R}-mNG-bearing gemmae exhibited very high levels of nuclear mNG fluorescence whereas lines expressing NLS-FL^{WT}-mNG did not unless they were treated with Bz (Fig. 1b-c; Fig. 3a). MpARF2-accumulating lines displayed a wide range of strong developmental defects, none of which were observed in NLS-FL^{WT}-mNG lines (Extended Data Fig. 5). Most NLS-FL^{E+R}-mNG lines were dwarfed, showed epinastic growth, ectopic apical notch formation, and failed to produce gemmae (Extended Data Fig. 5 & 6a). Some lines did form gemmae (#7 and #10), even though they mostly did so on the thallus, rather than inside gemmae cups (Extended Data Fig. 6b). However, these lines allowed us to explore effects of MpARF2 accumulation on gemmae development and auxin response. Mature gemmae showed defects in apical (meristematic) notch formation, often showing many more notches than the regular two notches (Fig. 3a; Extended Data Fig. 6c-d). EdU staining of S-phase cells confirmed the existence of supernumerary notches (Fig. 3b). As expected from B-ARF accumulation, NLS-FL^{E+R}-mNG gemmae showed a strong reduction in auxin response (Fig. 3c-d; Extended Data Fig. 6e). Thus, regulation of MpARF2 levels through proteasomal degradation is necessary for normal development and auxin response.

Studies in several species show that equivalent mutations stabilize Marchantia, Physcomitrium, Maize, and Arabidopsis ARFs, but given that these are all studied in separate contexts, it can not be concluded if these reflect the same mechanism. We therefore tested if these motifs are functionally equivalent by swapping the Physcomitrium PpARFb2 and Arabidopsis AtARF2 motifs into MpARF2 DBD. The NLS-DBD$^{PpARFb2\text{-}swap}$-mNG and NLS-DBD$^{AtARF2\text{-}swap}$-mNG proteins were unstable, yet accumulated when treated with Bz (Fig. 4a-c; Extended Data Fig. 7). Thus, the degradation mechanism is likely homologous between species.

Given that in Marchantia, both A- and B-ARFs are unstable[7], and having identified the minimal region that is both necessary and sufficient for MpARF2 degradation, we next asked if mechanisms

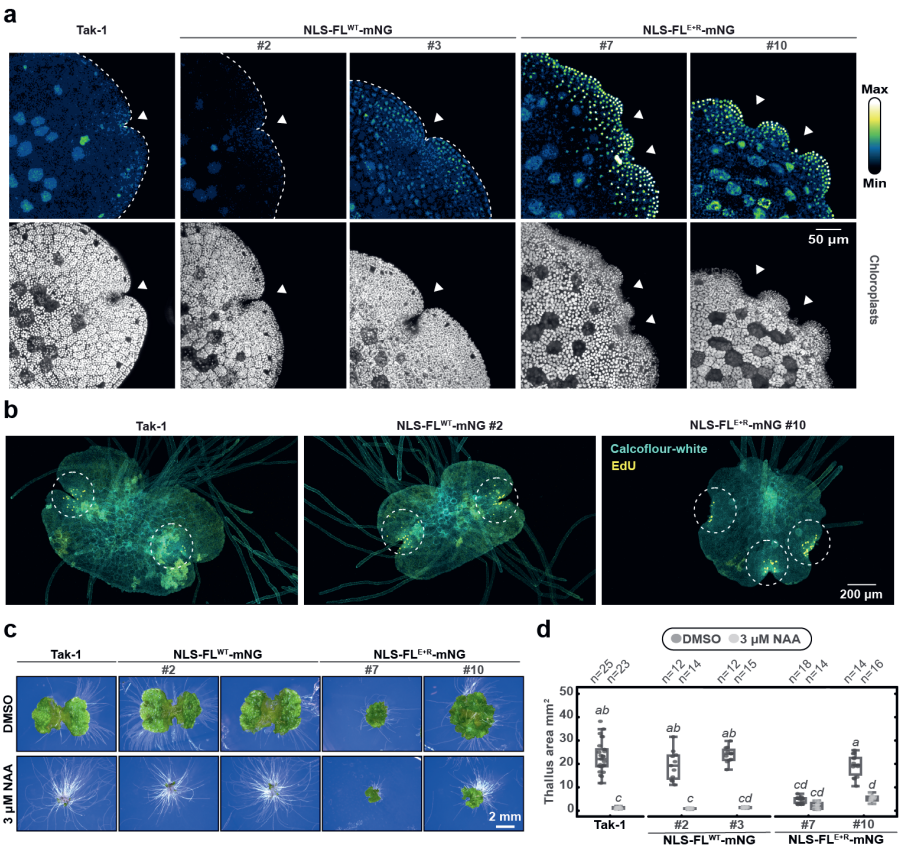


Fig. 3 | Biological significance of MpARF2 degradation.
a. Confocal images of Tak-1 wildtype -and transgenic gemmae expressing NLS-FL^{WT}-mNG or NLS-FL^{E+R}-mNG constructs. Chloroplast autofluorescence outlines gemmae morphology. Hashed numbers are independent transgenic lines. b. Confocal images of EdU staining in 3-day old gemmalings of S-phase nuclei (yellow), cell walls were stained with calcofluor-white (turquoise). c. Qualitative comparison of auxin response in gemmalings grown for 10 days on medium containing 3 µM NAA or DMSO, respectively. d. Quantification of projected thallus area of gemmalings shown in c. compared per one-way ANOVA (F=(9, 152)=122.6, $p\approx 2e^{-16}$) with Tukey post-hoc test with Benjamin-Hochberg correction (italics denote significant differences, p<.05). Boxplots show the following statistical parameters: central line, median; upper bound, first quartile; lower bound, third quartile; whiskers show the highest and lowest values, respectively, within 1.5*inter-quartile range (IQR). Statistical groups are determined by Tukey's Post-Hoc test (p < .05) following one-way ANOVA. Individual gemmae were selected randomly and grown as independent biological replicates, the sample size is. Raw data and exact p-values are provided as a Source Dataset.

of instability are universal among A- and B-ARFs. There is some conservation between MpARF1 and MpARF2 in the region required for MpARF2 (and Physcomitrium, Maize and Arabidopsis) instability (Fig. 2b). We tested if the equivalent region from MpARF1 could render MpARF2 unstable, i.e. we swapped this short motif into the

MpARF2 NLS-DBD-mNG (Fig. 2b). As a control, we included the equivalent region from the C-class MpARF3 which is stable in its native context[7]. While the NLS-DBD$^{MpARF3\text{-}swap}$-mNG protein accumulated to high levels even in the absence of Bz, we could hardly detect NLS-DBD$^{MpARF1\text{-}swap}$-mNG protein (Fig. 4a-c; Extended Data Fig. 7). When treated with Bz however, this protein accumulated to high levels (Fig. 4b-c; Extended Data Fig. 7). Thus, homologous motifs in MpARF1 and MpARF2 confer comparable protein instability. A- and B-ARFs derive from duplication in an ancestral AB-ARF gene, which in turn originates from a split of an ancestral ABC-ARF thereby forming the AB -and C-ARF clades[4,10], and neofunctionalized following this duplication (Fig. 2a)[10].

The finding that the same region in MpARF1 and MpARF2 can confer instability suggests that this feature has a single origin that predates the divergence of A- and B-ARFs. While the nature of the ancestral ABC and AB ARFs is not clear, extant representatives of these proteins are found in the sister lineages to land plants, the streptophyte algae[4]. We selected representative AB-ARFs of algae belonging to the Zygnematophyceae group, the lineage most closely related to land plants[11] (*Mesotaenium endlicherianum* MeARFab; *Spirogloea muscicola* SmARF2), as well as from Coleochaetophyceae (*Coleochaete scutata* CsARFab) and Klebsormidiophyceae (*Streptosarcina costaricana* ScARFab) clades. We also included a member of the Chlorokybophyceae (*Chlorokybus melkonianii* CmARF) representing the ABC-ARF clade[11]. We swapped the homologous motifs from these ARFs (Fig. 2b) into NLS-DBD-mNG. All of these swapped fusions were highly stable, mimicking behaviour of fusion proteins with mutated degron residues (Fig. 4a,c; Extended Data Fig. 7). This result is consistent with two interpretations: one would be that the ancestral state of either all ARFs or AB-ARFs included protein instability conferred by this motif, followed by subsequent loss in the lineages giving rise to the tested algal ARFs, which is unlikely. Alternatively, the ancestral ARF state was stable, and instability evolved in the lineage giving rise to land plants prior to A/B divergence (Fig. 4d). The very long evolutionary divergence times in this group of algae (>600 Mya[12]), and sparse species sampling makes such inferences problematic.

Our work identifies a minimal region for ARF degradation in Marchantia and shows that a key element required for instability is conserved among B-ARFs, even in Marchantia which has only a single copy. We show that MpARF2 instability is critical for normal development and auxin response. Our analysis of MpARF1 reveals that

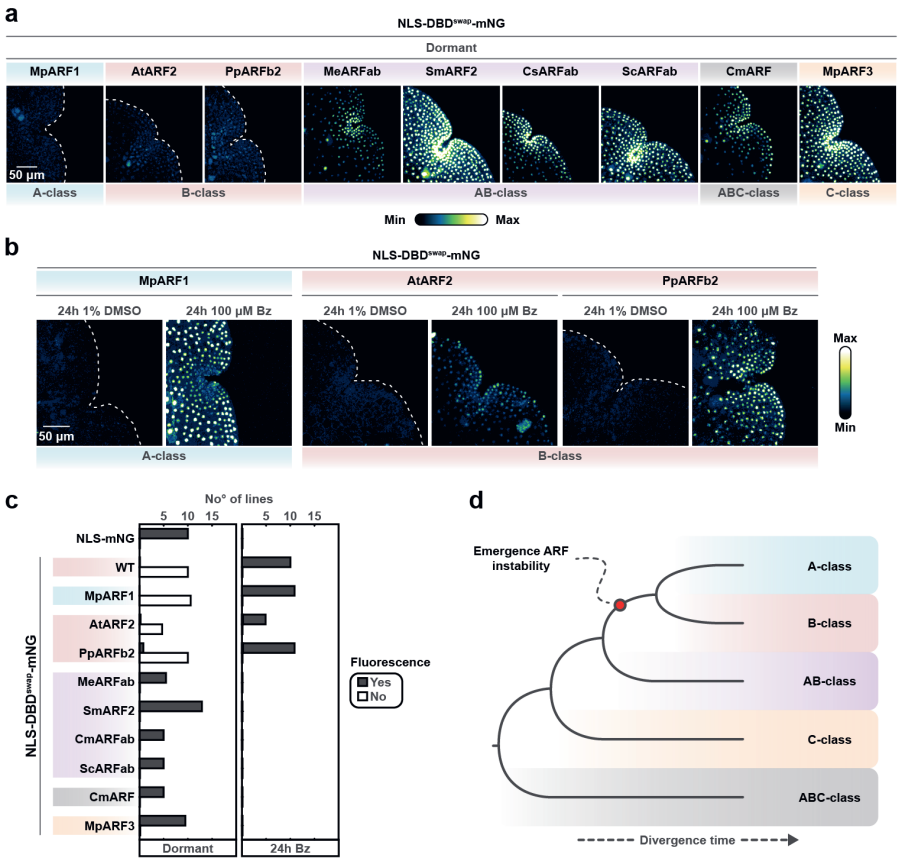


Fig. 4 | The evolutionary origin of ARF instability.
a. Fluorescence accumulation (assessed by confocal microscopy) of swaps of homologous motifs of different ARFs (representing major ARF classes) into NLS-DBD-mNG. **b.** Lines which showed no detectable fluorescence in dormant gemmae in a. were treated for 24h with Bz or DMSO and fluorescence accumulation was reassessed. **c.** Similar to Fig. 1d., the same controls were plotted. **d.** Schematic cladogram illustrating the hypothesized evolutionary relationship between known ARF clades and the emergence of the instability-conferring motif. **b-c** Bz, Bortezomib.

the capacity to mediate instability is very likely an ancestral property of the protein that predated the split between A- and B-ARFs.

While the minimal motif from MpARF1 can destabilize MpARF2 when transplanted, an interesting question is whether the same minimal region is also required for the degradation of MpARF1 under natural conditions. MpARF1 is unstable, and proteasome inhibition prevents decline of protein levels. This, however, differs from MpARF2, where proteasome inhibition not only prevents degradation but actually leads to protein hyperaccumulation[7]. While this may reflect different feedback controls triggered by either MpARF1

or MpARF2 accumulation, it may also reflect that mechanisms of degradation are not identical for the two proteins. Further analysis of sequence requirements for MpARF1 degradation should resolve this.

The minimal motif for ARF degradation is located within the DBD, close to the dimerization interface. An open question is if and how degradation and dimerization interact: does degradation prevent the accumulation of monomers? Does dimerization protect ARFs from degradation? Or are these two completely separate properties? Given how closely the two regions are linked, it may not be trivial to separately interfere with the two.

Based on genetic analysis of the Marchantia auxin response system[5,10], auxin-dependence only evolved after the A/B split[10]. We therefore infer that ARF instability either co-emerged with or preceded the origin of the auxin response system. A key future question is by what mechanism the minimal region confers instability. This region likely constitutes a protein-protein interaction interface that allows a Ubiquitin ligase, or another proteolysis adaptor protein, to bind. The fact that the S299N mutation does not stabilize MpARF2, while the orthologous mutation stabilizes Maize ZmARF28, suggests divergence in the degradation interface, and likely co-evolution with a partner protein. We expect that the future identification of other components in ARF degradation will help in understanding the mechanisms underlying ARF degradation, including an understanding of the sequence requirements in the minimal degradation motif. Identification of additional components will likely also help explain the diversity, and biological significance of ARF degradation across the many processes that auxin controls.

Methods

Sequence identification, alignment and phylogenetic analysis

Most ARF sequences have been previously identified [4]. Additional sequences have been retrieved through BLASTP analysis using reference databases for *Zea mays* (B73-NAM-5.0.55), *Ceratopteris richardii* (V2.1), *Selaginella kraussiana*, *Ceratodon purpureus* (GG1), and algal genomes of *Mesotaenium endlicherianum* (SAG12.97), *Chlorokybus melkonianii* (CCAC 0220, previously *C. atmophyticus*), *Zygnema circumcarinatum*, all accessed through Phycocosm. For *M. endlicherianum*, the v2.0 annotation was surveyed to obtain the MeARFab sequence. BLASTP cut-off was set to $10e^{-10}$ for algal searches. All sequences were first checked for the presence of ARF DNA binding domain features (*i.e.*: B3 DNA binding domain, PF02362; and Auxin_resp, PF06507) or discarded otherwise. Protein sequences were aligned with the *E-INS-i* algorithm of MAFFT version 7 (https://mafft.cbrc.jp/alignment/software/). Alignments were trimmed to keep the DBD sequences and manually curated. TrimAI was used on curated alignments to discard positions with more than 80% gaps (http://trimal.cgenomics.org/). The ModelFinder implementation in IQ-TREE was used on final alignments to choose JTT+I+G4 as substitution model based on the Akaike-and Bayesian Information Criterion. IQ-TREE was also used on the final alignment to build a maximum likelihood phylogenetic tree. Branch statistic support was inferred using Ultrafast bootstrap (5000 alignments), the SH-like approximate Likelihood Ratio Test, and Approximate Bayes Test. The resulting tree, rooted to the ABC-ARF CmARF, can be found at https://itol.embl.de/tree/13722425211476661730903969. The tree figure was manually adapted as a vectorial image keeping the scale parameters.

Structural analysis degron

The MpARF2 crystal structure was retrieved from PDB (https://www.rcsb.org/structure/6SDG)[5]. Structural visualisation was performed using Pymol (v2.3.4) software. To model the mutated versions of the MpARF2 DBD we employed AlphaFold2-multimer v2.2.2[13].

Plasmid construction

A genomic fragment of 1920 bp upstream of the Mp*ARF2*

startcodon was amplified with primers MdR298 and MdR299 (Supplementary Data Table 1). This region was used as promoter to drive expression of the transgenes. Next, the plasmid pMpGWB100, carrying a hygromycin resistance casette, was digested with the restriction enzyme XbaI (ThermoFisher Scientific) and the aforementioned Mp*ARF2* promoter was ligated downstream of an XbaI site followed by the mNeonGreen (mNG) coding sequence using NEBuilder HiFi DNA Assembly (New England Biolabs, Inc)[14]. Next, MpARF2 domains, the full length protein coding sequence, and mutant versions thereof were amplified from in-house plasmids using primer pairs specified in Supplementary Data Table 1 and introduced into the XbaI site flanked by the Mp*ARF2* promoter and mNG. The degron swap constructs were amplified in two fragments from the MpARF2 DBD with two primer pairs containing a non-complementary sequence to introduce the swap, these fragments were then integrated using HiFi DNA Assembly (Supplementary Data Table 1). Swaps were generated based on the alignment shown in Fig. 2b.

Plant growth conditions and transformation

For this study *Marchantia polymorpha* Takaragaike-1 (Tak-1) was used as wild-type. Plants were grown on ½ strength Gamborg B5 medium at 22°C with 40 µmol photons $m^{-2}s^{-1}$ continuous white fluorescent light. Tak-1 was transformed using agrobacterium-mediated delivery of transgenic constructs as described by Kubota et al., 2013[15]. Transgenic plants were selected on ½ Gamborg B5 with 10 mg/L hygromycin and 100 µg/ml cefotaxime.

EdU-labeling of S-phase cells

To visualize S-phase cells in 3-day old gemmalings, plants were cultured for 3 h in liquid ½ Gamborg B5 medium containing 20 µM 5-ethynyl-2'deoxyuridine (EdU) followed by fixation in 3.7% formaldehyde in phosphate buffer saline (PBS, pH 7.4) for 1h in a vacuum. Plants were then washed twice in PBS and permeabilized for 20 mins in 0.5% Triton X-100 in PBS. Next, plants were washed twice in PBS containing 3% BSA and placed in the EdU click-IT reaction mixture with the 594 Alexa FLUOR fluorophore in the dark for 1 h (Invitrogen). This was followed by two washes with PBS with 3% BSA after which samples were placed in ClearSee solution for 1-4 days, protected from light[16]. Cell walls were stained using calcofluor-white.

Confocal microscopy & Assessment of fusion protein stability

All microscopy was performed on a Leica SP8X-SMD confocal microscope fitted with hybrid detectors and a 40 MHz pulsed white-light laser. Data acquisition was performed using LasX (v3.5.7.23225) software. For mNeonGreen, the fluorophore was excited using 488 nm laser line at 12% power output. Fluorescence was detected between 500-570 nm with hybrid detectors set to photon counting mode with 1.00-24.50 ns time-gating active to suppress background fluorescence. For the EdU staining experiment, 594 Alexa FLUOR was excited with a 594 nm laser line at 9% laser power and fluorescence emission was captured between 600-660 nm (0.7-24.50 ns time-gating active). Z-stacks were acquired using an HC PL APO 20x/0.75 water immersion or APO CS 10x/0.40 dry objective. To display images, ImageJ (v1.52) was used to generate maximum-intensity projections.

When investigating stability of various fusion proteins, we screened T1 transgenic lines for fluorescence by imaging the apical notch region of dormant gemmae. When no fluorescence was detected, we treated these gemmae with Bortezomib (Cayman Chemical) for 24 h or the solvent DMSO (Sigma-Aldrich) as control and checked for fluorescence again. Transgenic lines that showed no fluorescence before and after Bortezomib treatment were excluded from the analysis.

Phenotypic analysis

For experiments assessing fluorescence accumulation, non-chimeric transgenic lines were established by growing a G_1 generation from gemmae of independent plants that appeared resistant to initial selection on hygromycin (T_1 generation). Gemmae from the G_1 generation were used for experiments. To assess the phenotypes of plants expressing the full length MpARF2-mNG fusion, we reported on phenotypes of 50-day old T_1 generation plants. For growth assays, dormant gemmae were micro dissected from the gemmae cups/thallus and if clearly distinguishable notches could be observed, these were counted. Next, the gemmae were placed onto ½ Gamborg B5 medium (in the case of NAA sensitivity, medium was supplemented with DMSO or 3 µM NAA) and grown at 22°C with 40 µmol photons $m^{-2}\,s^{-1}$ continuous white fluorescent light. After seven (general growth) or ten (NAA sensitivity) days, pictures were taken with a Canon EOS250D camera and thallus area was measured using ImageJ (v1.52). For higher magnification images a Leica M205

stereomicroscope was used. Statistical tests were performed in R (v4.2.1).

Statistics & reproducibility

Tests, parameters, additional statistical information and the nature of biological replicates are provided in figure descriptions. Sample sizes are shown within the figures themselves. No statistical method was used to predetermine sample size, sample sizes were determined according to field standards. Experiments were not randomized. When showing representative micrographs, data collected on two additional independent transgenic lines is provided in the Extended Data section.

Data availability

Data can be shared upon request. The full phylogenetic tree can be obtained from https://itol.embl.de/tree/1372242521147666 1730903969. Plasmids generated and used in this study are available upon request from the corresponding author. As long-term storage of *Marchantia polymorpha* lines is problematic, we can provide some lines analyzed in this study, contact the corresponding author for inquiries. We provide a source data file containing the raw data and statistical output for the phenotypic experiments contained in this paper.

Acknowledgements

We thank Sjoerd Woudenberg, Sophie Valk, and Juriaan Rienstra for help and advice, André Kuhn for comments on the manuscript, and Michael Prigge and Mark Estelle for helpful discussions. This work was supported by a grant from Netherlands Organization for Scientific Research (NWO; OCENW.M20.031 to J.W.B.), a Marie Skłodowska-Curie Individual Fellowship (H2020-MSCA-IF-2020 contract number to J.H.G.), and a Research Grant from the Human Frontiers Research Program (HFSP; grant RGP0015/2022 to D.W.).

Author Contributions

M.d.R.: Conceptualization; Data collection, analysis, and interpretation; Writing, editing and revising the manuscript. J.H.G.: Conceptualization; Data collection, analysis, and interpretation; Ed-

iting the manuscript. S.D.: Conceptualization. J.W.B.: Conceptualization; Data interpretation. D.W.: Conceptualization; Data interpretation; Writing, editing and revising the manuscript.

Competing interests

No competing interests are declared.

Extended Data

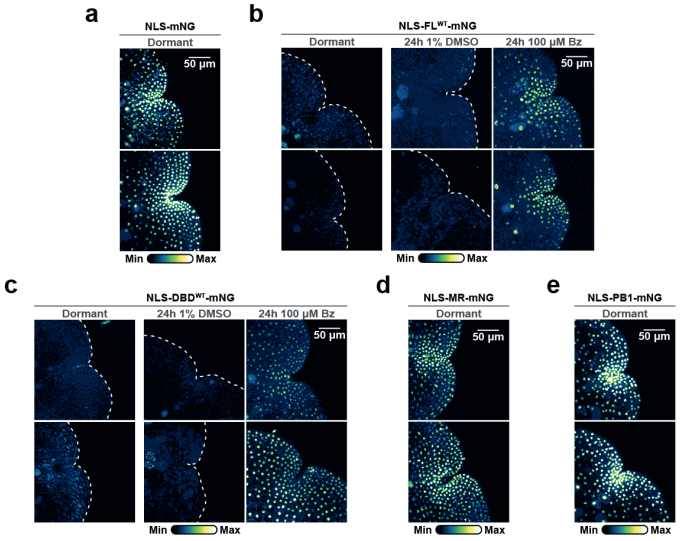


Fig. 1 | Assessment of stability of fusion proteins through confocal microscopy.
a.-e. Confocal images of *M. polymorpha* gemmae, showing representative expression of different fusion proteins as outlined in Fig. 1d. Here we show protein behavior in two additional independent lines for all panels in Fig. 1. Bz, Bortezomib.

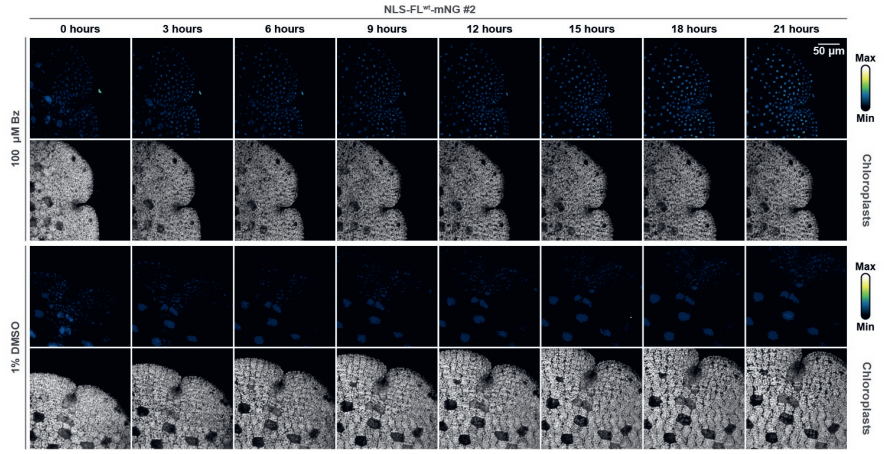


Fig. 2 | Dynamics and proteasome-dependence of NLS-FL^{wt}-mNG accumulation.
Time series of gemma expressing NLS-FL^{wt}-mNG treated with Bortezomib (Bz) or DMSO for 21 hours.

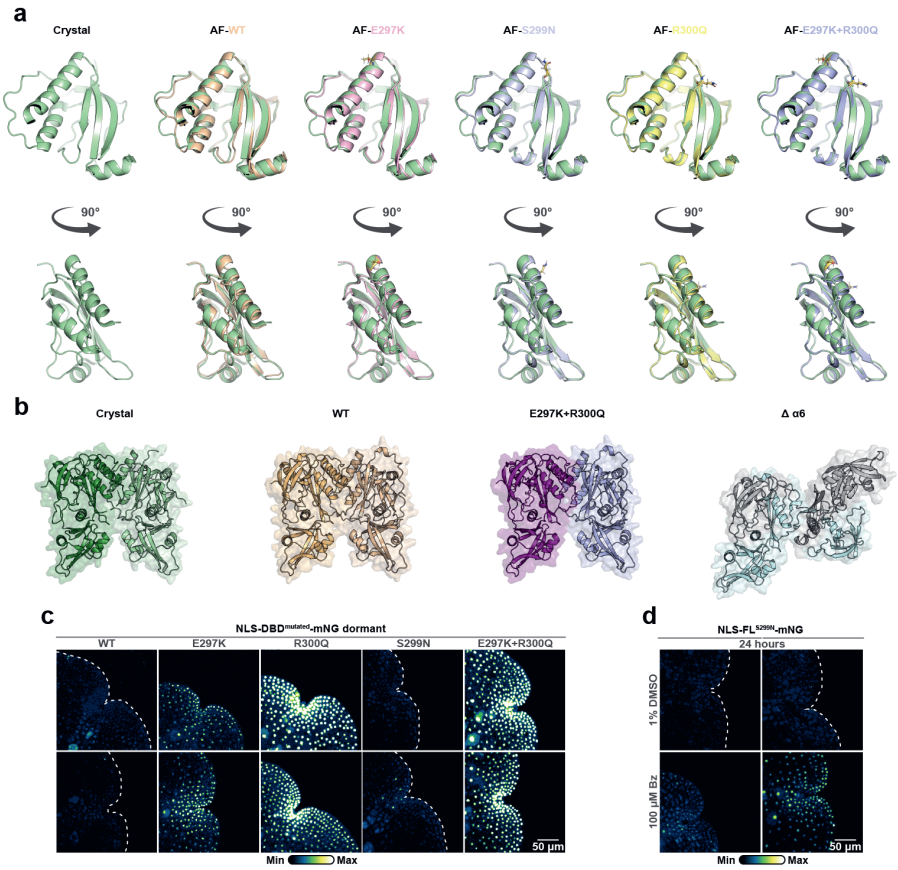


Fig. 3 | AlphaFold2 models of mutated residues and dimerization capacity. **a.** Overview of the introduced point mutations within the MpARF2 DBD. Mutations were visualized through AlphaFold2 modelling and projected onto the experimentally verified (X-ray crystallography) MpARF2 DBD shown in green. **b.** AlphaFold2 models of homodimerization of the WT MpARF2 DBD, the E297K+R300Q mutant, and a version where α-helix 6 was deleted (right) when compared to the structure of MpARF2 (left, green). **c.-d.** Confocal images of *M. polymorpha* gemmae, showing representative expression of different fusion proteins as outlined in Fig. 2d.-e. Here we show protein behavior in two additional independent lines for all panels in Fig. 2. Bz, Bortezomib.

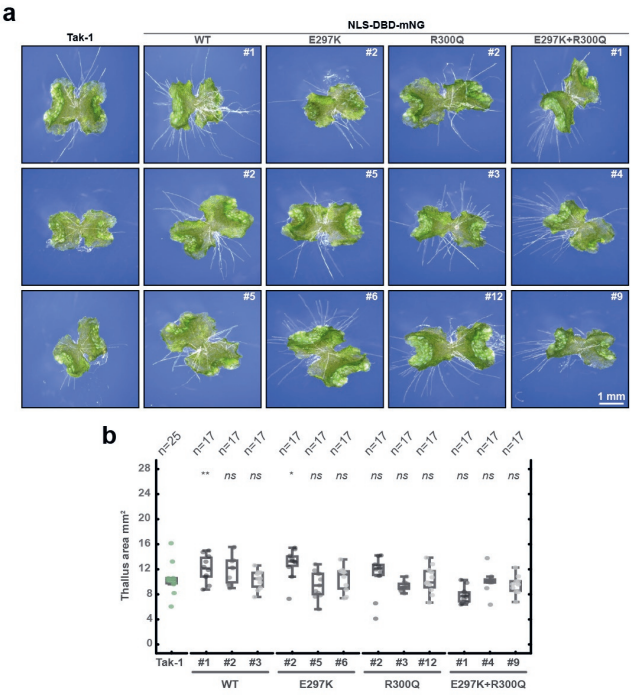


Fig. 4 | Expression of stabilized NLS-DBD-mNG fusions has no effect on Marchantia development.
a. Overview of phenotypes of seven day old gemmalings grown on ½ strength Gamborgs B5 medium wich express the NLS-DBD-mNG fusion proteins which harbour no mutations (WT) or mutations in key residues for stability as shown in Fig. 2d. **b.** Projected thallus area of aforementioned plants were measured and statisticaly compared by one-way ANOVA (F=(14, 216)=3.841 $P\approx7.94e^{-6}$) with Tukey post-hoc test (asterixes denote significant differences from Tak-1, * P<.05; ** P<.01). Boxplots show the following statistical parameters: central line, median; upper bound, first quartile; lower bound, third quartile; whiskers show the highest and lowest values, respectively, within 1.5*inter-quartile range (IQR). Individual gemmae were selected randomly and grown as independent biological replicates. The sample size is indicated and represents individual gemmalings. Raw data and exact p-values are provided as a Source Dataset.

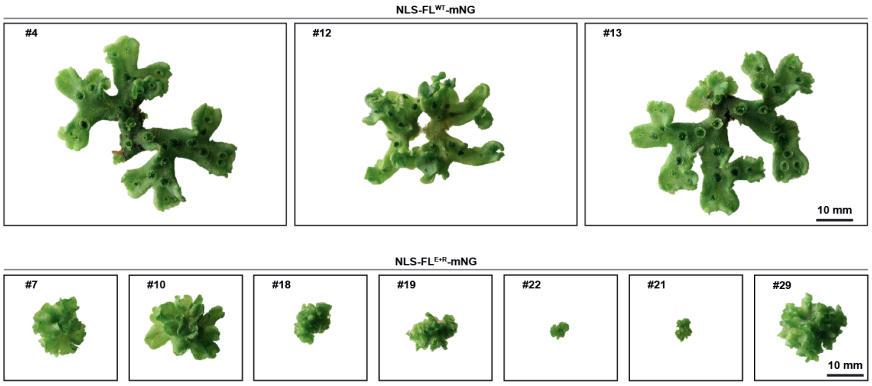


Fig. 5 | Expression of a stabilized full-length MpARF2 protein disturbs normal Marchantia development.
Overview of representative phenotypes of plants which survived T_1 selection on hygromycin-containing ½ Gamborgs B5 medium for 50 days. Compared here are multiple independent transgenic lines expressing NLS-FL^{WT}-mNG (top panel) and NLS-FL^{E+R}-mNG (bottom panel, harbours the E297K and R300Q mutations).

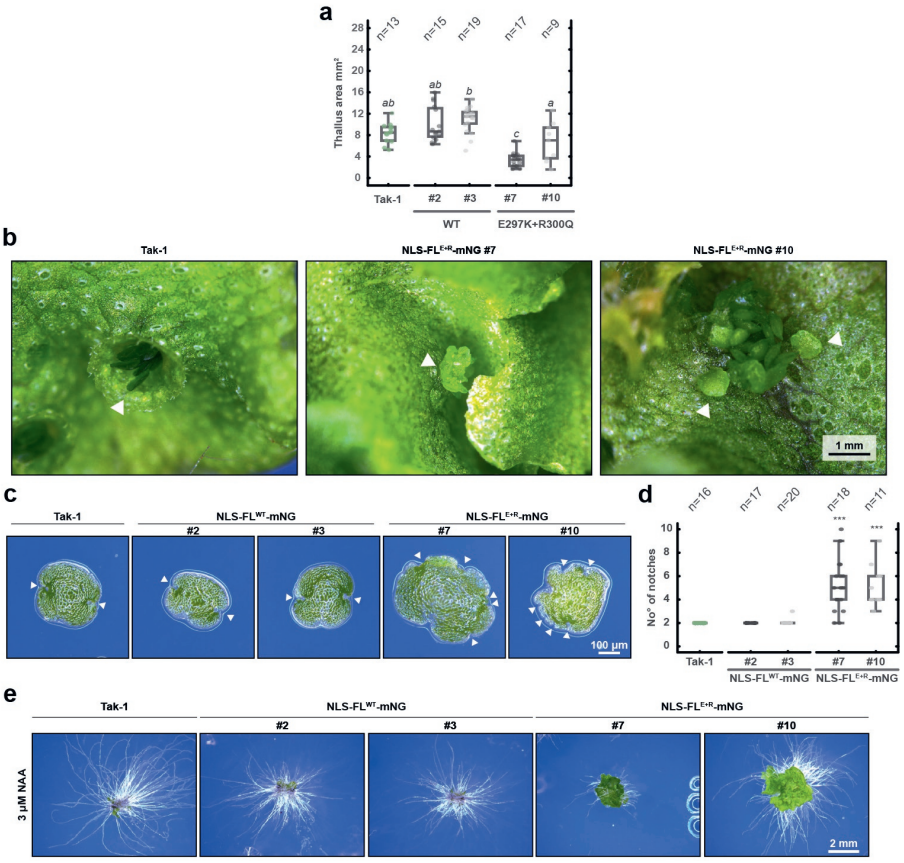


Fig. 6 | NLS-FL^{E+R}-mNG mutants exhibit pleitropic developmental defects and impaired auxin response.
a. Projected thallus area of seven day old gemmalings grown on ½ strength Gamborgs B5 medium. A comparison is made between the Tak-1 WT and plants wich express the NLS-FL^{WT}-mNG and NLS-FL^{E+R}-mNG fusion proteins (shown are two independent lines per construct). Thallus area was statisticaly compared by one-way ANOVA (F=(4, 68)=24.3, $p\approx1.65e^{-12}$) with Tukey post-hoc test (italics denote significant differences, $p<.05$). Boxplots show the following statistical parameters: central line, median; upper bound, first quartile; lower bound, third quartile; whiskers show the highest and lowest values, respectively, within 1.5*inter-quartile range (IQR). **b.** Detailed images of gemmae formation in gemma cups (Tak-1, left) and on the thallus (NLS-FL^{E+R}-mNG #7 and #10, wherein hashes indicate independent transgenic lines). **c.** Stereomicroscope images of dormant gemmae described in a. **d.** When clearly distinguishable apical notches of gemmae in c. were observed, these were counted and were statistically compared by a Chi-squared test (*** $p<.001$) to the Tak-1 WT. Boxplots show the following statistical parameters: central line, median; upper bound, first quartile; lower bound, third quartile; whiskers show the highest and lowest values, respectively, within 1.5*inter-quartile range (IQR). Individual gemmae were selected randomly and grown as independent biological replicates. The sample size is indicated and represents individual gemmae. **e.** Overview of gemmalings of plants described in a. were grown on 3 µM NAA containing ½ Gamborgs B5 medium for 17 days (same experiment as Fig. 3c but plants were grown for an additional seven days). For **a.** & **d.** the sample size is indicated and represents individual gemmalings, individual gemmae were selected randomly and grown as independent biological replicates. Source data and exact p-values are provided as a Source Dataset.

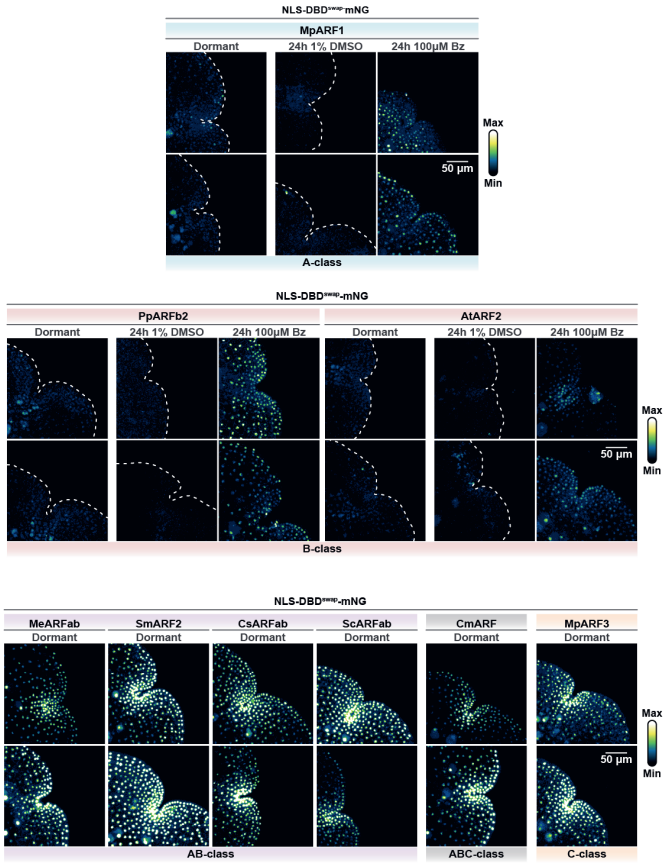


Fig. 7 | Investigation of the ability of homologous regions of ARF proteins from different Streptophyte species in conferring instability.
Confocal images of *M. polymorpha* gemmae, showing expression of different NLS-DBD-mNG fusion proteins with homologous sequences of other ARFs swapped. Here we show protein behaviour in two additional independent lines for all panels in Fig. 4. Bz stands for Bortezomib.

Supplementary Data Table 1 | Oligonucleotides used in this study.

Primer	Sequence 5′ > 3′	Description
MdR298	TGCATGCCTGCAGGTCGACTA-AAAGCCTGTAATCACACGACG	Fw promoter Mp*ARF2*
MdR299	GCTGTCTAGAGGTCG-GAACTTCTGTCTAAAATGC	Rv promoter Mp*ARF2*
MdR306	TTAGACAGAAGTTC-CGACCTATGTCAGAAG-CATCTTCCA	Fw Mp*ARF2* > $_{pro}$Mp*ARF2*::XbaI-mNG
MdR314	ATGCTGCCGCCGCCAAGCTG-CATGTCGTCGCCGCGCG	Rv Mp*ARF2* > $_{pro}$Mp*ARF2*::XbaI-mNG
MdR308	CCATGCGGCAAC-GAAGAAATCTCGATT	Fw introduce E297K mutation 2 fragment > $_{pro}$Mp*ARF2*::XbaI-mNG
MdR309	AATCGAGATTTCTTCGTTGC-CGCATGG	Rv introduce E297K mutation 2 fragment > $_{pro}$Mp*ARF2*::XbaI-mNG
MdR310	CGGAGAAATCTCAAT-TCTCTCTAATTT	Fw introduce R300Q 2 fragment > $_{pro}$Mp*ARF2*::XbaI-mNG
MdR311	AAATTAGAGAGAATT-GAGATTTCTCCG	Rv introduce R300Q 2 fragment > $_{pro}$Mp*ARF2*::XbaI-mNG
MdR312	ATGCGGCAACGAAGAAATCT-CAATTCTCTCT	Fw introduce E+R (E297K + R269Q) 2 fragment > $_{pro}$Mp*ARF2*::XbaI-mNG
MdR313	AGAGAGAATTGAGATTTCTTC-GTTGCCGCAT	Rv introduce E+R (E297K + R269Q) 2 fragment > $_{pro}$Mp*ARF2*::XbaI-mNG
MdR412	GCGGCAACGGAGAAAAATC-GATTCTCTCTAA	Fw introduce S299N 2 fragment > $_{pro}$Mp*ARF2*::XbaI-mNG
MdR413	TTAGAGAGAATCGATTTTTCTC-CGTTGCCGC	Rv introduce S299N 2 fragment > pA2_XbaI_mNG
MdR315	ATGCTGCCGCCGCCAAGCTG-GAAGGGCTCCACTTCCCATG	Rv Mp*ARF2* AD (DBD C-term.) > $_{pro}$Mp*ARF2*::XbaI-mNG
MdR317	ATGGCTCCAAAGAAGAA-GAGAAAGGTC	Fw Mp*ARF2* DBD+SV40 at N-term.
MdR318	TTAGACAGAAGTTC-CGACCTATGGCTC-CAAAGAAGAAG	Rv Mp*ARF2* DBD+SV40 at N-term.
MdR319	GGTTGTAAATTAGAGAGAATT-GAGATTTCTCCGTTGCCGC	Rv Mp*ARF2* R300Q 2 fragment > $_{pro}$Mp*ARF2*::XbaI-mNG
MdR320	GCGGCAACGGAGAAATCT-CAATTCTCTCTAATTTACAACCC	Fw Mp*ARF2* R300Q 2 fragment > $_{pro}$Mp*ARF2*::XbaI-mNG
MdR372	TTAGACAGAAGTTC-CGACCTATGGCTC-CAAAGAAGAAGAGAAAGG	Fw SV40 hifi o. hang > $_{pro}$Mp*ARF2*::XbaI-mNG
MdR373	ATGCTGCCGCCGCCAAGCT-GAACTGGACCTTGTTG-GAAATTTTGCGACG	Rv Mp*ARF2* MR hifi o. hang > $_{pro}$Mp*ARF2*::XbaI-mNG

Primer	Sequence 5′ > 3′	Description
MdR374	ATGCTGCCGCCGCCAAGCTG-CATGTCGTCGCCGCGCGCCC	Rv Mp*ARF2* PB1 hifi o. hang into XbaI+NLS
MdR381	TGGTTGTCCCTGCACTGC-CAGATGGGCAGCGGCCGC-GAGAAC	Rv swap degron Mp*ARF3* into Mp*ARF2* DBD longer o .hang
MdR382	CCCATCTGGCAGTGCAGGG-ACAACCATTCTCTCTAATTTA-CAACCCTCG	Fw swap degron Mp*ARF3* into Mp*ARF2* DBD
MdR424	GCCCATGCGCTAGCGAG-CAGTTCTCCATTCTCTCTA-ATTTACAACC	Fw swap degron Me*ARFab* into Mp*ARF2* DBD
MdR425	TGGAGAACTGCTCGCTAGCG-CATGGGCAGCGGCCGCGAGA	Rv swap degron Me*ARFab* into Mp*ARF2* DBD
MdR426	CCATGCGGTAAGGCACCTA-AAACCATTCTCTCTAATTTA-CAACCCT	Fw swap degron Cs*ARFab* into Mp*ARF2* DBD
MdR427	ATGGTTTTAGGTGCCTTAC-CGCATGGGCAGCGGCCGC-GAGAAC	Rv swap degron Cs*ARFab* into MpARF2 DBD
MdR428	CCATGGGGCAGCGTATGGA-CAACCATTCTCTCTAATTTA-CAACCCT	Fw swap degron Sc*ARFab* into Mp*ARF2* DBD
MdR429	AATGGTTGTCCATACGCTGC-CCCATGGGCAGCGGCCGC-GAGAAC	Rv swap degron Sc*ARFab* into Mp*ARF2* DBD
MdR430	ATGCGGCAGCGTCGGGACAG-ACATTCTCTCTAATTTACAAC-CCTCGA	Fw swap degron Cm*ARFabc* into Mp*ARF2* DBD
MdR431	GAATGTCTGTCCCGACGCTG-CCGCATGGGCAGCGGCCGC-GAGAAC	Rv swap degron Cm*ARFabc* into Mp*ARF2* DBD
MdR359	GTTCCCGTACTTATCGCATGG-GCAGCGGCCGCGAGA	Rv swap degron At*ARF2* into Mp*ARF2* DBD
MdR360	ATGCGATAAGTACGGGAAC-TATGTTCTCTCTAATTTACAAC-CCTCGATC	Fw swap degron At*ARF2* into Mp*ARF2* DBD
MdR389	CCCATGCGGCAATTTCGG-GATCTACATTCTCTCTAATTTA-CAACCCTCGATC	Fw swap degron Sm*ARF2* into Mp*ARF2* DBD

Primer	Sequence 5’ > 3’	Description
MdR390	AATGTAGATCCCGAAATTGC-CGCATGGGCAGCGGCCGC-GAGAACCCC	Rv swap degron Sm*ARF2* into Mp*ARF2* DBD
MdR353	TTCCCTCCCTTGACGCATGGG-CAGCGGCCGCGAGAA	Rv swap degron Pp*ARF2* into Mp*ARF2* DBD
MdR354	CCATGCGTCAAGGGAGG-GAATGCGATTCTCTCTAATTTA-CAACCC	Fw swap degron Pp*ARF2* into Mp*ARF2* DBD
MdR349	GAATCGAGAATTCGTCGCTGC-CGCATGGGCAGCGGCC	Rv swap degron Mp*ARF1* into Mp*ARF2* DBD
MdR350	CCGCTGCCCATGCGGCAGC-GACGAATTCTCGATTCTCTCTA-ATTTACAACCC	Fw swap degron Mp*ARF1* into Mp*ARF2* DBD

References

1 Vanneste, S. & Friml, J. Auxin: a trigger for change in plant development. *Cell* **136**, 1005–1016 (2009). https://doi.org/10.1016/j.cell.2009.03.001

2 Mockaitis, K. & Estelle, M. Auxin receptors and plant development: a new signaling paradigm. *Annu Rev Cell Dev Biol* **24**, 55–80 (2008). https://doi.org/10.1146/annurev.cellbio.23.090506.123214

3 Leyser, O. Auxin Signaling. *Plant Physiol* **176**, 465–479 (2018). https://doi.org/10.1104/pp.17.00765

4 Mutte, S. K. *et al.* Origin and evolution of the nuclear auxin response system. *Elife* **7** (2018). https://doi.org/10.7554/eLife.33399

5 Kato, H. *et al.* Design principles of a minimal auxin response system. *Nat Plants* **6**, 473–482 (2020). https://doi.org/10.1038/s41477-020-0662-y

6 Lavy, M. *et al.* Constitutive auxin response in Physcomitrella reveals complex interactions between Aux/IAA and ARF proteins. *Elife* **5** (2016). https://doi.org/10.7554/eLife.13325

7 Das, S. *et al.* Quantitative imaging reveals the role of MpARF proteasomal degradation during gemma germination. *Plant Commun*, 101039 (2024). https://doi.org/10.1016/j.xplc.2024.101039

8 de Roij, M., Borst, J. W. & Weijers, D. Protein degradation in the auxin response. *Plant Cell* (2024). https://doi.org/10.1093/plcell/koae125

9 Prigge, M. J. *et al.* Comparative mutant analyses reveal a novel mechanism of ARF regulation in land plants. *bioRxiv* (2023). https://doi.org/10.1101/2023.11.09.566459

10 Hernandez-Garcia, J. *et al.* Evolutionary origins and functional diversification of Auxin Response Factors. *Nat Commun* **15**, 10909 (2024). https://doi.org/10.1038/s41467-024-55278-8

11 de Vries, J. & Archibald, J. M. Plant evolution: landmarks on the path to terrestrial life. *New Phytol* **217**, 1428–1434 (2018). https://doi.org/10.1111/nph.14975

12 de Vries, J., Stanton, A., Archibald, J. M. & Gould, S. B. Streptophyte Terrestrialization in Light of Plastid Evolution. *Trends Plant Sci* **21**, 467–476 (2016). https://doi.org/10.1016/j.tplants.2016.01.021

13 Jumper, J. *et al.* Highly accurate protein structure prediction with AlphaFold. *Nature* **596**, 583–589 (2021). https://doi.org/10.1038/s41586-021-03819-2

14 Ishizaki, K. *et al.* Development of Gateway Binary Vector Series with Four Different Selection Markers for the Liverwort Marchantia polymorpha. *PLoS One* **10**, e0138876 (2015). https://doi.org/10.1371/journal.pone.0138876

15 Kubota, A., Ishizaki, K., Hosaka, M. & Kohchi, T. Efficient Agrobacterium-mediated transformation of the liverwort Marchantia polymorpha using regenerating thalli. *Biosci Biotechnol Biochem* **77**, 167–172 (2013). https://doi.org/10.1271/bbb.120700

16 Kurihara, D., Mizuta, Y., Sato, Y. & Higashiyama, T. ClearSee: a rapid optical clearing reagent for whole-plant fluorescence imaging. *Development* **142**, 4168–4179 (2015). https://doi.org/10.1242/dev.127613



Chapter 5
Diversification of functional requirements for proteolysis of Auxin Response Factors

Authors

Martijn de Roij[1], Esmée Heijdra[1], Jasper Lamers[1], Ryuichi Nishihama[2], Jan Willem Borst[1], Dolf Weijers[1,*]

Affiliations

[1] Laboratory of Biochemistry, Wageningen University, Stippeneng 4, 6708WE Wageningen, the Netherlands

[2] Department of Applied Biological Science, Faculty of Science and Technology, Tokyo University of Science, 2641 Yamazaki, Noda, Chiba 278-8510, Japan

* Corresponding author: dolf.weijers@wur.nl

This chapter has been published as:

de Roij, M. *et al.* Diversification of functional requirements for proteolysis of auxin response factors. *Nature Communications* (2026).

https://doi.org/10.1038/s41467-026-70440-0

Abstract

Auxin signaling through the Nuclear Auxin Pathway is essential for plant development and is mediated by competing A-class and B-class Auxin Response Factor (ARF) transcription factors. Recently, proteasomal ARF degradation through a degradation signal embedded within the DNA-Binding Domain, was identified as a key component of auxin response. Here, we investigate the structural requirements and biological relevance of ARF degradation in the bryophyte *Marchantia polymorpha*. We identify a critical residue for proteolysis of the repressive, B-class MpARF2, and find it to be functionally conserved in degradation of the activating, A-class MpARF1. Unlike MpARF2, however, impaired MpARF1 degradation had little effect on auxin response and development, suggesting differential integration in biological function. We find that MpARF2 degradation occurs across all developmental stages of the life cycle and is required for MpARF2 function during development. Our findings reveal a degradation mechanism targeting A -and B-class ARFs which shares the same origin but has evolved along unique evolutionary trajectories.

Introduction

Auxin is an important signaling molecule in plant development as it orchestrates several physiological processes[1]. While multiple mechanisms through which auxin elicits these responses have been revealed, the best characterized mode of action to date relies on the control of gene transcription through the Nuclear Auxin Pathway (NAP)[2,3]. The NAP revolves around three protein families, TRANSPORT INHIBITOR RESPONSE1/AUXIN SIGNALING F-BOX proteins (TIR1/AFBs), auxin/indole-3-acetic acid (Aux/IAA), and AUXIN RESPONSE FACTORS (ARFs)[4]. TIR1/AFBs are components of a SKP-CULLIN-F-BOX ubiquitin-ligase complex ($SCF^{TIR/AFB}$) and form a coreceptor complex together with Aux/IAA proteins in presence of auxin, which leads to ubiquitylation and subsequent degradation of Aux/IAAs by the proteasome[5-7]. Given the role of Aux/IAAs as ARF inhibitors, their degradation subsequently releases the ARFs from an inhibitory state leading to transcriptional activation of auxin-responsive genes[8,9]. ARFs are central in this system as they connect perception of auxin by TIR1/AFBs and Aux/IAAs to a transcriptional response which ultimately leads to physiological changes.

In land plants, ARFs contain an N-terminal DNA-binding domain (DBD), a middle region (MR), and a Phox and Bem 1 domain (PB1), and can be classified into three main subfamilies[10]. Two of these families, the A -and B-class ARFs, possess a highly conserved DNA-binding domain which show a substantial overlap in functionality and binding specificity of their target genes[11-13]. However, A-class ARFs tend to function as auxin-induced gene activators, whereas B-class ARFs are auxin-independent repressors[13,14]. A -and B-Class ARFs compete for DNA-binding sites in a stoichiometry-dependent way[13,14], and the relative abundance of A -and B-class ARFs within the nucleus therefore dictates cellular transcriptional responsiveness to auxin.

To maintain an appropriate ARF stoichiometry, plants rely on both transcriptional and post-translational control mechanisms[15,16]. In recent years, ARF proteolysis through the 26S proteasome has emerged as a critical node in auxin signaling[17-19]. Though various ARFs are known to be unstable, the precise molecular mechanisms and biological importance remain poorly understood[15].

Recent findings identified a conserved motif in the DBD that is critical for their proteasome-mediated degradation across diverse plant lineages[20,21]. Mutation of residues in this motif led to B-class ARF stabilization, which in turn represses the auxin response, ultimately leading to impaired development[20,21]. In the bryophyte

Marchantia polymorpha (hereafter Marchantia), each of the three major ARF families is represented by a single gene copy (A-class MpARF1, B-class MpARF2, and C-class MpARF3), making it an ideal, minimal system to dissect core principles of auxin signaling[22]. The sole B-class ARF MpARF2 carries the conserved degradation motif, and mutations in residues comprising this motif severely impacted normal development[21]. Swapping this motif of MpARF2 with homologous motifs of other ARFs, representing all known ARF classes across the green lineage, revealed that the instability conferred by this motif likely emerged in an ancestral AB-ARF that gave rise to the A -and B-class ARF clades[21-23]. While the importance of degradation through this motif was demonstrated in B-class ARFs, it remains unknown if, and to what extent, this instability was integrated in A-class ARF function. Furthermore, we systematically investigate sequence requirements of MpARF2 degradation, both through *in silico* and experimental approaches. In addition, previous studies focused on B-class ARF degradation during specific developmental stages[21], leaving the question of its relevance throughout the lifecycle largely unanswered. Here we provide detailed spatiotemporal information throughout the entire *M. polymorpha* lifecycle. Our work demonstrates how precise dosing of a B-class ARF through proteasome-mediated degradation contributes to auxin response and development.

Results

Structural requirements of MpARF2 degradation

We have previously demonstrated that a small loop in the MpARF2 DBD is required for regulated protein degradation. Single and double mutations in the E297 (E297K – a charge reversal) and R300 (R300Q – a loss of charge) residues radically decrease protein turnover, with severe consequences for development[21]. The mutations that were previously engineered were inspired by induced mutations in *Physcomitrium patens* ARFs that caused auxin-related phenotypes such as delayed gametophore formation and the ability to still form these gametophores when grown in high-auxin conditions[20]. However, given that no systematic analysis of the degradation region in any ARF has yet been reported, it is unclear what the requirements of this region for effective degradation are. Particularly because both mutations lead to a loss or reversal of charge, it is possible that this charge is critical for protein degradation. There is substantial variation in the degradation motif among ARFs, and the unstable B-class maize ZmARF28[20] lacks the charged residues, raising the question of what properties underlie protein instability.

To address such questions, we performed a systematic mutagenesis scan by replacing each residue flanking the E297 and R300 amino acids in MpARF2 with an alanine, except A294 and A295, which were substituted by a glycine (Fig. 1a). None of these mutations had a strong predicted effect on overall MpARF2 DBD folding (Supplementary Information Fig. 1a-d). We generated transgenic plants expressing the MpARF2 DBD fused to mNeonGreen (mNG) under control of the native Mp*ARF2* promoter in the Tak-1 background. We used only the DBD to prevent phenotypic effects, and because we previously found that remaining MpARF2 domains did not contribute to protein stability[21]. Fluorescence intensity was quantified in nuclei of transgenic gemmae using confocal microscopy as a proxy for protein stability. None of the A294G, A295G, T295G, T296A, E297A, K298A, S299A, and F301A mutations behaved significantly differently from the wild type (WT) protein, indicating that none of these residues are critical for protein degradation or that weak stabilizing effects could not be determined using this assay (Fig. 1a,b). In addition, we treated all lines with the proteasome inhibitor Bortezomib (Bz), and found that each accumulated, excluding the possibility that low protein accumulation observed was due to low expression levels (Supplementary Information Fig. 1e).

Intriguingly, in contrast to the E297K mutation[21], E297A fluo-

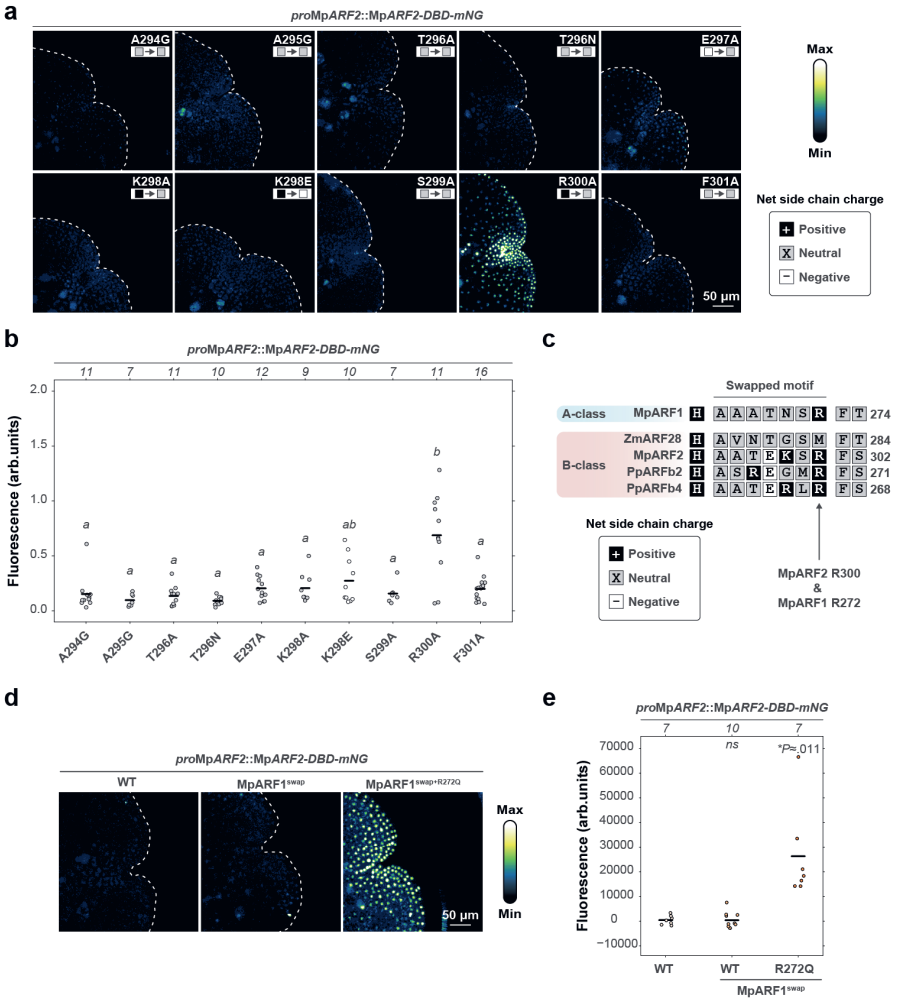


Fig. 1 | A positive charge is essential for MpARF degradation.
a. Representative confocal images showing fluorescence patterns in dormant gemmae expressing a *pro*Mp*ARF2*::Mp*ARF2-DBD-mNeonGreen* fusion with indicated mutations. Amino acid side chain charge is indicated. **b.** Quantification of overall fluorescence in several independent transgenic lines of which one is shown in (**a**). Letters in italics indicate significant differences determined per one-way ANOVA (F=(9,94)=6.322, P≈5.85x10^{-7}) and Tukey HSD post hoc test with Bonferroni correction (P<.05). **c.** Protein alignment of a selection of ARF proteins, amino acid side chain charge and the swapped motif are indicated. **d.** Representative confocal images of *pro*Mp*ARF2*::Mp*ARF2-DBD-mNeonGreen* fusions with indicated motif swaps. **e.** Quantification of (**d**), statistical differences from the WT were determined per two-sided T-test (P<.05). (**b** and **c**) The sample size is indicated above the figure, each replicate consists of a gemmae from an independent transgenic line. (**b** and **e**) Exact P-values are provided in the Source dataset.

rescence levels remained low (Fig. 1a,b), suggesting that the charge reversal, rather than loss of negative charge conferred E297K stability. The R300A mutation did induce protein stability (Fig. 1a,b),

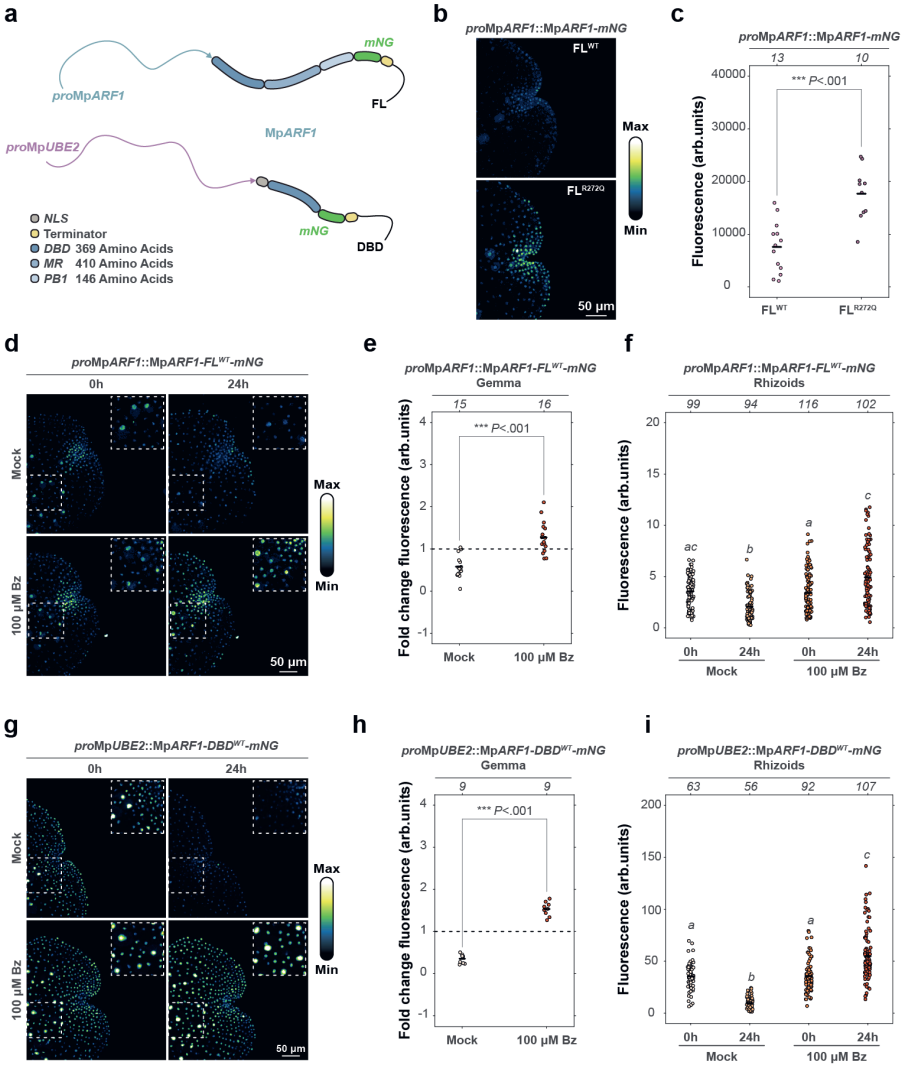


Fig. 2 | Requirements for MpARF1 proteolysis.
a. Diagram depicting genetic constructs encoding translational fusions to mNeonGreen (mNG) analyzed in this experiment; names correspond to other panels (**b**-**i**) in this figure. **b.** Representative confocal images showcasing *pro*Mp*ARF1*::Mp*ARF1-FL-mNG* accumulation patterns in dormant gemmae. **c.** Fluorescence intensity quantification of dormant gemmae expressing *pro*Mp*ARF1*::Mp*ARF1-FL-mNG*, both a wild type (WT) and R272Q mutant (R272Q) version, of which one is shown in (**b**). Fluorescence intensity was compared via two-sided T-test ($P<.05$). **d.** Representative confocal images showing *pro*Mp*ARF1*::Mp*ARF1-FL^{WT}-mNG* accumulation patterns in gemmae treated with Bortezomib (Bz) or Mock (DMSO) for 24 hours. The outlined portion of the image is enlarged. **e.** Quantification of fold change in overall fluorescence of *pro*Mp*ARF1*::Mp*ARF1-FL^{WT}-mNG* expressing gemmae, of which representatives are shown in (**d**), after 24 hours of treatment with Bortezomib (Bz) or Mock (DMSO). Fold change was compared per two-sided T-test ($P<.05$). (**f**) Mean fluorescence measured in individual nuclei of rhizoid initial cells before and after 24 hours of treatment with Bortezomib (Bz) or Mock (DMSO). **(continued on next page)**

Fig. 2 (continued) | Intensities were compared via Kruskal-Wallis test ($H(3)=74.539$, $P\approx4.548x10^{-16}$) with a Dunn post hoc test ($P<.05$). Same experiment as (**d** and **e**). **g.** Representative confocal images showing *pro*Mp*UBE2*::Mp*ARF1-DBD^{WT}-mNG* accumulation patterns in gemmae treated with Bortezomib (Bz) or Mock (DMSO) for 24 hours. An outlined portion of the image is enlarged. **h.** Quantification of fold change in overall fluorescence of *pro*Mp*UBE2*::Mp*ARF1-DBD^{WT}-mNG* expressing gemmae of which representatives are shown in (**g**). after 24 hours of treatment with Bortezomib (Bz) or Mock (DMSO). Fold change was compared per two-sided T-test ($P<.05$). **i.** Mean fluorescence measured in individual nuclei of rhizoid initial cells before and after 24 hours of treatment with Bortezomib (Bz) or Mock (DMSO). Intensities were compared via Kruskal-Wallis test ($H(3)=170.32$, $P\approx2.2x10^{-16}$) with a Dunn post hoc test ($P<.05$). Same experiment as (**g** and **h**). For (**c**, **e**, and **h**): sample size is indicated above the figures, each replicate consists of the average of a gemmae representing a total of three independent transgenic lines. For (**f** and **i**): sample size is indicated above the figure, each replicate consists of a measurement from an individual nucleus of a rhizoid initial cell. (**c**, **e**-**f**, **f**-**i**) Exact *P*-values are provided in the Source dataset.

hence loss of positive charge, rather than specific substitution to Q, caused R300Q stabilization. Collectively, these observations suggest that removal of the R300 positive charge or gain of E297K positive charge has a dramatic impact on protein instability. We therefore engineered a charge reversal in K298 (K298E) and found that this weakly and variably stabilized the protein (Fig. 1a,b), suggesting that interactions mediating protein degradation are likely driven by charges, yet these act in a localized manner.

In the maize ZmARF28 protein, a mutation equivalent to MpARF2 S299N causes stabilization[20], but we previously found that this mutation in MpARF2 did not impair degradation (Fig. 1c)[21]. Given the existence of one additional alcoholic residue in the MpARF2 degradation motif (T296), we mutated this threonine to asparagine (T296N) to test if the N side chain may influence stability in a different position in MpARF2. The T296N mutation did not affect protein stability (Fig. 1a,b). This suggests that the degradation motif in MpARF2 is lenient to mutation, but depends on positive charges, most prominently R300.

To analyze conservation of the positive charge conferred by R300, we generated a broad alignment of ARF sequences and compared biochemical properties (Supplementary Information Fig. 2a,b). Across the different ARF classes, ABC, AB, and C ARFs typically lacked a positive charge at the MpARF2 R300 position, whereas in A-class ARFs, and to a lesser extent in B-class ARFs, this charge is conserved (Supplementary Information Fig. 2a,b). Notably, both the A and B-class ARFs generally possess two conserved positive charges in two distinct configurations, different from patterns in charge distribution in the other ARF classes.

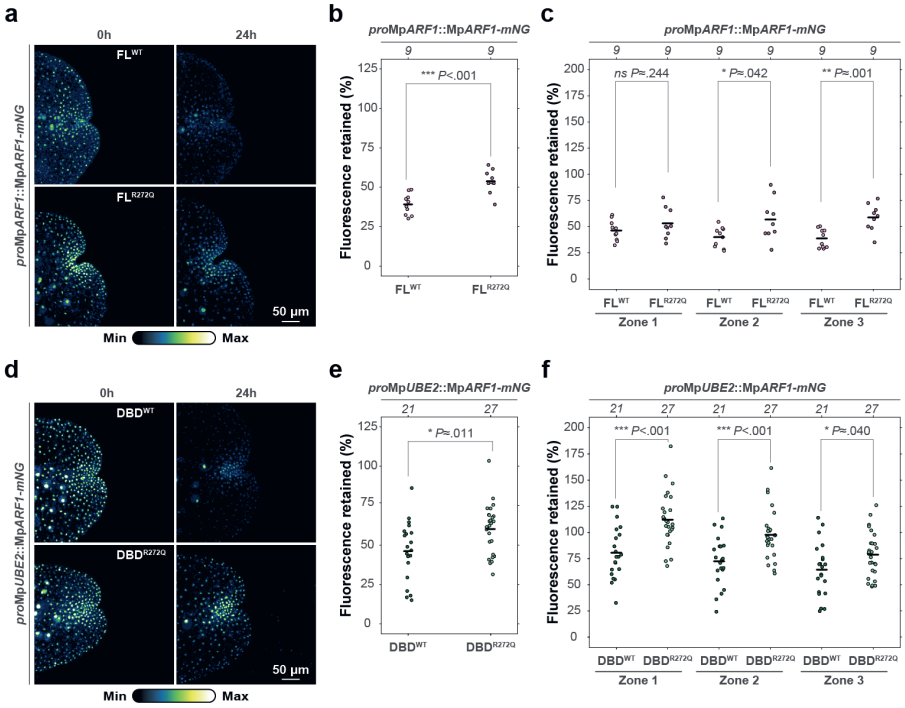


Fig. 3 | The R272Q mutation stabilizes MpARF1.
a. Representative confocal images showing *pro*Mp*ARF1*::Mp*ARF1-FL-mNG* accumulation patterns in individual gemmae in a dormant state (0 hours) and after germination (24 hours). **b.** Quantification of the overall level of fluorescence retained in *pro*Mp*ARF1*::Mp*ARF1-FL-mNG* after 24 hours of germination, compared by two-sided T-test ($P<.05$). **c.** Quantification of the level of fluorescence retained in three different zones of the apical notch, with Zone 1 corresponding to the zone most proximal to the apical cell, and Zone 3 being most distal of the apical cell, as illustrated in Supplementary Information Fig. 4e. Fluorescence retained was compared by two-sided T-test ($P<.05$). Same experiment as (**a** and **b**). **d.** Representative confocal images showing *pro*Mp*UBE2*::Mp*ARF1-DBD^{WT}-mNG* accumulation patterns in individual gemmae in a dormant state (0 hours) and after germination (24 hours). e. Quantification of the overall level of fluorescence retained in *pro*Mp*UBE2*::Mp*ARF1-DBD^{WT}-mNG* after 24 hours of germination, compared by T-test ($P<.05$). **f.** Quantification of the level of fluorescence retained in three different zones of the apical notch, with Zone 1 corresponding to the zone most proximal to the apical cell, and Zone 3 being most distal of the apical cell, as illustrated in Supplementary Information Fig. 4e. Fluorescence retained was compared by two-sided T-test ($P<.05$). Same experiment as (**d** and **e**). (**b** and **c**) Sample size is indicated above the figures, each replicate consists of the average of a gemmae (n=3) representing three independent transgenic lines in total. (**e** and **f**) Sample size is indicated above the figures, each replicate consists of the average of a gemmae (n=7-9) representing three independent transgenic lines in total. (**b**-**c** and **e**-**f**) Exact *P*-values are provided in the Source dataset.

The key single R300 degradation residue in MpARF2 is conserved in the A-class ARF MpARF1[21], indicative of a possibly conserved proteolytic degradation mechanism shared by the two classes (Fig. 1c; Supplementary Information Fig. 2a,b). We previously swapped the equivalent region from MpARF1 into the MpARF2 DBD

and observed conferred instability[21]. To test if this instability required the conserved arginine, we engineered the R272Q mutation within the MpARF2 DBD$^{MpARF1\ swap}$ fusion protein, and found this to have a drastic, stabilizing effect (Fig 1c,d; Supplementary Information Fig. 3a,b). Thus, protein degradation in Marchantia MpARF1 and MpARF2 relies on a critical arginine, and may be mediated by the same biochemical mechanism.

Regulated degradation of MpARF1

We previously hypothesized that proteasome-mediated proteolysis through the ARF DBD emerged in an ancestral AB-class ARF protein[21]. However, when following the accumulation of MpARF1 and MpARF2 in the same plant over time, either in presence or absence of a proteasome inhibitor, we found that dynamics of accumulation are rather different: proteasome inhibition leads to excess MpARF2 accumulation, whereas MpARF1 stops being degraded, but does not accumulate beyond regular levels[18]. It is therefore a question whether MpARF1 is actively degraded.

Given that the MpARF1 R272Q mutation stabilized MpARF2 when introduced as part of a region swap (Fig. 1d), we first engineered the same mutation in the full length MpARF1 protein (MpARF1-FL), and expressed this as an mNG fusion driven by the native Mp*ARF1* promoter (Fig. 2a). We found this mutation to weakly, but statistically significant, stabilize the MpARF1 protein (Fig. 2b,c). Notably, Bz treatment led to increased accumulation of MpARF1-FL (Fig. 2d,e,f). Next, to determine which protein domains confer MpARF1 instability, we expressed full length wild type (MpARF1-FL^{WT}) and R272Q MpARF1 (MpARF-FL^{R272Q}), as well as individual domains (MpARF1-DBD^{WT} and MpARF1-DBD^{R272Q}, MpARF1-MR, and MpARF1-PB1) as mNG fusions, which were expressed from the constitutive *UBIQUITIN-CONJUGATING ENZYME E2* promoter (*pro*Mp*UBE2)* to prevent autoregulation of the Mp*ARF1* promoter[24]. Interestingly, we found that MpARF1-FL accumulated at lower levels than each of its separate domains, indicative of a collective contribution to protein instability (Supplementary Information Fig. 4a,b). When expressed from the Mp*UBE2* promoter, we did not find a significant effect of the R272Q mutation on protein (domain) stability (Supplementary Information Fig. 2a,b). Fluorescence levels varied greatly between transgenics, particularly for the DBD-only lines, which may have occluded effects of the mutation (Supplementary Information Fig. 2a,b). Likewise, we observed the same variation when expressing the MpARF1-DBD from the Mp*ARF2* promoter (Supplementary In-

formation Fig. 2c,d). We therefore tested the effect of Bz treatment on *pro*Mp*UBE2*::Mp*ARF1-DBD*^{WT} lines and found this to cause increased accumulation (Fig 2g,h,i). We next observed protein accumulation over time following germination of gemmae in *pro*Mp*ARF1*::Mp*ARF-FL-mNG* and *pro*Mp*UBE2*::Mp*ARF1-DBD-mNG* lines in which the R272Q was engineered. In both these contexts, we found decline of the WT protein over time, and reduced decline induced by the R272Q mutation, across the meristematic region (Fig. 3a-f; Supplementary Information Fig. 2e). Thus, we conclude that the MpARF1 DBD confers instability, likely through the conserved R272.

Limited biological roles for MpARF1 instability

Given the *in vivo* degradation of MpARF1, and the minor but significant effect of the R272Q mutation, a key question is whether MpARF1 instability is required for normal development or auxin response. Unlike effects of MpARF2 stabilization[21], plants carrying *pro*Mp*ARF1*::Mp*ARF1-FL*^{R272Q}*-mNG* did not show obvious deviations from normal growth (Supplementary Information Fig. 4f), suggesting a minor effect, if any. However, plants did contain a wild-type copy of Mp*ARF1*, complicating interpretation. We therefore replaced the endogenous MpARF1 with a R272Q mutant version, by introducing the mutant transgene into the Mp*arf1-4* loss-of-function mutant, which is insensitive to auxin treatment (Supplementary Information Fig. 5a,b)[25]. While we found the R272Q mutation to cause slightly higher MpARF1 accumulation levels compared to WT in this background (Fig. 4a,b,c; Supplementary Information Fig. 5c), we did not observe substantial differences in phenotype when comparing Mp*arf1-4* complemented with WT or R272Q transgenes (Supplementary Information Fig. 6a). We examined air pore formation in both WT and R272Q, which did not show a significant difference between WT and R272Q, although some lines of both genotypes produced air pores slightly larger than Tak-1 (Supplementary Information Fig. 6b,c,d), We did observe a subtle difference in gemma cup formation as one transgenic line of R272Q showed a statistical significant delay in gemma cup formation compared to WT (Supplementary Information Fig. 7a,b,c). Similarly, one transgenic R272Q line produced gemmae which, like uncomplemented Mp*arf1-4*, often had three instead of the usual two apical notches (Supplementary Information Fig. 7d). We found no consistent difference in gemma germination between WT and R272Q (Supplementary Information Fig. 7e). Both WT and R272Q lines displayed similar rhizoid founder

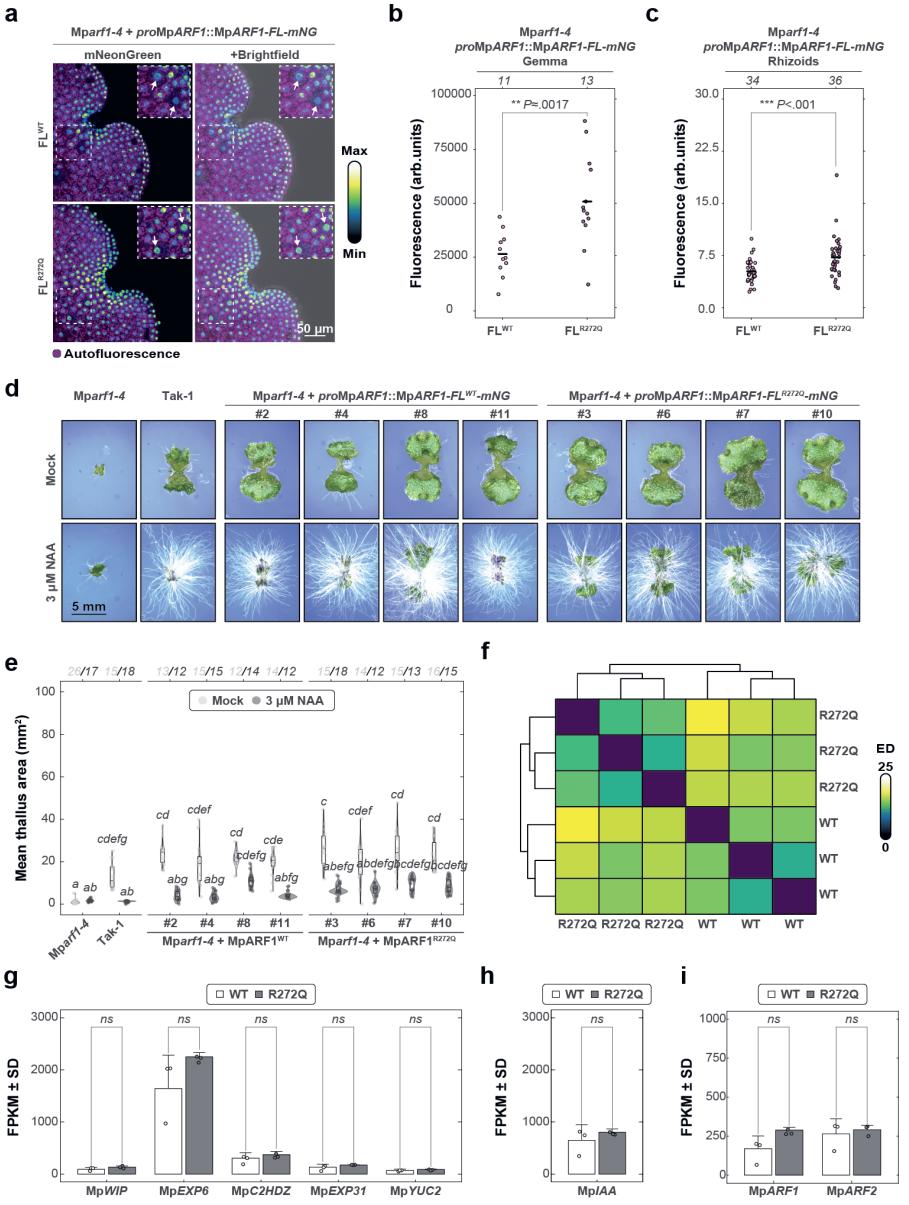


Fig. 4 | Functional analysis of MpARF1^{R272Q}.
a. Representative confocal images of accumulation patterns of dormant gemmae expressing *pro*Mp*ARF1*::Mp*ARF1-FL-mNG* in a M*parf1-4* background. Magenta shows chloroplast autofluorescence. A portion of the image is outlined and enlarged, and nuclei of rhizoid initial cells are indicated with an arrow. **b.** Quantification of overall fluorescence in several independent transgenic lines, of which one is shown in (**a**). Sample size is indicated above the figure and represents average fluorescence values for whole gemmae representing independent transgenic lines. **(continued on next page)**

Fig. 4 (continued) | c. Quantification of nuclear fluorescence in rhizoid initial cells of plants shown in (**a**). Sample size is indicated above the figure, each replicate consists of a measurement from an individual nucleus of a rhizoid initial cell. **d.** Qualitative assessment of auxin response in gemmalings grown for ten days on medium with Mock or NAA. Genotypes and independent transgenic lines are indicated above the figure. **e.** Quantification of projected thallus area of the experiment shown in (**d**). Projected thallus area was compared per Kruskal-Wallis test ($H(19)=243.77$, $P\approx 2.2x10^{-16}$) with a Dunn post hoc test ($P<.05$). Boxplots show the following statistical parameters: central line, median; upper bound, first quartile; lower bound, third quartile; whiskers show the highest and lowest values, respectively, within 1.5*inter-quartile range (IQR). Sample size is indicated above the figure and represents individual plants grown from gemmae. **f.** Heatmap representing clustering of transcriptomes determined by RNA-seq of three independent biological replicates of Mp*arf1-4* mutant lines complimented with a *pro*Mp*ARF1*::Mp*ARF1-FL^{WT}-mNG* or *pro*Mp*ARF1*::Mp*ARF1-FL^{R272Q}-mNG* copy, respectively. ED; Euclidean distance. **g.** Expression levels, represented as Fragments Per Kilobase Million of typical auxin-responsive genes in MpARF1^{WT} and MpARF1^{R272Q} complementation lines. **h.** Expression levels, represented as Fragments Per Kilobase Million of Mp*IAA* in *pro*Mp*ARF1*::Mp*ARF1-FL^{WT}-mNG* and *pro*Mp*ARF1*::Mp*ARF1-FL^{R272Q}-mNG* complementation lines. **i.** Expression levels, represented as Fragments Per Kilobase Million (FPKM) of Mp*ARF1* and Mp*ARF2* in MpARF1-FL^{WT} and MpARF1-FL^{R272Q} complementation lines. (**b**,**c**) Statistical differences were determined per two-sided T-test (*P<.05*) and sample size is indicated above the figures. (**g**-**i**) Bars represents means and error bars show standard deviation from the mean. Datapoints are shown (n=3). Statistical differences were determined per two-sided T-test (*P<.05*).

cell formation and rhizoid elongation (Supplementary Fig. 8a,b,c and Supplementary Information Fig. 9a,b,c) Both complementation genotypes displayed similar restoration of auxin response (Fig. 4d,e), and we did not find differences in sensitivity to auxin at a range of concentrations (Supplementary Information Fig. 10a,b).

To further examine the effects of altered protein accumulation on MpARF1 functions in gene expression regulation, we preformed RNA-seq analysis with Mp*arf1-4* mutant, complemented either with a wild-type Mp*ARF1* transgene, or with a transgene carrying the R272Q mutation. The two genotypes separated in hierarchical clustering (Fig. 4f; Supplementary Information Fig. 11a). We found 520 genes to be differentially expressed (172 up and 348 down), with no significant alterations in expression levels of known auxin-responsive genes (Fig. 4f,g; Supplementary Information Fig. 11b). Furthermore, no auxin-related GO terms were found to be enriched among differentially expressed genes (DEGs) (Supplementary Information Fig, 11c), and as the Mp*ARF1* and *2,* or Mp*Aux/IAA* genes were not differentially expressed we did not find evidence of transcriptional feedback regulation (Fig. 4h,i). These observations collectively suggest that reduction of MpARF1 degradation has a limited effect on MpARF1 function, both at the physiological and transcriptional levels.

A developmental map of MpARF2 degradation

While MpARF1 degradation does not appear to be critically required for development, interfering with MpARF2 degradation dramatically alters thallus development[21]. This identifies MpARF2 degradation as a key control mechanism in auxin response. We next explored the extent to which this mechanism operates in controlling development throughout the Marchantia life cycle. To first map MpARF2 degradation without confounding effects of resulting plant phenotypes, we imaged plants expressing either *pro*Mp*ARF2*::Mp*ARF2-DBD^{WT}-mNG* (DBD^{WT}) or the *pro*Mp*ARF2*::Mp*ARF2-DBD$^{E297K+R300Q}$-mNG* (DBD^{E+R}) double mutant.

In early stage developing dormant gemmae, the DBD^{E+R} mutant protein accumulated to high levels and broadly throughout the gemma, especially in the apical notch (Fig. 5b). In later stage dormant gemmae, MpARF2 levels seem to be lower, but DBD^{E+R} seemed to be somewhat constricted and is present in the apical notch and rhizoid initial cells (Supplementary Information Fig. 12a,b). Intriguingly, we have previously shown that MpARF2 is usually absent or barely detectable in rhizoid initial cells[18]. The presence of DBD^{E+R} therefore suggests that the Mp*ARF2* promoter is active in these cells but that MpARF2 abundance is regulated post-translationally through protein degradation. This is further supported by observation of signal in rhizoid initials in DBD^{WT} when treated with the proteasome inhibitor Bortezomib (Bz), as this treatment led to accumulation patterns similar to DBD^{E+R} (Supplementary Information Fig. 12c). As Mp*ARF2* expression is tightly linked to the meristematic apical notch zone[13,18], we next decided to investigate MpARF2 degradation in apical notches of plants at a more precise temporal resolution. Whereas DBD^{WT} was not detected during the investigated stages, DBD^{E+R} was present throughout most cells (Fig. 5c; Supplementary Information Fig. 12d,e). We verified that this was due to proteasome-mediated degradation, and not a lack of expression, by treating plants with Bz, which resulted in accumulation (Supplementary Information Fig. 12f). As stable lines expressing FL^{E+R} had problems in normal thallus growth, gemma and gemma cup formation, we examined thallus-related structures such as air pores, air chambers, ventral scales and gemmae cups for DBD^{WT} degradation. DBD^{E+R} signal was observed widely throughout the thallus, mostly in photosynthetically active tissues, and less so in cells that lacked chloroplasts, and in ventral scales (Fig. 5d,e). DBD^{E+R} was present throughout various cell types in gemmae cups, including cells comprising the wings, the stalks and in cells which form the floor of the gemma cup (Fig. 5d; Supplementary Information Fig. 12g). In air

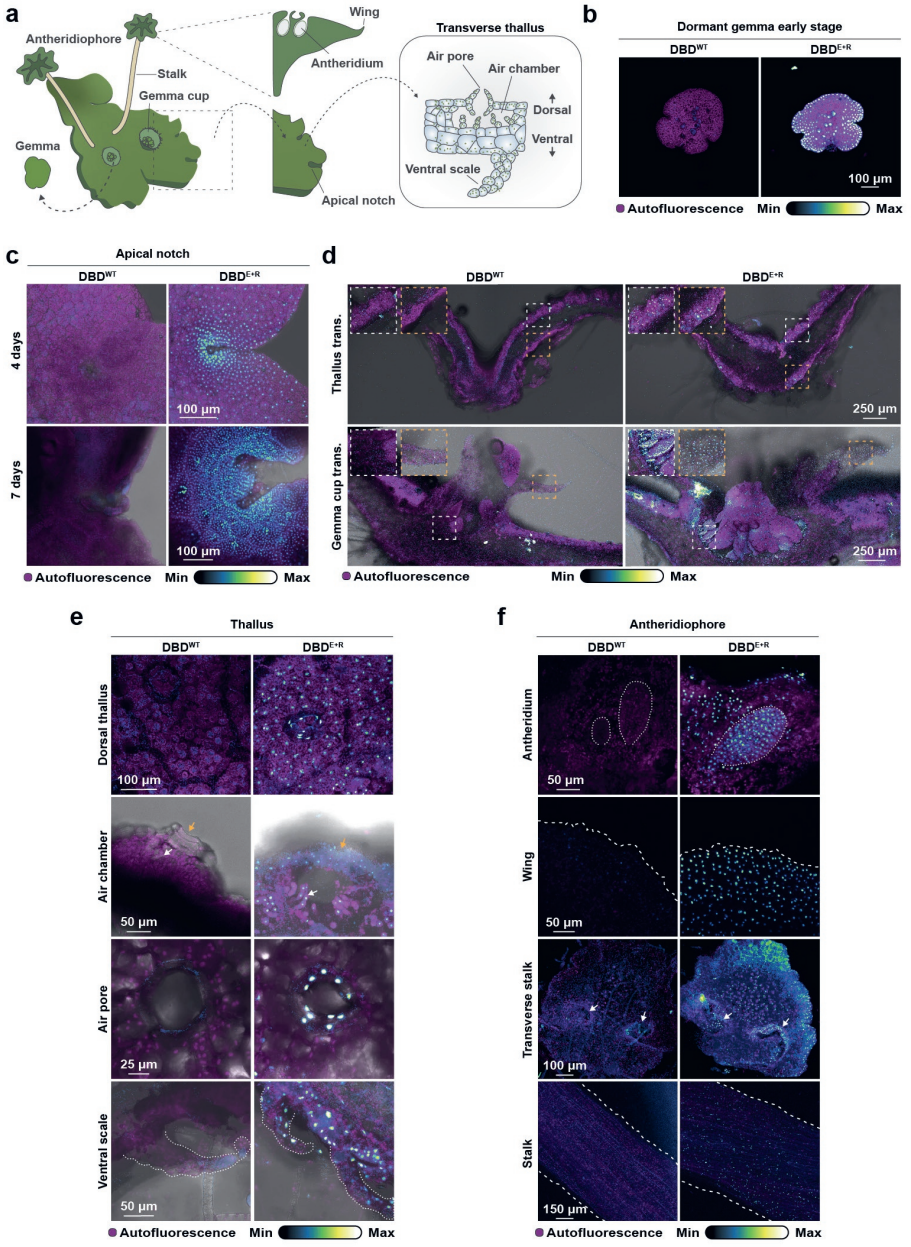


Fig. 5 | A spatial map of MpARF2 degradation.
a. Illustration of a mature *M. polymorpha* plant showing structures which were studied using confocal microscopy in this experiment. **b.**-**f.** Observations through confocal microscopy of accumulation patterns of a wild type (WT) and mutant (E297K+R300Q) copy of the MpARF2 DBD expressed from the Mp*ARF2* promoter fused to mNeonGreen, across different tissues. **b.** Early stage gemmae. **c.** Meristematic apical notches of plants grown from gemmae to a certain age, as indicated. **d.** Transverse cross sections of a gemmae cup and a thallus respectively. Certain structures are enlarged in the white and yellow boxes. **(continued on next page)**

Fig. 5 (continued) | e. Micrographs of mature thallus-related structures. Depicted here are a dorsal view of cells comprising the thallus, a dorsal view of an air pore, a transverse cross section of an air chamber (photosynthetic filaments (white arrow) and air pores (yellow arrow) are indicated), and ventral scales (outlined by white dotted lines). **f.** Micrographs showing structures found in antheridiophores. Highlighted are antheridia (outlined in white dotted lines), the wing, a transverse cross section of the stem (invaginations containing rhizoid bundles indicated by a white arrow), and a lateral view of the stem. (**b**-**f**) Micrographs represent 5 (**b**,**c**,**d**,**f**) or 6 (**e**) samples, respectively.

chambers DBD^{E+R} accumulated to high levels in the air pore cells, in the filamentous photosynthetic cells located in the air chambers themselves, and sometimes in the surrounding ground tissue (Fig. 5e).

Given that little is known about MpARF2 function and regulation in reproductive tissues, the gametangiophores, we investigated DBD^{E+R} accumulation in tissues which form the male antheridiophores (Fig. 5a). DBD^{E+R} accumulated throughout the stem, mostly in peripheral cells of the stem and around the invaginations which harbor rhizoid bundles (Fig. 5f). In cells which form the wing of the antheridiophore, DBD^{E+R} broadly accumulated (Fig. 5f). DBD^{E+R} was especially enriched in cells which give rise to the jacket around newly developing immature antheridia (Fig. 5f). Overall, these findings show that MpARF2 levels are tightly controlled through proteasomal degradation and that this degradation system is prominently active throughout the Marchantia lifecycle, enabling normal plant development.

Extended functions of MpARF2 degradation

To study the relevance of MpARF2 degradation beyond initial gemma development, we developed a conditional version of the MpARF2-$FL^{E297K+R300Q}$ protein expressed from its native promoter that can be activated, through excision of a floxed NLS-mScarlet3-tNOS cassette (abbreviated $mARF2^{flox}$), by treatment with both Dexamethasone (Dex) and heat shock (HS). MpARF2 activation would be visible by loss of mScarlet3 fluorescence and gain of mNG fluorescence (Fig. 6a). When $mARF2^{flox}$ plants were exposed to HS alone, we observed some leaky editing in the absence of Dex; however, plants simultaneously treated with HS and Dex showed stronger and broader editing patterns (Fig. 6b). Five days after induction, the leakiness of HS-treated plants seemed less severe, possibly due to selection against edited cells (Supplementary Information Fig. 13a). The $mARF2^{flox}$ plants did not display any phenotypic defects when compared to the Tak-1 wild-type background when not induced

(Supplementary Information Fig. 13b-e). To separate the effects of Dex and HS treatment, we included Tak-1 plants in all analyses and observed that 1 hour of HS had minimal effects on development and thallus size (Fig. 6c,d). We tested response to auxin in induced mARF2^{flox} gemmae and found clear auxin resistance and the characteristic phenotype found previously in stable MpARF2^{E+R} mutants (Fig. 6c,d; Supplementary Information Fig. 13f)[21]. This tells us that the mARF2^{flox} mimics the behavior of stable MpARF2^{E+R} mutants and that this system can be employed to study effects of MpARF2^{E+R} hyperaccumulation during thallus development.

Auxin regulates gemma cup development[26], a process which is difficult to study in stable mutants, as these generally do not form cups, or do so from abnormal thalli[21]. To study effects of MpARF2 stabilization on gemma cup development, we induced mARF2^{flox} after 7 days of cultivation and scored gemmae cup formation during the following 15 days. Strikingly, no gemmae cups were formed when mARF2^{flox} was induced even with only HS treatment (Fig. 6e). Gemma cup formation was not impaired in the Mock or Dex treated control groups and did not show morphological abnormalities (Fig. 6e; Supplementary Information Fig. 14a). In the previous experiments we found that MpARF2^{E+R} accumulates in antheridiophore associated tissues, whereas MpARF2^{WT} was maintained at low levels due to active degradation (Fig. 5f). We therefore analyzed the effect of impaired MpARF2 degradation on antheridiophore formation using the mARF2^{flox} system. We grew plants for 14 days and then induced both mARF2^{flox} and antheridiophore formation (with far red light), simultaneously. This developmental stage was also severely affected by induction of mARF2^{flox}, as plants did not form normal antheridiophores when induced with HS or HS and Dex contrasting strongly with the Mock and Dex controls, which formed normal antheridiophores (Fig. 6f; Supplementary Information Fig, 14b). Some induced mARF2^{flox} plants, however, formed undefined outgrowths (Supplementary Information Fig, 14b,c).

MpARF2 degradation is required for biological function

Plants expressing a stabilized copy of MpARF2 are strongly affected in auxin response and development, a defect that persists throughout development. However, given that an endogenous copy is still present, it is unclear what the impact would be of preventing the only MpARF2 copy from being degraded. Earlier attempts to generate Mp*arf2* loss-of-function mutants failed to recover mutants, and

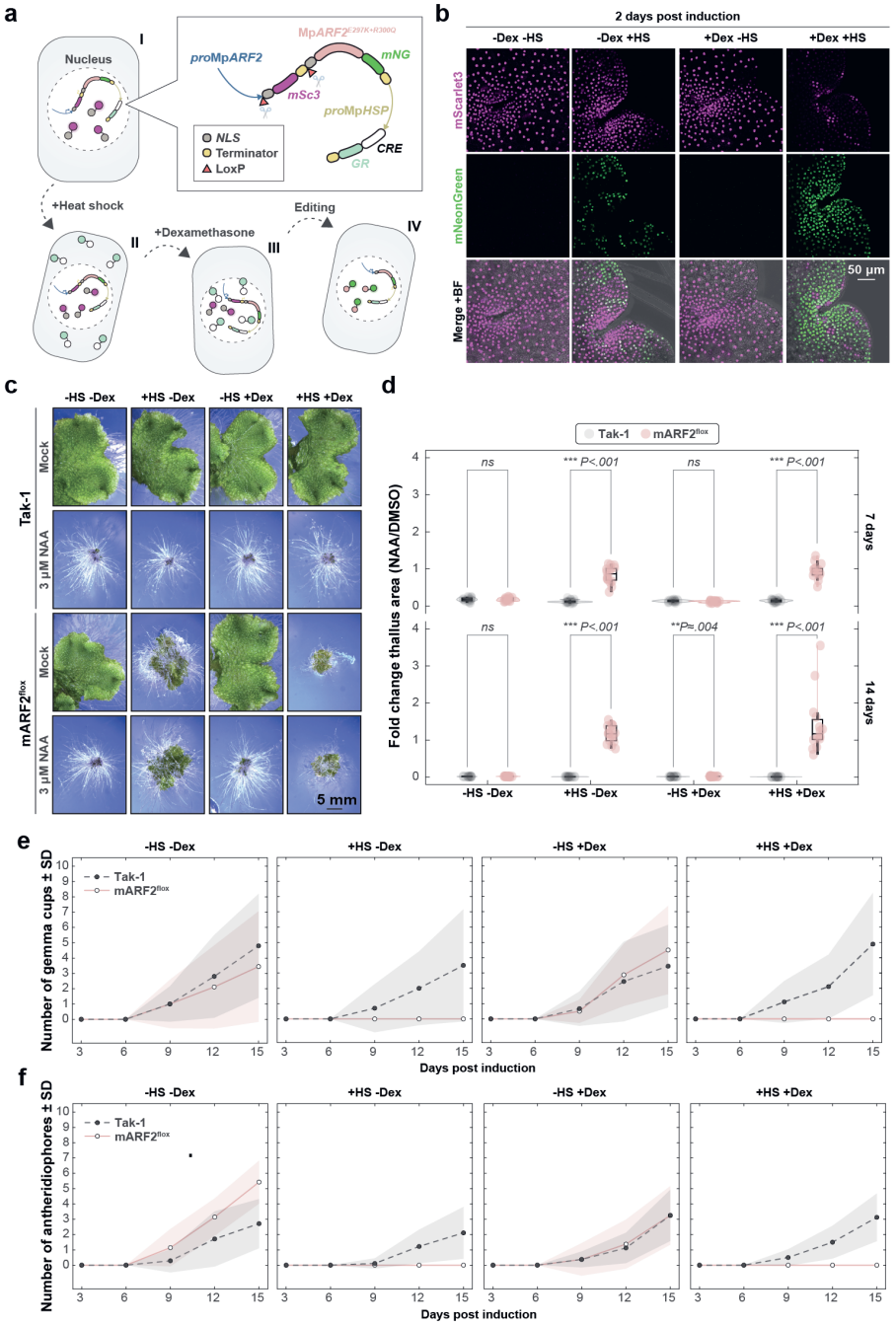


Fig. 6 | Conditional stabilization of MpARF2 reveals broad roles for its degradation in development.

a. Diagram illustrating the architecture of the inducible genetic construct, and how combined heat shock and Dexamethasone treatment leads to expression of mARF-2^{flox}. **(continued on next page)**

Fig. 6 (continued) | Abbreviations: mNG is mNeonGreen; mSc3 is mScarlet3; HSP is Heat Shock Protein; and GR is Glucocorticoid Receptor. **b.** Observations of editing patterns of the inducible construct through confocal microscopy two days after induction with heat shock and Dexamethasone treatment. Representative of 4 samples for each condition. **c.** Phenotype of Tak-1 and Inducible plants 14 days post induction with indicated treatments, grown on ½ Gamborg B5 medium supplemented with 3 µM NAA or Mock. **d.** Quantification of projected thallus area of plants shown in (**c**) relative growth of NAA treated plants was calculated versus their Mock control (i.e. a low fold change means a strong reduction in size due to NAA treatment). Fold change in projected thallus size was compared per Mann-Whitney U test (P<.05, two-tailed). Boxplots show the following statistical parameters: central line, median; upper bound, first quartile; lower bound, third quartile; whiskers show the highest and lowest values, respectively, within 1.5*inter-quartile range (IQR). **e.** Quantification of the number of gemma cups in Tak-1 and mARF2^{flox} plants measured during 15 days after induction with the indicated treatments. Shaded areas show standard deviations from the mean. **f.** Quantification of the number of antheridiophores in Tak-1 and mARF2^{flox} plants measured during 15 days after induction with the indicated treatments. Shaded areas show standard deviations from the mean. (**b**-**f**) Abbreviations treatments: HS is heat shock; and Dex is Dexamethasone.

we previously developed a floxed complementing MpARF2 to conditionally delete the only wild-type copy[13]. It is, however, impractical to complement this conditional mutant with specific protein versions. Recently, a stable Mp*arf2* allele was generated (Mp*arf2-1*)[27], which now allows assessing the biological function of specific variants. To test the requirement for regulated MpARF2 degradation, we complemented the Mp*arf2-1* mutant either with a *pro*Mp*ARF2*::Mp*ARF2-FL-*^{WT}*-mNG* (MpARF2^{WT}) or a *pro*Mp*ARF2*::Mp*ARF2-FL*$^{E297K+R300Q}$*-mNG* (MpARF2^{E+R}) copy. The uncomplemented Mp*arf2-1* mutant grows as a cell mass that retains the ability to proliferate and form rhizoid cells (Fig. 7a)[27]. The mutant fails to produce a flat thallus and its associated structures such as gemmae cups and midribs (Fig. 7a)[27]. Complementation with MpARF2^{WT} partially rescued the mutant phenotype (Fig. 7a). Some of the transgenic lines obtained could form thalli with air pores, however, a full restoration of the phenotype was not observed, suggesting that some expression signals are likely missing from the transgenic construct. Obtained lines still exhibited slower growth, abnormal apical notch formation and branching patterns when compared to Tak-1 (Fig. 7a). Some lines were able to produce gemmae cups and gemmae, one line produced gemmae without clearly defined notches, resulting in a round morphology (Fig. 7b; Supplementary Information Fig. 15a). These plants exhibited a relatively normal response to auxin (Supplementary Information Fig. 15b). In contrast, MpARF2^{E+R} plants failed to produce thalli with gemmae cups, and still appeared more or less like the Mp*arf2-1* mutant, even though they were able to grow faster (Fig. 7a). Excessive accumulation of MpARF2 leads to repression of the auxin response. Either way, these results show that regulated degradation

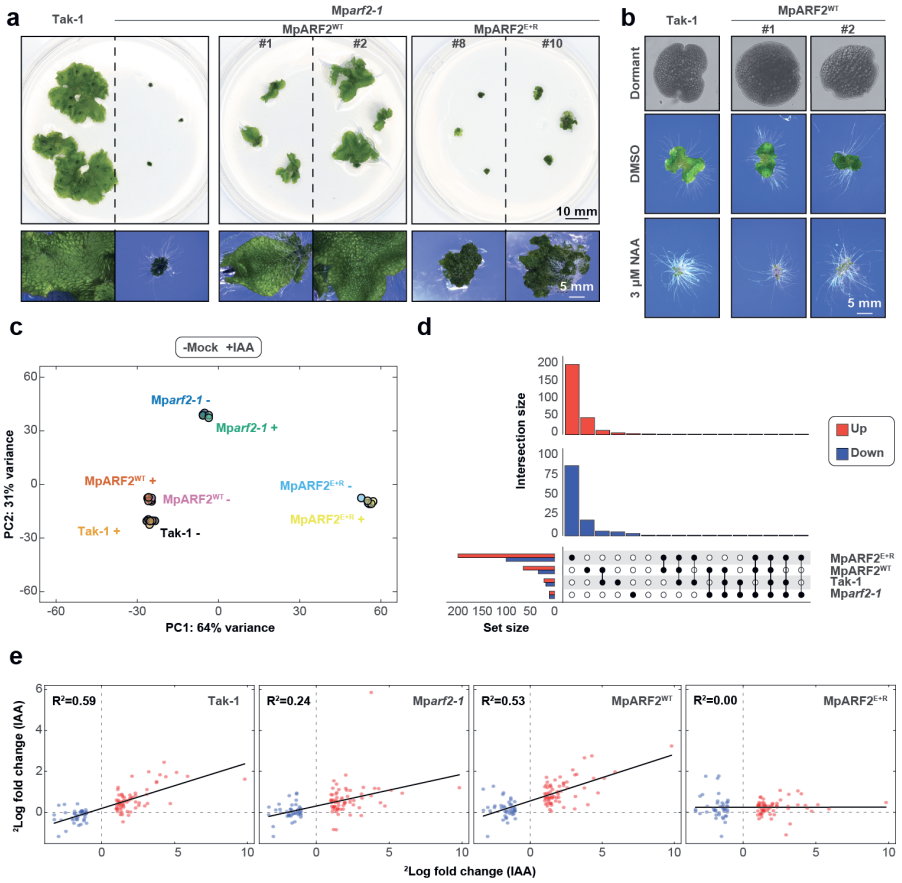


Fig. 7 | MpARF2 proteolysis is required for biological function.
a. Phenotypes of 20-day-old plants of the indicated genotypes, grown from tissue fragments. The lower panels show an enlargement of the plants imaged above. **b.** Gemma morphology and qualitative analysis of auxin response of 10-day-old gemmalings of Mp*arf2-1* mutant lines complemented with MpARF2^{WT} grown on NAA or Mock. The sample sizes reflected by these micrographs are represented in Supplementary Information Fig. 15a,b. **c.** Principal component analysis following transcriptome analysis of Tak-1, Mp*arf2-1*, and Mp*arf2-1* complementation lines (MpARF2^{WT} and MpARF2$^{E297K+R300Q}$, respectively) treated with IAA (indicated with +) or Mock (indicated with -). **d.** Upset plot showing unique and overlapping differentially expressed genes (determined per Wald statistical test with Benjamin-Hochberg correction for multiple comparison; -0.5<^{2}Log Fold Change>0.5, P_{adj}<.05) in the IAA-treated group versus the Mock control, per genotype. e. Relationship between fold changes of a set of auxin-responsive genes identified by Ref.[12] on the x-axis, and fold changes found in this experiment on the y-axis. R^2 value depicts fit of the linear regression model.

is required for MpARF2 function *in vivo*.

To address the impact of reduced MpARF2 degradation on MpARF2 function in transcriptional regulation, we grew fragments of Tak-1, Mp*arf2-1*, MpARF2^{E+R}, and MpARF2^{WT} plants for 14 days, de-

pleted endogenous auxin with the synthesis inhibitors Yucasin and L-Kynurenin[28], followed by treatment with 1 µM Indole-3-Acetic acid (IAA) or Mock for one hour. RNA-sequencing results showed strong clustering by genotype, eclipsing effects of the IAA treatment (Fig. 7c; Supplementary Information Fig. 16a). Notably, MpARF2^{WT} clustered together with Tak-1, whereas MpARF2^{E+R} clustered separately (Fig. 7c). MpARF2^{E+R} had the highest number of DEGs, showing no overlap with the other genotypes, indicating that these DEGs are not genes that are auxin-responsive (Fig. 7d). This was confirmed through GO-analysis, which showed that no auxin-related terms were found among terms enriched in genes differentially expressed in MpARF2^{E+R} (Supplementary Information Fig. 16b). We analyzed the expression of a set of previously described IAA-responsive DEGs[12] and found that both Tak-1 and MpARF2^{WT} showed highly similar expression of these genes (Fig. 7e). Unexpectedly, Mp*arf2-1* did not show a hypersensitive response, but rather a slightly dampened response to auxin (Fig. 7e). The transcriptional response to IAA was completely abolished in MpARF2^{E+R}, confirming that the physiological effects observed in these mutants are due to both a very strong repression of the auxin response system as well as unlicensed regulation of auxin-unrelated genes (Fig. 7e). These results confirm that MpARF2 degradation is essential for proper transcriptional homeostasis and responses to auxin, which, combined with effects on physiology, confirm its importance.

Discussion

Auxin is an important signaling molecule, deeply intertwined with plant development, and largely relies on transcriptional reprogramming. ARF proteins are an essential component of auxin signaling and their activity must be tightly regulated. Here, we report on significant divergence in degradation dynamics and functional consequences of MpARF family members, thereby offering insight into post-translational tuning of auxin signaling. More specifically, through a systematic analysis we demonstrate that a conserved arginine residue in the DBD is required for MpARF proteolysis. Our results further indicated that, the A-class MpARF1 is subjected to proteolysis, interference with its degradation through this arginine only resulted in mildly increased protein levels with negligible consequences on MpARF1 function and consequently, auxin signaling and plant development. This is in strong contrast to our finding that B-class MpARF2 degradation is critically required for biological function. We show that MpARF2 accumulates in essentially all cell- and tissue types across the Marchantia lifecycle when degradation is impaired, leading to severely derailed developmental programs. Finally, we demonstrate that MpARF2 function is contingent on its degradation through the proteosome, as dysregulation through proteolysis results in uncontrolled activity and a completely impaired transcriptional auxin response. Our findings point toward degradation mechanisms whose specificities are a product of evolutionary adaptation in the embryophyte lineage.

The A -and B-class ARFs represent two clades with deep evolutionary roots, and their common ancestry dates back to the very early stages of colonization of land by plants[23]. Most likely, the duplication of an ancestral AB-class ARF, which took place close to the origin of land plants (an event which likely occurred in an ancestor of all embryophytes), resulted in the lineages giving rise to the respective A -and B-class clades[23,29]. The A -and B-class ARFs then acquired specialized, antagonizing functions, wherein A-ARFs gained the ability to act as transcriptional activators while B-class ARFs tend to function as repressors[13,14,23]. In earlier work, we hypothesized that the DBD-mediated ARF instability arose in the AB-ARF ancestor of the A -and B-ARF clades, roughly 500-600 MYA[21]. Here we show that the same motif identified in B-ARF MpARF2 has similar, instability-conferring, properties within the context of the A-ARF MpARF1, thus providing further evidence supporting this hypothesis. However, the results presented here indicate that, although the DBDs of A -and B-ARFs are structurally and functionally deeply conserved, proteasomal degradation through signals embedded in this

DBD have either gained importance in B-ARFs or lost importance in A-ARFs[11,12]. Possibly, the ubiquitin-ligase adapter protein which targets ARFs may have coevolved with B-ARFs, resulting in higher binding affinity, and thus increased susceptibility for degradation. There is also the possibility of additional cofactors, which regulate substrate accessibility by the ubiquitin-ligase, which have evolved to target B-ARFs but not, or to lesser extent, A-ARFs. Such innovations would then enable more precise spatiotemporal control over MpARF2 levels, thereby permitting evolution of stronger repression capabilities and/or the ability to regulate new gene sets, whereas MpARF1 would only be weakly targeted and therefore evolved weaker abilities. Alternatively, B-ARFs might undergo post-translational modifications, of which there are sparse reports[20,30], which decrease its stability, e.g. by increasing affinity for the ubiquitin-ligase, whereas A-ARFs might be modified such that they are more protected from degradation. These theories require testing at the proteomics level. Many of these questions would be answered upon identification and proper functional characterization of said ubiquitin-ligase, which remains unidentified. A previously identified ubiquitin-ligase AUXIN RESPONSE FACTOR F-BOX1 (AFF1), which targets the Arabidopsis A-class ARFs AtARF7 and AtARF19[19], is not conserved in Marchantia and therefore, another ubiquitin-ligase must be involved.

Surprisingly, hampered MpARF1 degradation had barely any noticeable effects on MpARF1 function and plant development. We also observed that full-length MpARF1 proteins expressed from the *pro*Mp*UBE2* promoter accumulated to lower levels than each domain separately. Potentially, other domains of MpARF1 (the MR and PB1 domain) could, through a potential joint effort, contribute to its proteostasis. There are examples of A-class ARFs relying on their MR, such as AtARF7/19[19,31] and AtARF1[31], or on their PB1 domains[31,32] for degradation. Possibly, A-class ARFs have evolved multiple ways to be routed to the proteasome which are lacking or less-strong in B-class ARFs. Alternatively, MpARF1 degradation may not be solely reliant on R272, may require other protein domains, or might be of more significance under conditions not tested in this work. Furthermore, A-class ARF activity can also be inhibited through interactions with the Aux/IAA co-repressors, providing a reason for the lack of physiological effects when MpARF1 accumulation increased. Why then, did MpARF1 not lose degradation through the DBD? Since evolution of the DBD is known to be under high levels of evolutionary constraint, with little room for sub- or neofunctionalization[12], it is likely that the motif responsible for degradation is required for structural integrity of the MpARF1 DBD, and DNA-binding, thus pre-

venting changes to occur.

In summary, the work presented here reveals that, despite deep conservation of the ARF DBDs, the role of proteasome-mediated degradation has strongly diverged between A- and B-class ARFs, which likely reflects distinct evolutionary pressures and regulatory demands. The strict functional dependency of MpARF2 on proteolysis, which contrasts with the dispensability of MpARF1 degradation, may have been enabled or enforced by co-evolution with the degradation machinery or acquisition of unique regulatory mechanisms between the two classes during land plant evolution. Further deciphering of the precise mechanism of ARF proteolysis by the ubiquitin-proteasome system, which includes identifying the responsible ubiquitin-ligase, remains a crucial hurdle to address remaining questions, as answering these questions will be essential to fully understand tuning of auxin signaling. Ultimately, our findings suggest that diversification of functional requirements of ARF proteolysis may help explain how the simple signaling molecule auxin can orchestrate such a wide range of developmental processes in a precisely controlled manner.

Methods

Protein structure prediction & visualisation

The MpARF2 crystal structure was retrieved from PDB (https://www.rcsb.org/structure/6SDG)[13]. To model the MpARF1 structures, as well as the swap and mutated versions of the MpARF2 DBD, we employed AlphaFold2-multimer v2.2.2 with the default settings[33]. Structural visualisation was performed using Pymol (v2.3.4) software.

Net charge and sequence analysis

To quantify properties and evolutionary conservation of residues part of the degradation motif, we extracted this motif from an existing ARF resource[23]. For every organism in the dataset, we aligned ARF sequences with the Arabidopsis ARF sequences using Clustal Omega (default settings) and extracted the region flanking the degradation motif sequence using Arabidopsis AtARF5 as a reference. Next, all extracted regions were aligned together using Clustal Omega. These regions were used to create sequence LOGOs per ARF type (ABC, AB, A, B or C) using the ggseqlogo package (v0.2) in R. Furthermore, the net charge was calculated for every amino acid (windowsize = 1, Henderson-Hasselbalch equation) using the IDPR package (v1.8.0)[34] in R.

Plasmid construction

Plasmids which were generated for this study can be found in Supplementary Data Table 1. Promoters and cDNA-derived sequences were amplified through PCR from in-house plasmids mainly from Ref.[13,21,35]. The pMpGWB100 and pMpGWB300 backbones for the plasmids were from Ref.[36]. The motif swap of MpARF1 R272Q into the MpARF2 DBD-mNeonGreen fusion was generated based on the alignment in Ref.[21].

To generate the plasmids expressing MpARF2 fusion proteins (the mutagenesis screen, motif swaps and Mp*arf2-1* complementation) we used a *pro*Mp*ARF2* pMpGWB100 backbone (which contains an ~1.9kb *pro*Mp*ARF2* promoter upstream of an XbaI site, an in-frame mNeonGreen (mNG) coding sequence, followed by a tNOS[21]. Mutations were generated through site-directed PCR.

For MpARF1 fusion proteins, we generated *pro*Mp*UBE2* pMp-

GWB100 plasmids by inserting the ~3kb Mp*UBE2* promoter[35] into the XbaI site of pMpGWB100 together with the respective MpARF1 domains fused to mNG. For the *pro*Mp*MpARF2*::*NLS*-Mp*ARF1-DBD^{WT}-mNG* and *pro*Mp*MpARF2*::*NLS*- Mp*ARF1-DBD^{R272Q}-mNG* pMpGWB100 plamids we used the *pro*Mp*ARF2* pMpGWB100 backbone described above, and inserted the MpARF1 domains into the XbaI site. For MpARF1 complementation assays, we first cloned the full length MpARF1 sequences, C-terminally fused to mNG, into pDONR221 to generate pENTR221 MpARF1-FL^{WT}-mNG and pENTR221 MpARF1-FL-^{R272Q}-mNG. Next, expression vectors were generated through LR-reaction of entries and pHKDW046 (housed in the pMpGWB300 plasmid), which contains a ~4900bp Mp*ARF1* promoter upstream of the attR sites[13,36].

To clone mARF2^{flox}, we synthesized a fragment encoding a floxed SV40 Nuclear Localization Signal (NLS) fused to mScarlet3 (mSC3) and a tNOS terminator (loxP-NLS-mSc3-tNOS-loxP; Fig. 6a). We used our XbaI-digested *pro*Mp*ARF2* pMpGWB100 backbone (which contains an ~1.9kb *pro*Mp*ARF2* promoter cloned into the XbaI site, with the XbaI site regenerated) to insert the (from 5' to 3'): loxP-NLS-mSc3-tNOS-loxP fragment downstream of *pro*Mp*ARF2* together with the *MpARF2-mNG*-tNOS CDS and *pro*Mp*HSP*::*Cre-GR*-tNOS amplified from Ref.[37].

Oligonucleotide generation

Standard, desalted oligonucleotides were synthesized by IDT™. Oligonucleotides which were generated for this study can be found in Supplementary Data Table 2.

Plant growth conditions and transformation

For this study *Marchantia polymorpha* Takaragaike-1 (Tak-1) was used as the wild-type. Plants were grown on ½ strength Gamborg B5 medium (1% agar) at 22°C with 40 µmol photons $m^{-2}s^{-1}$ continuous white fluorescent light. Tak-1 was transformed using agrobacterium-mediated delivery of transgenic constructs as described by Ref.[38]. Transgenic plants were selected on ½ Gamborg B5 (1% agar) with 10 mg/L hygromycin and 100 µg/ml cefotaxime or 0.5 µM chlorsulfuron.

Analysis of genetically induced expression of MpARF2^{E+R}

Plants at the indicated developmental stages were placed in ½ strength Gamborg B5 medium, and treated with a 1 hour 37°C heat shock (HS) and/or 10 µM Dexamethasone (Dex, Sigma-Aldrich) dissolved in ethanol[37]. Afterwards, plants were placed back in their normal growth condition to recuperate, and phenotype parameters were scored. For determination of auxin response, gemmae were placed onto their respective media and immediately treated with 1 hour of HS.

For scoring of gemma cup formation, plants were grown from gemmae on ½ strength Gamborg B5 medium plates (1% agar) containing Mock (Ethanol) or Dex (10 µM) for seven days and were subsequently induced with 1 hour of HS. The number of gemma cups per plant were counted every three days using a Leica M205 stereomicroscope.

For scoring of antheridophore emergence, plants were grown from gemmae for 14 days from gemmae in plastic boxes, with ventilation, on ½ strength Gamborg B5 medium (1% agar) containing Mock (Ethanol) or Dex (10 µM). Plants were then induced with 1 hour of HS, and subsequently placed in 22°C with 40 µmol photons $m^{-2}s^{-1}$ continuous white fluorescent light supplemented with far-red light (50% power). The number of antheridiophores per plant were counted every three days using a Leica M205 stereomicroscope.

RNA-sequencing & Transcriptome analysis

For the Mp*arf2-1* mutant complementation, the indicated genotypes were ground into small fragments using a tissue homogenizer (Fisherbrand™ 150 homogenizer) and plated on ½ strength Gamborg B5 medium (1 % agar) and grown at 22°C with 40 µmol photons $m^{-2}s^{-1}$ continuous white fluorescent light for 14 days. Regenerated plant fragments were then cultured for 6 hours in liquid ½ strength Gamborg B5 medium with 50 µM Yuc and L-Kyn, respectively. Then, plantlets were washed and cultured in liquid ½ strength Gamborg B5 with 1 µM Indole-3-Acetic acid (Alfa Aesar), or an equal volume of DMSO in the mock condition, for 1 hour. Afterwards, plants were harvested, flash-frozen in liquid nitrogen and subsequently ground into a fine powder.

For Mp*arf1-4* mutant complementation analysis plants were grown for eight days from gemmae on standard ½ strength Gamborg B5 medium, without any treatments. Plants were then harvested

and directly frozen in liquid nitrogen and processed as described below.

For RNA extraction, ground tissue was incubated in 1 mL of TRIzol reagent for 5 min. at Room Temperature (RT). Next, 200 µL chloroform was added, samples were vortexed and incubated for an additional 3 min. at RT. Following this, samples were centrifuged for 15 min. at 12000g and 4°C, and the upper aqueous phase containing the RNA was transferred to a new tube and precipitated with 500 µL isopropanol for 10 min. at RT. Samples were then transferred to pink columns and processed further using the Qiagen RNeasy RNA purification kit, according to the manufacturer's instructions. RNA was sequenced using Illumina NovaSeq X plus by Novogene and checked for quality using FastQC (v0.11.9). Reads were then mapped to the *M. polymorpha* genome (v7.1) using Hisat2 (v2.2.1) and read counting was performed using FeatureCounts (v2.0.1). Read count normalization and differential expression analysis was performed through DEseq2 (v2.12), in which we excluded genes with a cumulative read count of <30 reads across all samples. We provide our analysis as a basic script on GitHub (https://git.wur.nl/bic/2025_auxinrespdiversification_martijn). Gene Ontology analysis was achieved using PlantRegMap using genelists as input of up -and downregulated genes respectively. PlantRegMap queries TAIR10 and UniProtKB databases to obtain GO terms, therefore most GO terms are based on homology to Arabidopsis.

In the Mp*arf1-4* mutant complementation experiment, Differentially Expressed Genes (DEGs) were defined as having a ^{2}Log Fold Change below and above -1 and 1, respectively (P_{adj}<.05). For the Mp*arf2-1* mutant complementation and auxin response experiment, we defined a ^{2}Log Fold Change below and above -0.5 and 0.5 as cutoffs, respectively (P_{adj} <.05).

Confocal microscopy & Assessment of fusion protein stability

Confocal microscopy was carried out with a Leica SP8X-SMD confocal microscope fitted with hybrid detectors and a 40 MHz pulsed white-light laser. Data acquisition was performed using LasX (v3.5.7.23225) software. The fluorophore mNeonGreen was excited using 488 nm laser line, and mScarlet3 with a 561 nm laser line. Fluorescence was detected between 500-570 nm (mNeonGreen) or 573-640 nm (mScarlet3) with hybrid detectors set to photon counting mode with 1.00-24.50 ns time-gating active to suppress background fluorescence. Z-stacks were acquired using an HC PL APO

20x/0.75 water immersion or APO CS 10x/0.40 air objective. The same settings were used for all samples within experiments. ImageJ (v1.52) was used to generate maximum-intensity projections, measure fluorescence intensities and produce micrographs for figures.

When investigating stability of MpARF2-DBD-mNG fusion proteins carrying different mutations, we screened T1 transgenic lines for fluorescence by imaging the apical notch region of dormant gemmae. When no fluorescence was detected, we treated these gemmae with Bortezomib (Cayman Chemical) for 24 h or the solvent DMSO (Sigma-Aldrich) as a Mock control and checked for fluorescence again. Transgenic lines which showed no nuclear mNeonGreen fluorescence after Bortezomib treatment were excluded from the analysis. To quantify average fluorescence, we generated ROIs by tracing the outline of gemmae. To measure the background signal, we created ROIs which excluded nuclei, obtained the average intensity and corrected the original measurement by subtraction of the average background signal per pixel. For quantification of rhizoid initial cells, we drew ROIs around the respective nuclei and measured the average intensity.

When imaging gemmae over time, an imaging chamber was created by placing five 25 µL Gene Frames (Thermo Scientific) onto an objective glass, which was then filled with ½ strength Gamborg B5 medium (1% agar) with the indicated treatments. Gemmae were placed onto the medium, and the imaging chambers were filled with Perfluordecalin (Sigma-Aldrich) to allow gas exchange. Chambers were sealed with a coverslip, when not being imaged, slides were placed in their normal growth conditions.

To quantify the projected area of rhizoid founder cells, dormant gemmae of 18-day-old old plants were stained with 10 µg/mL Propidium Iodide (PI) and directly imaged through confocal microscopy. PI and chlorophyll were excited at 490 nm and 560 nm, respectively. Fluorescence was detected between 568-641 nm (PI) or 685-700 nm (chlorophyll). The PI signal was segmented using a custom python script using the OpenCV package. First, the cell walls were segmented using the local NiBlack algorithm (windowsize 15) of OpenCV (v4.12.0). The thresholded image was dilated and eroded with a kernel of 3x3 and skeletonized. Cells and corresponding areas were then extracted using contour finder (OpenCV). The script for this analysis can be found in the following GitHub repository (https://git.wur.nl/bic/2026_rhizoidcellmeasurements_martijn). Rhizoid founder cells were manually annotated based on the lack of chlorophyll autofluorescence and the stronger PI staining.

Phenotype analysis

For experiments assessing fluorescence accumulation, non-chimeric transgenic lines were established by growing a G_1 generation from gemmae of independent plants that appeared resistant to initial selection on hygromycin or chlorsulfuron (T_1 generation). Gemmae from the G_1 generation were used for experiments. To assess the phenotypes of plants expressing the full length MpARF1 fusion proteins, we reported on phenotypes of 20-day old plants. To assess the morphology and formation of gemma cups and air pores, plants were grown for two and three weeks, respectively. Air pores were imaged in the central zone of plants, as this tissue is the oldest and fully differentiated (Supplementary Information Fig. 6c). To assess rhizoid elongation, plants were grown vertically for seven days, and the distance from the center of the thallus to the tip of the longest rhizoid (contacting the medium) was measured (Supplementary Information Fig. 7b). For growth assays, dormant gemmae were micro dissected from the gemmae cups/thallus and lightly placed onto the respective medium. For general overviews or thallus size quantifications, pictures were taken with a Canon EOS250D camera and thallus area was measured using ImageJ (v1.52). For higher magnification images a Leica M205 and Keyence VHX stereomicroscope fitted with a 20-200x VH-Z20R objective were used.

Statistics & reproducibility

Statistical tests were performed in R (v4.2.1). Tests, parameters, additional statistical information and the nature of biological replicates are provided in figure descriptions and Source Data. Sample sizes are shown within the figures themselves, and their nature is described in figure descriptions. No statistical method was used to predetermine sample size; sample sizes were determined according to field standards. Experiments were not randomized. Representative micrographs are shown which reflect the average values in the corresponding quantitative experiments (as indicated) or the number of individuals that are analyzed are explicitly stated in the figure legends.

Data and materials availability

Plasmids generated and used in this study are available upon request from the corresponding author. As long-term storage of *Marchantia polymorpha* lines is problematic, we can provide some lines analyzed in this study, contact the corresponding author for in-

quiries. The RNA-sequencing data generated in this study have been deposited on NCBI under BioProject accession code PRJNA1313408. The raw quantitative values measured and presented in this study are included in the Source Data file provided with this paper.

Code availability

The RNA-sequencing analysis script is deposited on GitHub (https://git.wur.nl/bic/2025_auxinrespdiversification_martijn). Similarly, the analysis script for rhizoid initial cell detection was also deposited on GitHub (https://git.wur.nl/bic/2026_rhizoidcellmeasurements_martijn).

Acknowledgments

We would like to thank Jorge Hernández-García, Jiashu Chu, Eduardo Flores-Sandoval, and Juriaan Rienstra for helpful discussions regarding this work. Furthermore, we thank Danilo dos Santos Pereira for assistance with the transcriptome analysis and creating the GitHub repositories, and Emi Hainiwa, Hidemasa Suzuki, and Takayuki Kohchi for their efforts in isolating the Mp*arf2-1* mutant. This work has been supported by the Netherlands Organization for Scientific Research (NWO; OCENW.M20.031 M.d.R., J.W.B.), Research Grant from the Human Frontiers Research Program (HFSP; grant RGP0015/2022 D.W.), and European Research Council (CoG Catch; grant 101000981 J.L.). JSPS KAKENHI (JP18H04836, JP20H04884, and JP22H04733, R.N.), and Tokyo University of Science Research Grants (R.N.).

Author contributions

Conceptualization: M.d.R, D.W.

Methodology: M.d.R, D.W.

Investigation: M.d.R., E.H., D.W., J.L., R.N.

Visualization: M.d.R.

Supervision: J.W.B., D.W.

Writing—original draft: M.d.R, D.W.

Writing—review & editing: M.d.R, D.W.

Competing interests

All other authors declare they have no competing interests.

Supplementary Information

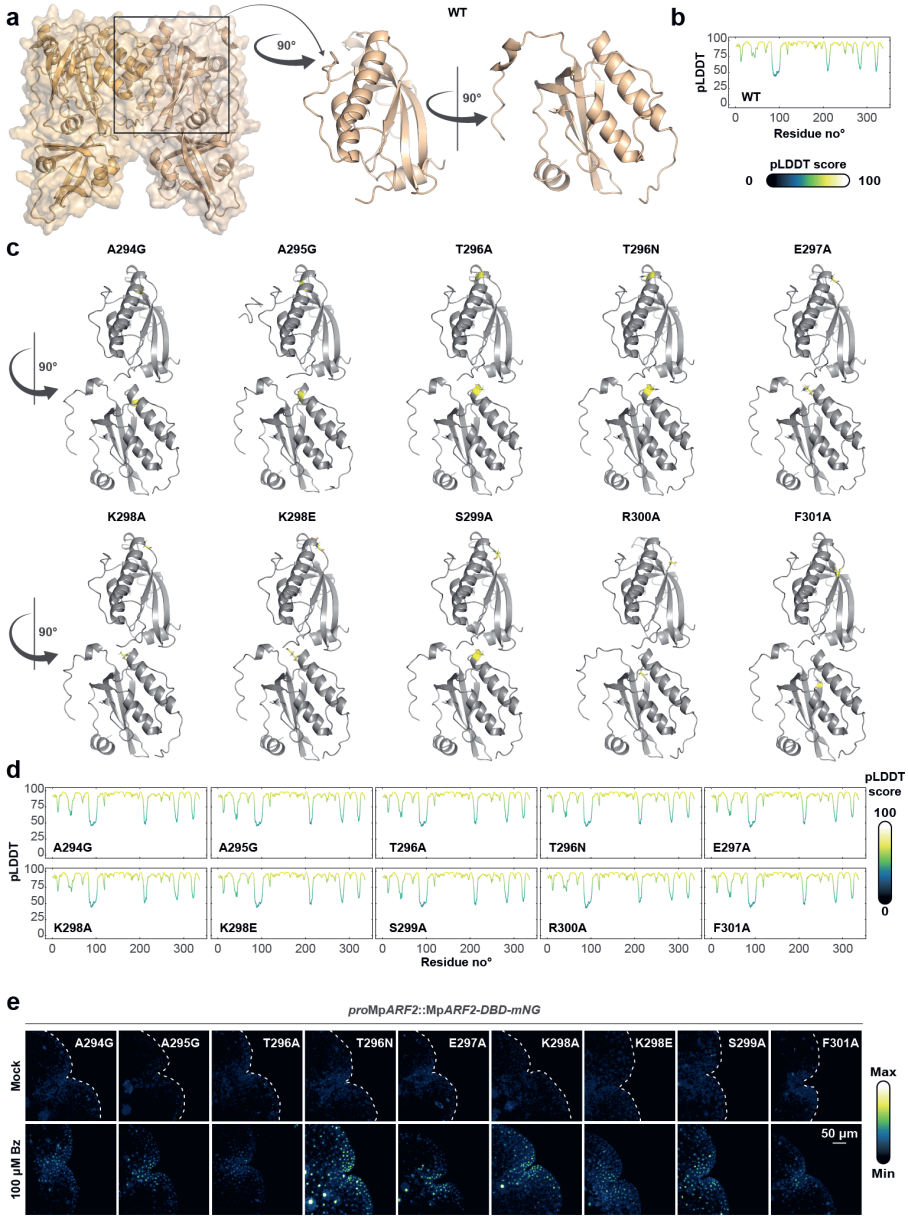


Fig. 1 | Structural modeling and stability of MpARF2 DBD variants.
a. Structural models generated by AlphaFold2 of the MpARF2 DBD (orange) as a homodimer, and the structure containing the loop with relevant residues is outlined and enlarged. **b.** The predicted Local Distance Difference Test (pLDDT) score for the AlphaFold2 model presented in (**a**). **c.** AlphaFold2 models of the MpARF2 DBD with indicated point mutations, the relevant residue is colored by element (yellow).

(continued on next page)

Fig. 1 (continued) | d. The predicted Local Distance Difference Test (pLDDT) scores for the AlphaFold2 models presented in (**c**) **e.** Accumulation patterns of *pro*M-p*ARF2*::Mp*ARF2-DBD-mNeonGreen* fusions, carrying the indicated mutations, treated for 24 hours with Bortezomib (Bz) or Mock.

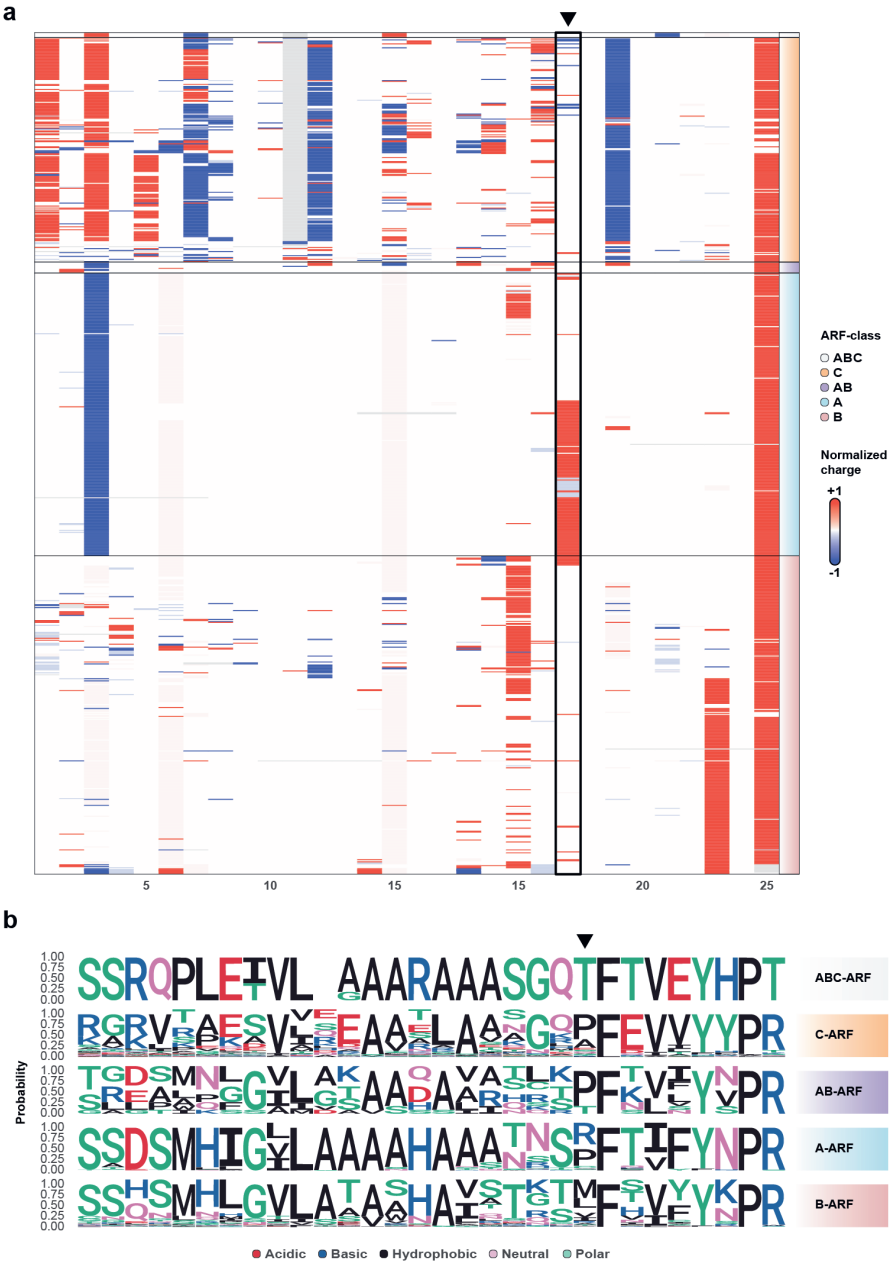


Fig. 2 | A broad alignment of ARF sequences shows charge conservation. **a.** Protein sequence alignment of 852 streptophyte-derived ARF sequences representing the A, B, AB, C, and ABC clades, as indicated. Normalized amino acid side chain charges are shown for the region of interest. **(continued on next page)**

Fig. 2 (continued) | b. LOGO analysis depicting residue conservation of amino acids comprising the degradation-conferring motif, color coded by biochemical properties. (**a** and **b**) MpARF1 R272 and MpARF2 R300 are indicated by a black triangle.

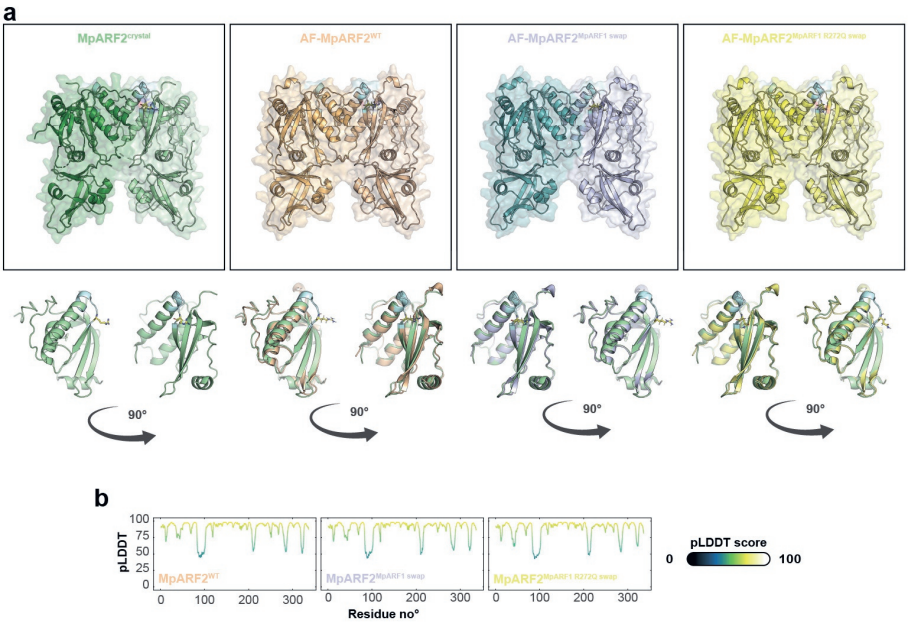


Fig. 3 | Structural modeling of the MpARF2 DBD and mutant versions.
a. Structure of the MpARF2 DBD crystal (green) separately and overlain on Alpha-Fold2 models of a WT (orange) and mutant versions of the MpARF2 DBD as indicated. **b.** The predicted Local Distance Difference Test (pLDDT) scores for the AlphaFold2 models presented in (**a**)

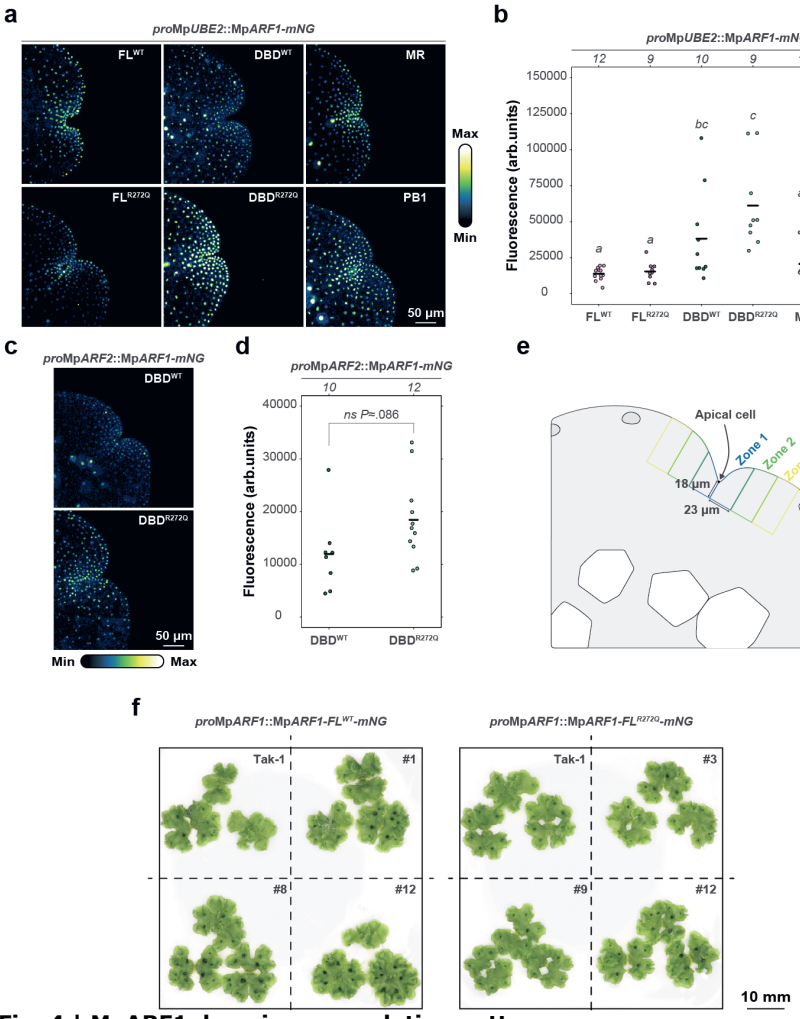


Fig. 4 | MpARF1 domain accumulation patterns.
a. Representative confocal images of accumulation patterns of dormant gemmae expressing protein fusions of MpARF1 to mNeonGreen as indicated. Fusion proteins are expressed from the constitutive Mp*UBE2* promoter. **b.** Quantification of overall fluorescence in a number of independent transgenic lines of which one is shown in (**a**). Sample size is shown above the figure and corresponds to measurements of a gemma each from an independent transgenic line. Letters in italics indicate significant differences determined per one-way ANOVA (F=(5,56)=12.83, P≈2,54x10^{-8}) and Tukey HSD post hoc test with Bonferroni correction (P<.05). **c.** Representative confocal images of MpARF1 DBD-mNeonGreen fusions expressed from a *pro*Mp*ARF2* promoter. **d3.** Quantification of overall fluorescence in gemmae, same experiment as (**c**), compared by T-test (P<.05). Sample size is shown above the figure and corresponds to measurements of a gemma each from an independent transgenic line. **e.** Illustration showing an arbitrary subdivision of the apical notch meristematic region into three zones, positioned relative to the apical cell. **f.** Representation of the overall morphology of 20-day old Tak-1 plants and Tak-1 plants carrying an extra copy of *pro*Mp*ARF1*::Mp*ARF1-FL*^{WT}*-mNG* or *pro*Mp*ARF1*::Mp*ARF1-FL*^{R272Q}*-mNG*. (**b** and **e**) Exact *P*-values are provided in the Source dataset. (**a** and **b**). Abbreviations: FL; Full Length, DBD; DNA-binding domain, MR; Middle Region, PB1; Phox and Bem 1.

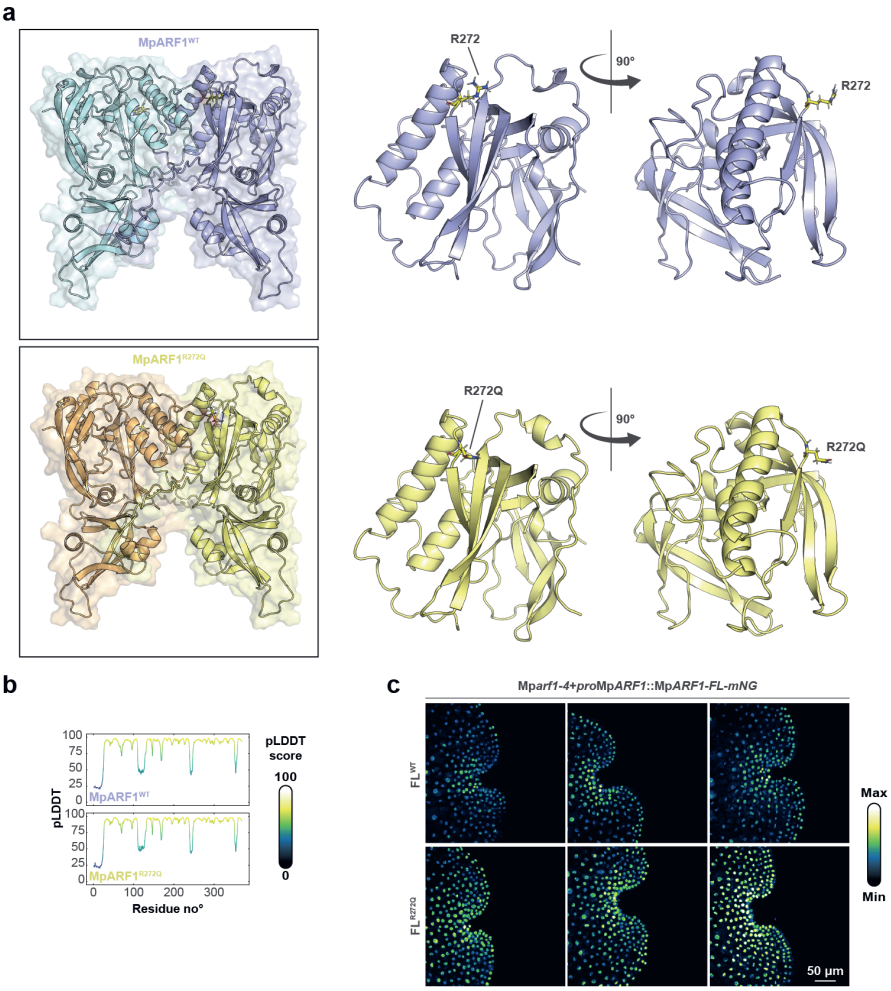


Fig. 5 | Structural predictions and *in vivo* analysis of the MpARF1 DBD R272Q variant.
a. AlphaFold2 models of the MpARF1 DBD structure as a homodimer (WT in blue and purple, R272Q mutant in orange and yellow), and a zoomed in region harboring the R272 or R272Q residue (highlighted). **b.** The predicted Local Distance Difference Test (pLDDT) scores for the AlphaFold2 models presented in (**a**). **c.** Three additional, independent, transgenic lines of the Mp*arf1-4* mutant complemented with *pro*Mp*ARF1*::Mp*ARF1-FL*^{WT}*-mNG* (FL^{WT}) and *pro*Mp*ARF1*::Mp*ARF1-FL*^{R272Q}*-mNG* (FL^{R272Q}) proteins, to supplement micrographs shown in Main Fig. 4a. These lines represent the means of Main Fig. 4b.

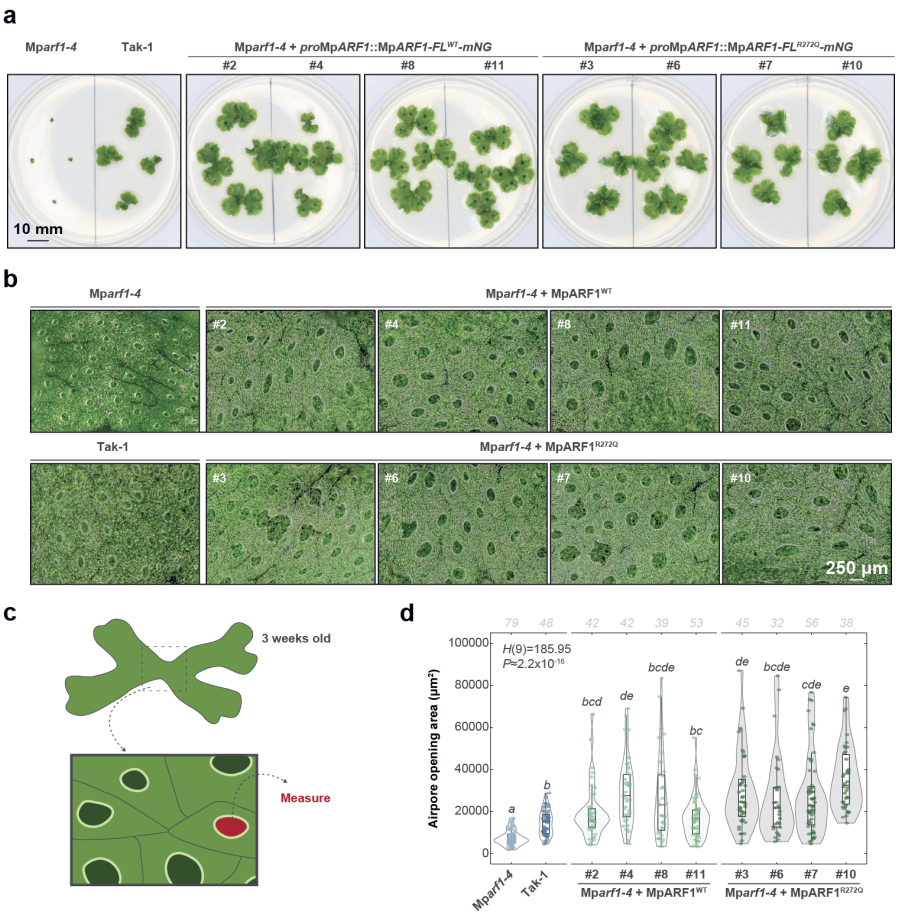


Fig. 6 | Restoration of air pore formation in Mp*arf1-4* by a WT or R272Q Mp*ARF1* copy.
a. Overall phenotypes of plants aged 20 days, grown from gemmae, of the indicated phenotypes. **b.** Detailed images of air pores in differentiated tissues of the indicated genotypes which were grown for three weeks from gemmae. **c.** Illustration highlighting in which tissue of three-week old plants air pores were imaged and how air pore opening area was measured. **d.** Quantification of the total surface area of air pores (as shown in **c**) of indicated genotypes. Air pore opening area was statistically compared by Kruskal-Wallis with Dunn post hoc test ($P<.05$), test statistics are shown within the figure. Italics denote significant differences. Exact *P*-values are provided in the Source dataset and sample size is shown above the figure. Italics denote significant differences.

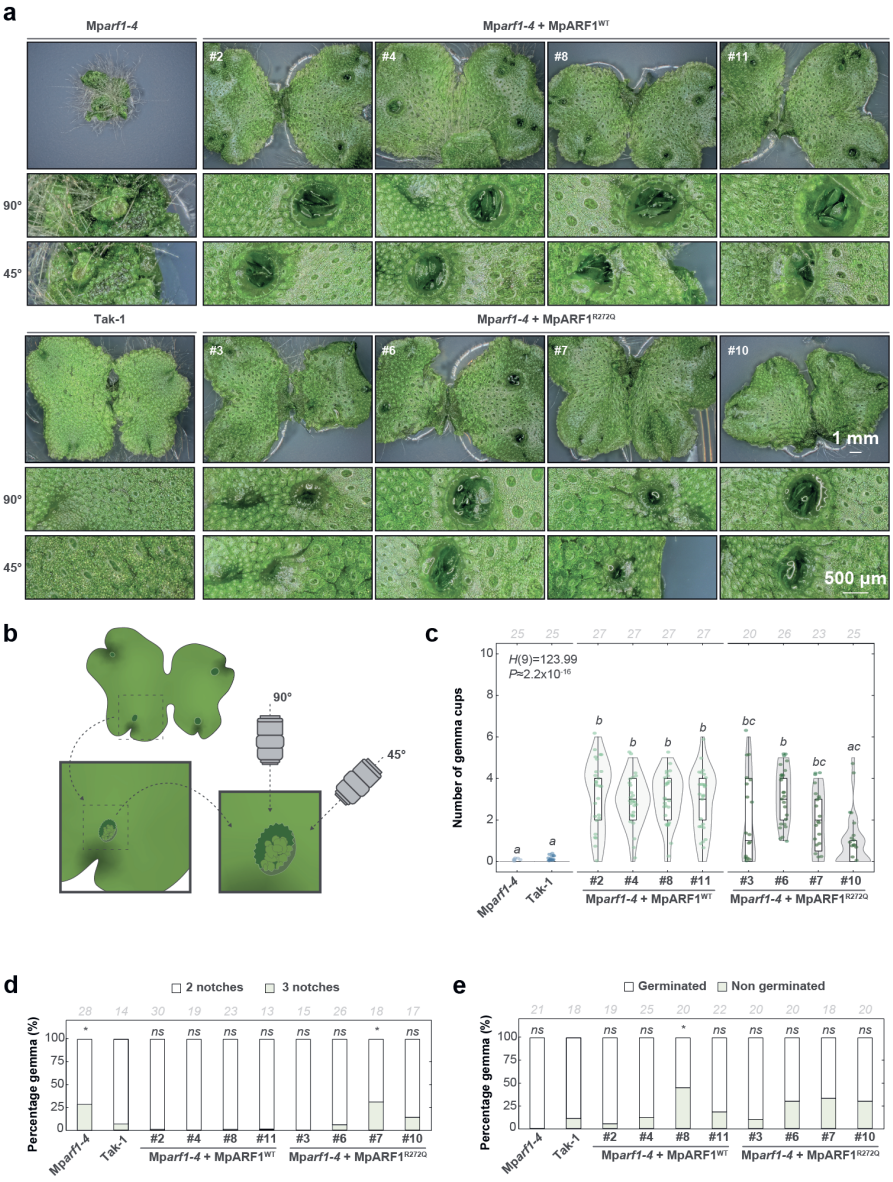


Fig. 7 | Restoration of gemma and gemma cup formation in Mp*arf1-4* by a WT or R272Q Mp*ARF1* copy.
a. Overall phenotypes of plants aged 14 days, grown from gemmae, of the indicated phenotypes. Gemma cup formation was assessed, and gemma cups were imaged from above (90°) or the side (45°). **b.** Illustration showing imaging angles of images shown in (**a**). **c.** The number of gemma cups containing gemmae was quantified and statistically compared by Kruskal-Wallis with Dunn post hoc test (P<.05), test statistics are shown within the figure. Italics denote significant differences. **d.** Comparison of the number of apical notches found in gemmae of the indicated genotypes. **e.** Comparison of the percentage of germinated and non-germinated gemmae (after 24 hours of growth) of the indicated genotypes. **(continued on next page)**

Fig. 7 (continued) | (**d** and **e**) Frequencies were compared per Fishers exact test (* *P*<0.05) versus Tak-1, ns is not-significant. (**c,d,e**) Exact *P*-values are provided in the Source dataset and sample size is shown above the figure. Italics denote significant differences.

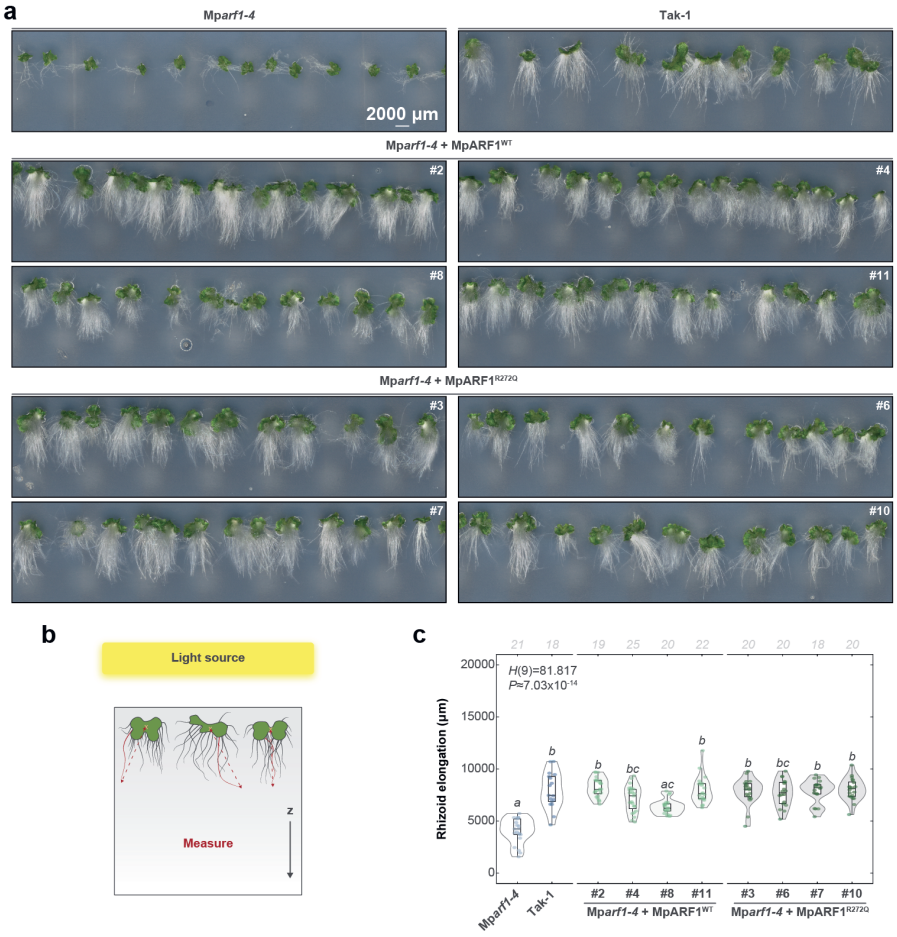


Fig. 8 | Restoration of rhizoid elongation in Mp*arf1-4* by a WT or R272Q Mp*ARF1* copy.
a. Quantitative comparison of seven-day-old gemmalings of the indicated genotypes grown vertically to assess rhizoid formation and elongation. **b.** schematic illustration showing how quantification of rhizoid elongation was performed, a straight line from the center of the thallus was drawn towards the tip of the longest rhizoid. **c.** Quantification of rhizoid elongation (as shown in **b**) of the indicated genotypes. Rhizoid length was statistically compared by Kruskal-Wallis with Dunn post hoc test (*P*<.05), test statistics are shown within the figure. Exact *P*-values are provided in the Source dataset and sample size is shown above the figure. Italics denote significant differences.

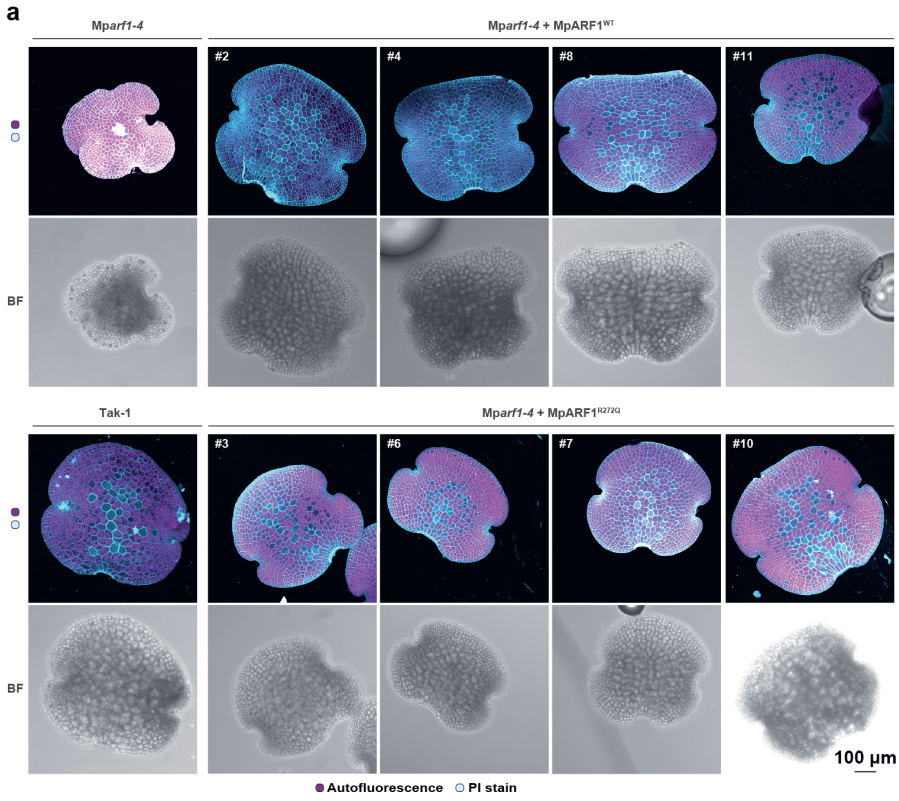


Fig. 9 | Rhizoid initial cell size is not affected in the R272Q mutant.
a. Confocal images of dormant gemmae of the indicated. Plasma membranes were stained with propidium iodide (PI) shown in cyan. Chloroplast autofluorescence was captured and is shown in magenta, this shows positioning of rhizoid initial cells. **b.** schematic illustration showing how quantification of rhizoid initial cell size was performed. Rhizoid initial cells can be recognized by size (larger than surrounding cells) and shape (more angular) and a lack of large chloroplasts. Rhizoid initial cells were outlined using an in-house script (and manually curated) and their surface area was measured. **c.** Quantification of rhizoid initial cell surface area (as shown in **b**) of the indicated genotypes. Cell size was statistically compared by Kruskal-Wallis with Dunn post hoc test (P<.05), test statistics are shown within the figure. Exact P-values are provided in the Source dataset and sample size is shown above the figure. Italics denote significant differences.

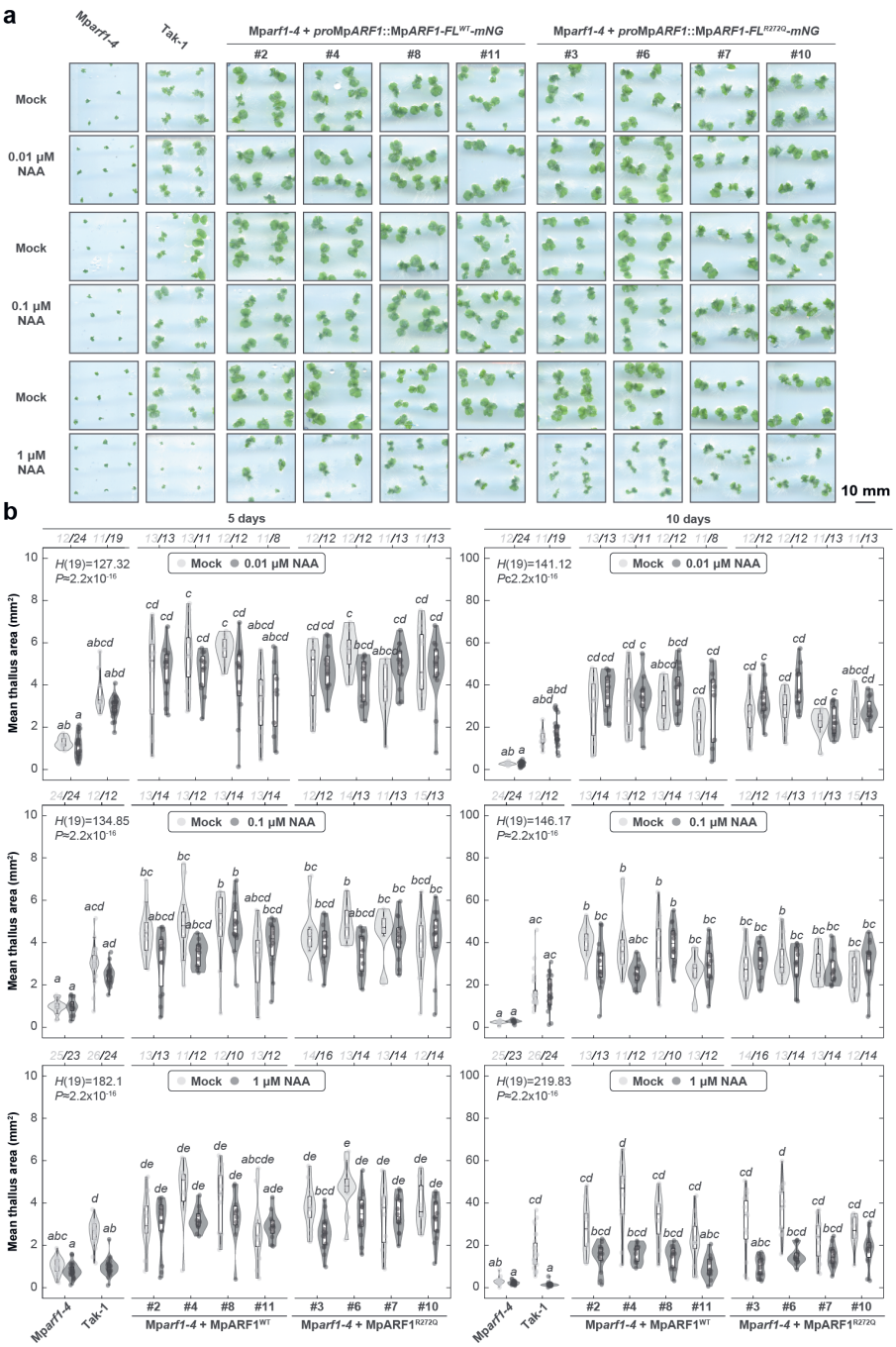


Fig. 10 | Sensitivity of Mp*arf1-4* complementation lines to a range of NAA concentrations.
a. Overview of general growth of the indicated genotypes (top) grown on a range of NAA concentrations (left) for five days. **(continued on next page)**

Fig. 10 (continued) | b. Quantification of projected thallus area of plants of indicated genotypes grown on medium with 1, 0.1 and 0.01 µM NAA for five and seven days, respectively. Projected thallus areas was statistically compared by Kruskal-Wallis with Dunn post hoc test (P<.05), test statistics are shown within the figures. Italics denote significant differences.

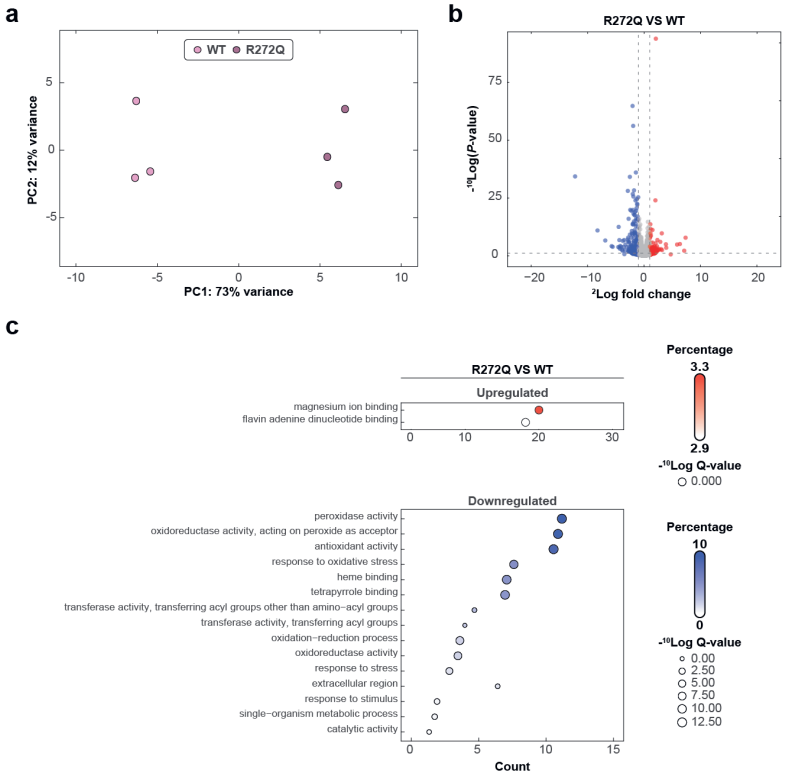
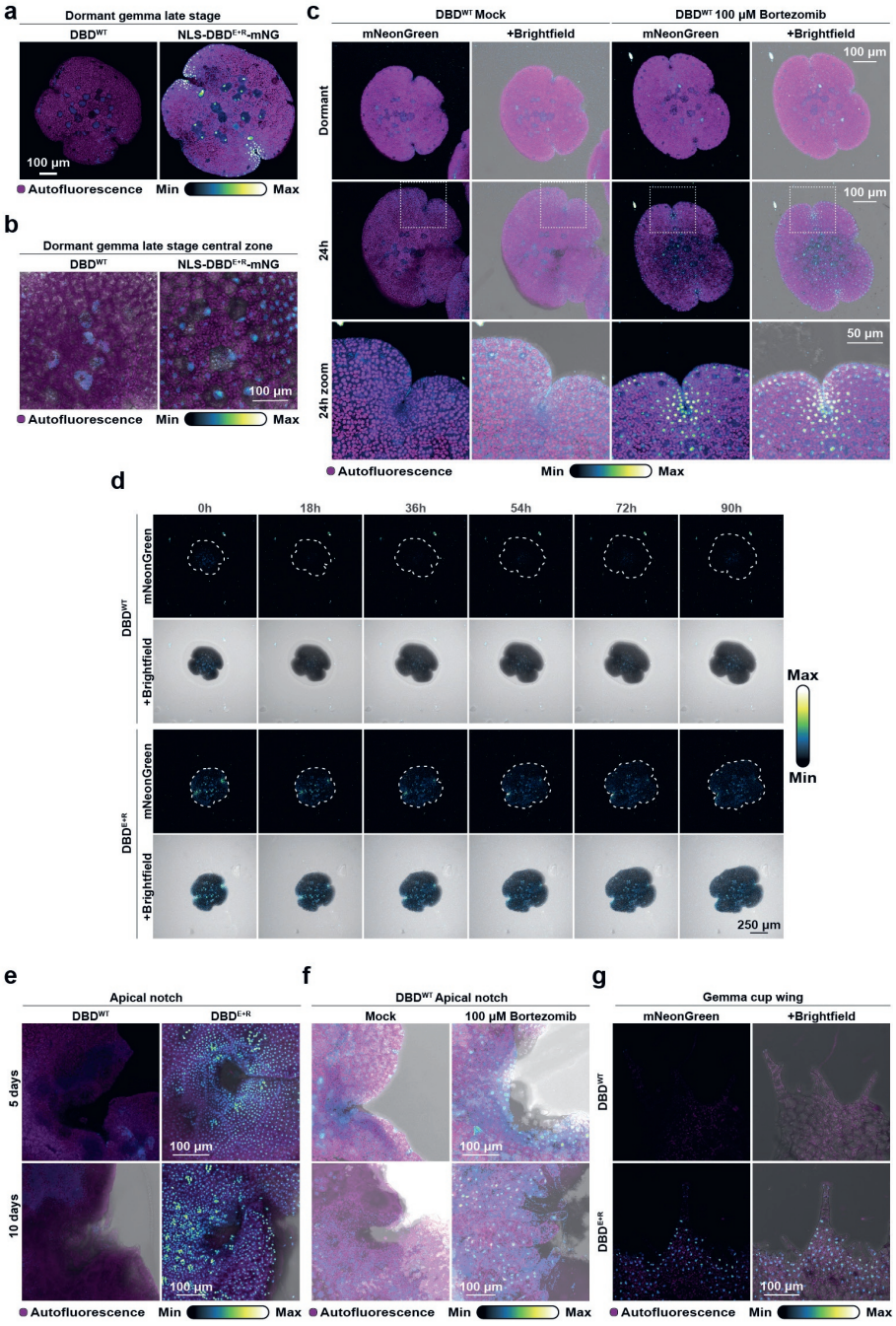
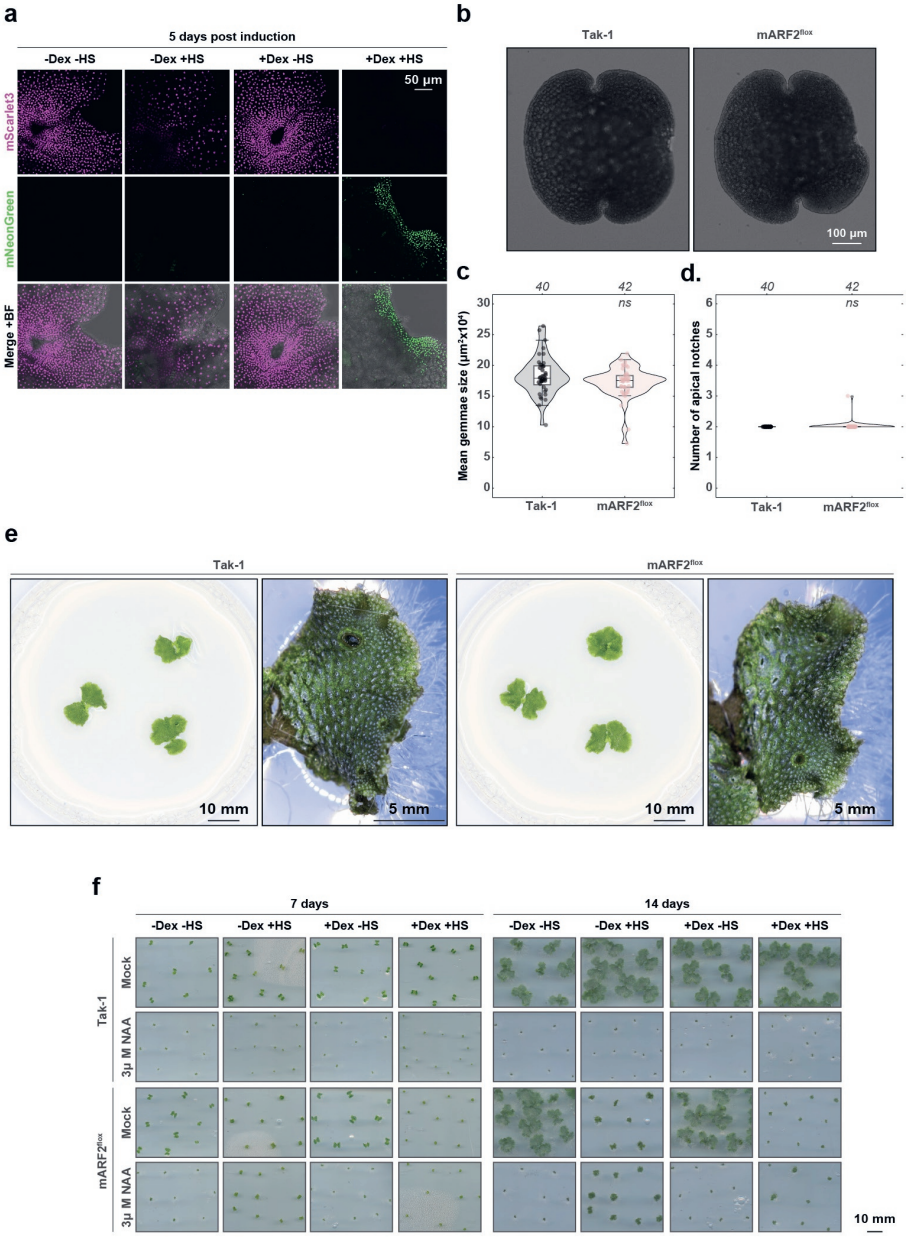


Fig. 11 | Transcriptome analysis of Mp*arf1-4* complementation lines.
a. Principal component analysis of eight-day old plants of the Mp*arf1-4* mutant complemented with MpARF1 FL^{WT} and FL^{R272Q} copies. Three biological replicates for both genotypes were studied. **b.** Volcano plot showing differentially expressed genes between Mp*arf1-4* complemented with *pro*Mp*ARF1*::Mp*ARF1-FL*^{WT}*-mNG* and *pro*Mp*ARF1*::Mp*ARF1-FL*^{R272Q}*-mNG*. Genes were deemed differentially expressed when -1<^{2}Log(Fold Change)>1 and P_{adj}<.05. Genes which were significantly downregulated are blue, genes which are significantly upregulated are red. **c.** Differentially expressed genes of (**b**) were used as input for gene ontology enrichment analysis. Only two terms were significantly enriched in the upregulated gene set and are shown in red, the top 15 for the downregulated gene set is shown in blue.



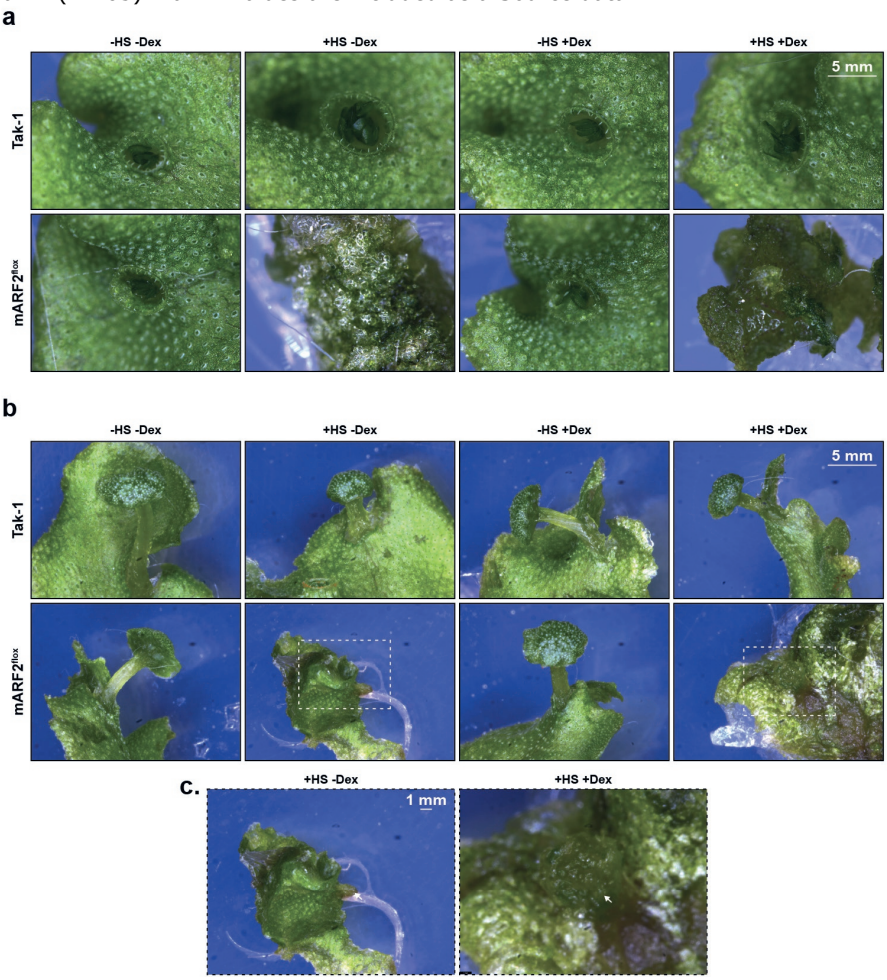
Supplementary Fig. 12 | Developmental regulation and proteasome-dependent accumulation of MpARF2.
a. Micrographs depicting DBD^{WT} or DBD^{E+R} expressing gemmae in a late developmental stage. **(continued on next page)**

Supplementary Fig. 12 (continued) | b. Zoom in on central cells of a gemmae expressing DBD^{WT} or DBD^{E+R}. **c.** DBD^{WT} treated with 100 μM Bortezomib (Bz) or Mock, for 24 hours. A portion of the image is outlined and enlarged below. **d.** Timeseries experiment of gemmae expressing DBD^{WT} or DBD^{E+R} imaged during the early stages of gemmae germination at indicated timepoints. **e.** Accumulation patterns of DBD^{WT} or DBDE+R in apical notches of plants of indicated ages. **f.** DBD^{WT} accumulation patterns in apical notches treated with 100 μM Bortezomib (Bz) or Mock, for 24 hours. Plants are five days (top row) and ten days (bottom row) old, respectively. **g.** DBD^{WT} or DBD^{E+R} accumulation patterns in wings of gemma cups. (**a** to **g**) Abbreviations: DBD^{WT} is *pro*Mp*ARF2*::*MpARF2-DBD^{WT}-mNG* and DBD^{E+R} is *pro*Mp*ARF2*::Mp*ARF2-DBD^{E+R}-mNG*.



Supplementary Fig. 13 | Characterization of mARF2^{flox} editing and baseline developmental phenotypes.
a. Micrographs showing representative editing patterns of mARF2^{flox} five days after induction with heat shock (HS) and Dexamethasone (Dex) treatment. BF; Brightfield. **b.** Morphology of gemmae of Tak-1 and mARF2^{flox} plants without induction. **c.** Mean dormant gemmae size of Tak-1 and uninduced mARF2^{flox} plants. Boxplots show the following statistical parameters: central line, median; upper bound, first quartile; lower bound, third quartile; whiskers show the highest and lowest values, respectively, within 1.5*inter-quartile range (IQR). **(continued on next page)**

Supplementary Fig. 13 (continued) | d. Average number of apical notches per gemmae of Tak-1 and uninduced mARF2^{flox} plants, same experiment as (**c**). Boxplots show the following statistical parameters: central line, median; upper bound, first quartile; lower bound, third quartile; whiskers show the highest and lowest values, respectively, within 1.5*inter-quartile range (IQR). **e.** Phenotypic overview of uninduced mARF2^{flox} and Tak-1 plants, grown from gemmae for 14 days in normal growth conditions and on medium without treatment. **f.** Overview of general growth of Tak-1 and mARF2^{flox} plants grown on 3 µM NAA or Mock. Plants received a variety of treatments, as indicated by the different combinations of heat shock (HS) and Dexamethasone (Dex), shown above the figure. (**c** and **d**) Sample size (individual gemmae) is indicated above the figure. T-tests were used to determine statistical differences from Tak-1 (P<.05). Raw P-values are included as a Source data.



Supplementary Fig. 14 | Conditional mARF2^{flox} induction disrupts organogenesis.
a. Representative images showing gemmae cup morphology of Tak-1 and mARF2^{flox} plants which received HS and/or Dex treatments. **b.** Representative images of the morphology of antheridiophores (or in mARF2^{flox} +HS and +HS+Dex, putative antheridiophore-related structures) of Tak-1 and mARF2^{flox} plants which received the indicated HS and/or Dex treatments. **c.** Enlargement of the outlined regions shown in (**b**). (**a** to **c**) Abbreviations; heat shock (HS) and Dexamethasone (Dex).

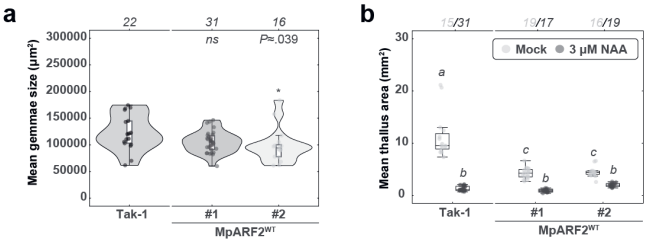


Fig. 15 | Growth phenotypes of MpARF2-FL^{WT}–complemented Mp*arf2-1* plants.
a. Mean gemma size of gemmae from Tak-1 as well as from the Mp*arf2-1* mutant plants complemented with *pro*Mp*ARF2*::Mp*ARF2-FL^{WT}-mNG*. Size was compared per T-test (P<.05). **b.** Projected thallus area of gemmalings grown on µM NAA or Mock for ten days. Compared are Tak-1 plants and Mp*arf2-1* mutant plants complemented with *pro*Mp*ARF2*::Mp*ARF2-FL^{WT}-mNG*. Mean projected thallus area was compared by Kruskal-Wallis test (H(5)=101.38, $P\approx 2.2\times10^{-16}$) with a Dunn post hoc test (P<.05). (**a** and **b)** Exact P-values can be found in the Source data. Boxplots show the following statistical parameters: central line, median; upper bound, first quartile; lower bound, third quartile; whiskers show the highest and lowest values, respectively, within 1.5*inter-quartile range (IQR).

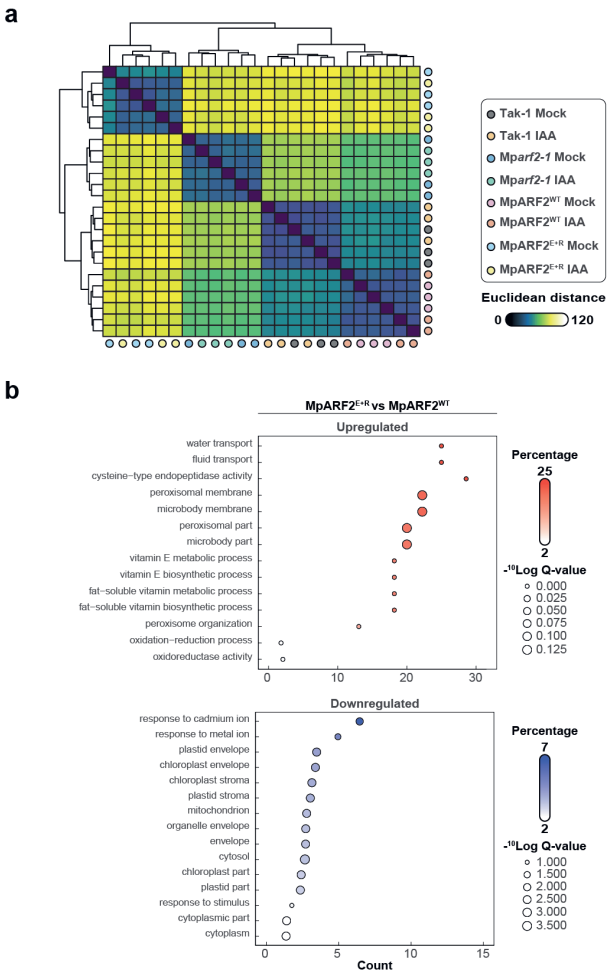


Fig. 16 | Transcriptomes of Mp*arf2-1* mutant complementation lines.
a. Hierarchical clustering of color-coded genotypes (Tak-1, the Mp*arf2-1* mutant and complementation lines), treated with Mock or IAA, as indicated. **b.** Gene Ontology (GO) analysis, depicting the top 15 most enriched GO terms found in the up -and downregulated gene sets of MpARF2^{E+R} vs MpARF2^{WT} in Mock conditions.

Supplementary Data Table 1 | Plasmids used in this study.

no°	Backbone	Plant^{res}	Bacterial^{res}	Contains
1	pMpGWB100	Hygromycin	Spectinomycin	*pro*Mp*UBE2*::*NLS*-Mp*ARF1-DBD*^{WT}-*mNG*-tNOS
2	pMpGWB100	Hygromycin	Spectinomycin	*pro*Mp*UBE2*::*NLS*- Mp*ARF1-DBD*^{R272Q}-*mNG*-tNOS
3	pMpGWB100	Hygromycin	Spectinomycin	*pro*Mp*UBE2*::*NLS*- Mp*ARF1-FL*^{WT}-*mNG*-tNOS
4	pMpGWB100	Hygromycin	Spectinomycin	*pro*Mp*UBE2*::*NLS*- Mp*ARF1-FL*^{R272Q}-*mNG*-tNOS
5	pMpGWB100	Hygromycin	Spectinomycin	*pro*Mp*UBE2*::*NLS*- Mp*ARF1-MR-mNG*-tNOS
6	pMpGWB100	Hygromycin	Spectinomycin	*pro*Mp*UBE2*::*NLS*- Mp*ARF1-PB1-mNG*-tNOS
7	pMpGWB100	Hygromycin	Spectinomycin	*pro*Mp*UBE2*::*NLS*- Mp*ARF1-FL*^{WT}-*mNG*-tNOS
8	pMpGWB100	Hygromycin	Spectinomycin	*pro*Mp*ARF1*::*NLS*- Mp*ARF1-FL*^{R272Q}-*mNG*-tNOS
9	pMpGWB100	Hygromycin	Spectinomycin	*pro*Mp*ARF2*::*NLS*- Mp*ARF1-DBD*^{WT}-*mNG*-tNOS
10	pMpGWB100	Hygromycin	Spectinomycin	*pro*Mp*ARF2*::*NLS*- Mp*ARF1-DBD*^{R272Q}-*mNG*-tNOS
11	pMpGWB300	Chlorsulfuron	Spectinomycin	*pro*Mp*ARF1*:: Mp*ARF1-FL*^{WT}-*mNG*-tNOS
12	pMpGWB300	Chlorsulfuron	Spectinomycin	*pro*Mp*ARF1*:: Mp*ARF1-FL-*^{R272Q}-*mNG*-tNOS
13	pMpGWB100	Hygromycin	Spectinomycin	*pro*Mp*ARF2*::*NLS*- Mp*ARF2-DBD*^{WT}-*mNG*-tNOS
14	pMpGWB100	Hygromycin	Spectinomycin	*pro*Mp*ARF2*::*NLS*- Mp*ARF2-DBD*$^{E297K+R300Q}$-*mNG*-tNOS
15	pMpGWB100	Hygromycin	Spectinomycin	*pro*Mp*ARF2*::*NLS*- Mp*ARF2-FL*^{WT}-*mNG*-tNOS
16	pMpGWB100	Hygromycin	Spectinomycin	*pro*Mp*ARF2*::*NLS*- Mp*ARF2-FL*$^{E297K+R300Q}$-*mNG*-tNOS
17	pMpGWB100	Hygromycin	Spectinomycin	mARF2^{flox}
18	pMpGWB100	Hygromycin	Spectinomycin	*pro*Mp*ARF2*::*NLS*- Mp*ARF2-DBD*^{A294G}-*mNG*-tNOS
19	pMpGWB100	Hygromycin	Spectinomycin	*pro*Mp*ARF2*::*NLS*- Mp*ARF2-DBD*^{A295G}-*mNG*-tNOS
20	pMpGWB100	Hygromycin	Spectinomycin	*pro*Mp*ARF2*::*NLS*- Mp*ARF2-DBD*^{T296N}-*mNG*-tNOS
21	pMpGWB100	Hygromycin	Spectinomycin	*pro*Mp*ARF2*::*NLS*- Mp*ARF2-DBD*^{E297A}-*mNG*-tNOS

no°	Backbone	Plant^{res}	Bacterial^{res}	Contains
22	pMpGWB100	Hygromycin	Spectinomycin	*pro*Mp*ARF2*::*NLS*- Mp*ARF2-DBD*^{K298A}-*mNG*-tNOS
23	pMpGWB100	Hygromycin	Spectinomycin	*pro*Mp*ARF2*::*NLS*- Mp*ARF2-DBD*^{K298E}-*mNG*-tNOS
24	pMpGWB100	Hygromycin	Spectinomycin	*pro*Mp*ARF2*::*NLS*- Mp*ARF2-DBD*^{S299A}-*mNG*-tNOS
25	pMpGWB100	Hygromycin	Spectinomycin	*pro*Mp*ARF2*::*NLS*- Mp*ARF2-DBD*^{R300A}-*mNG*-tNOS
26	pMpGWB100	Hygromycin	Spectinomycin	*pro*Mp*ARF2*::*NLS*- Mp*ARF2-DBD*^{F301A}-*mNG*-tNOS
27	pMpGWB100	Hygromycin	Spectinomycin	*pro*Mp*ARF2*::*NLS*-Mp*ARF2-DBD*$^{MpARF1\ swap}$-*mNG*-tNOS
28	pMpGWB100	Hygromycin	Spectinomycin	*pro*Mp*ARF2*::*NLS*-Mp*ARF2-DBD*$^{MpARF1\ swap+R272Q}$-*mNG*-tNOS

Supplementary Data Table 2 | Oligonucleotides used in this study.

Primer	Sequence (5′ > 3′)	Description
MdR329	CCGCTGCCCATGGGGCAACGGAGAAAT	Fw A294G in Mp*ARF2*
MdR330	GATTTCTCCGTTGCCCCATGGGCAGCGG	Rv A294G in Mp*ARF2*
MdR331	GCTGCCCATGCGGGAACGGAGAAATCTC	Fw A295G in Mp*ARF2*
MdR332	GAGATTTCTCCGTTCCCGCATGGGCAGC	Rv A295G in Mp*ARF2*
MdR333	GCCCATGCGGCAAATGAGAAATCTC-GATTC	Fw T296N in Mp*ARF2*
MdR334	GAATCGAGATTTCTCATTTGCCGCATG-GGC	Rv T296N in Mp*ARF2*
MdR335	CTGCCCATGCGGCAGCGGAGAAATCTC-GA	Fw T296A in Mp*ARF2*
MdR336	TCGAGATTTCTCCGCTGCCGCATGGGCA	Rv T296A in Mp*ARF2*
MdR337	CCCATGCGGCAACGGCGAAATCTCGAT	Fw E297A in Mp*ARF2*
MdR338	ATCGAGATTTCGCCGTTGCCGCATGGG	Rv E297A in Mp*ARF2*
MdR339	CATGCGGCAACGGAGGCATCTCGATTC	Fw K298A in Mp*ARF2*
MdR340	GAATCGAGATGCCTCCGTTGCCGCATG	Rv K298A in Mp*ARF2*
MdR341	CCATGCGGCAACGGAGGAATCTCGATT	Fw K298E in Mp*ARF2*
MdR342	AATCGAGATTCCTCCGTTGCCGCATGG	Rv K298E in Mp*ARF2*
MdR343	GCGGCAACGGAGAAAGCTCGAT-TCTCTCTAATT	Fw S299A in Mp*ARF2*
MdR344	AATTAGAGAGAATCGAGCTTTCTC-CGTTGCCGC	Rv S299A in Mp*ARF2*

Primer	Sequence (5′ > 3′)	Description
MdR345	GCGGCAACGGAGAAATCTGCAT-TCTCTCTAATTTAC	Fw introduce R300A in MpARF2
MdR346	GTAAATTAGAGAGAATGCAGATTTCTC-CGTTGCCGC	Rv introduce R300A in MpARF2
MdR347	CGGCAACGGAGAAATCTCGAG-CCTCTCTAATTTAC	Fw introduce F301A in MpARF2
MdR348	GTAAATTAGAGAGGCTCGAGATTTCTC-CGTTGCCG	Rv introduce F301A in MpARF2
MdR375	CGATTGCCCTCGGTTCTTTTATGGCTC-CAAAGAAGAAGAGAAAGG	Fw SV40 to clone with hifi into *proMpARF1*::XbaI-mNG at XbaI site
MdR376	ATGCTGCCGCCGCCAAGCTGTAACG-GCTCAATTTCCCACAGAGAC	Rv MpARF1 DBD with hifi into *proMpARF1::XbaI-mNG at XbaI site*
MdR377	CATGCTGCCGCCGCCAAGCTGCTG-CATAAATTGGCTATCATTTATAC	Rv A1 MR with hifi into *proMpARF1*::XbaI-mNG at XbaI site
MdR378	ATGCTGCCGCCGCCAAGCTGGGGGCAC-CCCCGCTGGGCAT	Rv A1 PB1 with hifi into *proMpARF1*::XbaI-mNG at XbaI site
MdR379	GCCACCAATAGCCAATTCACTATCTTTTAC	Fw A1 DBD R272Q mutation for 2 fragment assembly
MdR380	GTAAAAGATAGTGAATTGGCTATTGGT-GGC	Rv A1 DBD R272Q mutation for 2 fragment assembly
MdR432	CCGCTGCCCATGCGGCAGCGACGAAT-TCTCAATTCTCTCTAATTTACAACCC	Fw swap MpARF1 R272Q mutation
MdR433	GGGTTGTAAATTAGAGAGAATTGAGAAT-TCGTCGCTGCCGCATGGGCAGCGG	Rv swap MpARF1 R272Q mutation
MdR439	GTGCCAAGCTTGCATGCCTGCAGGTC-GACTACGGGGCGGATAAAAATTTTGG	Fw *pro*Mp*UBE2* to clone into pMpGWB100 XbaI
MdR440	CTTCTTTGGAGCCATGGGCACCAGCAC-CGCCAAGCG	Rv *pro*Mp*UBE2* to clone with NLS-something into pMp-GWB100 XbaI
MdR441	GCGGTGCTGGTGCCCATGGCTC-CAAAGAAGAAGAGAAAGG	Fw NLS SV40 to clone with *pro*Mp*UBE2* into pMpGWB100 XbaI
MdR442	GGAAATTCGAGCTCGGTACCCGGG-GATCCTTTACTTGTACAGCTCGTCCATGC	Rv mNG to clone into pMp-GWB100 XbaI
MdR443	GGGGACAAGTTTGTACAAAAAAGCAG-GCTTAATGTCAGAAGCATCTTCCATCAC	Fw MpARF2 CDS (no NLS) to clone into pDONR221 linearized
MdR444	ACGAAGTTATCAAGGTCGGAACTTCT-GTCTAAAATGCTAG	Rv pMpARF2 to amplify pMp-GWB100 XbaI to linearize and clone mARF2^{flox}
MdR445	GTCATAGCTGTTTCCTGTGTGAAATTGT-TATCCGC	Fw pGWBO100 to amplify pMpGWB100 XbaI to linearize and clone mARF2^{flox}

Primer	Sequence (5′ > 3′)	Description
MdR446	ACAGAAGTTCCGACCTTGATAACTTCG-TATAGCAT	Fw lox mSc3 to clone mARF-2^{flox}
MdR447	ATGCTTCTGACATTGGATAACTTCGTATA-ATGTATGCTATACGAAGTTATAGC	Rv lox mSc3 to clone mARF2^{flox}
MdR448	ATACGAAGTTATCCAATGTCAGAAG-CATCTTCCATCACTC	Fw MpARF2 CDS (no NLS) to clone mARF2^{flox}
MdR449	TAATGGCTGCGCGCCTGATCTAGTAA-CATAGATGACACCGCG	Rv MpARF2 CDS (binds tNOS, no NLS) to clone mARF2^{flox}
MdR450	TCTATGTTACTAGATCAGGCGCGCAGC-CATTATAGC	Fw *proHSP*, to clone CRE-GR-tNOS into mARF2^{flox}
MdR451	GCTATGACGATCTAGTAACATAGATGA-CACCGCGC	Rv tNOS to clone CRE-GR-tNOS into mARF2^{flox}
MdR452	AAAGCAGGCTTAATGGCTCCAAAG	Fw attb+NLS to genotype plants
MdR453	CATCGCCGATACCAGTAATAGTTCCC	Rv MpARF1 DBD near AD domain to genotype plants
MdR454	ATGGCTCCAAAGAAGAAGAGAAAGGTC	Fw NLS to genotype plants
MdR455	GCCATCTAAGCGGGTCGACATC	Rv MpARF1 DBD near AD domain to genotype plants
MdR456	GGAATTTAGAAAGATTTCATGCG	Fw *proHSP* to seq
MdR457	CTGGCATTTCTGGGGATTGC	Fw CRE to seq
MdR491	GCAGCCGCCACCAATAGCCAATTCAC-TATCTTTTAC	Fw R272Q MpARF1 2 fragment assembly
MdR492	GCCGCCACCAATAGCCAATTCAC-TATCTTTTACAATCCCAG	Fw R272Q MpARF1 2 fragment assembly

References

1 Vanneste, S., Pei, Y. & Friml, J. Mechanisms of auxin action in plant growth and development. *Nat Rev Mol Cell Biol* (2025). https://doi.org/10.1038/s41580-025-00851-2

2 Leyser, O. Auxin Signaling. *Plant Physiol* **176**, 465–479 (2018). https://doi.org/10.1104/pp.17.00765

3 Lavy, M. & Estelle, M. Mechanisms of auxin signaling. *Development* **143**, 3226–3229 (2016). https://doi.org/10.1242/dev.131870

4 Chapman, E. J. & Estelle, M. Mechanism of auxin-regulated gene expression in plants. *Annu Rev Genet* **43**, 265–285 (2009). https://doi.org/10.1146/annurev-genet-102108-134148

5 Gray, W. M., Kepinski, S., Rouse, D., Leyser, O. & Estelle, M. Auxin regulates SCF(TIR1)-dependent degradation of AUX/IAA proteins. *Nature* **414**, 271–276 (2001). https://doi.org/10.1038/35104500

6 Dharmasiri, N., Dharmasiri, S. & Estelle, M. The F-box protein TIR1 is an auxin receptor. *Nature* **435**, 441–445 (2005). https://doi.org/10.1038/nature03543

7 Kepinski, S. & Leyser, O. The Arabidopsis F-box protein TIR1 is an auxin receptor. *Nature* **435**, 446–451 (2005). https://doi.org/10.1038/nature03542

8 Ulmasov, T., Murfett, J., Hagen, G. & Guilfoyle, T. J. Aux/IAA proteins repress expression of reporter genes containing natural and highly active synthetic auxin response elements. *Plant Cell* **9**, 1963–1971 (1997). https://doi.org/10.1105/tpc.9.11.1963

9 Vernoux, T. *et al.* The auxin signalling network translates dynamic input into robust patterning at the shoot apex. *Mol Syst Biol* **7**, 508 (2011). https://doi.org/10.1038/msb.2011.39

10 Roosjen, M., Paque, S. & Weijers, D. Auxin Response Factors: output control in auxin biology. *J Exp Bot* **69**, 179–188 (2018). https://doi.org/10.1093/jxb/erx237

11 Boer, D. R. *et al.* Structural basis for DNA binding specificity by the auxin-dependent ARF transcription factors. *Cell* **156**, 577–589 (2014). https://doi.org/10.1016/j.cell.2013.12.027

12 Rienstra, J., Carrillo-Carrasco, V. P., de Roij, M., Hernandez-Garcia, J. & Weijers, D. A conserved ARF-DNA interface underlies auxin-triggered transcriptional response. *Proc Natl Acad Sci U S A* **122**, e2501915122 (2025). https://doi.org/10.1073/pnas.2501915122

13 Kato, H. *et al.* Design principles of a minimal auxin response system. *Nat Plants* **6**, 473–482 (2020). https://doi.org/10.1038/s41477-020-0662-y

14 Lavy, M. *et al.* Constitutive auxin response in Physcomitrella reveals complex interactions between Aux/IAA and ARF proteins. *Elife* **5** (2016). https://doi.org/10.7554/eLife.13325

15 de Roij, M., Borst, J. W. & Weijers, D. Protein degradation in the auxin response. *Plant Cell* (2024). https://doi.org/10.1093/plcell/koae125

16 Liu, L., Yahaya, B. S., Li, J. & Wu, F. Enigmatic role of auxin response factors in plant growth and stress tolerance. *Front Plant Sci* **15**, 1398818 (2024). https://doi.org/10.3389/fpls.2024.1398818

17 Lakehal, A. *et al.* A Molecular Framework for the Control of Adventitious Rooting by TIR1/AFB2-Aux/IAA-Dependent Auxin Signaling in Arabidopsis. *Mol Plant* **12**, 1499–1514 (2019). https://doi.org/10.1016/j.molp.2019.09.001

18 Das, S. *et al.* Quantitative imaging reveals the role of MpARF proteasomal degradation during gemma germination. *Plant Commun*, 101039 (2024). https://

doi.org/10.1016/j.xplc.2024.101039
19 Jing, H. *et al.* Regulation of AUXIN RESPONSE FACTOR condensation and nucleo-cytoplasmic partitioning. *Nat Commun* **13**, 4015 (2022). https://doi.org/10.1038/s41467-022-31628-2
20 Prigge, M. J. *et al.* Comparative mutant analyses reveal a novel mechanism of ARF regulation in land plants. *Nat Plants* **11**, 821–835 (2025). https://doi.org/10.1038/s41477-025-01973-3
21 de Roij, M., Hernandez Garcia, J., Das, S., Borst, J. W. & Weijers, D. ARF degradation defines a deeply conserved step in auxin response. *Nat Plants* **11**, 717–724 (2025). https://doi.org/10.1038/s41477-025-01975-1
22 Mutte, S. K. *et al.* Origin and evolution of the nuclear auxin response system. *Elife* **7** (2018). https://doi.org/10.7554/eLife.33399
23 Hernandez-Garcia, J. *et al.* Evolutionary origins and functional diversification of Auxin Response Factors. *Nat Commun* **15**, 10909 (2024). https://doi.org/10.1038/s41467-024-55278-8
24 Romani, F. *et al.* The landscape of transcription factor promoter activity during vegetative development in Marchantia. *Plant Cell* **36**, 2140–2159 (2024). https://doi.org/10.1093/plcell/koae053
25 Kato, H. *et al.* The Roles of the Sole Activator-Type Auxin Response Factor in Pattern Formation of Marchantia polymorpha. *Plant Cell Physiol* **58**, 1642–1651 (2017). https://doi.org/10.1093/pcp/pcx095
26 Kato, H., Yasui, Y. & Ishizaki, K. Gemma cup and gemma development in Marchantia polymorpha. *New Phytol* **228**, 459–465 (2020). https://doi.org/10.1111/nph.16655
27 Flores-Sandoval, E. *et al.* The B-class auxin response factor MpARF2 is essential for meristem organization in free-living plant gametophytes. *Curr Biol* (2025). https://doi.org/10.1016/j.cub.2025.11.015
28 Nishimura, T. *et al.* Yucasin is a potent inhibitor of YUCCA, a key enzyme in auxin biosynthesis. *Plant J* **77**, 352–366 (2014). https://doi.org/10.1111/tpj.12399
29 Harris, B. J. *et al.* Divergent evolutionary trajectories of bryophytes and tracheophytes from a complex common ancestor of land plants. *Nat Ecol Evol* **6**, 1634–1643 (2022). https://doi.org/10.1038/s41559-022-01885-x
30 Zhao, S., Zhang, M. L., Ma, T. L. & Wang, Y. Phosphorylation of ARF2 Relieves Its Repression of Transcription of the K+ Transporter Gene HAK5 in Response to Low Potassium Stress. *Plant Cell* **28**, 3005–3019 (2016). https://doi.org/10.1105/tpc.16.00684
31 Salmon, J., Ramos, J. & Callis, J. Degradation of the auxin response factor ARF1. *Plant J* **54**, 118–128 (2008). https://doi.org/10.1111/j.1365-313X.2007.03396.x
32 Cavalleri, A. *et al.* Auxin-dependent post-translational regulation of MONOPTEROS in the Arabidopsis root. *Cell Rep* **43**, 115083 (2024). https://doi.org/10.1016/j.celrep.2024.115083
33 Jumper, J. *et al.* Highly accurate protein structure prediction with AlphaFold. *Nature* **596**, 583–589 (2021). https://doi.org/10.1038/s41586-021-03819-2
34 McFadden, W. M. & Yanowitz, J. L. idpr: A package for profiling and analyzing Intrinsically Disordered Proteins in R. *PLoS One* **17**, e0266929 (2022). https://doi.org/10.1371/journal.pone.0266929
35 Sauret-Gueto, S. *et al.* Systematic Tools for Reprogramming Plant Gene Expression in a Simple Model, Marchantia polymorpha. *ACS Synth Biol* **9**, 864–882 (2020). https://doi.org/10.1021/acssynbio.9b00511

36 Ishizaki, K. *et al.* Development of Gateway Binary Vector Series with Four Different Selection Markers for the Liverwort Marchantia polymorpha. *PLoS One* **10**, e0138876 (2015). https://doi.org/10.1371/journal.pone.0138876

37 Nishihama, R., Ishida, S., Urawa, H., Kamei, Y. & Kohchi, T. Conditional Gene Expression/Deletion Systems for Marchantia polymorpha Using its Own Heat-Shock Promoter and Cre/loxP-Mediated Site-Specific Recombination. *Plant Cell Physiol* **57**, 271–280 (2016). https://doi.org/10.1093/pcp/pcv102

38 Kubota, A., Ishizaki, K., Hosaka, M. & Kohchi, T. Efficient Agrobacterium-mediated transformation of the liverwort Marchantia polymorpha using regenerating thalli. *Biosci Biotechnol Biochem* **77**, 167–172 (2013). https://doi.org/10.1271/bbb.120700



Chapter 6

A forward genetic screen for mutants defective in Auxin Response Factor degradation

Authors

Martijn de Roij[1], Michael Prigge[2], Danilo dos Santos Pereira[1], Jan Willem Borst[1], Mark Estelle[2], and Dolf Weijers[1,*]

Affiliations

[1] Laboratory of Biochemistry, Wageningen University, Stippeneng 4, 6708WE Wageningen, the Netherlands

[2] Department of Cell and Developmental Biology, School of Biological Sciences, University of California San Diego, La Jolla, California, USA

* Corresponding author: dolf.weijers@wur.nl

Abstract

Auxin controls plant development largely through transcriptional regulation mediated by Auxin Response Factors (ARFs), whose abundance is critical for determining auxin-responsive gene expression. In particular, the stoichiometry between activating A-class and repressing B-class ARFs must be tightly regulated, yet the molecular mechanisms controlling ARF protein stability remain poorly understood. Previous work has shown that many B-class ARFs are intrinsically unstable and targeted for degradation by the 26S proteasome via a deeply conserved mechanism acting on their DNA-binding domain. Here, we use a forward genetic approach to identify genes required for B-ARF degradation in the moss *Physcomitrium patens*. We used UV irradiation mutagenesis and screened for auxin-resistant mutants with aberrant accumulation of a PpARFb2–YFP protein. Several UV-induced mutants displayed PpARFb2–YFP levels well outside the normal range, leading to the identification of candidate mutations and genes. However, targeted knock-out of these candidates in a non-mutagenized background using CRISPR–Cas9 failed to reproduce the elevated PpARFb2–YFP accumulation. These results indicate that the identified genes are unlikely to directly or individually control PpARFb2 degradation or auxin signaling. We discuss possible explanations for this outcome, such as genetic redundancy, indirect transcriptional or physiological effects in UV-mutagenized lines, and limitations inherent to the screening assumptions. Together, this work underlines the challenges of identifying regulators of ARF degradation and demonstrates the complexity of quantitatively controlling auxin signaling through protein turnover.

Introduction

The signaling molecule auxin has profound influence on plant morphology and is a key regulator of plant development[1]. Auxin controls development through a transcriptional regulatory system, the Nuclear Auxin Pathway (NAP)[2,3]. Central to this system are Auxin Response Factor (ARF) transcription factor proteins[4]. ARFs typically contain three domains, an N-terminal DNA-binding domain (DBD), a middle region (MR), and a C-terminal Phox and Bem 1 domain (PB1)[5,6]. In land plants, three ARF subfamilies are defined, the auxin-modulated transcriptionally activating A-class ARFs and the B-and C-class ARFs, which are repressors[7,8]. Whereas C-class ARFs seem to regulate non-auxin related genes, A-and B-class ARFs target overlapping gene sets[7,9]. Whether a gene becomes activated or repressed is determined by the A-and B-class ARF stoichiometry, as these two ARF classes compete for DNA-binding in a concentration-dependent manner[10]. The abundance of proteins can be regulated by quantitative tuning of transcription, translation, or by protein degradation[11], however if and to what extent such processes regulate ARF levels remains poorly understood.

In thesis chapters 3[11], 4[12], 5[13] and in Prigge et al., 2024[14] we show that a large group of B-class ARF family members, from various divergent plant lineages, are unstable. This instability relies on the 26S proteasome and requires specific residues in a defined, conserved region in the DNA-Binding Domain (DBD)[12,14]. This region was originally identified through the analysis of auxin-resistant mutants in *P. patens* and a morphological mutant in maize[14]. Mapping these mutations identified lesions in the Pp*ARFb2* -and *4*, and Zm*ARF28* (from *Zea mays*) genes, which led to increased protein stability and drastic accumulation, with strong effects on auxin response and development[14]. In line with this, homologous residues in AtARF2 (from *Arabidopsis thaliana*) also controlled stability, although the functional impact of these findings remains to be unclear[14]. Based on this, missense mutations (i.e. the charge reversals E266K and R269Q) in these two key residues in Pp*ARFb2* were identified as crucial for normal regulation of Pp*ARFb2* levels through the proteasome[14]. Similarly, we show that homologous residues in MpARF1 -and 2 (from *Marchantia polymorpha*) are equally important in proteasomal regulation in chapter 4 and 5[12]. Taken together, these findings suggest that there is a deep level of mechanistic conservation of this degradation in land plants.

Proteins are routed to the proteasome following post-translational modification with ubiquitin, which is typically ligated onto a

substrate by ubiquitin-ligase enzymes. Usually, this process requires additional molecular factors and can be substantially influenced by e.g. protein (mis)folding, co-ligands, and post-translational modifications of the substrate[11]. The ubiquitin-ligase and other factors controlling ARF degradation remain largely elusive[11]. Identification of such factors is a crucial step in unlocking key details in the biochemistry and evolution of ARF degradation[11]. However, there have been sparse efforts on a specific, targeted investigation on factors regulating ARF degradation. Here we make use of the moss *Physcomitrium patens* (*P. patens*) as a well-established platform for carrying out genetic screens and report on an extensive genetic screen aimed at the identification of factors regulating ARF degradation.

Results

Candidate mutants display increased PpARFb2 accumulation

We first set out to recapitulate the findings presented in Prigge et al., 2025 in our lab conditions. In our hands, the *P. patens* line expressing YFP-tagged Pp*ARFb2-YFP* (the YFP sequence was knocked-in at the native Pp*ARFb2* locus) exhibited highly unstable behaviour, congruent with previous reports[14], and accumulated to barely detectable levels (Fig. 1a).

However, drastic accumulation can be observed upon treatment with proteasome inhibitor Bortezomib (Bz), or when introducing the E266K and R269Q mutations (Fig. 1a,b and Fig. 2a,b). In chapter 4, we show that a homologous region of PpARFb2 can be substituted into the MpARF2 DBD, and that this chimeric protein remains unstable in *Marchantia* and is degraded in a similar manner as the native MpARF2 protein[12]. This, combined with the findings that in MpARF2 the E297K and R300Q mutations inhibited degradation, suggests that both ARFs are degraded via a similar and conserved mechanism, which was further confirmed by experimental and *in-silico* analyses of the degradation conferring-motif in chapter 5[13].

To identify and characterize molecular factors required for ARF degradation, we employed *P. patens* for a large-scale genetic mutagenesis screen. We used UV-light as a mutagen to induce *de novo* mutations in the Pp*ARFb2-YFP* or the Pp*ARFb2-YFP*$^{\Delta hyg}$ backgrounds. We predicted that mutants defective in Pp*ARFb2-YFP* would present as auxin resistant, similar to the intragenic PpARFb2$^{E266K+R269Q}$ mutant[14]. For this reason, we pre-screened for auxin-resistant plants to create a strong selection pressure for the desired phenotype. This was done to drastically enhance the efficiency of the screen, and have a filtering step that would limit the number of individuals that would need to be analyzed by fluorescence microscopy. Mutants that displayed signs of auxin resistance were then examined for increased YFP signal using confocal microscopy (Fig. 3). Increased PpARFb2-YFP signal could be indicative of a compromised ability to target PpARFb2 to the proteasome and may thus lead to the identification of key regulators driving this process.

From large amounts of mutagenized tissue, we isolated between 1100-1300 auxin-resistant clones. Analyzing these using confocal microscopy led to the identification of 15 mutants in

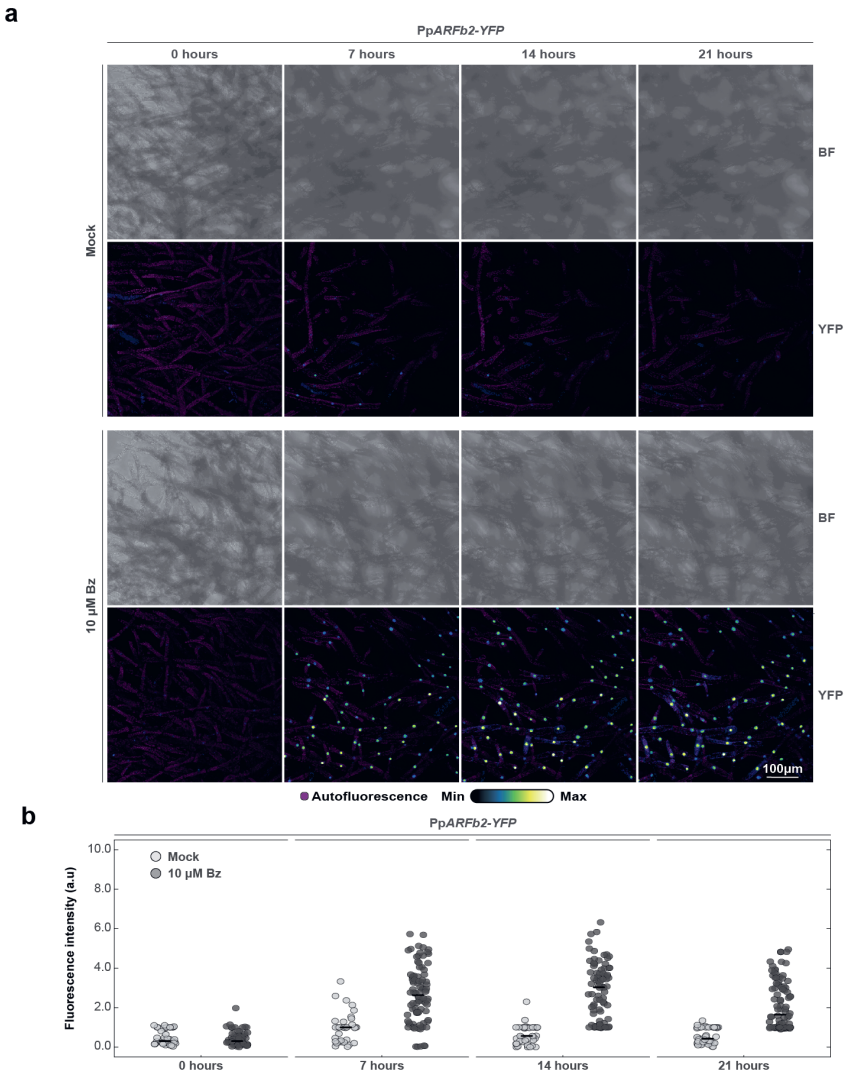


Fig. 1 | PpARFb2 instability relies on the 26S proteasome.
a. Confocal images of a *P. patens* line expressing PpARFb2-*YFP*, wherein the YFP gene was knocked in at the native Pp*ARFb2* locus. Plants were treated with Mock or 10 µM Bortezomib (Bz) for 21 hours and imaged at regular intervals. The colored scale corresponds to YFP fluorescence intensity and chloroplast autofluorescence is shown in magenta. BF stands for brightfield. **b.** Quantification of YFP fluorescence signals in nuclei of plants part of the experiment shown in (**a**).

the PpARFb2-YFP background (narF series) and 1 mutant in the PpARFb2-YFP$^{\Delta hyg}$ background (narW series) which presented increased YFP signal (Fig. 4-6). Each mutant which displayed significant increased amounts of YFP (which was judged by eye) was isolated and grown for a further 7 days and examined again. Often,

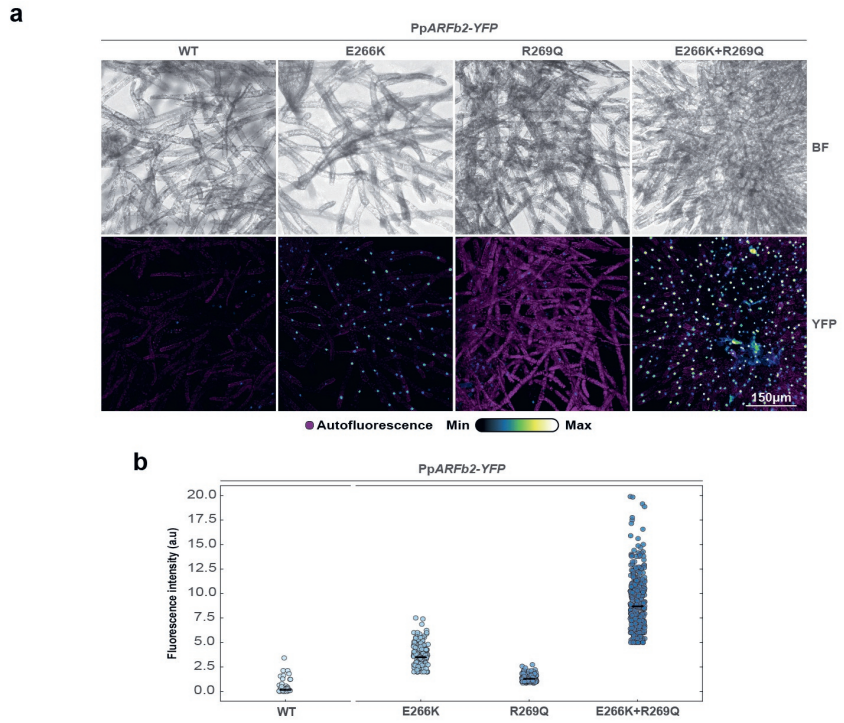


Fig. 2 | E266 and R269 are crucial residues for PpARFb2 degradation.
a. Confocal images of a *P. patens* line expressing Pp*ARFb2-YFP*, wherein the YFP gene was knocked in at the native Pp*ARFb2* locus. Shown here is wild type (WT) accumulation and accumulation of mutant versions of Pp*ARFb2*, as indicated. The coloured scale corresponds to YFP fluorescence intensity and chloroplast autofluorescence is shown in magenta. BF stands for brightfield. **b.** Quantification of YFP fluorescence signals in nuclei of plants part of the experiment shown in (**a**).

when imaging WT cells using our microscopy settings, only >10% of nuclei displayed detectable YFP signal. We screened for mutants in which >80-90% of nuclei appeared fluorescent. During the screen, we noticed that several mutants that would present themselves as promising after 7 days, would appear WT after 14 days, and individual mutants displaying such an unstable phenotype were therefore excluded from further analysis.

Given that mutations that directly stabilize B-ARFs had originally been identified in a similar genetic screen in Physcomitrium, we asked whether any of the newly identified mutants were likewise intragenic mutations in the fluorescently tagged ARF. We therefore amplified a region in PpARF2b that encompasses the known instability domain from the panel of mutants and sequenced these. This identified a total of nine independent mutants which carried the

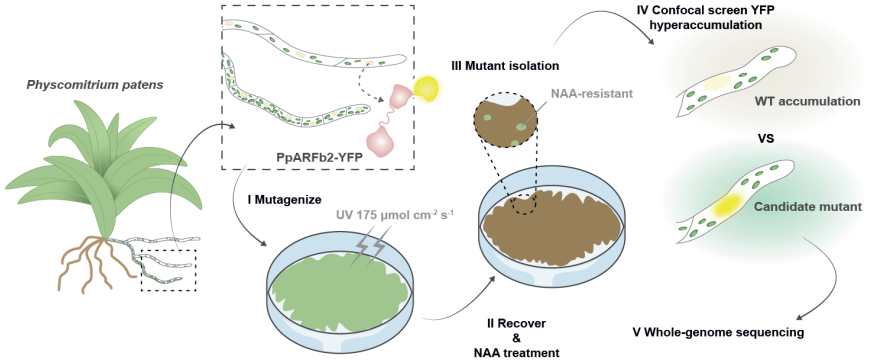


Fig. 3 | A forward genetic approach to identify mutants impaired in PpARFb2 degradation.
Schematic diagram depicting the experimental set-up for the forward genetic screen. Steps are numbered, in order, in roman numerals (I to V). In short, the Pp*ARFb2-YFP* background was homogenized, mutagenized and selected for auxin resistance. Next, resistant mutants were screened for increased YFP signal and if this was consistently observed, mutants were sent for whole genome sequencing.

E266K mutation (Fig. 4-6; Supplementary Information Fig. 1). As expected, the mutants which carried E226K (three are shown) exhibited high levels of PpARFb2-YFP and auxin resistance (Fig. 4-6; Supplementary Information Fig. 5). This strongly suggests that our screen was nearing saturation.

Genomes of candidate mutants contain numerous disruptive mutations

The 16 mutants which did not carry intragenic Pp*ARFb2* mutations were subjected to Whole Genome Sequencing (WGS; Supplementary Information Fig. 1).

In order to map potentially causative mutations, sequencing reads were both compared to the reference genome and to the non-mutagenized background strain. Next, the disruptive effect of Single Nucleotide Polymorphisms (SNPs), which were mutant-specific and which did not occur in the non-mutagenized background, was predicted using SNPeff[15]. This yielded a dataset containing SNPs that fell within coding regions of genes and were predicted to have a disruptive effect on gene function. The number of candidate mutations per mutant ranged from 9 (narF104) to 91 (narW20) SNPs, whereas the number of candidate genes per mutant fell within the range of 8 (narF104) to 79 (narW20; i.e. some genes carried multi-

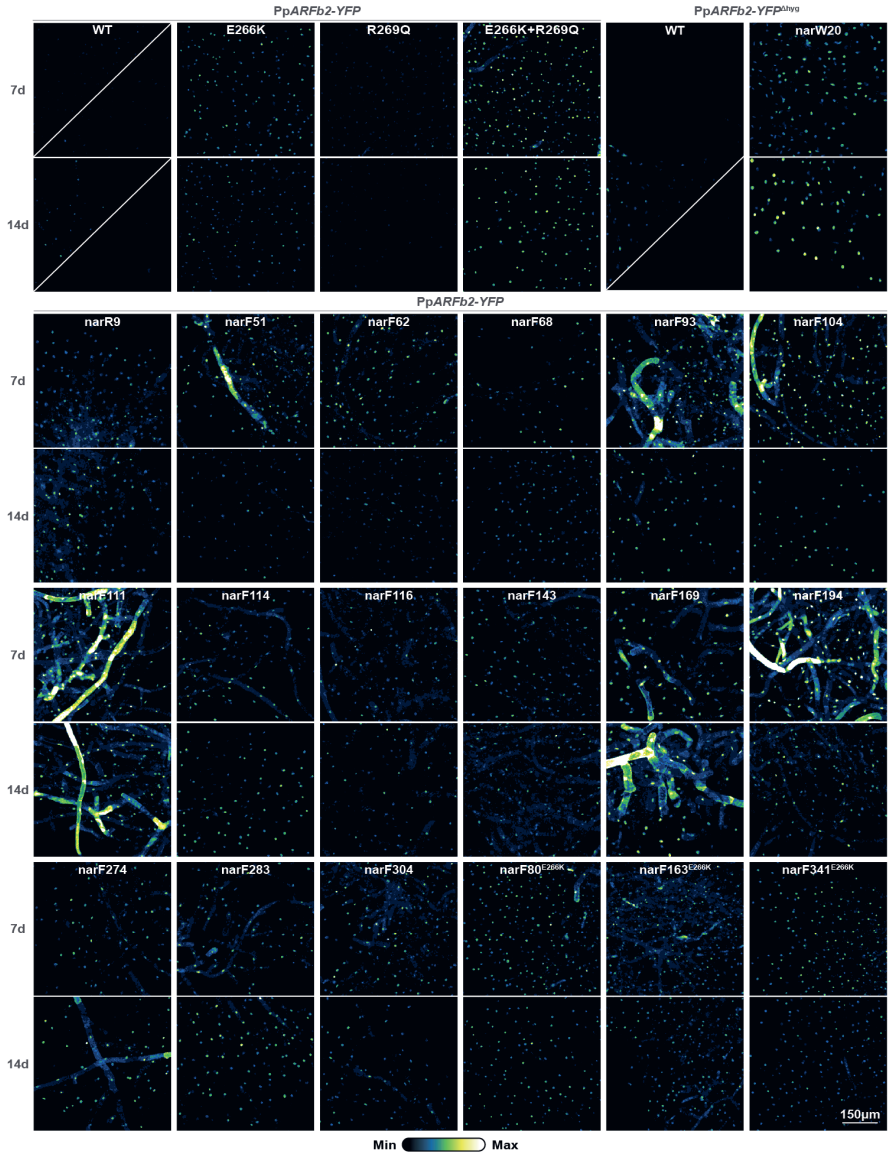


Fig. 4 | PpARFb2-YFP signal is elevated in 25 mutants.
Overview of YFP fluorescence signals in 19 mutants identified in the screen as described in Fig. 3. Shown here is an impression of the YFP signal in wild type (WT), E266K, R269Q, and E266K+R269Q double mutants for comparison. Mutants identified in this screen are named narW, narR or narF (and subsequently numbered). The narR and narF series are generated in the Pp*ARFb2-YFP* background and the narW20 mutant is generated in the Pp*ARFb2-YFP*$^{\Delta hyg}$ background. Plants were imaged at 7 days and after 14 days of growth from homogenization. For the WT, 2 images are shown (divided diagonally) to show variation in observed YFP signal. The colored scale corresponds to YFP fluorescence intensity.

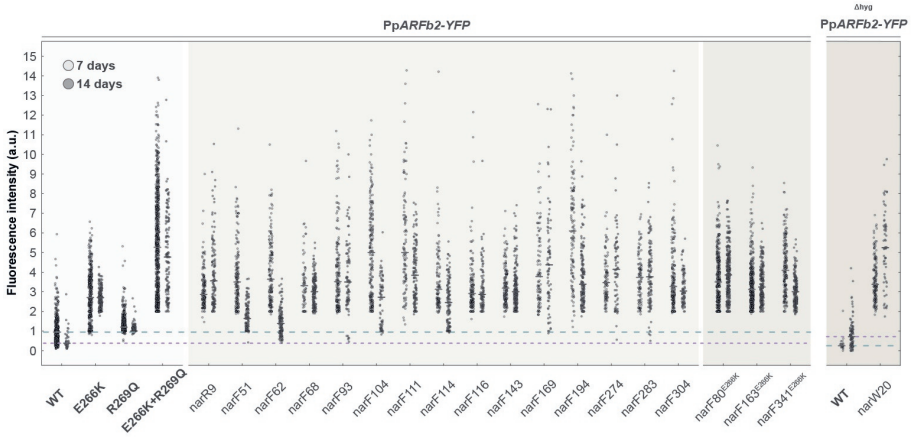


Fig. 5 | Quantification of YFP signal in 19 mutants.
Quantification of YFP fluorescence intensity of nuclei of mutants shown in Fig. 4. Nuclei were measured of plants aged 7 and 14 days respectively (see legend). Mean fluorescence signals for the WT at 7 and 14 days are shown as dashed (blue) and dotted (magenta) lines, respectively.

ple SNPs; Supplementary Information Fig. 2a,b).

In total, 462 SNPs, spread across 251 genes, and the 16 mutants were identified (Supplementary Information Fig. 2c-e). Each mutant represented a set of uniquely mutated genes as well as overlapping genes between mutants (Supplementary Information Fig. 2f). Closer inspection of the latter category revealed that mutations in overlapping genes are likely artefacts of read-mapping, as these genes often locate within highly repetitive regions within the genome. Due to the repetitive nature of these regions, we observed signs of falsely mapped reads; we therefore excluded these genes from analysis. Word cloud analysis of gene functional annotation did not show enrichment of annotation terms related to the Ubiquitin Proteasome System (UPS), or auxin (Supplementary Information Fig. 2g,h). Finally, we selected a candidate gene set of 13 genes based on annotation (Fig. 7 and Fig. 8; Supplementary Information Fig. 3a,b).

To select candidate genes, we focused on genes which either exhibited high-impact mutations (such as premature stop codons) or encoded proteins linked to the UPS (such as ubiquitin ligases), as well as proteins containing domains that are known from the literature to play a role in molecular systems targeting substrate proteins to the proteasome (Fig. 7 and Fig. 8). We obtained functional annotations for all genes in the dataset and queried for known UPS-asso-

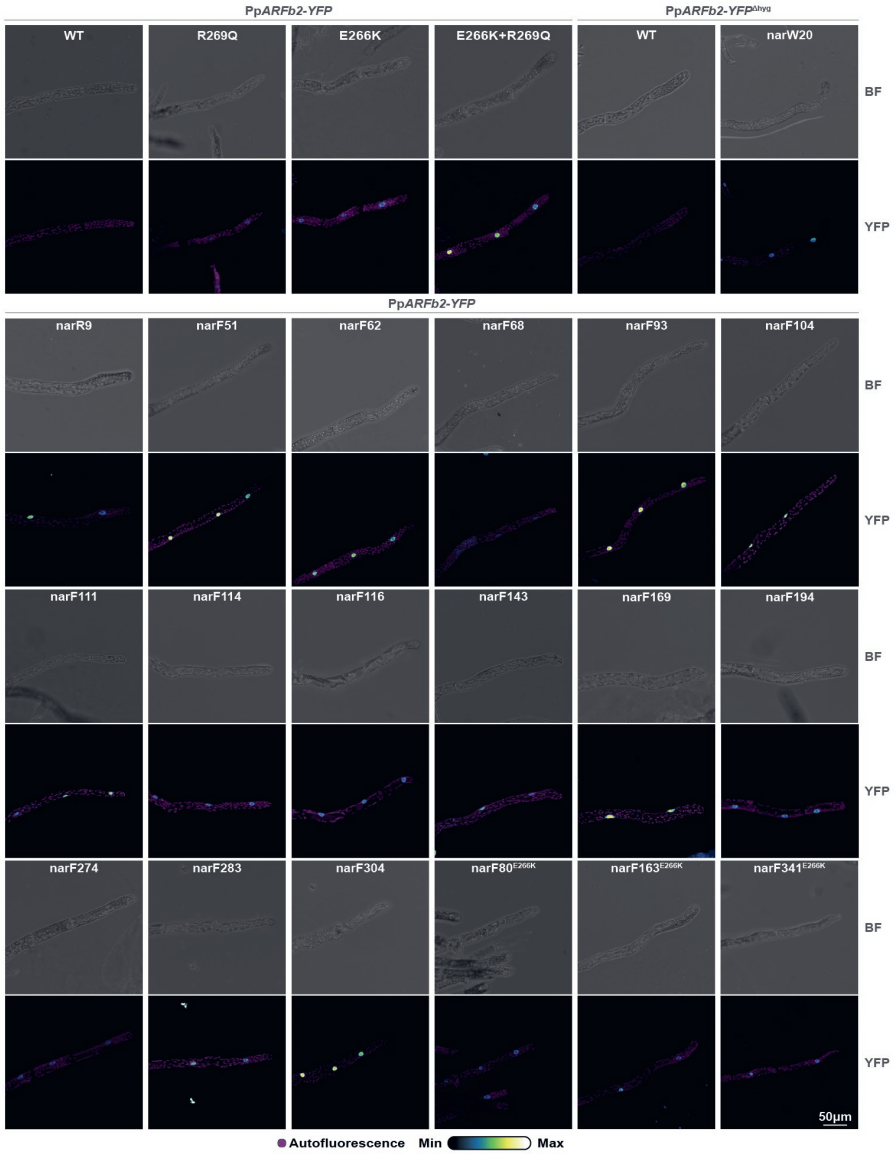


Fig. 6 | Confocal images of PpARFb2-YFP signal in caulonema cells of the identified mutants.
Confocal images of caulonema tissue the same mutants depicted in Fig. 4 at higher magnification. Shown here is an impression of the YFP signal in wild type (WT), E266K, R269Q, and E266K+R269Q double mutants for comparison. Mutants identified in this screen are named narW, narR or narF (and subsequently numbered). The narR and narF series are generated in the Pp*ARFb2-YFP* background and the narW20 mutant is generated in the Pp*ARFb2-YFP*$^{\Delta hyg}$ background. Plants were imaged after 14 days of growth from homogenization. The coloured scale corresponds to YFP fluorescence intensity and chloroplast autofluorescence is shown in magenta. BF stands for brightfield.

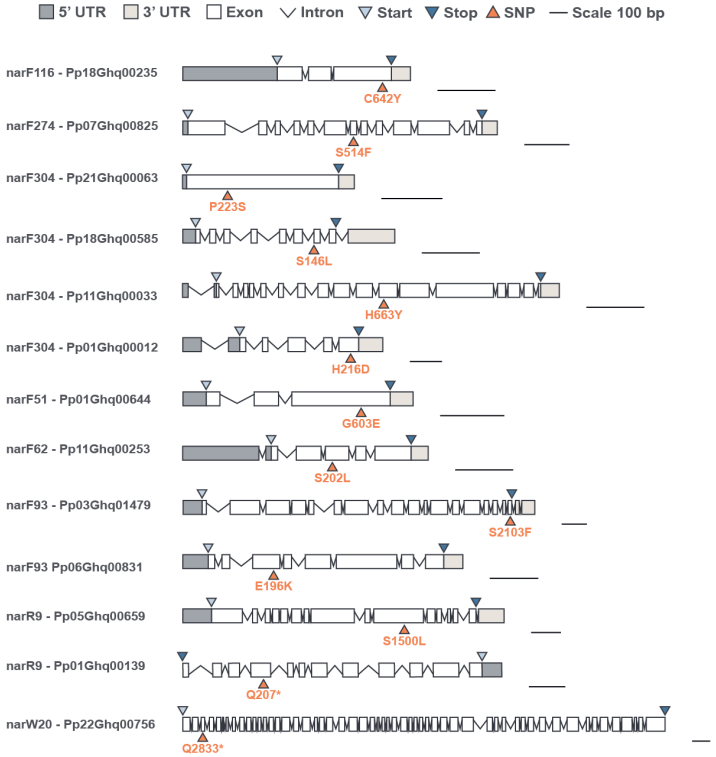


Fig. 7 | Nar mutants carry exonic SNPs resulting in amino acid substitutions.
Gene models of the selected candidate genes and which mutations occurred (and their intragenic location, in orange) in the indicated nar mutant. Gene models are based on RNA-sequencing[8], and for some (Pp01Ghq00139 and Pp22Ghq00756) Untranslated Regions (UTRs) are uncertain. The scalebar for each gene model indicates a length of 100 base pairs.

ciated protein domains such as "RING", "U-box", "BTB", "Ubiquitin", "HECT", "Proteasome", "E3", "Anaphase Promoting Complex" etc. We manually curated all genes and flagged genes which possessed such properties as potential candidates, which left us with 13 total candidate genes (Fig. 7). Two of the selected genes, Pp01Ghq00139 and Pp22Ghq00756, had premature stop codons, whereas the other selected genes all carried SNPs resulting in amino acid substitutions (Fig. 7). Next we explored the potential causality between these mutations and the nar phenotype.

CRISPR-Cas9-mediated verification of candidate mutations

The selection of 13 candidate genes were targeted for mutation by expressing a CRISPR-Cas9 system and respective gRNA

Table 1 | Overview of CRISPR-Cas9 induced mutations in candidate genes.

Line	Gene	Lesion
T380-5	Pp18Ghq00235 RING/U-box	Δ1147 bp + 5 bp; frameshift
T380-12	Pp18Ghq00235 RING/U-box	Δ1788 bp; e1-3'utr deletion
T381-6	Pp6Ghq00825 kelch repeat	Δ1984 bp; frameshift
T381-11	Pp6Ghq00825 kelch repeat	Δ1977 bp + 1 bp; in frame
T381-16	Pp6Ghq00825 kelch repeat	Δ1982 bp; in frame
T382-3	Pp21Ghq00063 MET-10+/Kelch	Δ2001 bp; in frame
T382-10	Pp21Ghq00063 MET-10+/Kelch	Δ2001 bp; in frame
T382-12	Pp21Ghq00063 MET-10+/Kelch	Δ2001 bp; in frame
T384-20	Pp11Ghq00033 RING/HEAT/U-box	Δ3645 bp; frameshift
T384-21	Pp11Ghq00033 RING/HEAT/U-box	Δ3629 bp; in frame
T385-7	Pp01Ghq00012 BIG BROTHER RING/U-box	Δ885 bp; frameshift
T385-11	Pp01Ghq00012 BIG BROTHER RING/U-box	Δ875 bp; frameshift
T386-20	Pp01Ghq00644 MAGPIE ZFP	Δ1993 bp + 3 bp; 5'utr-e3
T386-22	Pp01Ghq00644 MAGPIE ZFP	Δ1999 bp; 5'utr-e3
T387-3	Pp11Ghq00253 SKP2A	Δ1348 bp; frameshift
T387-5	Pp11Ghq00253 SKP2A	Δ1540 bp; frameshift
T388-10	Pp03Ghq01479 GED1/PRT6	Δ8,626+4 bp; in frame
T388-3	Pp03Ghq01479 GED1/PRT6	Δ8,629+14 bp; in frame
T389-2	Pp06Ghq00831 BTB/POZ	Δ1,943 + 7 bp (frameshift/stop) then Δ7 bp
T389-4	Pp06Ghq00831 BTB/POZ	Δ2,858 + 23 bp; stop in insertion
T390-1	Pp05Ghq00659 KAK/UPL3 HECT	Δ2,749 bp; in frame
T390-2	Pp05Ghq00659 KAK/UPL3 HECT	Δ2,748 bp; frameshift
T391-2	Pp01Ghq00139 LEUNIG homolog	Δ9,334 + 3 bp; entire coding region deleted
T391-3	Pp01Ghq00139 LEUNIG homolog	Δ9,335 + 32 bp; entire coding region deleted
T392-3	Pp22Ghq00756 Dynein-1-α HC	Δ3,102 bp; frameshift
T392-4	Pp22Ghq00756 Dynein-1-α HC	Δ3,112 bp; in frame

guides in the Pp*ARFb2-YFP* background. Each transformant was given a numerical identifier (the letter T followed by a three-digit number, which corresponds to the target gene, and a hyphened singular number which corresponds to an independent transgenic line (Table 1).

The resultant transformants were screened for mutations through PCR (c). For each candidate gene, we recovered at

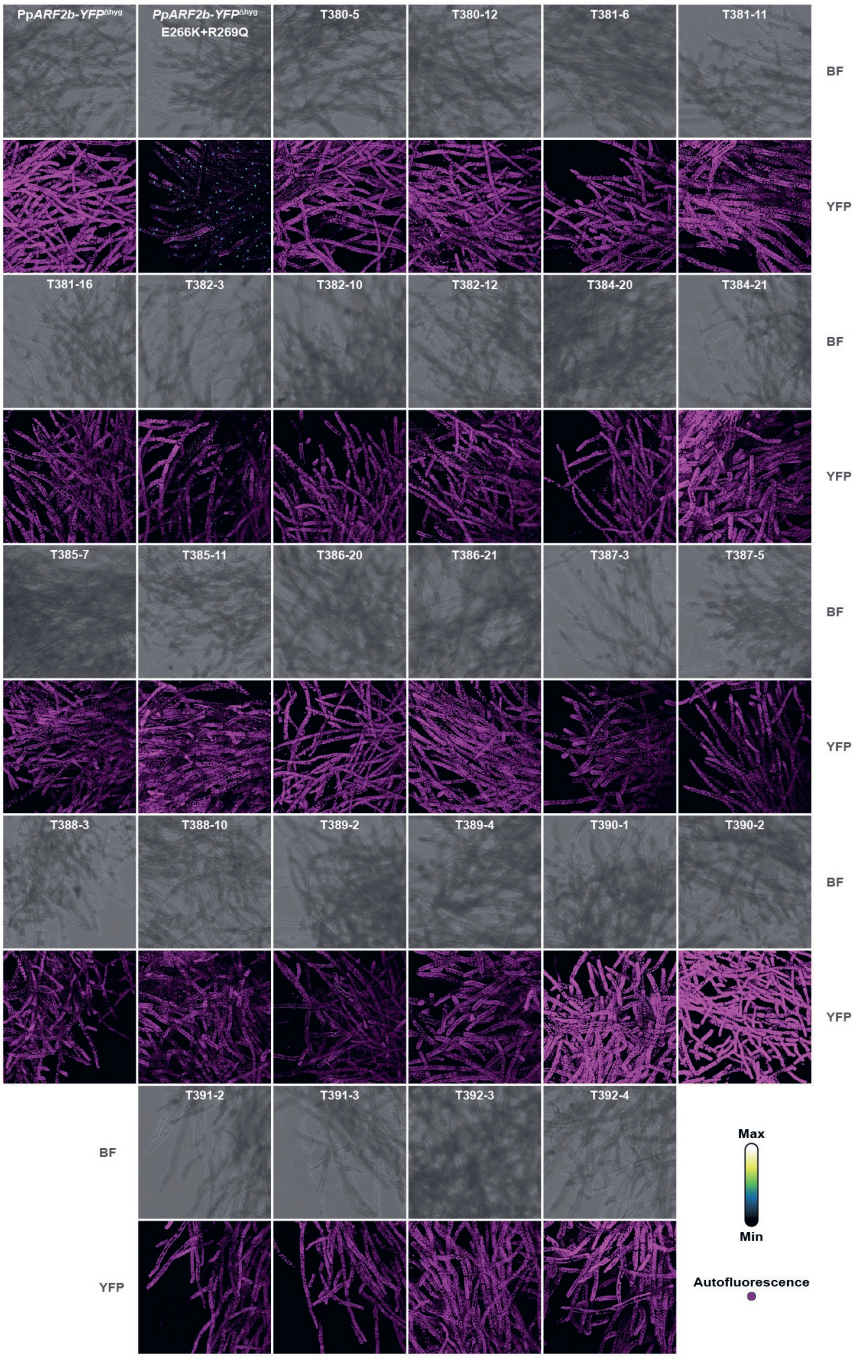


Fig. 8 | Confocal imaging of Pp*ARFb2-YFP* CRISPR-Cas9 mutants reveals no substantial increase in YFP signal.

Confocal images CRISPR-Cas9 generated knock out mutants which correspond to mutants described in Table 1. **(continued on next page)**

Fig. 8 (continued) | Mutants are all generated in the Pp*ARFb2-YFP*$^{\Delta hyg}$ background, which is shown for comparison, along with a, stabilized, E266K+R269Q version. Plants were imaged after 14 days of growth from homogenization. The colored scale corresponds to YFP fluorescence intensity and chloroplast autofluorescence is shown in magenta. BF stands for brightfield.

least two, independent mutant lines with lesions in the coding region, which were then verified using sequencing, with exception of Pp18Ghq00585 (Table 1; Supplementary Information Fig. 3b). Pp18Ghq00585 encodes a PBA1/PSB1 Proteasome Subunit 1, and its deletion is likely lethal[16]. For the 12 other genes, we obtained large deletions, frameshifts, and in the case of T389-4 (Pp06Ghq00831), a premature stop codon, all predicted to have knock-out effects (Table 1). None of the obtained mutants had a particularly strong effect on the phenotype, with T389-2 and T389-4 (corresponding to Pp06Ghq00831) being the exception, as these lines displayed drastic phenotypic defects, strongly resembling the phenotype initially observed for the PpARFb2$^{E266K+R269Q}$ mutant[14]. This phenotype displays strongly impaired gametophore formation and a round colony morphology (Supplementary Information Fig. 4 and 5). However, T389-2 and T389-4 did not prove to be particularly resistant to high levels of auxin, whereas the PpARFb2$^{E266K+R269Q}$ is (Supplementary Information Fig. 5)[14]. To verify if the targeted genes were involved in regulation of PpARFb2-YFP degradation, the newly generated mutant lines were subjected to confocal microscopy and screened for increased YFP fluorescence signal once more. None of the mutant lines which analyzed showed the expected increase in YFP signal and therefore did not recapitulate the phenotype observed in the initial mutant obtained through UV-mutagenesis (Fig. 8). We therefore conclude that we were unsuccessful in our efforts to isolate mutants defective in PpARFb2-YFP degradation.

Discussion

Auxin has profound control over plant development and does so in large part through a transcriptional pathway that revolves around ARF transcription factors. ARF levels must be finely tuned to achieve appropriate auxin responses. Here, we employed a forward genetic screen to identify molecular factors targeting *P. patens* PpARFb2 to the proteasome for degradation. We report on a number of mutants that display levels of PpARFb2-YFP which fall well out of the normal range, thereby leading to a set of potentially causative candidate mutations and genes. When these genes were targeted for knock-out in the non-mutagenized background strain using CRISPR-Cas9, we did not recapitulate the abnormal accumulation of PpARFb2-YFP which was observed in the original, UV-mutagenized, mutant. Together, these findings suggest that we did not identify genes which are responsible for PpARFb2 degradation, and these genes appear unlikely to be involved in auxin signaling.

Various interpretations can explain this experimental outcome. For example, the mutations we discovered could be gain-of-function mutations and knock out of the genes would therefore not restore the initial phenotype but would rather weaken it. This could not be the case for MdR12 and MdR13 as these genes were truncated due to premature stop codons, and a resultant gain-of-function phenotype would therefore be highly unlikely. Furthermore, the genome of *P. patens* has undergone genomic duplications and presents extensive genetic redundancy[17]. It is therefore possible that genetic redundancy has masked effects of our CRISPR-Cas9 generated knock-out mutants, wherein the knocked-out gene copy can be compensated for by one or multiple paralogues leading to unhindered degradation of PpARFb2. However, if these genes have a high degree of conservation, it is plausible that alternative paralogous copies are also targeted by the gRNA, creating higher order mutants. Hitting redundant paralogues using the random UV-light as a mutagen is extremely unlikely and therefore does not satisfactorily explain the apparent high levels of PpARFb2 in our initial UV-mutants, but the lack of such an effect in the CRISPR-Cas9 mutants.

Potentially, a disturbed transcriptome in the UV-mutants could lead to elevated PpARFb2-YFP levels. Transcriptional effects can be caused by mutations in genes encoding for proteins which play a role several layers upstream of actual regulation of Pp*ARFb2* transcription, and such a transcriptional network would be extremely difficult to untangle. qPCR on the Pp*ARFb2* gene, or a complete

transcriptome analysis, would be a start to decipher this problem, but falls outside the scope of this work. Another possibility is that, due to often carrying many mutations, the mutants are in a different developmental or physiological state than the wild-type and may therefore represent a different level of PpARFb2-YFP. We can, however, conclude from the data presented here that none of the selected candidate genes are likely responsible for such a transcriptional effect.

In addition, there are certain crucial assumptions which underly the genetic screen. For example, we assume that mutants in which PpARFb2 ARF degradation is perturbed will display consistently high levels of PpARFb2-YFP and that such mutants are resistant to high levels of auxin (Fig. 3). The latter is a defendable assumption, as we, and others, have shown that disturbing B-class ARF degradation will lead to (often extreme) auxin-resistant phenotypes[12,14]. However, this assumption has a definitive effect on the success of the screen, and if wrong, would render the screen ineffective. In this case, two mutations would be required for individuals to be isolated in our screen: one causing auxin resistance and another caused PpARFb2 accumulation. This would make recapitulation of the stable PpARFb2 phenotype impossible. Furthermore, it is possible that there are physiological stages in which even a stabilized PpARFb2 might not appear overly abundant, and it is possible that such physiological stages resulted in false negatives during the initial screening of the UV-mutants or are obscuring effects in the follow-up CRIPSR-Cas9 mutants. The latter scenario is however quite unlikely, as most of the CRISPR-Cas9 mutants have weak phenotypes.

Given that we have screened a total of 1100-1300 mutants and recovered nine independent mutants which possessed the intragenic E266K PpARFb2 mutation (0.69%-0.81%) suggest we have reached some level of saturation. We therefore conclude that a genetic screen, as described in this chapter, is unlikely to lead to discovery of crucial factors driving PpARFb2 degradation, and other methods should be explored to progress towards such crucial discoveries.

Methods

Plant growth conditions

Moss (*Physcomitrium patens*) reporter lines were obtained from Michael Prigge (UCSD) and grown on BCD medium, or BCD supplemented with 5 mM ammonium tartrate (BCDAT). Propagation occurred through direct transfer of protonema tissue. Plants were grown in 16 hours of light and 8 hours of darkness, at 25 degrees. Open trays filled with water were placed in the growth cabinet to increase humidity.

UV-mutagenesis

We used a similar approach as was described in previous work (see Ref.[18]). In short, one week old plates of $_{pro}$*DR5*::*dsRED*/Pp*ARFb2-YFP* or $_{pro}$*DR5*::*dsRED*/Pp*ARFb2-YFP*$^{\Delta hyg}$ (started from homogenized tissue) were homogenized again and plated onto sterile cellophanes, which were placed on BCDAT medium plates. Next, plant fragments were allowed to grow for one week, thereby forming protonema, and weire then subjected to irradiation with 175 mJ/cm^2 UV light using a Stratalinker UV Crosslinker (Stratagene™). The irradiated tissue was allowed to recover in the dark for 24 hours, and then the cellophanes were moved to fresh BCD plates supplemented with 5 µM NAA. Mutants, as described in Fig. 3, were selected for auxin resistance 4-6 weeks after initial placement onto BCD + NAA.

Whole Genome Sequencing and variant calling of nar mutants

Tissue of the isolated nar mutants and background strains was isolated, frozen in liquid nitrogen, and ground to powder using glass beads. DNA was extracted using the Zymo™ Research Quick-Plant DNA/Seed Miniprep kit, and quality and concentration was verified using a Qubit™ dsDNA Quantification assay. DNA was then shipped on dry ice to BGI Hongkong, checked for integrity prior to library construction using an Agilent™ 5400 fragment analyzer, and the DNA library was prepared with the DNBseq kit. DNA was sequenced using the DNBseq platform which generated pair-ended reads of 150 bp. The quality of raw reads and the presence of sequencing adapters were inspected with FastQC (v0.12.1) and handled with fastp (v1.0.1)[19] using the default parameters. Quality filtered reads were aligned onto the reference genome of *P. patens* (v6)[20] using

bwa-mem2 (v2.2.1)[21]. Each resulting BAM file was ordered according to their genomic position using samtools sort (v1.22.1).

Mutations which occurred in the non-mutagenized background strains were identified by comparison to the reference and masked. Then variable sites in the nar mutants were called and the effect of the identified SNPs were predicted using SNPeff (v5.4)[15]. For further analysis we only included protein modifiers classified as "MISSENSE" (a change in amino acid due to a SNP) or "NONSENSE" (the codon changes into a stop codon due to a SNP). Variants in non-coding regions, or variants occurring in non-coding genes, were excluded from analysis.

Phenotyping

To report on phenotypes of mutants, we always homogenized fully developed plants in sterile demi water, and the cell suspension was then plated onto respective medium. To study colony morphology, we used a Keyence VHX stereomicroscope fitted with a 20-200x VH-Z20R objective.

CRISPR-Cas9 mutagenesis

Candidate gene sequences were scanned for potential CRISPR guide sequences using CRISPOR[22], and pairs of guides were chosen that have high "RS3" scores and flank either the entire gene or large regions encoding conserved domains. Forward and reverse oligos containing the guide sequences were synthesized, phosphorylated, annealed, and Golden-Gate assembled into dual-guide CRISPR/Cas9 constructs using the pMP2284 vector and the pMP2316 'bridge' plasmid[14]. pMP2316 contains the sgRNA scaffold sequence and an *U6* promoter from *Funaria hygrometrica*[23] flanked by BsaI sites with overhangs compatible for the 3' overhang of the first guide oligos and the 5' overhang or the second guide oligos. The assembled constructs contain $_{pro}$Zm*Ubi::Cas9* divergently transcribed from $_{pro}$Pp*U6::sgRNA1/*Fh*U6::sgRNA2* with a $_{pro}$*35S::hdh* hygromycin selection cassette.

Protoplasts of the Pp*ARFb2-YFPt DR5::DsRed* strain were transformed as previously described (see Ref.[24]) with modifications (see Ref.[14]). After 4 days, transformants were selected for 1 week with 15 mg/l hygromycin B, after which several dozen individual transformants were picked. Deletion mutants were identified by PCR with primers outside the CRISPR targets followed by sequencing

the products (Supplementary Information Fig. 3a). PCR with one of the outside primers and an internal primer was used to detect WT and mosaic transformants with an intact gene present in some cells (Supplementary Information Fig. 3a, Supplementary Data Table 1).

The mutants were grown for 21 days on BCD media alone or supplemented with either 3.5 mM ammonium tartrate (BCDAT) or 5 µM NAA (BCD+NAA). Plants were photographed with a Nikon SMZ1500 microscope (0.5× objective and 1× zoom) with a DS-Ri1 camera. DsRed fluorescence was captured with a TRITC filter cube and a 1.5s exposure time.

Keyence microscopy

Six-day-old protonemata for mutants and parent lines were transferred to wells of 48-well plates containing 900 µl solid media overlain with 20 µl liquid media, both containing 100 mM bortezomib or 0.1% DMSO. The following day, Z-stacked images for bright-field and YFP (2s exposure) were captured with a 10× objective with a Keyence BZ-X810 microscope.

Confocal microscopy

Confocal images were obtained using a Leica SP8X-SMD confocal microscope using a HC PL APO 20x/0.75 objective. For excitation of YFP, a 488 nm 40 MHz pulsed white-light laser line was used. YFP fluorescence was detected between 500-550 nm with hybrid detectors set to photon counting mode and 1.00-24.50 ns time-gating active to suppress autofluorescence. To produce micrographs, maximum projection z-stacks were generated through ImageJ (v1.52).

For Bortezomib treatment, freshly prepared Bortezomib (Cayman Chemical™) was added into BCDAT medium to a final concentration of 10 µM. Gene frames (Thermo Fisher™) were utilized to create imaging chambers with BCDAT agarose pads (containing respective treatments). Protonema tissue was then placed onto the agarose pads and chambers were filled with Perfluordecalin (Sigma-Aldrich) to allow gas exchange and sealed with a coverslip. Plants were imaged at the indicated time intervals.

Acknowledgements

We gratefully acknowledge Peter van Gisbergen for advice on moss culturing and Janneke Bloem for providing a UV Stratalinker. This work has been supported by the Netherlands Organization for Scientific Research (NWO; OCENW.M20.031 M.d.R., J.W.B.) and the Experimental Plant Sciences graduate school (outgoing travel grant, M.d.R.).

Supplementary Information

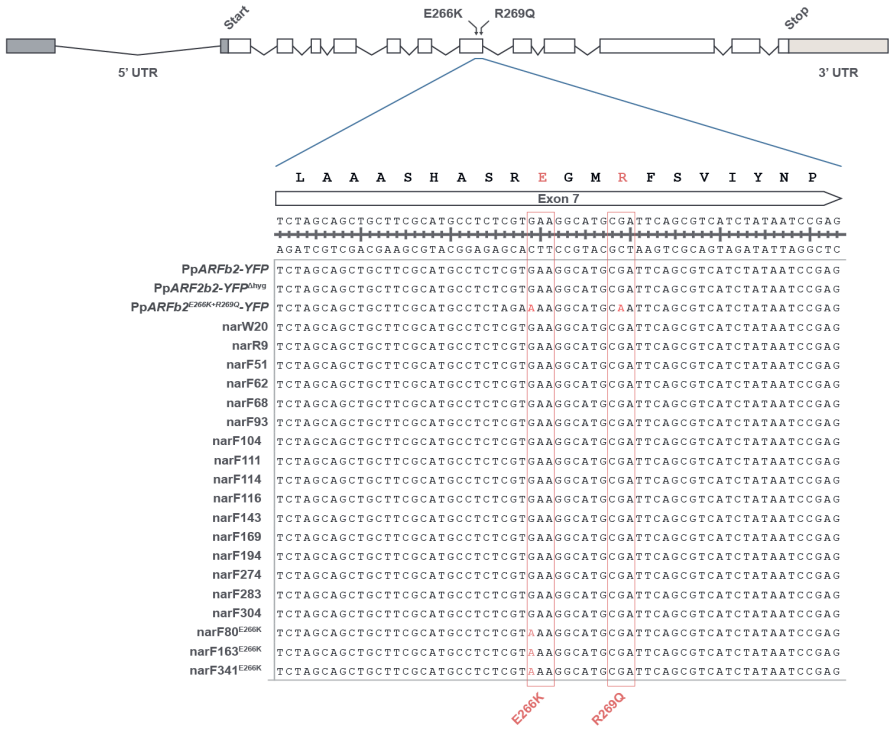


Fig. 1 | Alignment of sequencing reads nar mutants to Pp*ARFb2* gene model.
Shown here are sequencing results aligned to the Pp*ARFb2* gene, exon 7 is highlighted as exon 7 contains the codons encoding the crucial E266 and R269 residues, in red SNPs leading to E266K and R269Q substitutions, respectively.

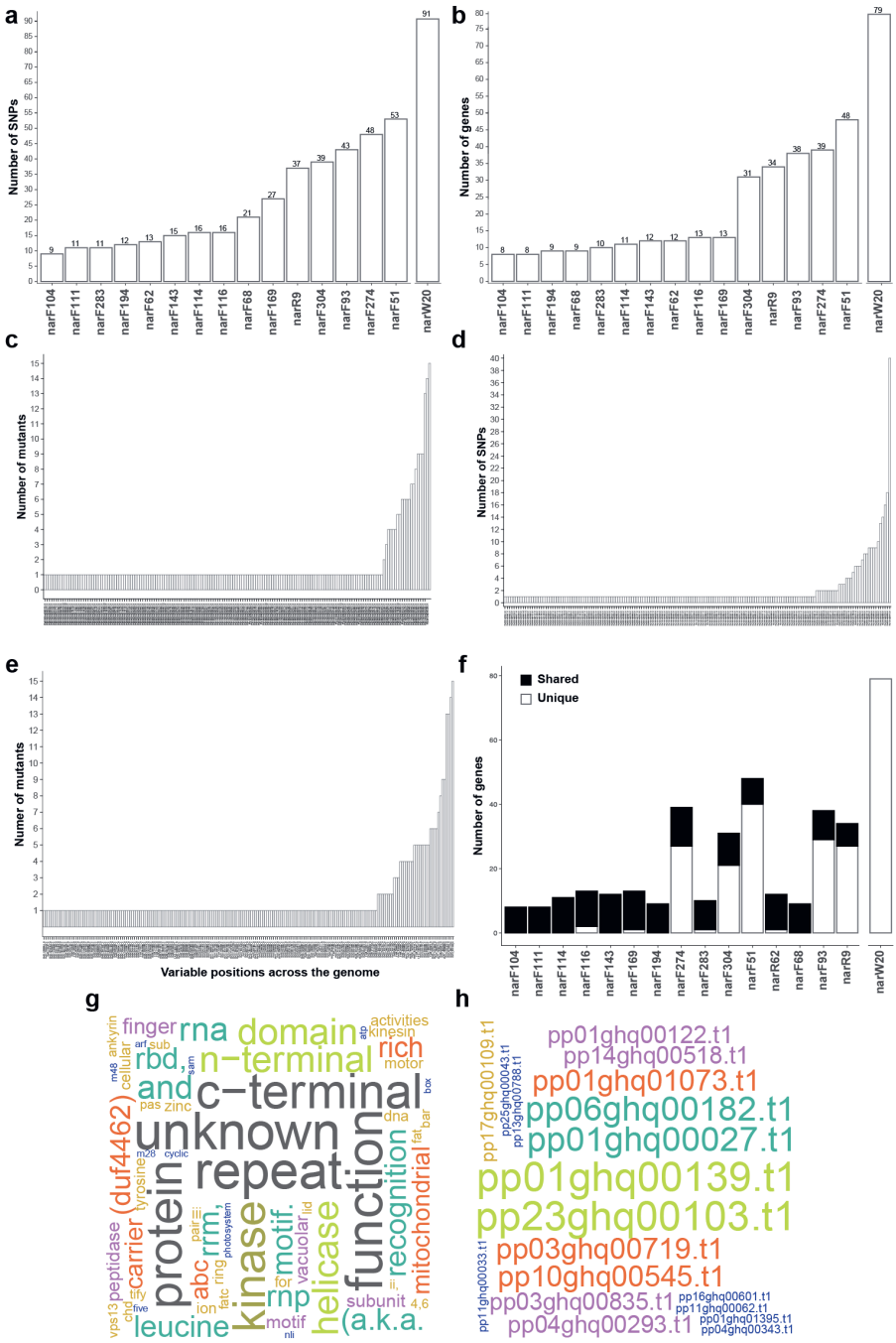


Fig. 2 | Overview of the mutational landscape in nar mutants.
a. The number of total SNPs identified in the nar mutants which passed through the quality control cut-off which had a predicted disruptive effect on gene function. **b.** The total number of genes affected in each nar mutant. **(continued on next page)**

Fig. 2 (continued) | c. The number of SNPs for each gene which was shown to carry mutations. **d.** The number of times a specific SNP has occurred in the nar mutants. **e.** An overview of each identified variable position over the P. patens genome, and the occurrence of each variable position across the nar mutants. **f.** Overlap and uniqueness of genes across the nar mutants. **g.** Word cloud of gene ontology terms, size of each word corresponds to the relative number of times it occurs in the dataset. **h.** Word cloud of gene IDs, size of each word corresponds to the relative number of times it occurs in the dataset.

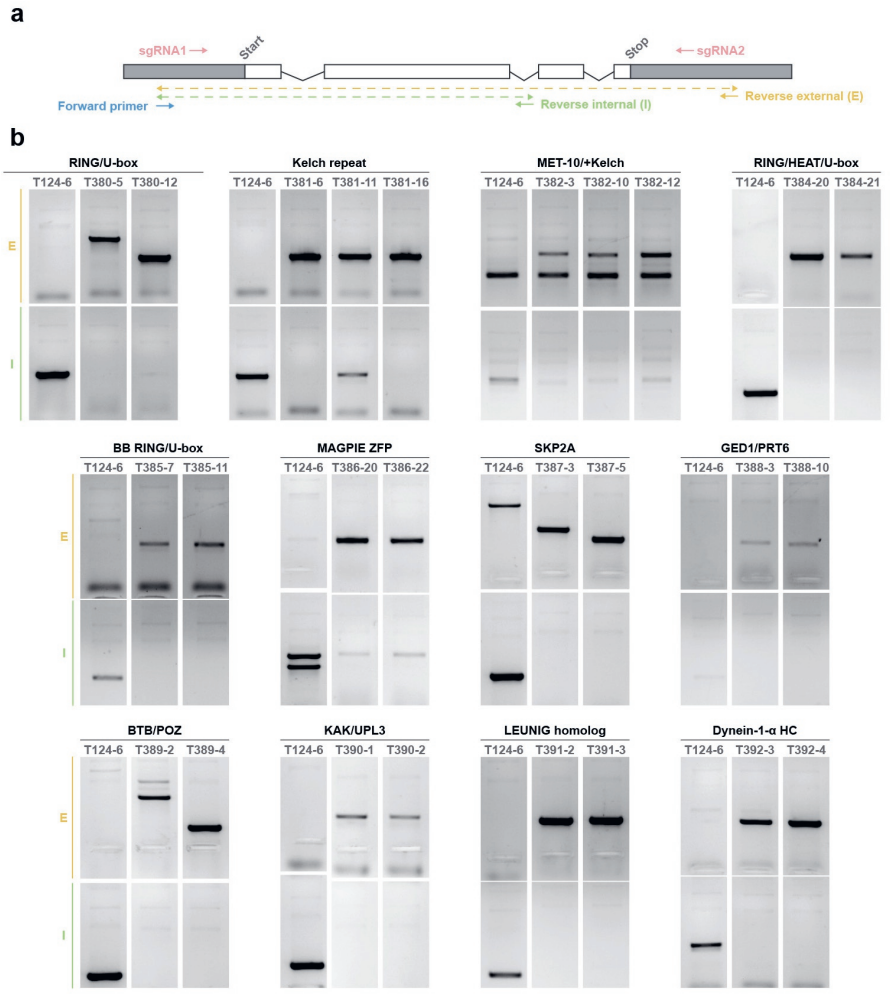


Fig. 3 | Agarose gel electrophoresis reveals large deletions in CRISPR-Cas9 mutants.
a. Hypothetical gene model showing how genotyping primer pairs are positioned relative to the gRNAs used to direct the Cas9 enzyme to the DNA, colors of the amplicons and primer pairs correspond to (**b**). **b.** Genotyping results shown through gel electrophoresis, T124-6 corresponds to the wild type background strain and thus depicts unedited PCR results of the non-edited gene.

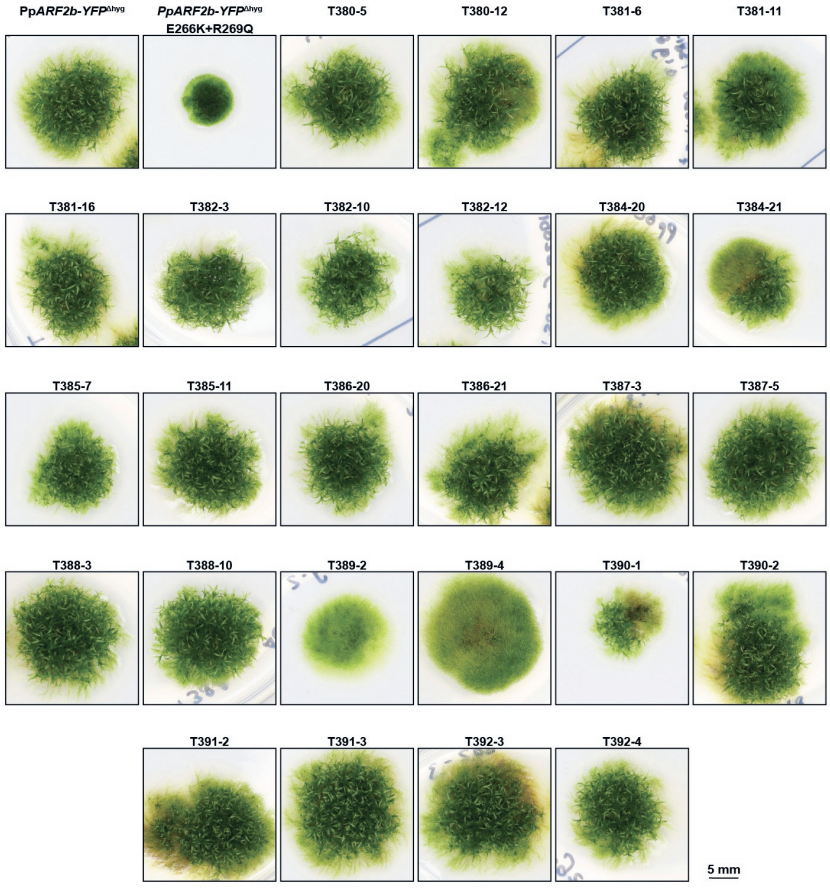


Fig. 4 | Overview of colony morphology CRISPR-Cas9 mutants.
Phenotypes of 14 – day old plants grown as spot inoculants (ie homogenized tissue was suspended in sterile demi water, and drops of this suspension were plated onto BCDAT medium). CRISPR-Cas9 mutants (T-series) can be compared to the unmutated background (Pp*ARFb2-YFP*$^{\Delta hyg}$) and the Pp*ARFb2-YFP*$^{E266K+R269Q}$ mutant.



Fig. 5 | Overview of morphology and auxin response CRISPR-Cas9 mutants.
Phenotypes of 14 – day old plants grown as spot inoculants. Homogenized tissue was suspended in sterile demi water, and drops of this suspension were plated onto BCD, BCDAT (+NH_4), and BCD + NAA medium. CRISPR-Cas9 mutants (T-series) can be compared to the unmutated background (Pp*ARFb2-YFP*$^{\Delta hyg}$) and the Pp*ARFb2-YFP*$^{E266K+R269Q}$ mutant. For each NAA treated colony, *Dr5::DsRED* signal is shown as a proxy for the transcriptional auxin response.

Supplementary Data Table 1 | Oligonucleotides used in this study.

Primer	Sequence 5'>3'	Description
MdR1-cr1F	CCATTGGTAGACTTGTGTGAACGAGT	gRNA Pp18Ghq00236
MdR1-cr1R	TAAAACTCGTTCACACAAGTCTACCA	gRNA Pp18Ghq00236
MdR1-cr2F	TATGCTTGGCATAGAGTAGTAAG	gRNA Pp18Ghq00236
MdR1-cr2R	AAACCTTACTACTCTATGCCAAG	gRNA Pp18Ghq00236
MdR2-cr1F	CCATGCTGAGGACAGAAAGCGTGAGT	gRNA Pp6Ghq00825
MdR2-cr1R	TAAAACTCACGCTTTCTGTCCTCAGC	gRNA Pp6Ghq00825
MdR2-cr2F	TATGGCCGGATGCCGCTATGCAG	gRNA Pp6Ghq00825
MdR2-cr2R	AAACCTGCATAGCGGCATCCGGC	gRNA Pp6Ghq00825
MdR3-cr1F	CCATTCGCGGGCAGAGTTGATCTGGT	gRNA Pp21Ghq00063
MdR3-cr1R	TAAAACCAGATCAACTCTGCCCGCGA	gRNA Pp21Ghq00063
MdR3-cr2F	TATGTGGGTGCTCGACACTGAGA	gRNA Pp21Ghq00063
MdR3-cr2R	AAACTCTCAGTGTCGAGCACCCA	gRNA Pp21Ghq00063
MdR5-cr1F	CCATCCGACCTCACTACAAATGCGGT	gRNA Pp11Ghq00033
MdR5-cr1R	TAAAACCGCATTTGTAGTGAGGTCGG	gRNA Pp11Ghq00033
MdR5-cr2F	TATGCCGCCTGATAGAATCACCA	gRNA Pp11Ghq00033
MdR5-cr2R	AAACTGGTGATTCTATCAGGCGG	gRNA Pp11Ghq00033
MdR6-cr1F	CCATCACTTCCGATGCCTCATCAGGT	gRNA Pp01Ghq00012
MdR6-cr1R	TAAAACCTGATGAGGCATCGGAAGTG	gRNA Pp01Ghq00012
MdR6-cr2F	TATGACAGGCAGCCGAACAGCGG	gRNA Pp01Ghq00012
MdR6-cr2R	AAACCCGCTGTTCGGCTGCCTGT	gRNA Pp01Ghq00012
MdR7-cr1F	CCATGGCTAGGGACGATGCACCCAGT	gRNA Pp11Ghq00253
MdR7-cr1R	TAAAACTGGGTGCATCGTCCCTAGCC	gRNA Pp11Ghq00253
MdR7-cr2F	TATGCTGCTGATTACCAGGACCA	gRNA Pp11Ghq00253
MdR7-cr2R	AAACTGGTCCTGGTAATCAGCAG	gRNA Pp11Ghq00253
MdR8-cr1F	CCATGTGGCGCATATCCTATGTCTGT	gRNA Pp03Ghq01479
MdR8-cr1R	TAAAACAGACATAGGATATGCGCCAC	gRNA Pp03Ghq01479
MdR8-cr2F	TATGGGTTCAGGAAACTCTGGTG	gRNA Pp03Ghq01479
MdR8-cr2R	AAACCACCAGAGTTTCCTGAACC	gRNA Pp03Ghq01479
MdR9-cr1F	CCATGTGGACCGACTGCACAACAGGT	gRNA Pp06Ghq00831
MdR9-cr1R	TAAAACCTGTTGTGCAGTCGGTCCAC	gRNA Pp06Ghq00831
MdR9-cr2F	TATGCGGATTACGAGTAATCAGG	gRNA Pp06Ghq00831
MdR9-cr2R	AAACCCTGATTACTCGTAATCCG	gRNA Pp06Ghq00831

Primer	Sequence 5'>3'	Description
MdR10-cr1F	CCATGCTAGATTACACGAGGCTGGGT	gRNA Pp06Ghq00831
MdR10-cr1R	TAAAACCCAGCCTCGTGTAATCTAGC	gRNA Pp06Ghq00831
MdR10-cr2F	TATGGTACATTTAGAAGAAGCCG	gRNA Pp06Ghq00831
MdR10-cr2R	AAACCGGCTTCTTCTAAATGTAC	gRNA Pp06Ghq00831
MdR11-cr1F	CCATGAGGCGTCGCAACCTTCGGGGT	gRNA Pp05Ghq00659
MdR11-cr1R	TAAAACCCCGAAGGTTGCGACGCCTC	gRNA Pp05Ghq00659
MdR11-cr2F	TATGTGGGCGGAGGATCTCGAGG	gRNA Pp05Ghq00659
MdR11-cr2R	AAACCCTCGAGATCCTCCGCCCA	gRNA Pp05Ghq00659
MdR12-cr1F	CCATGGTTTCCCTTCCCTCTCACGGT	gRNA Pp01Ghq00139
MdR12-cr1R	TAAAACCGTGAGAGGGAAGGGAAACC	gRNA Pp01Ghq00139
MdR12-cr2F	TATGGGCATGACAGAATGCAGAG	gRNA Pp01Ghq00139
MdR12-cr2R	AAACCTCTGCATTCTGTCATGCC	gRNA Pp01Ghq00139
MdR13-cr1F	CCATGAGCATGATGAGCCCCACAGGT	gRNA Pp22Ghq00756
MdR13-cr1R	TAAAACCTGTGGGGCTCATCATGCTC	gRNA Pp22Ghq00756
MdR13-cr2F	TATGGGATGCTCTAAGGCCACCA	gRNA Pp22Ghq00756
MdR13-cr2R	AAACTGGTGGCCTTAGAGCATCC	gRNA Pp22Ghq00756
MdR1-Fwd	TCGATCTGGGTGCTCTTGTGG	genotyping Pp18Ghq00236
MdR1-iRev	CTGCACACTCCAACCCTTCCT	genotyping Pp18Ghq00236
MdR1-Rev	TCGATTCCTCCATTCCAGTGCTT	genotyping Pp18Ghq00236
MdR2-Fwd	TGCAGAGATGGTGAAGGAGGC	genotyping Pp6Ghq00825
MdR2-iFwd	TCGATTGTTGCTAAGTCTCTGTTACCA	genotyping Pp6Ghq00825
MdR2-Rev	AGCAACACCTGTAACTTCCCACA	genotyping Pp6Ghq00825
MdR3-Fwd	GAGTGTTTCGGAGTTGGCGTG	genotyping Pp21Ghq00063
MdR3-iRev	GATGCCATGCTCGCCTTTACC	genotyping Pp21Ghq00063
MdR3-Rev	AGGGCCATCAACAATCAGGGT	genotyping Pp21Ghq00063
MdR5-Fwd	TGACTACGACTGGTTGCTATGACTT	genotyping Pp11Ghq00033
MdR5-iFwd	GCGGTTCTTGCATGTCAGGG	genotyping Pp11Ghq00033

Primer	Sequence 5'>3'	Description
MdR5-Rev	TGGCCACGGTCAAATGAAACAA	genotyping Pp11Ghq00033
MdR6-Fwd	TGGTTCCCTTGAAGAGATGGTGT	genotyping Pp01Ghq00012
MdR6-iRev	GCTCCGCAAGTGAAAAGGACAA	genotyping Pp01Ghq00012
MdR6-Rev	CCATTTCAACAGTGCAGCGGA	genotyping Pp01Ghq00012
MdR7-Fwd	TGTCTTGAAAATGAAGCGCAGTGT	genotyping Pp11Ghq00253
MdR7-iFwd	CGTACGTTGCGAAGACTTCCG	genotyping Pp11Ghq00253
MdR7-Rev	CAGAGGGTGTCAACGGAAGGT	genotyping Pp11Ghq00253
MdR8-Fwd	ATGCGTGCAATATTCGACTATGGG	genotyping Pp03Ghq01479
MdR8-iRev	CCCAGCCTCTGTAATGCCCTT	genotyping Pp03Ghq01479
MdR8-Rev	TGAAGACTCATGACAAGGACGAGAA	genotyping Pp03Ghq01479
MdR9-Fwd	CTTTTGTGCCACTGTTGATCTCCA	genotyping Pp06Ghq00831
MdR9-iRev	ACCTTCCTCTTCACAATGCCCT	genotyping Pp06Ghq00831
MdR9-Rev	GCTGCCCAAGGTTATGTAGTGC	genotyping Pp06Ghq00831
MdR10-Fwd	AGGGGTGATATCGTTTTCTTCAGTCA	genotyping Pp06Ghq00831
MdR10-iRev	ATCTTGCTCCTGACCAACGCT	genotyping Pp06Ghq00831
MdR10-Rev	ACCTTTCACGCATTCCTGAACAAA	genotyping Pp06Ghq00831
MdR11-Fwd	ATGGTTCAGGCAGTGGGTAGAG	genotyping Pp05Ghq00659
MdR11-iRev	GTCCTTCGATGCCAACACGC	genotyping Pp05Ghq00659
MdR11-Rev	TCCACCCTATCCACCTCCCC	genotyping Pp05Ghq00659
MdR12-Fwd	AGGCTCCACACACACACAAATG	genotyping Pp01Ghq00139
MdR12-iRev	TACTTGACCGCCTCGTGTACC	genotyping Pp01Ghq00139
MdR12-Rev	GCAATTAAGTGGCCCTCATGCA	genotyping Pp01Ghq00139

Primer	Sequence 5'>3'	Description
MdR13-Fwd	AAGCCACACATCCTCCCTTCC	genotyping Pp22Ghq00756
MdR13-iFwd	TGTGGGATGAGGGAGAGCAGA	genotyping Pp22Ghq00756
MdR13-Rev	TGAGTGAAAATTTGCCTGCCAGT	genotyping Pp22Ghq00756

References

1 Vanneste, S., Pei, Y. & Friml, J. Mechanisms of auxin action in plant growth and development. *Nat Rev Mol Cell Biol* (2025). https://doi.org/10.1038/s41580-025-00851-2

2 Mockaitis, K. & Estelle, M. Auxin receptors and plant development: a new signaling paradigm. *Annu Rev Cell Dev Biol* **24**, 55–80 (2008). https://doi.org/10.1146/annurev.cellbio.23.090506.123214

3 Leyser, O. Auxin Signaling. *Plant Physiol* **176**, 465–479 (2018). https://doi.org/10.1104/pp.17.00765

4 Chapman, E. J. & Estelle, M. Mechanism of auxin-regulated gene expression in plants. *Annu Rev Genet* **43**, 265–285 (2009). https://doi.org/10.1146/annurev-genet-102108-134148

5 Roosjen, M., Paque, S. & Weijers, D. Auxin Response Factors: output control in auxin biology. *J Exp Bot* **69**, 179–188 (2018). https://doi.org/10.1093/jxb/erx237

6 Cance, C., Martin-Arevalillo, R., Boubekeur, K. & Dumas, R. Auxin response factors are keys to the many auxin doors. *New Phytol* **235**, 402–419 (2022). https://doi.org/10.1111/nph.18159

7 Kato, H. *et al.* Design principles of a minimal auxin response system. *Nat Plants* **6**, 473–482 (2020). https://doi.org/10.1038/s41477-020-0662-y

8 Lavy, M. *et al.* Constitutive auxin response in Physcomitrella reveals complex interactions between Aux/IAA and ARF proteins. *Elife* **5** (2016). https://doi.org/10.7554/eLife.13325

9 Flores-Sandoval, E., Eklund, D. M. & Bowman, J. L. A Simple Auxin Transcriptional Response System Regulates Multiple Morphogenetic Processes in the Liverwort Marchantia polymorpha. *PLoS Genet* **11**, e1005207 (2015). https://doi.org/10.1371/journal.pgen.1005207

10 Boer, D. R. *et al.* Structural basis for DNA binding specificity by the auxin-dependent ARF transcription factors. *Cell* **156**, 577–589 (2014). https://doi.org/10.1016/j.cell.2013.12.027

11 de Roij, M., Borst, J. W. & Weijers, D. Protein degradation in the auxin response. *Plant Cell* (2024). https://doi.org/10.1093/plcell/koae125

12 de Roij, M., Hernandez Garcia, J., Das, S., Borst, J. W. & Weijers, D. ARF degradation defines a deeply conserved step in auxin response. *Nat Plants* **11**, 717–724 (2025). https://doi.org/10.1038/s41477-025-01975-1

13 de Roij, M. *et al.* Diversification of functional requirements for proteolysis of auxin response factors. *Nature Communications* (2026). https://doi.org/10.1038/s41467-026-70440-0

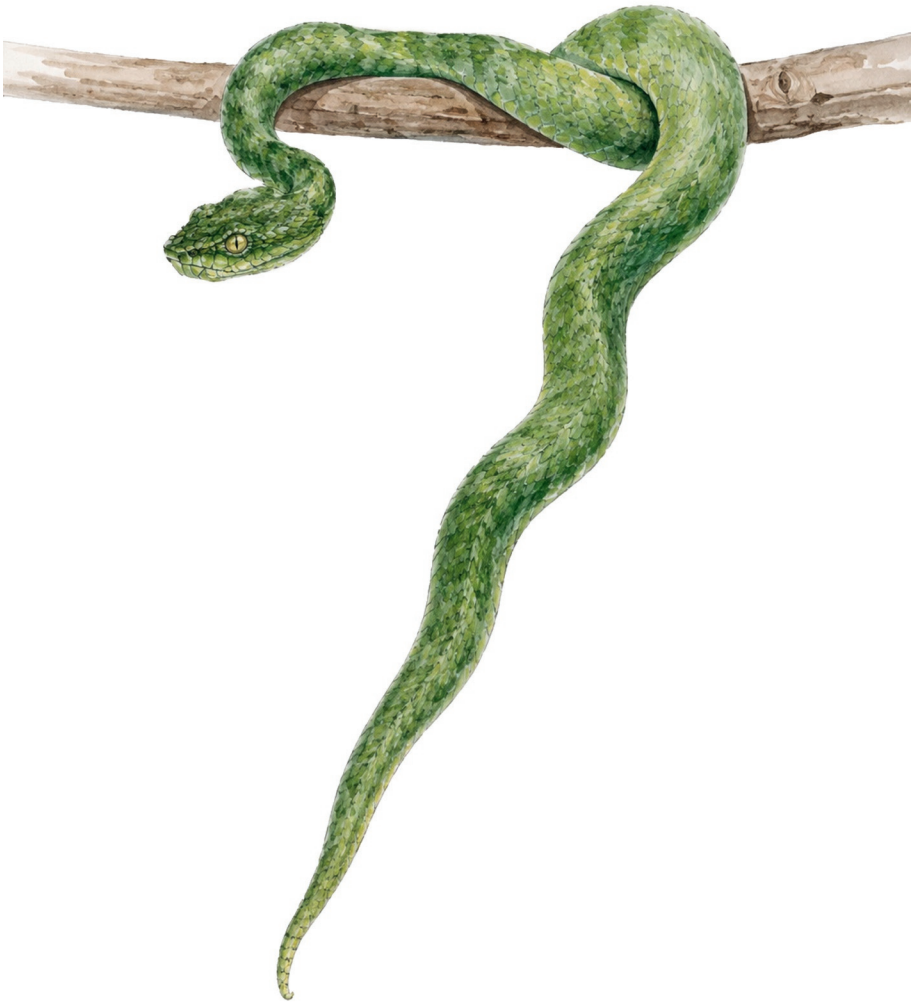
14 Prigge, M. J. *et al.* Comparative mutant analyses reveal a novel mechanism of ARF regulation in land plants. *Nat Plants* **11**, 821–835 (2025). https://doi.org/10.1038/s41477-025-01973-3

15 Cingolani, P. *et al.* A program for annotating and predicting the effects of single nucleotide polymorphisms, SnpEff: SNPs in the genome of Drosophila melanogaster strain w1118; iso-2; iso-3. *Fly (Austin)* **6**, 80–92 (2012). https://doi.org/10.4161/fly.19695

16 Fung, D. *et al.* Evidence supporting a catalytic pentad mechanism for the proteasome and other N-terminal nucleophile enzymes. *Nat Commun* **16**, 2949 (2025). https://doi.org/10.1038/s41467-025-58077-x

17 Rensing, S. A. *et al.* An ancient genome duplication contributed to the abundance of metabolic genes in the moss Physcomitrella patens. *BMC Evol Biol* **7**,

130 (2007). https://doi.org/10.1186/1471-2148-7-130
18 Bascom, C., Jr. *et al.* Clade-D auxin response factors regulate auxin signaling and development in the moss Physcomitrium patens. *PLoS Biol* **21**, e3002163 (2023). https://doi.org/10.1371/journal.pbio.3002163
19 Chen, S., Zhou, Y., Chen, Y. & Gu, J. fastp: an ultra-fast all-in-one FASTQ preprocessor. *Bioinformatics* **34**, i884–i890 (2018). https://doi.org/10.1093/bioinformatics/bty560
20 Bi, G. *et al.* Near telomere-to-telomere genome of the model plant Physcomitrium patens. *Nat Plants* **10**, 327–343 (2024). https://doi.org/10.1038/s41477-023-01614-7
21 Vasimuddin, M., Misra, S., Li, H. & Aluru, S. in *2019 IEEE International Parallel and Distributed Processing Symposium (IPDPS)* 314–324 (2019).
22 Concordet, J. P. & Haeussler, M. CRISPOR: intuitive guide selection for CRISPR/Cas9 genome editing experiments and screens. *Nucleic Acids Res* **46**, W242–W245 (2018). https://doi.org/10.1093/nar/gky354
23 Kirbis, A. *et al.* Comparative analysis using a chromosome-scale genome assembly for Funaria hygrometrica suggests greater collinearity in mosses than in seed plants. *Commun Biol* **8**, 330 (2025). https://doi.org/10.1038/s42003-025-07749-x
24 Cove, D. J. *et al.* Transformation of the moss Physcomitrella patens using direct DNA uptake by protoplasts. *Cold Spring Harb Protoc* **2009**, pdb prot5143 (2009). https://doi.org/10.1101/pdb.prot5143



Chapter 7

Mapping the MpARF2 proximal interactome identifies putative degradation regulators

Authors

Martijn de Roij[1], Mark Roosjen[1], Clint Heijstek[1], Catherina Albrecht[1], Jorge Hernández García[1] & Dolf Weijers[1,*]

Affiliations

[1] Laboratory of Biochemistry, Wageningen University, Stippeneng 4, 6708WE Wageningen, the Netherlands

* Corresponding author: dolf.weijers@wur.nl

Parts of this chapter have been submitted for publication as:

Hernández-García, J., *et al.* Subnuclear cofactor partitioning underlies auxin-dependent transcriptional regulation. *Cell* (2026).

Abstract

Auxin signaling in land plants relies on Auxin Response Factors transcription factors (ARFs), whose protein abundance critically shapes transcriptional output. Although ARFs are regulated through ubiquitin–proteasome–mediated degradation, the factors responsible for targeting ARFs for proteolysis remain largely unknown. Here, we investigated the interactome of the unstable MpARF2 from *Marchantia polymorpha* using TurboID-based proximity labeling. By comparing the interactome of a wild type MpARF2 protein with a stabilized mutant, we identified a set of MpARF2-proximal proteins, including candidate ubiquitin ligases and a protein kinase, selectively associated with the unstable protein. Targeted disruption of selected candidates using CRISPR–Cas9 in a MpARF2 reporter background failed to yield edited alleles, despite repeated attempts. These findings suggest that MpARF2 degradation may involve essential factors for viability in Marchantia, or otherwise genetically constrained components of the ubiquitin–proteasome system. Together, this work defines the MpARF2 proximal proteome, identifies possible proteolysis regulators, and highlights challenges in genetically dissecting transcription factor proteolysis in plants.

Introduction

After its initial discovery, auxin has taken up position in the field of plant science as a central and crucial signaling molecule for plant development[1]. Auxin exercises developmental control through a variety of ways, one of which is the Nuclear Auxin Pathway (NAP)[2,3]. The NAP converts the molecular auxin signal into a transcriptional response, and the Auxin Response Factor (ARF) transcription factor proteins are key regulators during this process[4,5]. In land plants, canonical ARFs are comprised of three protein domains, a DNA-binding domain (DBD) at the N-terminus, a middle region (MR), and a Phox and Bem 1 domain (PB1) at the C-terminus[5,6]. Canonical land plant ARFs are classified into three subfamilies, A, B, and C-class ARFs[7]. These subfamilies are functionally distinct, with A-class ARFs acting as auxin-inducible transcriptional activators and B-class ARFs as auxin-independent repressors of auxin-responsive genes[8,9]. C-class ARFs appear to regulate a different gene set and seem to have functionally diverged away from the classic auxin-response system[8,10]. A -and B-class ARFs regulate gene expression through a competition-based model, DNA-binding of either class is thought to be influenced by DNA-binding kinetics, and crucially, protein stoichiometry[8,9,11]. This model suggests that accurate and well-timed tuning of the transcriptional auxin response requires appropriate control over ARF protein levels, for example through transcriptional or post-translational regulation[12].

Recently, roles of ARF proteolysis through the ubiquitin-proteasome system (UPS) have emerged as important, ancient, and evolutionarily conserved mechanisms for post-translational control over ARF stoichiometry[12-15]. In a concerted effort, we and others have unraveled the post-translational control of ARF degradation through the UPS[13-15]. Mainly, we identified residues of ARF proteins (positioned in the DBD) which were integral for degradation, transcriptional auxin response, and development[13-15]. However, external factors, such as an ubiquitin-ligase, the enzyme targeting substrate proteins to the 26S proteasome for proteolysis, or other proteins which steer ARF degradation, remain elusive[12].

In chapter 5 we reported on a genetic screen in which we induced genome-wide mutations to identify such factors, but the screen proved unsuccessful in identifying causal mutations (see Chapter 5). Here, we employ a proteomic approach to identify these factors in *Marchantia polymorpha*. As the genome of *Marchantia* typically has little genetic redundancy, it is a genetically tractable system. We therefore use *in vivo* TurboID-based proximity labelling

to identify proteins that interact with the unstable MpARF2, but not with a stable, mutant version (E296K+R300Q)[13].

Results

Expression of translational MpARF2 fusions to TurboID

To obtain a holistic overview of the MpARF2 interactome, we generated a set of different translational fusion proteins (Fig. 1). The MpARF2 DBD is sufficient to confer degradation through the proteasome to an otherwise stable mNeonGreen (mNG) protein[13], suggesting that all components required for this instability are present in the DBD and other domains are not required. We therefore fused the MpARF2 wild type (DBD^{WT}-sYFP-turboID) and E297K+R300Q (DBD^{E+R}-sYFP-turboID) mutant DBDs to a Nuclear Localization Signal (NLS) and a superfolder Yellow Fluorescent Protein (sYFP), wherein the MpARF2 DBDs would function as bait for potential interactors (Fig. 1). By comparing both the unstable and stabilized MpARF2 variants, we aimed to enrich for factors specifically associated with degradation rather than generic ARF interactors. These fusion proteins were expressed from a minimal 1.9kb Mp*ARF2* promoter in a Tak-1 background (Fig. 1). To account for unspecific biotinylation we included a negative control with the MpARF2 DBD excluded (1.9NLS-sYFP-turboID; Fig. 1). We also generated a full length (FL) wild type MpARF2 version, wherein we fused to entire MpARF2 protein (i.e. all three domains) to sYFP and turboID (FL-^{WT}-sYFP-turboID) and expressed this from a 3kb Mp*ARF2* promoter (Fig. 1). We then used this construct to complement the Mp*arf2-1* knock-out mutant[16]. Again, to identify false positives, we included a negative control 3NLS-sYFP-turboID which we expressed in a Tak-1 background (Fig. 1).

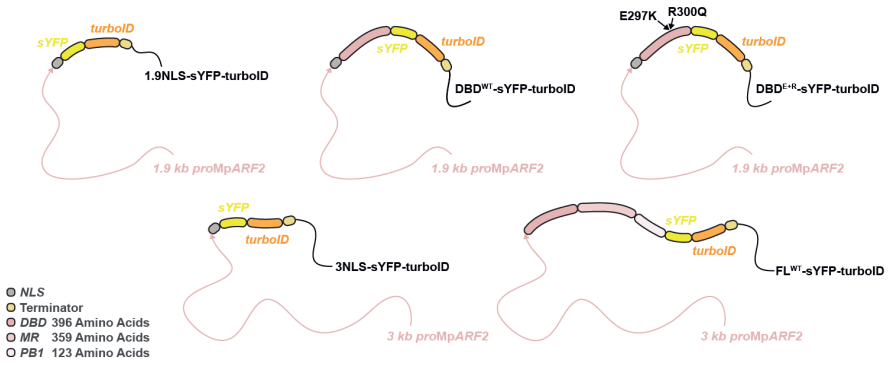


Fig. 1 | Diagram of the genetic translational Mp*ARF2-turboID* fusions. Overview of the translational fusion proteins generated for, and used in, this chapter. The Mp*ARF2* coding regions for the DBD, MR, and PB1 are indicated in pink, and their sizes in amino acids are shown in the figure legend. sYFP stands for superfolder Yellow Fluorescent Protein, and NLS for Nuclear Localization Signal. Names of each construct are shown in black and are used consistently throughout this chapter.

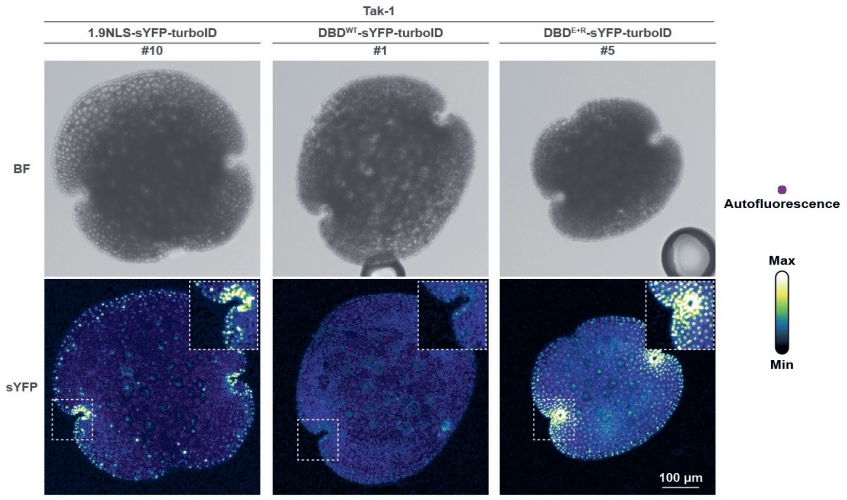


Fig. 2 | Expression patterns of turboID fusion proteins.
Expression of sYFP signal assessed by confocal microscopy in dormant gemmae. The genotypes correspond to the genetic constructs shown in Fig. 1. BF stands for brightfield and chloroplast autofluorescence is shown in magenta. The apical notch is enlarged and shown as an inset.

As expected, the DBD^{WT}-sYFP-turboID was highly unstable *in vivo* and accumulated to barely detectable levels (Fig. 2). This was in stark contrast to the DBD^{E+R}-sYFP-turboID and 1.9NLS-sYFP-turboID constructs, which accumulated to high levels, indicative of the impaired degradation of the construct (Fig. 2).

Interestingly, we recovered two FL^{WT}-sYFP-turboID complementation lines (#1 and #3) in the Mp*arf2-1* background which produced relatively normal thalli and gemma cups with gemmae, which the uncomplemented knock-out mutant fails to develop (Fig. 3a,b). In these lines, MpARF2 levels appeared similar to levels observed in the MpARF2-mNG knock-in lines[17]. Both FL^{WT}-sYFP-turboID #1 and #3 displayed delayed formation of gemma cups relative to Tak-1. However, gemma morphology was rather typical (Fig. 3a,c) and these gemmae showed a qualitatively and quantitatively restored auxin response (Fig. 3e,d)[16]. Again, 3NLS-sYFP-turboID was highly stable and accumulated to very high levels as this construct lacked MpARF2 to confer degradation.

TurboID reveals the MpARF2 interactome

In Chapter 5 we show that MpARF2 degradation is pervasive throughout the Marchantia lifecycle and occurs in almost all developmental stages (see Chapter 5). We also show that in 7-day old

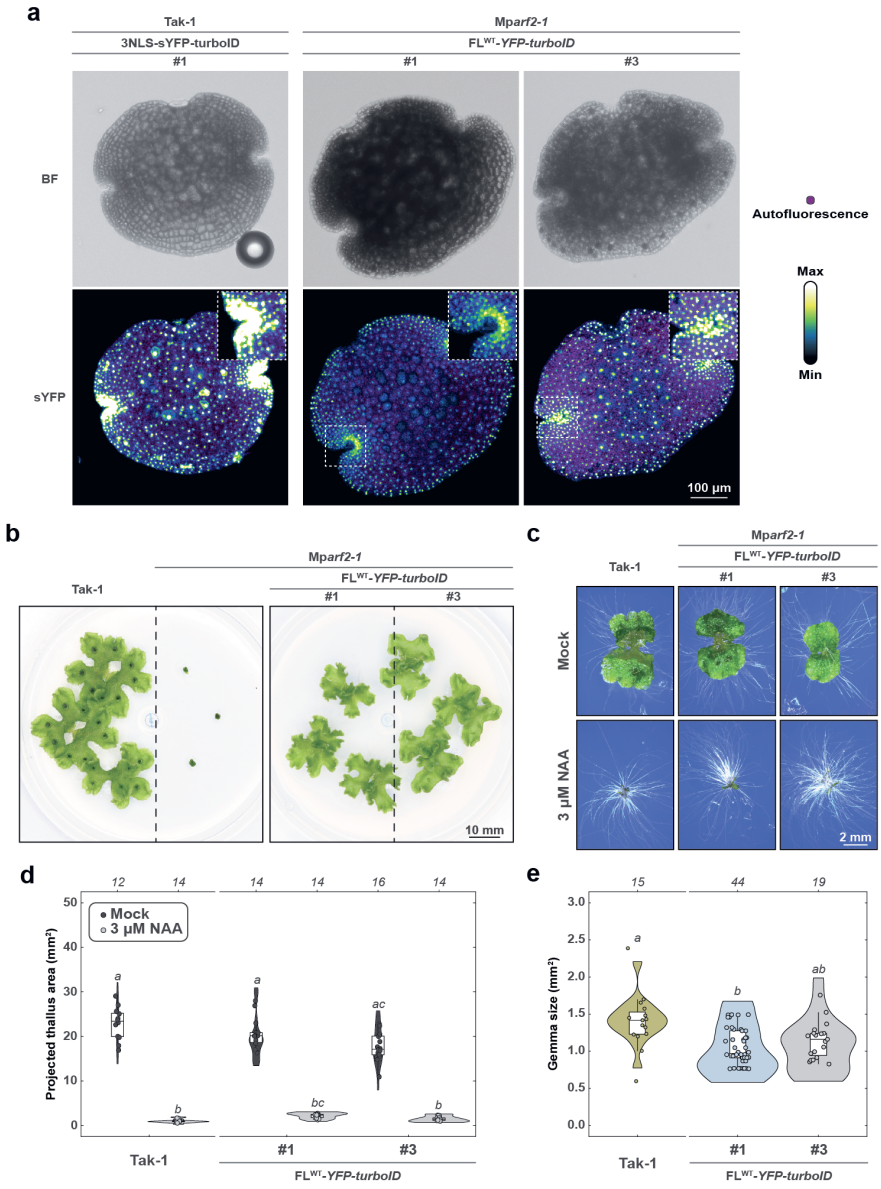


Fig. 3 | Expression of turboID fusion proteins and mutant complementation.
a. Expression of sYFP signal assessed by confocal microscopy. The genotypes correspond to the genetic constructs shown in Fig. 1. BF stands for brightfield and chloroplast autofluorescence is shown in magenta. The apical notch is enlarged and shown as an inset. Note that the 3NLS-sYFP-turboID line is generated in the Tak-1 background, and the FL^{WT}-sYFP-turboID lines are generated in the Mp*arf2-1* knock-out mutant background. **b.** Overview of the phenotypes of 20-day old plants showing the complementation ability of FL^{WT}-sYFP-turboID. **c.** Qualitative assessment of the restoration of auxin response of the Mp*arf2-1* knock-out mutant complemented with FL^{WT}-sYFP-turboID. **(continued on next page)**

Fig. 3 (continued) | d. Quantification of thallus size of 7-day old Tak-1 and Mp*arf2-1* knock-out mutants complemented with FL^{WT}-sYFP-turboID. Plants were grown on Mock medium, or medium supplemented with 3 μM NAA. **e.** Quantification of gemma size of Tak-1 and the Mp*arf2-1* knock-out mutant complemented with FL^{WT}-sYFP-turboID. (**d,e**) Sizes were compared between groups per Kruskal-Wallis test with a Dunn post hoc test (P<.05). Italics denote significant differences per group. Sample size is indicated above the figure.

plants, cellular MpARF2 levels remain low by this degradation (see Chapter 5). Therefore, we treated the aforementioned plant lines, as well as Tak-1, at an age of 7 days, with 50 μM biotin dissolved in water for 24 hours, after which they were harvested and flash frozen in liquid nitrogen. Cells were lysed, followed by a nuclear extraction using a sucrose gradient, and an enrichment of biotinylated proteins. LC-MS/MS mass spectrometry was used to analyze the identity of enriched, biotinylated proteins. Due to the extremely high abundance of the 1.9NLS-sYFP-turboID and 3NLS-sYFP-turboID controls *in vivo*, using these as the negative control resulted in the loss of most interactions due to their highly stable nature. We therefore excluded these controls from analysis and compared the proteomes identified in DBD^{WT}-sYFP-turboID, DBD^{E+R}-sYFP-turboID, and FL^{WT}-sYFP-turboID to the Tak-1 control. Doing so resulted in a total number of 159 and 78 enriched proteins in DBD^{WT}-sYFP-turboID and FL^{WT}-sYFP-turboID, respectively (Fig. 4a). Among proteins significantly enriched in FL^{WT}-sYFP-turboID we identified several TFs such as MpISWI, MpC3H16, MpbHLH44, MpGARP6, MpRRB, MpCAMTA, MpVAL, MpHLP1, MpARID2, and MpTRIHELIX33. We also recovered auxin response-related proteins, such as MpTPL and MpncIAA. These confirmed that we have been successful in labelling proteins proximal to MpARF2. Furthermore, we identified MpARF3 as a potential interactor of MpARF2. To search for potential regulators of MpARF2 degradation, we identified 27 genes encoding the enriched proteins in DBD^{WT}-sYFP-turboID and FL^{WT}-sYFP-turboID, but not DBD^{E+R}-sYFP-turboID (Fig. 4b).

We next queried the functional annotations of these genes for terms indicative of a role in the UPS. We specifically searched for proteins annotated as ubiquitin-ligases or UPS associated, such as "E3", "Proteasome", "Ubiquitin", "degradation", "proteolysis", "RING", "U-box", "BTB", "POZ", "HECT", "Anaphase Promoting Complex" etc. In doing so, we identified two genes: Mp3g04110 and Mp5g07060, which were annotated as potential ubiquitin ligases and both were not enriched in DBD^{E+R}-sYFP-turboID (Fig. 4a,b). Mp3g04110 encodes a protein with a RING/U-box domain, which is typically responsible for ligation of ubiquitin moieties to a substrate. Mp3g04110 is annotated as Vacuolar protein sorting protein 11 C terminal, which

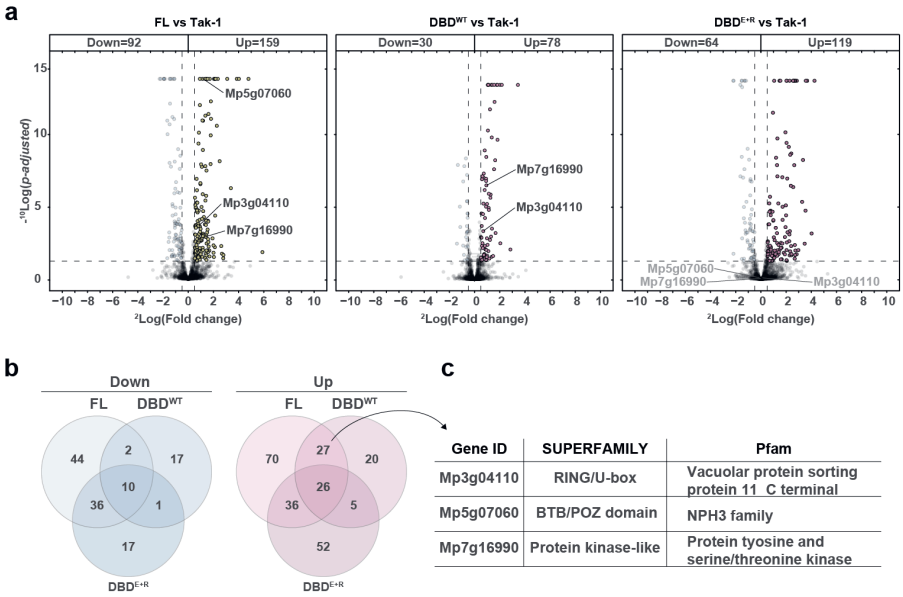


Fig. 4 | Analysis of enriched biotinylated proteins compared to Tak-1.
a. Volcano plot showing proteins which are significantly enriched (Up) or reduced (Down) compared to Tak-1 in the indicated genotypes. Genotypes correspond to Fig. 1. We defined enriched proteins as having a ^{2}Log Fold change > 0.5 and a $P_{adj} < .05$. Datapoints have a solid, non-opaque fill color when enriched, and are transparent when not. The three candidate genes are highlighted. **b.** Venn diagrams showing which proteins are uniquely enriched or reduced, and which ones are shared between genotypes. **c.** The three candidate genes which were enriched in the FL^{WT}-sYFP-turboID and the DBD^{WT}-sYFP-turboID genotypes but were not enriched in the DBD$^{E297K+R300Q}$-sYFP-turboID. Shown here are their SUPERFAMILY and Pfam annotation.

was shown to be important for vacuole biogenesis in Arabidopsis, and the homozygous mutant is likely embryo-lethal[18]. Mp5g07060 is annotated as a phototropic-responsive NPH3 family protein, but to our knowledge remains uncharacterized *in planta*. Furthermore, we observed that a protein tyrosine and serine/threonine kinase, Mp7g16990, was enriched in both DBD^{WT}-sYFP-turboID and FL-^{WT}-sYFP-turboID but was lost in DBD^{E+R}-sYFP-turboID. Again, to our knowledge, Mp7g16990 has not been characterized in the literature. Potentially, Mp7g16990 is part of a MpARF2 degradation module, wherein MpARF2 proteolysis requires phosphorylation by this kinase, which is potentially abolished by the E269K+R300Q mutation. Other identified genes did not show clear links to proteolysis by the 26S proteasome and mostly were related to chloroplast biogenesis and function. We therefore selected Mp3g04110, Mp5g07060, and Mp7g16990 as potentially interesting candidates for mutagenesis with CRISPR-Cas9 to investigate their role in MpARF2 degradation

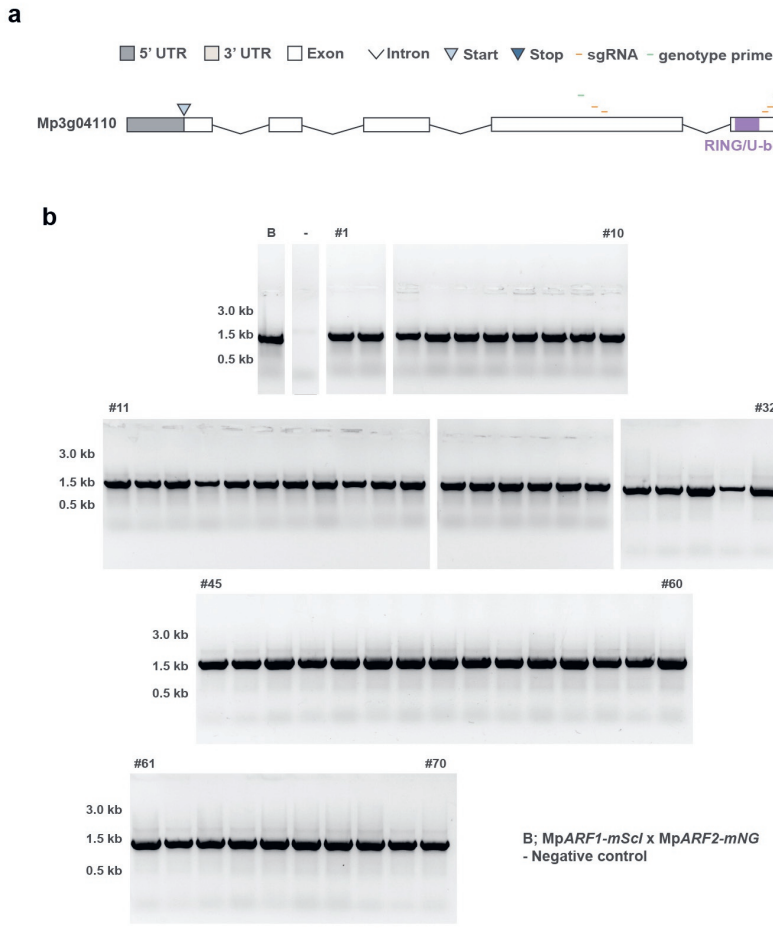


Fig. 5 | PCR reveals no gene editing of Mp3g04110.
a. Gene model of Mp3g04110, the RING/U-box encoding regions are highlighted in magenta. Recognition sites of the used sgRNAs are indicated, as well as the binding sites of the genotyping primers. **b.** Agarose electrophoresis assessment of the genotyping PCR using the primer pairs shown in (**a**). As a control, the background (Mp*ARF1-mScI* x Mp*ARF2-mNG*) line, which is unedited, was amplified.

(Fig. 4c).

CRISPR-Cas9 targeting of candidate genes failed to produce knock-out mutants

We targeted Mp3g04110, Mp5g07060, and Mp7g16990 with a dual-guide CRISPR-Cas9 system, to delete coding regions of putatively crucial domains, in the Mp*ARF1-mScarlet-I* x Mp*ARF2-mNeonGreen* double knock-in reporter[17]. If a knock-out mutant is successfully generated, we can verify involvement of that gene in MpARF

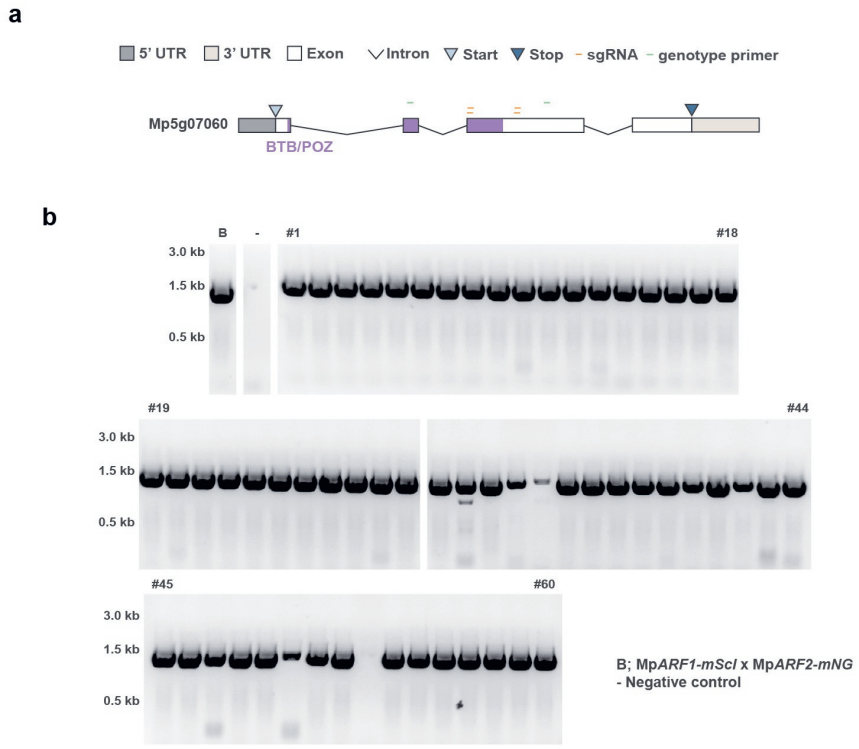


Fig. 6 | PCR reveals no gene editing of Mp5g07060.
a. Gene model of Mp5g07060, the BTB/POZ encoding regions are highlighted in magenta. Recognition sites of the used sgRNAs are indicated, as well as the binding sites of the genotyping primers. **b.** Agarose electrophoresis assessment of the genotyping PCR using the primer pairs shown in (**a**). As a control, the background (Mp*ARF1-mScI* x Mp*ARF2-mNG*) line, which is unedited, was amplified.

degradation by analysis of mScarlet-I (mScI) and mNeonGreen (mNG) fluorescence levels.

For Mp3g04110 we attempted to delete a large portion of the 3' coding region which includes the exon coding for the RING/U-box domain (Fig. 5a). We obtained 70 putatatively transgenic lines which survived two rounds of chlorsulfuron selection. However, genotyping PCR and amplicon sequencing indicated that none of these lines were edited (Fig. 5a,b).

Similarly, for Mp5g07060 we targeted an exon encoding a significant portion of the BTB/POZ domain, which is the domain that should be crucial for ubiquitin-ligase activity (Fig. 6a). A total of 60 lines were obtained after antibiotic selection, and again, none of these lines displayed editing (Fig. 6a,b).

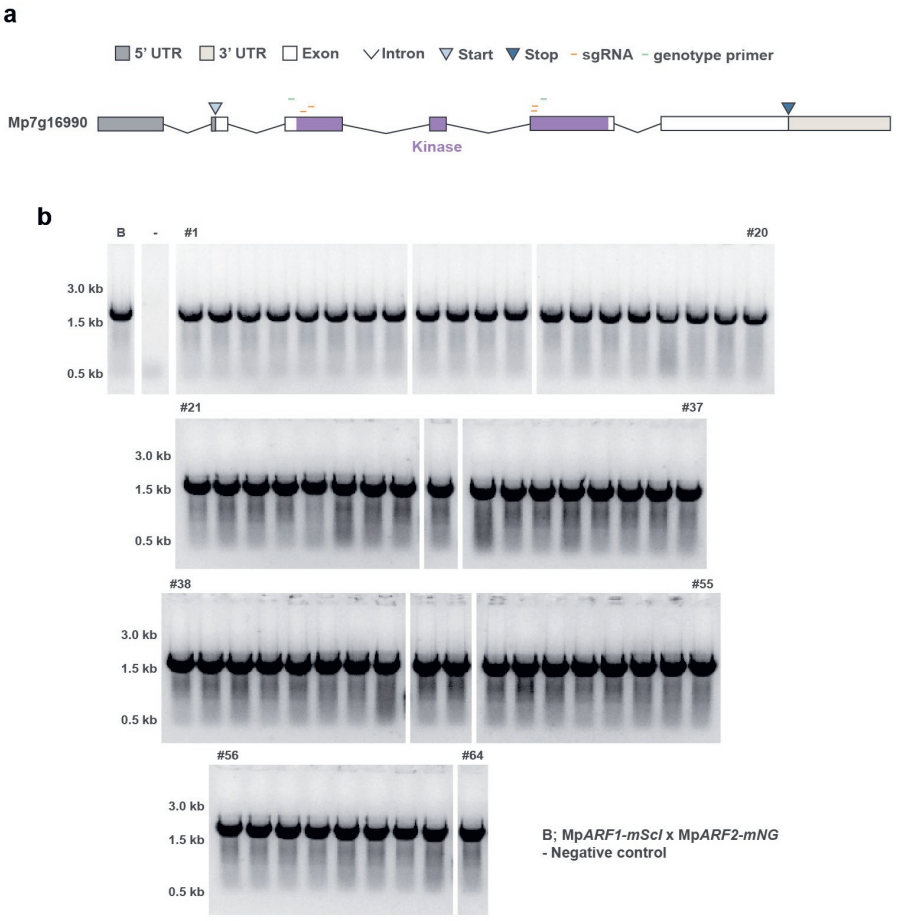


Fig. 7 | PCR reveals no gene editing of Mp7g16990.
a. Gene model of Mp7g16990, the kinase domain encoding regions are highlighted in magenta. Recognition sites of the used sgRNAs are indicated, as well as the binding sites of the genotyping primers. **b.** Agarose electrophoresis assessment of the genotyping PCR using the primer pairs shown in (**a**). As a control, the background (Mp*ARF1-mScI* x Mp*ARF2-mNG*) line, which is unedited, was amplified.

Lastly, we attempted to delete the kinase domain of Mp7g16990, and obtained 64 lines after selection, but none of these lines appeared edited (Fig. 7a,b).

In conclusion, we were unsuccessful in generating the desired knock-out mutants.

Discussion

The signaling molecule auxin is crucial for plant development and acts through a transcriptional pathway, with the ARF transcription factors at its core[2,3]. ARF concentrations determine transcriptional responses and therefore require accurate quantitative tuning[12]. ARF protein levels are regulated through the 26S proteasome, but key mechanistic insights, such as factors driving this process, remain enigmatic[12-15]. In this chapter we use a proteomic approach to identify proteins which interact with MpARF2 and may regulate its stability. We focus on proteins that may post translationally modify MpARF2 or are known to be connected to the UPS. By screening the MpARF2 interactome using proximity labelling, we identify potential candidates and targeted them for mutagenesis using CRISPR-Cas9 genome editing tools. However, we failed to recover edited alleles for the candidate genes we selected and therefore could not verify their involvement in MpARF degradation.

We did not observe gene editing which prohibited us from assessing if our selection of genes were involved in the regulation of MpARF2 stability. Possibly, knock out of any of these three genes is lethal, or may interfere with survival during the chlorsulfuron selection, which would render generating knock-out alleles impossible. Alternatively, although we have used four different combinations of gRNAs for each gene, it is possible that the designed gRNAs are inefficient in targeting Cas9 to the DNA to induce double-strand breaks resulting in deletions. Reducing the function of these candidates through partial knock-down or conditional knockout may offer solutions. For example, expressing artificial microRNA's or inducible or tissue-specific expression of Cas9 may help circumvent lethality.

We opted for a TurboID-based approach as this technique is often used to detect weak and/or transient *in vivo* interactions[19-21]. Some of the identified putative interactors are known DNA-binding TFs, suggesting that we have successfully labelled nuclear proteins that associate with DNA and potentially MpARF2. Similarly, we have recovered a known MpARF2 interactor (MpTPL). We therefore believe that TurboID can be successfully used to label proteins in close proximity to MpARF2 *in vivo*. However, identification of factors involved in MpARF2 degradation may require alternative genetic strategies that are better suited. For example, Yeast 2 Hybrid (Y2H) screens have been successfully used in the past to identify ubiquitin-ligase-substrate modules[22-25]. Using MpARF2 as a bait in a Y2H screen may identify such interactions. However, TF have been notoriously difficult to use in Y2H screens due to autoactivation of

the system[26-29]. To circumvent this, a truncated version of MpARF2 can be used, with just the DBD as bait, as this is sufficient for degradation[13]. Other interactions, unconnected to MpARF2 degradation, may also be selected against by using the MpARF2 DBD as the sole bait.

We believe that reverse genetic strategies show promising initial results, and further exploration of the MpARF2 degradation mechanism would benefit from additional reverse genetic approaches. We also report on Mp*arf2-1* mutants, which could be complemented with a Mp*ARF2-sYFP-turboID* transgene, thus suggesting that in this context, the MpARF2 protein is functional when coupled to the TurboID enzyme. These plants can be used as valuable resources for studying the interactomes of auxin signaling components. Furthermore, the inability to generate loss-of-function alleles for multiple, mechanistically distinct candidate genes suggests that MpARF2 degradation may rely on essential or highly buffered components of the UPS. Together, our results suggest that ARF proteolysis is governed by a robust and possibly essential regulatory network, rather than a single dedicated E3 ubiquitin-ligase, once again highlighting the importance of quantitative control in auxin signaling.

Methods

Generation of genetic constructs

We used the in-house pHKDW037 plasmid to amplify the Mp*ARF2* promoter and Mp*ARF2* CDS. We amplified *sYFP-turboID* from a plasmid provided by Jorge Hernández-García. These were combined into the XbaI site of pMpGWB100[30] using NEB™ HiFi. We used the plasmids generated in Ref.[13] to amplify the 1.9kb Mp*ARF2* promoter and DBD^{WT} and DBD^{E+R} sequences, and these were also combined into the XbaI site of pMpGWB100 as described above. The NLS controls were generated by amplification of *sYFP-TurboID* with a primerset containing the SV40 NLS sequence.

We used the dual-guide CRISPR-Cas9 system as developed by Ref.[31]. Briefly, 20 nucleotide gRNA oligo's were designed using the CasFinder (default settings) tool on MarPolBase and were designed against the target genes based on the version of the Marchantia genome (v7.1). High scoring gRNA oligo's were blasted against the Marchantia genome to check for off target hits. We selected 2 gRNAs towards the 5' en of the region of interest, and 2 gRNAs against the 3' end, so four differ combinations could be made. Next, single stranded gRNA oligo's were annealed to their reverse complement by incubating 1 µL of the forward and reverse oligo's (at a concentration of 100 µM) in 8 µL water at 37°C for 30 min, followed by 95°C for 5 min, and a ramp down towards RT (20°C) at 5°C per min. The annealed oligo's were then directly cloned into the L1ck2 and L1ck3 vectors using T4 DNA ligase and the BbsI restriction enzyme[31]. The L2 plasmids were generated by SapI type IIS restriction Loop assembly[31]. Plasmid identity was verified using DNA sequencing.

Plasmids and oligonucleotides which were generated for this study can be found in Supplementary Data Table 1 and 2, respectively.

Transformation of plants

Tak-1 and the Mp*arf2-1* mutant were transformed using agrobacterium-mediated delivery of transgenic constructs as described by Ref.[32]. Transgenic plants were selected on ½ Gamborg B5 (1% agar) with 10 mg/L hygromycin or 0.5 mg/L chlorsulfuron, and 100 µg/mL cefotaxime for two rounds. Afterwards, plants were screened for sYFP signal by confocal microscopy, see below.

Phenotyping

Marchantia plants of the indicated genotypes were placed on ½ strength Gamborg B5 medium (1% agar) for 7 (NAA response) or 20 (general growth) days, respectively. Growth conditions were 22°C with 40 µmol photons $m^{-2}s^{-1}$ continuous white, fluorescent light. Takaragaike-1 (Tak-1) was used as the wild type. For the assessment of NAA response, plants were grown on medium containing 3 µM NAA or Mock (DMSO), respectively. A canon 250d camera fitted with a 18-135 mm lens was used to obtain pictures thallus, and projected thallus areas were measured using imageJ (v1.52). Detailed, high magnification images were obtained using a Leica M205 stereomicroscope.

Confocal microscopy

Confocal microscopy was carried out with a Leica SP8X-SMD confocal microscope fitted with hybrid detectors and a 40 MHz pulsed white-light laser. Data acquisition was performed using LasX (v3.5.7.23225) software. The fluorophore sYFP was excited using 488 nm laser line. Fluorescence was detected between 500-570 nm with hybrid detectors set to photon counting mode with 1.00-24.50 ns time-gating active to suppress background fluorescence. Z-stacks were acquired using an HC PL APO 20x/0.75 water immersion or APO CS 10x/0.40 air objective. The same settings were used for all samples within experiments. ImageJ (v1.52) was used to generate maximum-intensity projections and produce micrographs for figures.

TurboID and LC-MS/MS

Plants of the indicated genotypes (Fig. 1) as well as the Tak-1 control were grown for 14 days on sterile mesh on standard ½ strength Gamborgs B5 medium. First seven-day old plants were submerged in 40 mL sterile dH_2O with 50 µM Biotin for 24 hours, after which they were harvested and flash frozen in liquid nitrogen. Next, plant material was ground into a fine powder in liquid nitrogen.

For nuclear extraction, we added NIB (20 mM Tris pH 7.5, 25% glycerol, 20 mM KCL, 2 mM EDTA, 2.5 mM $MgCl_2$, 250 mM sucrose, 1 mM DTT and 1x CPI) in a 1:1 ratio and resuspended the material through rotation for 20 min at 4°C head over tail. The homogenate was then filtered through a 100 µm nylon filter. The

nuclei were then pelleted by centrifugation for 15 min at 3000 RPM at 4°C. The resultant pellet was then resuspended in 10 mL of NIBT and mixed through pipetting, after which the nuclei were pelleted once more by centrifugation for 5 min at 3000 RPM at 4°C. The nuclei pellet volume was determined, and then 2 volumes of lysis buffer was added in a 1:1 ratio (50 mM Tris pH 8.0, 150 mM NaCl, 2 mM $MgCl_2$, 1 mM EDTA, 1 mM DTT, 1% NP40, 0.5% sodium deoxycholate, 0.1% SDS 10% glycerol and 1xCPI). Samples were then sonicated in a 4°C water bath (>2 mL volume) for 10 cycles of 15s on and 30s off. This was followed by centrifugation at max speed for 30 minutes at 4°C. The supernatant was then collected, and free biotin was removed through loading onto 3kDa Amicon™ filters with a max volume of 15 mL and dead volume of 250 µL. The supernatant was filtered for 30 min 3000g at room temperature (RT). Filters were washed twice using 5 mL lysis buffer and centrifugation for 15 min at 3000g at RT. The concentrated lysate was resuspended to a final volume of 1 mL lysis buffer. We then proceeded with protein concentration measurements. We used the bicinchoninic acid assay (BCA) from ThermoScientific™ in a 96 well plate format to assess protein concentrations. Protein concentrations were calculated from linear regressions.

Next, we enriched samples for biotinylated proteins using a magnetic streptavidin bead enrichment approach. We used 100 µL of NEB™ magnetic streptavidin bead slurry per sample, beads were washed 3 times before use. Samples were incubated overnight (20 hours) on a rotating wheel at 4°C, followed by three washes with 1 mL lysis buffer. Next, beads were washed three times with 1 mL lysis buffer without detergents, and three times with 1 mL 50 mM Ammonium Bicarbonate (ABC). Afterwards, beads were resuspended in 100 µL 50 mM ABC with 50 mM Acrylamide and incubated for 30 min at RT. Next, the supernatant was collected and added to 100 µL ABC with 0.5 µg Trypsin, which was incubated overnight (19 hours) at RT.

Following incubation, samples were acidified using 10% TFA until a pH of 2-3 was reached. We made C18 microcolumns by fitting plugs of C18 membrane material into a 200 µL pipette tip and adding 50 µL of 10 mg Lichoprep C18 mix with methanol, which were then centrifugated for 1 min at 1500g. Next, we added 50 µL 0.1% Formic acid and centrifuged for 1 min at 1500g, followed by another centrifugation of 50 µL 0.1% Formic Acid with 5% Acetonitrile for 1 min at 1500g. Columns were then washed once more with 50 µL 0.1% Formic acid in 5% Acetonitrile and centrifugated for 1 min at 1500g. The acidified samples were then loaded onto the column

which was followed by 20 min of centrifugation at 400g. Columns were then washed with 100 µL 0.1% Formic acid in 5% acetonitrile and centrifuged for 1 min at 1500g. The washed peptides were then eluted in clean 0.5 mL Eppendorf™ tubes with 30 µL 80% acetonitrile, 0.1% Formic acid with centrifugation for 2 min at 1500g. Samples were then vacuum centrifuged at 45◦C V-AQ until ~5 µL sample volume remained. Samples were then resuspended to a total volume of 10 µL with 0.1% Formic acid.

Analysis LC MS/MS data

Nano liquid chromatography–tandem mass spectrometry (nLC–MS/MS) analysis was performed as previously described[33]. A volume of 5 ul peptide samples were loaded directly onto a 0.10 * 250 mm ReproSil-Pur 120 C18-AQ 1.5 µm beads analytical column (prepared in-house) at a constant pressure of 825 bar (flow rate of circa 700 nL/min) with 1 ml/l HCOOH in water and eluted at a flow of 0.5 ul/min with a 30 min linear gradient from 9% to 34% acetonitrile in water with 1 ml/l formic acid with a Vanquish Neo. An electrospray potential of 3.5 kV was applied directly to the eluent via a stainless-steel needle fitted into the waste line of a micro cross that was connected between the nLC and the analytical column. Full scan positive mode FTMS spectra were measured between m/z 380 and 1400 on a Exploris 480 (Thermo electron, San Jose, CA, USA) in the Orbitrap at resolution (60000). MS and MSMS AGC targets were set to 300%, 100% respectively or maximum ion injection times of 50 ms (MS) and 30 ms (MSMS) were used. HCD fragmented (Isolation width 1.2 m/z, 28% normalized collision energy) MSMS scans of 2-5+ charged peaks in the MS scan were recorded in data dependent mode in a cycle time of 1.1 s (Resolution 15000, threshold $2x10^4$, 15 s exclusion duration for the selected m/z +/- 10 ppm).

Thermo RAW files were searched using MSFragger version 4.1 with the standard workflow LFQ-MBR against the MpTak (v7.1) protein database from MarpolBase. Combined protein files were analyzed using the DEP2 package. Intensity data was ^{2}Log transformed, normalized using variance stabilization and missing values imputed using a mixed imputation approach of knn for MAR and QRLIC for MNAR. Differentially enriched proteins were identified using limma with empirical bayes and a FDR threshold of 0.05.

Generation of CRISPR-Cas9 mutants

Dual gRNA plasmids were used to transform the MpARF1-mScI x MpARF2-mNG double knock in background. By using a dual guide system, we aimed to generate deletions in the CDS of the target genes. Transformants were subjected to two rounds of chlorsulfuron selection (see above) and surviving plants were screened for gene editing using ThermoFisher™ Phire Plant Direct PCR mastermix. Genotyping primers flanked the gRNA recognition sites, and amplicon size was analyzed using 1% agarose gel electrophoresis (Fig. 5a, 6a, and 7a).

Statistics & reproducibility

Statistical tests were performed in R (v4.2.1). Tests and their parameters as well as sample sizes are shown within the figures themselves. No statistical method was used to predetermine sample size; sample sizes were determined according to field standards. Experiments were not randomized.

Acknowledgements

We are very grateful to Anna Jonkers for repeating a PCR reaction. We thank Cecilia Borassi and Sjoerd Woudenberg for help during the harvesting of the biotin-treated plants. This work has been supported by the Netherlands Organization for Scientific Research (NWO; OCENW.M20.031 M.d.R., J.W.B.).

Supplementary Data Table 1 | Plasmids used in this study.

No°	Backbone	Plant^{res}	Bacterial^{res}	Contains
1	OP-005	Chlorsulfuron	Spectinomycin	dual gNRA targetting Mp3g04110 + CAS9
2	OP-005	Chlorsulfuron	Spectinomycin	dual gNRA targetting Mp3g04110 + CAS9
3	OP-005	Chlorsulfuron	Spectinomycin	dual gNRA targetting Mp3g04110 + CAS9
4	OP-005	Chlorsulfuron	Spectinomycin	dual gNRA targetting Mp3g04110 + CAS9
5	OP-005	Chlorsulfuron	Spectinomycin	dual gNRA targetting Mp5g07060 + CAS9
6	OP-005	Chlorsulfuron	Spectinomycin	dual gNRA targetting Mp5g07060 + CAS9
7	OP-005	Chlorsulfuron	Spectinomycin	dual gNRA targetting Mp5g07060 + CAS9
8	OP-005	Chlorsulfuron	Spectinomycin	dual gNRA targetting Mp5g07060 + CAS9
9	OP-005	Chlorsulfuron	Spectinomycin	dual gNRA targetting Mp7g16990 + CAS9
10	OP-005	Chlorsulfuron	Spectinomycin	dual gNRA targetting Mp7g16990 + CAS9
11	OP-005	Chlorsulfuron	Spectinomycin	dual gNRA targetting Mp7g16990 + CAS9
12	OP-005	Chlorsulfuron	Spectinomycin	dual gNRA targetting Mp7g16990 + CAS9
13	pHKDW037	Hygromycin	Spectinomycin	MpA*RF2* FL CDS fused to sYFP and turboID expressed from *pro*Mp*ARF2*
14	pHKDW037	Hygromycin	Spectinomycin	NLS CDS fused to sYFP and turboID expressed from *pro*Mp*ARF2*
15	pMpGWB100	Hygromycin	Spectinomycin	MpA*RF2* DBDWT CDS fused to sYFP and turboID expressed from *pro*Mp*ARF2*
16	pMpGWB100	Hygromycin	Spectinomycin	MpA*RF2* DBDE+R CDS fused to sYFP and turboID expressed from *pro*Mp*ARF2*
17	pMpGWB100	Hygromycin	Spectinomycin	NLS CDS fused to sYFP and turboID expressed from *pro*Mp*ARF2*

Supplementary Data Table 2 | Oligonucleotides used in this study.

Primer	Sequence 5'>3'	Description
MdR434	CCAGATCCACCTGATCCGC-CCACTTCCCATGGTGAGACCC	Rv Mp*ARF2* DBD + sYFP + tID > pMpGWB100 XbaI
MdR435	GGGTCTCACCATGGGAAGTGGGCG-GATCAGGTGGATCTGGAGGCTC	Fw Mp*ARF2* DBD + link. sYFP + tID > pMpGWB100 XbaI
MdR436	GGGGAAATTCGAGCTCGGTACCCG-GGGATCCTTTACTGAAGTTTTTCCG-CGC	Rv Mp*ARF2* DBD + sYFP + tID > pMpGWB100 XbaI
MdR437	CCAGATCCACCTGATCCGC-CGACCTTTCTCTTCTTCTTTGGAGCC	Rv NLS + sYFP+tID > pMp-GWB100 XbaI
MdR438	CAAAGAAGAAGAGAAAGGTCGGCG-GATCAGGTGGATCTGG	Fw pMp*ARF2* NLS + sYFP + tID > pMpGWB100 XbaI
MdR460	CTCGGCTTTATAAGGAAGTCATGGGT	gRNA1.1 Mp3g04110
MdR461	TAAAACCCATGACTTCCTTATAAAGC	gRNA1.2 Mp3g04110 (rev complement + overhangs of MR460)
MdR462	CTCGTCAGTTGGTGCGTAACTCAGGT	gRNA2.1 Mp3g04110
MdR463	TAAAACCTGAGTTACGCACCAACTGA	gRNA2.2 Mp3g04110 (rev complement + overhangs of MR462)
MdR464	CTCGAAAGGAGACTCCTAGTTTGAGT	gRNA3.1 Mp3g04110
MdR465	TAAAACTCAAACTAGGAGTCTCCTTT	gRNA3.2 Mp3g04110 (rev complement + overhangs of MR464)
MdR466	CTCGATTGCGGATTACTTTGGAAGGT	gRNA4.1 Mp3g04110
MdR467	TAAAACCTTCCAAAGTAATCCGCAAT	gRNA4.2 Mp3g04110 (rev complement + overhangs of MR468)
MdR468	CTCGTCCCGTTGGTCTCGCGATGCGT	gRNA5.1 Mp5g07060
MdR469	TAAAACGCATCGCGAGACCAACG-GGA	gRNA5.2 Mp5g07060 (rev complement + overhangs of MR470)
MdR470	CTCGCGTTGGTCTCGCGATGCGG-GGT	gRNA6.1 Mp5g07060
MdR471	TAAAACCCCGCATCGCGAGAC-CAACG	gRNA6.2 Mp5g07060 (rev complement + overhangs of MR472)
MdR472	CTCGATGTCGTGAACAGATTGCGCGT	gRNA7.1 Mp5g07060
MdR473	TAAAACGCGCAATCTGTTCACGACAT	gRNA7.2 Mp5g07060 (rev complement + overhangs of MR474)
MdR474	CTCGTGTCGTGAACAGATTGCGCAGT	gRNA8.1 Mp5g07060
MdR475	TAAAACTGCGCAATCTGTTCACGACA	gRNA8.2 Mp5g07060 (rev complement + overhangs of MR476)
MdR476	CTCGTGCAACTCTTCACAATTCGAGT	gRNA9.1 Mp7g16990
MdR477	TAAAACTCGAATTGTGAAGAGTTGCA	gRNA9.2 Mp7g16990 (rev complement + overhangs of MR478)
MdR478	CTCGCGATCGCGTCCGCATCCTGTGT	gRNA10.1 Mp7g16990
MdR479	TAAAACACAGGATGCGGACGC-GATCG	gRNA10.2 Mp7g16990 (rev complement + overhangs of MR480)

Primer	Sequence 5'>3'	Description
MdR480	CTCGTATGGTGTGGACCTCGTTCGGT	gRNA11.1 Mp7g16990
MdR481	TAAAACCGAACGAGGTCCACACCATA	gRNA11.2 Mp7g16990 (rev complement + overhangs of MR482)
MdR482	CTCGGGACCTCGTTCGAGGGATCAGT	gRNA12.1 Mp7g16990
MdR483	TAAAACTGATCCCTCGAACGAGGTCC	gRNA12.2 Mp7g16990 (rev complement + overhangs of MR484)
MdR484	CAATAGTGGCAACCTCCTACCA	genotype Mp3g04410 CRISPR fw
MdR485	GCTCACGCAAATGACGAGTTAG	genotype Mp3g04410 CRISPR rv
MdR486	GATGTCGTGGTCATTGTCGG	genotype Mp5g07060 CRISPR fw
MdR487	GTCCGTTTGTTGCAAGAAGCAC	genotype Mp5g07060 CRISPR rv
MdR488	GCAGCAAAATCGTGGAGTGATG	genotype Mp7g16990 CRISPR fw
MdR489	GAGCAACGGAATACCGAATTCTC	genotype Mp7g16990 CRISPR rv
MdR490	GTCGAAGCGTCACGAGAGAT	sequence L1ck2 or ck3 gRNA insertion
MdR493	CCATCTCCGGTCGACTTTGTTCATG	genotype Mp3g04410 CRISPR fw
MdR494	ACGGTTGGCACCGCTCACGC	genotype Mp3g04410 CRISPR rv
MdR495	GTTCTGGCAACGGATGTCCCGAG	genotype Mp5g07060 CRISPR fw
MdR496	GATGCGTTGTACGATGTCCACATCG	genotype Mp5g07060 CRISPR rv
MdR497	GGGCGGTGATTCGTTTGGACCTTC	genotype Mp7g16990 CRISPR fw
MdR498	GTCCCCATCCATGGAACTGGTTCAGA	genotype Mp7g16990 CRISPR rv

References

1 Vanneste, S., Pei, Y. & Friml, J. Mechanisms of auxin action in plant growth and development. *Nat Rev Mol Cell Biol* (2025). https://doi.org/10.1038/s41580-025-00851-2
2 Mockaitis, K. & Estelle, M. Auxin receptors and plant development: a new signaling paradigm. *Annu Rev Cell Dev Biol* **24**, 55–80 (2008). https://doi.org/10.1146/annurev.cellbio.23.090506.123214
3 Leyser, O. Auxin Signaling. *Plant Physiol* **176**, 465–479 (2018). https://doi.org/10.1104/pp.17.00765
4 Chapman, E. J. & Estelle, M. Mechanism of auxin-regulated gene expression in plants. *Annu Rev Genet* **43**, 265–285 (2009). https://doi.org/10.1146/annurev-genet-102108-134148
5 Roosjen, M., Paque, S. & Weijers, D. Auxin Response Factors: output control in auxin biology. *J Exp Bot* **69**, 179–188 (2018). https://doi.org/10.1093/jxb/erx237
6 Cance, C., Martin-Arevalillo, R., Boubekeur, K. & Dumas, R. Auxin response factors are keys to the many auxin doors. *New Phytol* **235**, 402–419 (2022). https://doi.org/10.1111/nph.18159
7 Hernandez-Garcia, J. *et al.* Evolutionary origins and functional diversification of Auxin Response Factors. *Nat Commun* **15**, 10909 (2024). https://doi.org/10.1038/s41467-024-55278-8
8 Kato, H. *et al.* Design principles of a minimal auxin response system. *Nat Plants* **6**, 473–482 (2020). https://doi.org/10.1038/s41477-020-0662-y
9 Lavy, M. *et al.* Constitutive auxin response in Physcomitrella reveals complex interactions between Aux/IAA and ARF proteins. *Elife* **5** (2016). https://doi.org/10.7554/eLife.13325
10 Flores-Sandoval, E., Eklund, D. M. & Bowman, J. L. A Simple Auxin Transcriptional Response System Regulates Multiple Morphogenetic Processes in the Liverwort Marchantia polymorpha. *PLoS Genet* **11**, e1005207 (2015). https://doi.org/10.1371/journal.pgen.1005207
11 Boer, D. R. *et al.* Structural basis for DNA binding specificity by the auxin-dependent ARF transcription factors. *Cell* **156**, 577–589 (2014). https://doi.org/10.1016/j.cell.2013.12.027
12 de Roij, M., Borst, J. W. & Weijers, D. Protein degradation in the auxin response. *Plant Cell* (2024). https://doi.org/10.1093/plcell/koae125
13 de Roij, M., Hernandez Garcia, J., Das, S., Borst, J. W. & Weijers, D. ARF degradation defines a deeply conserved step in auxin response. *Nat Plants* **11**, 717–724 (2025). https://doi.org/10.1038/s41477-025-01975-1
14 de Roij, M. *et al.* Diversification of functional requirements for proteolysis of auxin response factors. *Nature Communications* (2026). https://doi.org/10.1038/s41467-026-70440-0
15 Prigge, M. J. *et al.* Comparative mutant analyses reveal a novel mechanism of ARF regulation in land plants. *Nat Plants* **11**, 821–835 (2025). https://doi.org/10.1038/s41477-025-01973-3
16 Flores-Sandoval, E. *et al.* The B-class auxin response factor MpARF2 is essential for meristem organization in free-living plant gametophytes. *Curr Biol* (2025). https://doi.org/10.1016/j.cub.2025.11.015
17 Das, S. *et al.* Quantitative imaging reveals the role of MpARF proteasomal degradation during gemma germination. *Plant Commun*, 101039 (2024). https://doi.org/10.1016/j.xplc.2024.101039

18 Tan, X., Wei, J., Li, B., Wang, M. & Bao, Y. AtVps11 is essential for vacuole biogenesis in embryo and participates in pollen tube growth in Arabidopsis. *Biochem Biophys Res Commun* **491**, 794–799 (2017). https://doi.org/10.1016/j.bbrc.2017.07.059
19 Branon, T. C. *et al.* Efficient proximity labeling in living cells and organisms with TurboID. *Nat Biotechnol* **36**, 880–887 (2018). https://doi.org/10.1038/nbt.4201
20 Zhang, Y. *et al.* TurboID-based proximity labeling reveals that UBR7 is a regulator of N NLR immune receptor-mediated immunity. *Nat Commun* **10**, 3252 (2019). https://doi.org/10.1038/s41467-019-11202-z
21 Cho, K. F. *et al.* Proximity labeling in mammalian cells with TurboID and split-TurboID. *Nat Protoc* **15**, 3971–3999 (2020). https://doi.org/10.1038/s41596-020-0399-0
22 Miao, Y. & Zentgraf, U. A HECT E3 ubiquitin ligase negatively regulates Arabidopsis leaf senescence through degradation of the transcription factor WRKY53. *Plant J* **63**, 179–188 (2010). https://doi.org/10.1111/j.1365-313X.2010.04233.x
23 Lv, Q., Zhang, L., Zan, T., Li, L. & Li, X. Wheat RING E3 ubiquitin ligase TaDIS1 degrade TaSTP via the 26S proteasome pathway. *Plant Sci* **296**, 110494 (2020). https://doi.org/10.1016/j.plantsci.2020.110494
24 Yu, Y. *et al.* The Chinese wild grapevine (Vitis pseudoreticulata) E3 ubiquitin ligase Erysiphe necator-induced RING finger protein 1 (EIRP1) activates plant defense responses by inducing proteolysis of the VpWRKY11 transcription factor. *New Phytol* **200**, 834–846 (2013). https://doi.org/10.1111/nph.12418
25 Abramovitch, R., Janjusevic, R., Stebbins, E. & Martin, G. B. Type III effector AvrPtoB requires intrinsic
E3 ubiquitin ligase activity to suppress
plant cell death and immunity. *Proc Natl Acad Sci U S A* **103**, 5 (2006). https://doi.org/doi 10.1073 pnas.0507892103
26 Vidal, M. & Legrain, P. Yeast forward and reverse 'n'-hybrid systems. *Nucleic Acids Res* **27**, 10 (1999). https://doi.org/https://doi.org/10.1093/nar/27.4.919
27 Titz, B. *et al.* Transcriptional activators in yeast. *Nucleic Acids Res* **34**, 955–967 (2006). https://doi.org/10.1093/nar/gkj493
28 Dreze, M. *et al.* High-quality binary interactome mapping. *Methods Enzymol* **470**, 281–315 (2010). https://doi.org/10.1016/S0076-6879(10)70012-4
29 Shivhare, D., Musialak-Lange, M., Julca, I., Gluza, P. & Mutwil, M. Removing auto-activators from yeast-two-hybrid assays by conditional negative selection. *Sci Rep* **11**, 5477 (2021). https://doi.org/10.1038/s41598-021-84608-9
30 Ishizaki, K. *et al.* Development of Gateway Binary Vector Series with Four Different Selection Markers for the Liverwort Marchantia polymorpha. *PLoS One* **10**, e0138876 (2015). https://doi.org/10.1371/journal.pone.0138876
31 Sauret-Gueto, S. *et al.* Systematic Tools for Reprogramming Plant Gene Expression in a Simple Model, Marchantia polymorpha. *ACS Synth Biol* **9**, 864–882 (2020). https://doi.org/10.1021/acssynbio.9b00511
32 Kubota, A., Ishizaki, K., Hosaka, M. & Kohchi, T. Efficient Agrobacterium-mediated transformation of the liverwort Marchantia polymorpha using regenerating thalli. *Biosci Biotechnol Biochem* **77**, 167–172 (2013). https://doi.org/10.1271/bbb.120700
33 Kuhn, A. *et al.* RAF-like protein kinases mediate a deeply conserved, rapid auxin response. *Cell* **187**, 130–148 e117 (2024). https://doi.org/10.1016/j.cell.2023.11.021



Chapter 8

General Discussion

Authors

Martijn de Roij[1]

Affiliations

[1] Laboratory of Biochemistry, Wageningen University, Stippeneng 4, 6708WE Wageningen, the Netherlands

ARF proteolysis

AUXIN RESPONSE FACTOR (ARF) transcription factors (TFs) are central components of the Nuclear Auxin Pathway (NAP) and play essential roles in nearly all aspects of plant growth and development[1-4]. Phylogenetic analyses indicate that the ARF proteins originated in the common ancestor of the streptophyte lineage and subsequently duplicated to form A/B- and C-type ARFs, of which descendants are still found in extant streptophyte algae[5,6]. Further duplication events gave rise to the A -and B-ARFs in the last common ancestor (LCA) of land plants[5,7]. Following the colonization of land, these classes expanded in size and diversified[5-7]. ARFs act as crucial regulators that bridge auxin perception to a transcriptional response[3]. As ARF classes are functionally distinct, the qualitative and quantitative nuclear ARF landscape shapes the auxin response.

Much attention has been devoted to understand how ARFs achieve specificity through their DNA-binding preferences toward auxin response elements (AuxREs), binding kinetics, and differences in binding-site architecture and dimerization capacity[3,8-17]. However, it is increasingly clear that ARF activity is also extensively controlled at the post-translational level as the stability of ARF proteins are regulated by the Ubiquitin Proteasome System (UPS; reviewed in **Chapter 2**)[18]. Targeted ARF turnover enables cells to fine-tune auxin responses across space and time, ensuring appropriate developmental outcomes. Despite the central role of ARFs in auxin signaling, our understanding of how and why ARF stability and turnover are regulated, how conserved these mechanisms are across embryophyte lineages, and how these diversified during plant evolution remains limited. Addressing these questions is essential to achieve a comprehensive understanding of the NAP. In this thesis I have focused on elucidating the mechanisms and evolutionary conservation of 26S proteasome-dependent ARF degradation and its role in shaping auxin-responsive transcriptional networks.

Roles of ARF proteolysis

In **Chapter 3** we generated a spatiotemporal map of accumulation patterns of auxin response proteins in *Marchantia*, revealing that these patterns are both spatially and dynamically distinct[19]. A pronounced and consistent difference in cell-specific accumulation levels and localization between the antagonizing A-class MpARF1 and B-class MpARF2 was observed[19]. Studying these stoichiometries during the early stages of gemma germination revealed that these patterns are not static but rapidly changed due to ARF proteolysis,

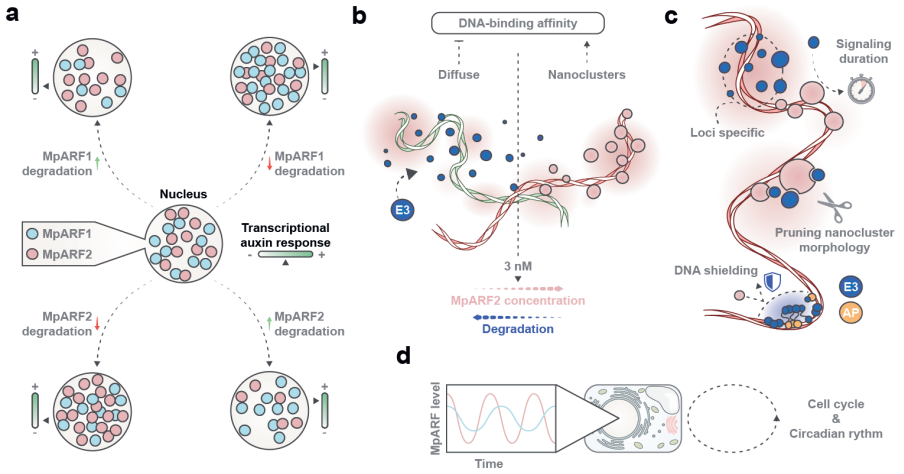


Fig. 1 | Conceptual roles of ARF proteolysis in auxin signaling.

a. Model illustrating how differential degradation of the antagonistic transcription factors MpARF1 (A-class activator, blue) and MpARF2 (B-class repressor, pink) dynamically reshapes their intracellular stoichiometry and thereby modulates transcriptional auxin responses. Changes in degradation rates alter the MpARF1:MpARF2 ratio, shifting transcriptional output without requiring changes in gene expression. **b.** Concentration-dependent changes in MpARF2 organization and DNA-binding behavior. At low concentrations MpARF2 is diffuse, whereas above a threshold (~3 nM) they assemble into spherical nanoclusters. This transition alters DNA-binding affinity and sequence specificity. Because ARF abundance is controlled by proteasome-mediated degradation, proteolysis can determine whether ARFs exist in diffuse or clustered states. **c.** Potential local functions of ARF degradation at the chromatin. Degradation may sculpt nanocluster morphology, limit cluster size, affect signaling duration, or selectively remove ARFs at specific genomic loci. Protection of specific DNA elements may occur by if the E3 ligase targeting ARFs can be anchored to the DNA, either directly, or through interactions with ancillary proteins (abbreviated AP). **d.** Hypothetically oscillatory ARF levels could occur through regulated proteolysis and may link auxin responsiveness to periodic biological processes such as the cell cycle or circadian rhythms.

which is mediated by the 26S proteasome[19]. ARF degradation reshaped the MpARF1 and MpARF2 stoichiometry, increasing the ratio of MpARF1, thus enhancing the NAP auxin responsiveness, which was mirrored by an increase in transcriptional auxin response even when auxin levels decreased[19]. This, combined with measurements illustrating that dynamics of MpARF1 and 2 degradation were markedly different, deem it plausible that active ARF degradation functions as a key mechanism to regulate the stoichiometric balance between A -and B-ARFs (Fig. 1a)[19].

Aux/IAA degradation enables rapid derepression in response to auxin, as reflected by the short MpIAA half-life (>10 minutes) measured in **Chapter 3**[19]. ARF degradation may therefore serve as a complementing regulatory layer to modulate the cellular auxin response capacity (Fig. 1a). The dynamic range of cellular tran-

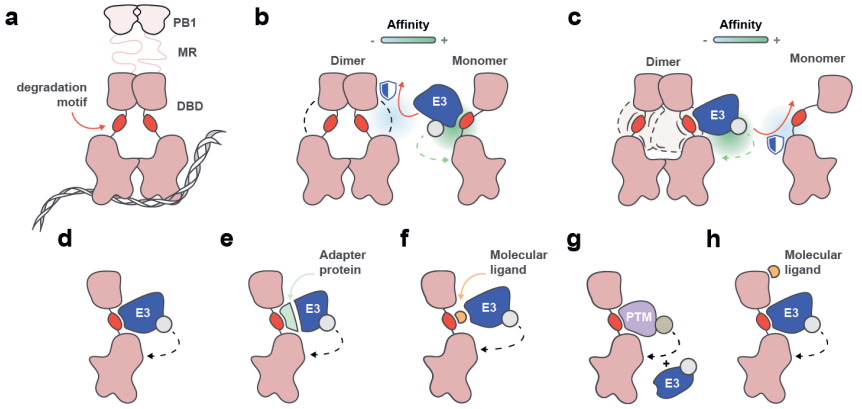


Fig. 2 | Structural and mechanistic models for ARF proteasomal degradation.
a. Domain architecture of a representative ARF protein highlighting the DNA-binding domain (DBD), middle region (MR), and PB1 oligomerization domain. The conserved degradation motif (red) is located in a surface-exposed loop of the DBD, positioned near the dimerization interface. **b.–c.** Alternative models for dimerization-dependent ARF recognition by the cognate E3 ubiquitin-ligase. **b** The degradation motif is more accessible in the monomeric state, allowing higher E3 affinity and preferential ubiquitylation of monomers. Dimerization shields the motif and reduces degradation efficiency. **c** The E3 ligase preferentially recognizes a structural conformation presented in the ARF dimer. Dimerization enhances degron accessibility or creates a composite recognition interface, increasing ligase affinity. **d.–h.** Mechanistic hypotheses for recruitment of the ubiquitin machinery. **d** The positively charged residue (R300) within the degradation motif forms a charge-based docking interface with a negatively charged surface patch on the E3 ligase. **e** An intermediate adaptor protein bridges the ARF substrate to the E3 ligase complex, providing combinatorial specificity. **f** Binding of a small molecular ligand to the charged surface patch stabilizes E3 engagement. **g** Post Translational Modifications (PTM) near or within the degradation motif create or expose a binding site for the ubiquitin ligase, integrating additional signaling inputs. **h** interaction with the E3 ligase is assisted through an allosteric interaction of the ARF protein with a small molecule.

scriptional competence may be shaped by ARF degradation, thereby introducing two separate, tunable, kinetic layers of control over transcriptional output (Fig. 1a).

Quantitative control over ARF levels may be especially important in light of recent findings, wherein ARFs were found to form concentration-dependent nanoclusters, affecting valency and DNA-binding behaviour[20]. Through *in vitro* studies, this work identified a sharp transition window around 3 nM, a physiologically feasible concentration, where MpARF2 switches from a diffuse distribution to clustered, nanoscopic assemblies (Fig. 1b)[20]. This transition drastically changed DNA-binding affinity and sequence specificity (Fig. 1b)[20]. As intracellular ARF concentrations are directly impacted

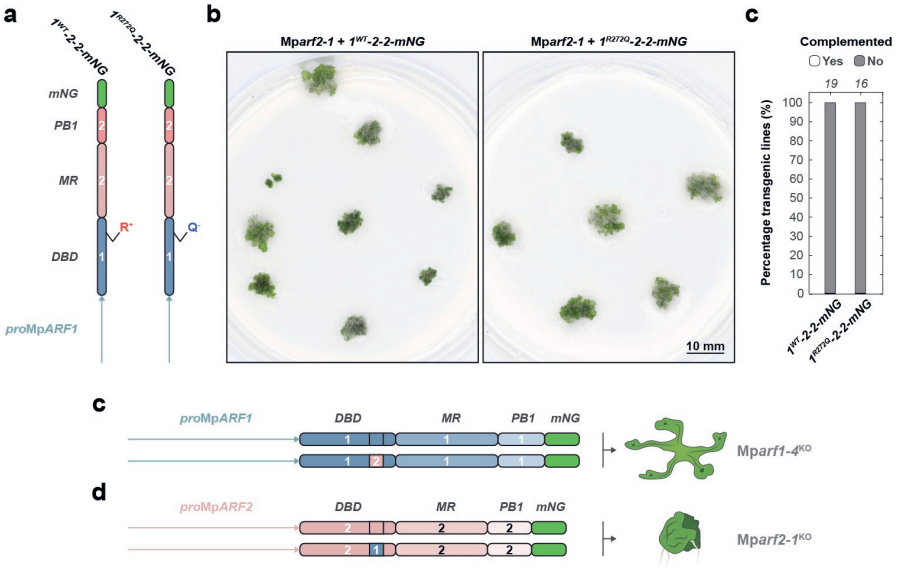


Fig. 3 | Stabilization of the MpARF1 DNA-binding domain does not restore MpARF2 function in chimeric constructs.
a. Schematic representation of chimeric MpARF constructs, fused to mNeonGreen (mNG). The wild-type protein and a stabilized variant carrying the R272Q substitution in the MpARF1 DNA-binding domain (DBD) are shown. Domain organization includes the DNA-binding domain (DBD), middle region (MR), PB1 oligomerization domain, and the fluorescent mNG tag. **b.** Complementation assay in *Marchantia*. Chimeric MpARF proteins (shown in **a**) expressed in the Mp*arf2-1* mutant background. Representative transformants grown on agar plates post-selection are shown. Neither the wild-type chimera (1^{WT}-2-2-mNG) nor the stabilized mutant (1^{R272Q}-2-2-mNG) restored the phenotype of the Mp*arf2-1* mutant. **c.** Quantification of complementation efficiency. The percentage of independent transgenic lines showing phenotypic rescue is shown for each construct (corresponding to **a**). No complementation was observed for either chimera, indicating functional incompatibility of the MpARF1 DBD within this MpARF2 protein context. **d.** Experimental strategy for testing degradation motif function by domain swapping. Constructs containing domain combinations from MpARF1 and MpARF2 were designed to evaluate the contribution of the DNA-binding domain to protein function in Mp*arf1-4* and Mp*arf2-1* mutant backgrounds.

by degradation, the latter may therefore dictate if ARFs are present in diffuse or clustered states, thereby influencing DNA-binding and possibly transcriptional regulation (Fig. 1b). "Trimming" of ARF clusters may alter nanocluster morphology, be highly local, and only occur at specific loci (Fig. 1c). Similarly, switching the ARF clustering state through degradation may be subject to temporal regulation affecting e.g. signaling duration (Fig. 1b,c). Testing this *in vivo* represents an important direction for future research.

While regulation of ARF stoichiometry appears as one of the major roles for ARF degradation, additional roles may exist. In

Chapter 5 we show that MpARF2 accumulates in nearly all tissues when its degradation is perturbed[21]. Continuous synthesis and degradation of a protein is metabolically costly and therefore raises questions regarding its function. If rapid Aux/IAA proteolysis enables fast activation of the NAP system, B-class ARF degradation may allow fast attenuation. Blocking of constitutive B-class ARF degradation could act as a transient brake, resulting in rapid accumulation of B-ARFs and thus repression of the auxin response system. On the other hand, slowing or pausing A-ARF degradation, while Aux/IAA levels remain constant, can rapidly activate the auxin response system (Fig. 1a). However, in **Chapter 5** we show that interference with A-class MpARF1 degradation through the R272Q mutation has limited biological consequences, contradicting this hypothesis. This may mean we have not identified critical determinants of MpARF1 stability, or that, in this context, repression plays a more dominant role than activation. Such rapid proteomic plasticity is characteristic of biological systems involved in stress responses or cell cycle control, requiring the ability to rapidly respond[22,23]. Numerous studies have shown that genetic manipulation of UPS components in plants directly impact stress tolerance (reviewed in Ref.[22,24-26]). In **Chapter 3** we tested influence of some stress signaling hormones (abscisic acid[27] and jasmonic acid[28-30] on MpARF degradation, but did not observe clear effects[19]. Perhaps multiple, converging signals are required, or observation of altered ARF degradation requires alternative, more sensitive, experimental assays. Future studies thoroughly examining environmental conditions and stress signaling networks may reveal additional regulatory inputs into ARF turnover.

Another promising research direction involves investigating ARF accumulation dynamics during the cell cycle. Cell cycle progression and regulation heavily rely on the UPS[23,31-35]. Although auxin and ARFs have been shown to be directly involved in cell cycle regulation in angiosperms, involvement of auxin in cell division regulation in *Marchantia* remains poorly understood[36-43]. Close monitoring of ARF levels during mitosis could reveal oscillatory patterns, which can be indicative of cell-cycle-dependent regulation as has been shown for other TFs in animals and yeast (Fig. 1d)[44-51]. Rhythmic patterns maybe also suggest involvement of ARF degradation in developmental processes with a pulsatile nature, such as the circadian rhythm (Fig. 1d).

An alternative possibility for the seemingly wasteful continuous ARF degradation is that ARF degradation acts as a quality control mechanism, surveying the ARF population for protein misfold-

ing, damage, DNA-binding -or oligomerization states. It is widely accepted that damaged or misfolded proteins are dispensed through the UPS, although most demonstrative studies were performed using animal and yeast systems[52-59]. All components required for ARF degradation are present in the DBD[60], and will therefore often reside in proximity to the DNA. Possibly, certain DNA elements are shielded from ARF binding through guarding by a directly or indirectly DNA-associated E3 ligase (Fig. 1c). Occupation of chromatin or DNA elements by specific factors, single proteins or E3-containing complexes, could label ARFs for degradation when these approach, thereby protecting these DNA binding sites (Fig. 1c).

Furthermore, the positioning of the ARF degradation motif, close to the DBD dimerization domain (see **Chapter 4** and **5**)[21,60,61], is of note. This raises the possibility that ARF dimerization states guides their degradation. For example, the degradation motif can be inaccessible to the degradation machinery in an ARF dimer due to shielding by the larger dimeric assembly (Fig. 2a,b). Alternatively, the ARF dimer might be a better target for the degradation machinery as the latter may require structural conformations or additional interactions presented in the dimeric, but not monomeric, form (Fig. 2a,c). These hypotheses can be tested using *in vivo* techniques capable of measuring protein oligomerization states such as Fluorescence Correlation Spectroscopy[62,63] or Number and Brightness analysis[64]. Because ARF concentration differences between WT and artificially stabilized ARFs may confound such measurements, concentration-independent techniques like Förster Resonance Energy Transfer – Fluorescence Lifetime Imaging techniques may provide a more robust alternative[65,66].

Mechanisms of ARF proteolysis

Although **Chapter 4** and **5** provide significant insights into ARF degradation and its molecular mechanism, many questions surrounding this topic remain unresolved[21,60]. Most of our findings concern the identification of sequence features, and the importance of their chemical properties, within the MpARF proteins themselves[21,60,61]. However, degradation of proteins by the 26S proteasome implies many other components, most notably an E3 ubiquitin-ligase enzyme that targets and ubiquitylates substrate proteins, causing their degradation[32]. Despite extensive efforts and a dual approach to identify these components in **Chapters 6** and **7**, regulators of ARF degradation remain unknown. Unlike methods for identification of substrates of known E3 ligases[67-71], standardized

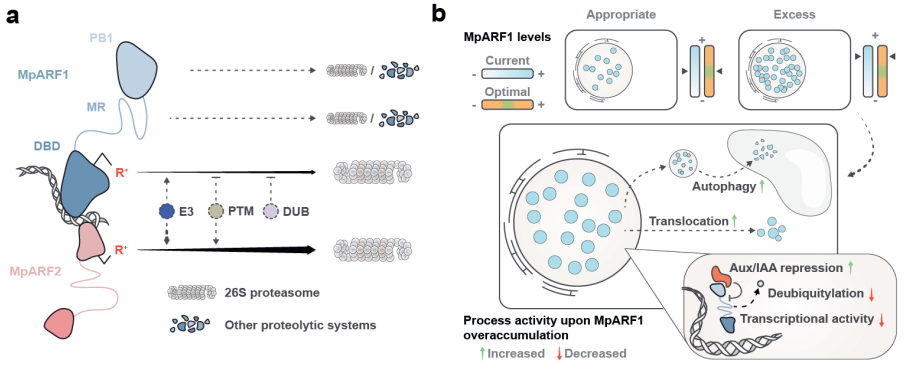


Fig. 4 | Models for differential ARF degradation and buffering systems. **a.** Model illustrating multiple proteolytic pathways that may regulate ARF protein abundance. In addition to degradation via the 26S proteasome, ARFs may be regulated through alternative proteolytic systems or by post-translational modification pathways including ubiquitylation and deubiquitylation (DUB). **b.** Conceptual framework for buffering and maintaining optimal MpARF1 activity. Under appropriate conditions MpARF1 levels support balanced transcriptional activity, whereas excessive accumulation may activate compensatory buffering mechanisms. Elevated MpARF1 may increase repression by Aux/IAA proteins, reduce transcriptional activity through deubiquitylation or other regulatory mechanisms, and thereby maintain auxin signaling homeostasis.

strategies for reverse identification of E3 ligases targeting a known substrate, are limited.

Future, alternative, strategies like Yeast-Two-Hybrid screens, which were previously shown to identify E3 ligase-substrate modules,[72-76], can be used. Similarly, a suppressor screen, using the non-auxin responsive (nar) phenotype described in **Chapter 6** would accommodate a high throughput genetic approach, and could potentially identify gain-of-function mutations in the E3 ligase or its positive regulators. Ideally, a weak allele of the stabilized PpARF2 (i.e. PpARFb2^{R269Q})[61] would be utilized as opposed to a more strongly stabilized PpARF2 (e.g. PpARFb2^{E266k} or PpARFb2$^{E266k+R269Q}$)[61] as these might be completely immune to degradation, regardless of increased E3 ligase activity. Alternatively, modification of the TurboID proximity labelling assay presented in **Chapter 7** may lead to better results. Modification of the MpARF2 DBD bait fragment, such as truncations, may reduce non-degradation related interactions. Furthermore, moving or removing the sYFP tag, moving the TurboID enzyme to the MpARF2 N-terminus, pharmacologically blocking ARF degradation during biotinylation, replacing TurboID with another biotin ligase, or performing TurboID experiments under developmental or environmental conditions enhancing ARF degradation may improve results.

Identification of the cognate E3 ligase responsible for ARF remains a crucial step in addressing core questions regarding the mechanism of proteasome-mediated ARF degradation. We can, however, speculate on the nature, composition, and architecture of this mechanism based on the available data presented in this thesis.

Firstly, we identified a motif in a small loop facing outward of the MpARF2 DBD homodimer structure (see **Chapter 4**)[60] and in **Chapter 5** demonstrated a particularly critical role for a positive charge conferred by an Arginine residue[21].

A parsimonious hypothesis is that R300 participates in electrostatic interactions with a negatively charged residue or motif in the E3 ligase (Fig, 2a,d). Alternatively, the motif may form a docking site for adapter proteins bridging the E3 ubiquitin-ligase to the ARF substrate (Fig. 2a,e). Another possibility is that the charged surface of the motif binds an unknown molecular ligand (e.g. a phytohormone, signaling molecule or element) thereby allowing binding of cofactors or the ubiquitin-ligase enzyme (Fig. 2a,f). There are established examples of such molecular glues(reviewed in Ref.[77]), with auxin perception by TIR1 and Aux/IAA as a famous and therapeutically applicable example (reviewed in **Chapter 2**[18]). It is known that mutations in the motif can prevent ubiquitylation and thereby degradation[61], however we do not know if these mutations affect the process of ubiquitylation directly. Possibly, the charged motif is directly post translationally modified (PTM) through e.g. (de)SUMOylation or (de)phosphorylation or is required for interactions with PTM-inducing enzymes (Fig. 2a,g). PTMs or ligand binding may also allosterically affect E3-ARF interactions (Fig. 2a,h). Lastly, substrate proteins are often guided to and unfolded at the proteasome by ancillary proteins (reviewed in Ref.[78,79]). Reception and processing of substrates by the proteasome depends on the nature and modifications of substrate-conjugated ubiquitin signals, and interactions with cofactors, such as chaperone proteins[80-85]. Currently, such proteasome-engaging cofactors as well as ARF ubiquitylation sites remain unknown and these require identification for a complete perspective on the mechanisms of ARF degradation.

Combinations of these models with multiple adapter proteins, multimeric E3 ubiquitin-ligase complexes, combinatorial requirements of adapter proteins and molecular ligands, or PTM-dependent ubiquitin-ligase interactions are possibilities. Structural studies, like X-ray crystallography[86] or cryo-electron microscopy[87], resolving ARFs in complex with degradation-controlling proteins will uncover crucial mechanistic details. In conclusion, the data presented here

clearly highlights identifying the ubiquitin-ligase and/or cofactors regulating ARF degradation as key next steps in comprehensively understanding auxin signaling.

Evolution of ARF proteolysis

Comparative phylogenetic and biochemical analysis of the degradation-conferring motif presented in **Chapter 4** demonstrated that the MpARF1 degradation motif could substitute the homologous motif of MpARF2, conferring degradation[60]. Similarly, motif swaps of B-class ARFs of other, distantly related, plant species like *Physcomitrium patens* and *Arabidopsis thaliana* could confer instability, indicative of possibly synonymous mechanisms[60]. These findings suggest that degradation arose in an A/B-class ancestral protein which ultimately gave rise to the A -and B-class clades prior to their split, likely during the earliest stages of land plant evolution.

Further support for this model came from **Chapter 5**, in which we showed that the positive charge of the MpARF2 R300 residue was conserved as R272 in MpARF1, and that the R272Q mutation within the MpARF1 protein led to slight stabilization[21]. However, despite a seemingly shared degradation motif, the two proteins display markedly different degradation dynamics and related functional relevance. A core question arising from this data therefore involves the contradiction between the seemingly ancient and shared conservation of the degradation mechanism among A -and B-class MpARF members, contrasted by a significant divergence in degradation dynamics and developmental relevance[21].

In **Chapter 5** we explore possible explanations for these phenomena, focusing both on the evolution of the mechanism and the differences between MpARF1 -and 2 as substrates, suggesting that other MpARF1 domains also contribute to its quantitative regulation. Replacing the MpARF1 DBD with that of MpARF2 could not fully restore protein function[14], which, however is achieved through swapping the MpARF2 DNA-binding B3 subdomain into MpARF1[9]. Thus, regions outside the B3 were functionally incongruent between both MpARFs, such as the dimerization domains or perhaps the degradation mechanism. To explore this hypothesis in this discussion, I generated novel chimeric proteins consisting of the MpARF1 DBD and MpARF2 MR and PB1 domains both with WT sequences (1^{WT}-2-2) and with the R272Q stabilizing mutation (1^{R272Q}-2-2) introduced into the MpARF1 DBD (Fig. 3a). I used these chimeras to complement the Mp*arf2-1* mutant. Both 1^{WT}-2-2 and 1^{R272Q}-2-2 could not

rescue the mutant phenotype, thus showing that, within the context of these chimeras, the DBD of MpARF1 and 2 are not functionally interchangeable (Fig. 3b,c). While informative, this experiment does not separate the underlying causes of functional DBD divergence between MpARF1 and 2, as swapping the full DBD may simultaneously alter DNA-binding properties, broader structural and/or intramolecular incompatibility, or degradation dynamics. To isolate functional differences in ARF stability and possible domain contributions, we propose a targeted motif-swap experiment in which only the minimal degradation motif is exchanged between the two MpARF proteins (Fig. 3c,d). Specifically, the MpARF1 degradation motif would be introduced into the MpARF2 full-length protein followed by assessing of its ability to complement the Mp*arf2-1* mutant. Reciprocally, the MpARF2 degradation motif would be inserted into MpARF1 and tested for its ability to rescue the Mp*arf1-4* mutant. Unlike full DBD swaps, this approach should lead to better preservation of overall structural architecture and DNA-binding properties. This experiment tests if there are quantitatively different, yet transferable, degradation signals in the motifs of both MpARFs, and how these contribute to protein function.

We observed that interfering with MpARF1 degradation through the R272Q mutation did not noticeably interfere with its ability to complement Mp*arf1-4* (see **Chapter 5**)[21]. Possibly, the MpARF1 MR and/or PB1 domains contain signals for degradation through the UPS or other proteolytic systems, such as autophagy (Fig. 4a,b). Mechanisms of ubiquitylation itself may also differ between MpARF1 and 2; the E3 ligase might have higher preference or affinity for MpARF2, which can be a direct biochemical property or can be influenced by (de)stabilizing PTMs (Fig. 4a). Alternatively, MpARF1 can be unassigned from UPS-mediated degradation by deubiquitinating enzymes (Fig. 4a,b)[88]. Other buffering systems might prevent potential undesired effects of excess MpARF1 accumulation, such as MpARF1 inactivation by translocation, increased Aux/IAA repression, or decreased DNA-binding and/or transcriptional activity (Fig. 4b).

The degradation-conferring motif swap experiments presented in **Chapter 4**, together with the phylogenetic and molecular analyses in **Chapter 5** and complementary work by colleagues[61], demonstrate that ARF degradation operates across multiple, distantly related plant lineages. This broad conservation raises the question of how universally maintained the mechanism truly is. Deep phylogenetic analyses of motif sequence and charge conservation reveal substantial variation[21], a finding that appears paradoxical given that

perturbation of B-class ARF degradation is consistently detrimental to development[21,60,61], implying strong evolutionary constraint. One possibility is that lineage-specific diversification of the motif enables fine-tuning of degradation kinetics to accommodate increasingly complex developmental and regulatory demands. At the same time, the ancient incorporation of degradation into the NAP has created a dependency as ARF proteolysis is no longer auxiliary but integral to proper development. Disruption of this mechanism, whether through intragenic ARF mutations (see **Chapter 6**) or impaired E3 ligase function, is consistently deleterious[21,60,61]. Understanding how plants have evolutionarily stabilized such a powerful, yet vulnerable regulatory mechanism will require systematic cross-lineage investigation, integrating phylogenetics, biochemistry, and developmental genetics.

Closing Perspective

The work presented in this thesis establishes proteasome-mediated ARF degradation as a central mechanism in auxin signaling. The differential reliance of A -and B-class ARFs on proteolysis illustrates how subtle quantitative tuning of protein levels can profoundly impact developmental outcomes.

While important mechanistic questions remain, most notably, the identity of the ARF-targeting E3 ubiquitin-ligase, the main themes and findings presented in this thesis provide a solid foundation for future research on ARF proteolysis-driven transcriptional and developmental control. By integrating evolutionary, biochemical, and developmental approaches and perspectives, this thesis highlights how quantitative post-translational ARF regulation enables the simple signaling molecule auxin to orchestrate highly complex developmental programs across plant lineages.

References

1 Bowman, J. L. *et al.* Insights into Land Plant Evolution Garnered from the Marchantia polymorpha Genome. *Cell* **171**, 287–304 e215 (2017). https://doi.org/10.1016/j.cell.2017.09.030

2 Flores-Sandoval, E., Eklund, D. M. & Bowman, J. L. A Simple Auxin Transcriptional Response System Regulates Multiple Morphogenetic Processes in the Liverwort Marchantia polymorpha. *PLoS Genet* **11**, e1005207 (2015). https://doi.org/10.1371/journal.pgen.1005207

3 Weijers, D. & Wagner, D. Transcriptional Responses to the Auxin Hormone. *Annu Rev Plant Biol* **67**, 539–574 (2016). https://doi.org/10.1146/annurev-arplant-043015-112122

4 Vanneste, S., Pei, Y. & Friml, J. Mechanisms of auxin action in plant growth and development. *Nat Rev Mol Cell Biol* (2025). https://doi.org/10.1038/s41580-025-00851-2

5 Hernandez-Garcia, J. *et al.* Evolutionary origins and functional diversification of Auxin Response Factors. *Nat Commun* **15**, 10909 (2024). https://doi.org/10.1038/s41467-024-55278-8

6 Carrillo-Carrasco, V. P., Hernandez-Garcia, J., Mutte, S. K. & Weijers, D. The birth of a giant: evolutionary insights into the origin of auxin responses in plants. *EMBO J* **42**, e113018 (2023). https://doi.org/10.15252/embj.2022113018

7 Mutte, S. K. *et al.* Origin and evolution of the nuclear auxin response system. *Elife* **7** (2018). https://doi.org/10.7554/eLife.33399

8 Rienstra, J., Hernandez-Garcia, J. & Weijers, D. To bind or not to bind: how AUXIN RESPONSE FACTORs select their target genes. *J Exp Bot* **74**, 6922–6932 (2023). https://doi.org/10.1093/jxb/erad259

9 Rienstra, J., Carrillo-Carrasco, V. P., de Roij, M., Hernandez-Garcia, J. & Weijers, D. A conserved ARF-DNA interface underlies auxin-triggered transcriptional response. *Proc Natl Acad Sci U S A* **122**, e2501915122 (2025). https://doi.org/10.1073/pnas.2501915122

10 Boer, D. R. *et al.* Structural basis for DNA binding specificity by the auxin-dependent ARF transcription factors. *Cell* **156**, 577–589 (2014). https://doi.org/10.1016/j.cell.2013.12.027

11 Freire-Rios, A. *et al.* Architecture of DNA elements mediating ARF transcription factor binding and auxin-responsive gene expression in Arabidopsis. *Proc Natl Acad Sci U S A* **117**, 24557–24566 (2020). https://doi.org/10.1073/pnas.2009554117

12 Martin-Arevalillo, R. *et al.* Synthetic deconvolution of an auxin-dependent transcriptional code. *Cell* **188**, 2872–2889 e2824 (2025). https://doi.org/10.1016/j.cell.2025.03.028

13 Cance, C., Martin-Arevalillo, R., Boubekeur, K. & Dumas, R. Auxin response factors are keys to the many auxin doors. *New Phytol* **235**, 402–419 (2022). https://doi.org/10.1111/nph.18159

14 Kato, H. *et al.* Design principles of a minimal auxin response system. *Nat Plants* **6**, 473–482 (2020). https://doi.org/10.1038/s41477-020-0662-y

15 Ulmasov, T., Hagen, G. & Guilfoyle, T. J. ARF1, a transcription factor that binds to auxin response elements. *Science* **276**, 1865–1868 (1997). https://doi.org/10.1126/science.276.5320.1865

16 Fontana, M. *et al.* Cooperative action of separate interaction domains promotes high-affinity DNA binding of Arabidopsis thaliana ARF transcription factors. *Proc Natl Acad Sci U S A* **120**, e2219916120 (2023). https://doi.org/10.1073/

pnas.2219916120
17 Mironova, V. V., Omelyanchuk, N. A., Wiebe, D. S. e. a. & Levitsky, V. G. Computational analysis of auxin responsive elements in the Arabidopsis thaliana L. genome. . *BMC Genomics* **15** (2014). https://doi.org/10.1186/1471-2164-15-S12-S4
18 de Roij, M., Borst, J. W. & Weijers, D. Protein degradation in the auxin response. *Plant Cell* (2024). https://doi.org/10.1093/plcell/koae125
19 Das, S. *et al.* Quantitative imaging reveals the role of MpARF proteasomal degradation during gemma germination. *Plant Commun*, 101039 (2024). https://doi.org/10.1016/j.xplc.2024.101039
20 Arfman, K. *et al.* Nanoclustering of a plant transcription factor enables strong yet specific DNA binding. (2025). https://doi.org/10.1101/2025.11.05.686732
21 de Roij, M. *et al.* Diversification of functional requirements for proteolysis of auxin response factors. *Nature Communications* (2026). https://doi.org/10.1038/s41467-026-70440-0
22 Stone, S. L. The role of ubiquitin and the 26S proteasome in plant abiotic stress signaling. *Front Plant Sci* **5**, 135 (2014). https://doi.org/10.3389/fpls.2014.00135
23 Sadanandom, A., Bailey, M., Ewan, R., Lee, J. & Nelis, S. The ubiquitin-proteasome system: central modifier of plant signalling. *New Phytol* **196**, 13–28 (2012). https://doi.org/10.1111/j.1469-8137.2012.04266.x
24 Yee, D. & Goring, D. R. The diversity of plant U-box E3 ubiquitin ligases: from upstream activators to downstream target substrates. *J Exp Bot* **60**, 1109–1121 (2009). https://doi.org/10.1093/jxb/ern369
25 Chen, L. & Hellmann, H. Plant E3 ligases: flexible enzymes in a sessile world. *Mol Plant* **6**, 1388–1404 (2013). https://doi.org/10.1093/mp/sst005
26 Lyzenga, W. J. & Stone, S. L. Abiotic stress tolerance mediated by protein ubiquitination. *J Exp Bot* **63**, 599–616 (2012). https://doi.org/10.1093/jxb/err310
27 Ghosh, T. K. *et al.* Abscisic acid-induced gene expression in the liverwort Marchantia polymorpha is mediated by evolutionarily conserved promoter elements. *Physiologia plantarum* **156**, 13 (2015). https://doi.org/https://doi.org/10.1111/ppl.12385
28 Liang, Y. *et al.* The wound-activated ERF15 transcription factor drives Marchantia polymorpha regeneration by activating an oxylipin biosynthesis feedback loop. *Sci Adv* **8**, eabo7737 (2022). https://doi.org/10.1126/sciadv.abo7737
29 Monte, I. *et al.* Ligand-receptor co-evolution shaped the jasmonate pathway in land plants. *Nat Chem Biol* **14**, 480–488 (2018). https://doi.org/10.1038/s41589-018-0033-4
30 Penuelas, M. *et al.* Jasmonate-Related MYC Transcription Factors Are Functionally Conserved in Marchantia polymorpha. *Plant Cell* **31**, 2491–2509 (2019). https://doi.org/10.1105/tpc.18.00974
31 Genschik, P., Marrocco, K., Bach, L., Noir, S. & Criqui, M. C. Selective protein degradation: a rheostat to modulate cell-cycle phase transitions. *J Exp Bot* **65**, 2603–2615 (2014). https://doi.org/10.1093/jxb/ert426
32 Vierstra, R. D. The ubiquitin-26S proteasome system at the nexus of plant biology. *Nat Rev Mol Cell Biol* **10**, 385–397 (2009). https://doi.org/10.1038/nrm2688
33 Marrocco, K., Thomann, A., Parmentier, Y., Genschik, P. & Criqui, M. C. The APC/C E3 ligase remains active in most post-mitotic Arabidopsis cells and is required for proper vasculature development and organization. *Development* **136**,

1475–1485 (2009). https://doi.org/10.1242/dev.035535
34 Capron, A., Okresz, L. & Genschik, P. First glance at the plant APC/C, a highly conserved ubiquitin-protein ligase. *Trends Plant Sci* **8**, 83–89 (2003). https://doi.org/10.1016/S1360-1385(02)00028-6
35 Gusti, A. *et al.* The Arabidopsis thaliana F-box protein FBL17 is essential for progression through the second mitosis during pollen development. *PLoS One* **4**, e4780 (2009). https://doi.org/10.1371/journal.pone.0004780
36 Jurado, S. *et al.* The Arabidopsis cell cycle F-box protein SKP2A binds to auxin. *Plant Cell* **22**, 3891–3904 (2010). https://doi.org/10.1105/tpc.110.078972
37 Feng, Z., Sun, X., Wang, G., Liu, H. & Zhu, J. LBD29 regulates the cell cycle progression in response to auxin during lateral root formation in Arabidopsis thaliana. *Ann Bot* **110**, 1–10 (2012). https://doi.org/10.1093/aob/mcs019
38 Berckmans, B. *et al.* Auxin-dependent cell cycle reactivation through transcriptional regulation of Arabidopsis E2Fa by lateral organ boundary proteins. *Plant Cell* **23**, 3671–3683 (2011). https://doi.org/10.1105/tpc.111.088377
39 Ai, H. *et al.* Auxin-dependent regulation of cell division rates governs root thermomorphogenesis. *EMBO J* **42**, e111926 (2023). https://doi.org/10.15252/embj.2022111926
40 Himanen, K. *et al.* Auxin-mediated cell cycle activation during early lateral root initiation. *Plant Cell* **14**, 2339–2351 (2002). https://doi.org/10.1105/tpc.004960
41 Wang, J. *et al.* Dual regulations of cell cycle regulator DPa by auxin in Arabidopsis root distal stem cell maintenance. *Proc Natl Acad Sci U S A* **120**, e2218503120 (2023). https://doi.org/10.1073/pnas.2218503120
42 Schruff, M. C. *et al.* The AUXIN RESPONSE FACTOR 2 gene of Arabidopsis links auxin signalling, cell division, and the size of seeds and other organs. *Development* **133**, 251–261 (2006). https://doi.org/10.1242/dev.02194
43 Di Mambro, R. *et al.* Auxin minimum triggers the developmental switch from cell division to cell differentiation in the Arabidopsis root. *Proc Natl Acad Sci U S A* **114**, E7641–E7649 (2017). https://doi.org/10.1073/pnas.1705833114
44 Son, S. H. *et al.* SUMOylation-mediated PSME3-20S proteasomal degradation of transcription factor CP2c is crucial for cell cycle progression. *Sci Adv* **9**, 18 (2023). https://doi.org/10.1126/sciadv.add4969
45 D'Annibale, S. *et al.* Proteasome-dependent degradation of transcription factor activating enhancer-binding protein 4 (TFAP4) controls mitotic division. *J Biol Chem* **289**, 7730–7737 (2014). https://doi.org/10.1074/jbc.M114.549535
46 Mark, K. G. & Rape, M. Ubiquitin-dependent regulation of transcription in development and disease. *EMBO Rep* **22**, e51078 (2021). https://doi.org/10.15252/embr.202051078
47 Clijsters, L. *et al.* Cyclin F Controls Cell-Cycle Transcriptional Outputs by Directing the Degradation of the Three Activator E2Fs. *Mol Cell* **74**, 1264–1277 e1267 (2019). https://doi.org/10.1016/j.molcel.2019.04.010
48 Emanuele, M. J. *et al.* Global identification of modular cullin-RING ligase substrates. *Cell* **147**, 459–474 (2011). https://doi.org/10.1016/j.cell.2011.09.019
49 Wang, X. *et al.* VprBP/DCAF1 Regulates the Degradation and Nonproteolytic Activation of the Cell Cycle Transcription Factor FoxM1. *Mol Cell Biol* **37** (2017). https://doi.org/10.1128/MCB.00609-16
50 Argentini, M., Barboule, N. & Wasylyk, B. The contribution of the RING finger domain of MDM2 to cell cycle progression. *Oncogene* **19**, 3849–3857 (2000). https://doi.org/10.1038/sj.onc.1203737

51 Leng, R. P. *et al.* Pirh2, a p53-induced ubiquitin-protein ligase, promotes p53 degradation. *Cell* **112**, 779–791 (2003). https://doi.org/10.1016/s0092-8674(03)00193-4
52 Hiller, M. M., Finger, A., Schweiger, M. & Wolf, D. H. ER Degradation of a Misfolded Luminal Protein by the Cytosolic Ubiquitin-Proteasome Pathway. *Science* **273**, 3 (1996). https://doi.org/10.1126/science.273.5282.1725
53 Zavodszky, E., Peak-chew, S., Juszkiewicz, S., Narvaez, A. J. & Hedge, R. S. Identification of a quality-control factor that monitors failures during proteasome assembly. *Science* **373**, 6 (2021). https://doi.org/10.1126/science.abc6500
54 Wang, F., Song, W., Brancati, G. & Segatori, L. Inhibition of endoplasmic reticulum-associated degradation rescues native folding in loss of function protein misfolding diseases. *J Biol Chem* **286**, 43454–43464 (2011). https://doi.org/10.1074/jbc.M111.274332
55 Rousseau, E., Kojima, R., Hoffner, G., Djian, P. & Bertolotti, A. Misfolding of proteins with a polyglutamine expansion is facilitated by proteasomal chaperones. *J Biol Chem* **284**, 1917–1929 (2009). https://doi.org/10.1074/jbc.M806256200
56 Zhang, H. *et al.* PDE1 inhibition facilitates proteasomal degradation of misfolded proteins and protects against cardiac proteinopathy. *Sci Adv* **5**, eaaw5870 (2019). https://doi.org/10.1126/sciadv.aaw5870
57 Comyn, S. A., Young, B. P., Loewen, C. J. & Mayor, T. Prefoldin Promotes Proteasomal Degradation of Cytosolic Proteins with Missense Mutations by Maintaining Substrate Solubility. *PLoS Genet* **12**, e1006184 (2016). https://doi.org/10.1371/journal.pgen.1006184
58 Berner, N., Reutter, K. R. & Wolf, D. H. Protein Quality Control of the Endoplasmic Reticulum and Ubiquitin-Proteasome-Triggered Degradation of Aberrant Proteins: Yeast Pioneers the Path. *Annu Rev Biochem* **87**, 751–782 (2018). https://doi.org/10.1146/annurev-biochem-062917-012749
59 Cummings, C. J. *et al.* Chaperone suppression of aggregation and altered subcellular proteasome localization imply protein misfolding in SCA1. *Nat Genet* **19**, 148–154 (1998). https://doi.org/10.1038/502
60 de Roij, M., Hernandez Garcia, J., Das, S., Borst, J. W. & Weijers, D. ARF degradation defines a deeply conserved step in auxin response. *Nat Plants* **11**, 717–724 (2025). https://doi.org/10.1038/s41477-025-01975-1
61 Prigge, M. J. *et al.* Comparative mutant analyses reveal a novel mechanism of ARF regulation in land plants. *Nat Plants* **11**, 821–835 (2025). https://doi.org/10.1038/s41477-025-01973-3
62 Elson, E. L. Fluorescence correlation spectroscopy: past, present, future. *Biophys J* **101**, 2855–2870 (2011). https://doi.org/10.1016/j.bpj.2011.11.012
63 Kim, S. A., Heinze, K. G. & Schwille, P. Fluorescence correlation spectroscopy in living cells. *Nat Methods* **4**, 963–973 (2007). https://doi.org/10.1038/nmeth1104
64 Cutrale, F. *et al.* Using enhanced number and brightness to measure protein oligomerization dynamics in live cells. *Nat Protoc* **14**, 616–638 (2019). https://doi.org/10.1038/s41596-018-0111-9
65 Chen, H., Puhl, H. L., 3rd, Koushik, S. V., Vogel, S. S. & Ikeda, S. R. Measurement of FRET efficiency and ratio of donor to acceptor concentration in living cells. *Biophys J* **91**, L39–41 (2006). https://doi.org/10.1529/biophysj.106.088773
66 Hoppe, A., Christensen, K. & Swanson, J. A. Fluorescence resonance energy transfer-based stoichiometry in living cells. *Biophys J* **83**, 3652–3664 (2002). https://doi.org/10.1016/S0006-3495(02)75365-4

67 Huang, H. T. *et al.* Ubiquitin-specific proximity labeling for the identification of E3 ligase substrates. *Nat Chem Biol* **20**, 1227–1236 (2024). https://doi.org/10.1038/s41589-024-01590-9

68 O'Connor, H. F. *et al.* Ubiquitin-Activated Interaction Traps (UBAITs) identify E3 ligase binding partners. *EMBO Rep* **16**, 1699–1712 (2015). https://doi.org/10.15252/embr.201540620

69 Mukhopadhyay, U. *et al.* A ubiquitin-specific, proximity-based labeling approach for the identification of ubiquitin ligase substrates. *Sci Adv* **10**, eadp3000 (2024). https://doi.org/10.1126/sciadv.adp3000

70 Watanabe, M. *et al.* A substrate-trapping strategy to find E3 ubiquitin ligase substrates identifies Parkin and TRIM28 targets. *Commun Biol* **3**, 592 (2020). https://doi.org/10.1038/s42003-020-01328-y

71 Barroso-Gomila, O. *et al.* BioE3 identifies specific substrates of ubiquitin E3 ligases. *Nat Commun* **14**, 7656 (2023). https://doi.org/10.1038/s41467-023-43326-8

72 Miao, Y. & Zentgraf, U. A HECT E3 ubiquitin ligase negatively regulates Arabidopsis leaf senescence through degradation of the transcription factor WRKY53. *Plant J* **63**, 179–188 (2010). https://doi.org/10.1111/j.1365-313X.2010.04233.x

73 Lv, Q., Zhang, L., Zan, T., Li, L. & Li, X. Wheat RING E3 ubiquitin ligase TaDIS1 degrade TaSTP via the 26S proteasome pathway. *Plant Sci* **296**, 110494 (2020). https://doi.org/10.1016/j.plantsci.2020.110494

74 Yu, Y. *et al.* The Chinese wild grapevine (Vitis pseudoreticulata) E3 ubiquitin ligase Erysiphe necator-induced RING finger protein 1 (EIRP1) activates plant defense responses by inducing proteolysis of the VpWRKY11 transcription factor. *New Phytol* **200**, 834–846 (2013). https://doi.org/10.1111/nph.12418

75 Abramovitch, R., Janjusevic, R., Stebbins, E. & Martin, G. B. Type III effector AvrPtoB requires intrinsic E3 ubiquitin ligase activity to suppress plant cell death and immunity. *Proc Natl Acad Sci U S A* **103**, 5 (2006). https://doi.org/doi 10.1073 pnas.0507892103

76 Zhuang, M., Guan, S., Wang, H., Burlingame, A. L. & Wells, J. A. Substrates of IAP ubiquitin ligases identified with a designed orthogonal E3 ligase, the NEDDylator. *Mol Cell* **49**, 273–282 (2013). https://doi.org/10.1016/j.molcel.2012.10.022

77 Kozicka, Z. & Thoma, N. H. Haven't got a glue: Protein surface variation for the design of molecular glue degraders. *Cell Chem Biol* **28**, 1032–1047 (2021). https://doi.org/10.1016/j.chembiol.2021.04.009

78 Inobe, T. & Matouschek, A. Paradigms of protein degradation by the proteasome. *Curr Opin Struct Biol* **24**, 156–164 (2014). https://doi.org/10.1016/j.sbi.2014.02.002

79 Yu, H. & Matouschek, A. Recognition of Client Proteins by the Proteasome. *Annu Rev Biophys* **46**, 149–173 (2017). https://doi.org/10.1146/annurev-biophys-070816-033719

80 Maestro-Lopez, M. *et al.* Structures of the 26S proteasome in complex with the Hsp70 co-chaperone Bag1 reveal a mechanism for direct substrate transfer. *Sci Adv* **12** (2026). https://doi.org/10.1126/sciadv.adz3026

81 Verma, R., Oania, R., Fang, R., Smith, G. T. & Deshaies, R. J. Cdc48/p97 mediates UV-dependent turnover of RNA Pol II. *Mol Cell* **41**, 82–92 (2011). https://doi.org/10.1016/j.molcel.2010.12.017

82 Rape, M. *et al.* Mobilization of processed, membrane-tethered SPT23 transcription factor by CDC48(UFD1/NPL4), a ubiquitin-selective chaperone. *Cell* **107**, 667–677 (2001). https://doi.org/10.1016/s0092-8674(01)00595-5

83 Beskow, A. *et al.* A conserved unfoldase activity for the p97 AAA-ATPase in proteasomal degradation. *J Mol Biol* **394**, 732–746 (2009). https://doi.org/10.1016/j.jmb.2009.09.050
84 Barthelme, D. & Sauer, R. T. Identification of the Cdc48*20S proteasome as an ancient AAA+ proteolytic machine. *Science* **337**, 843–846 (2012). https://doi.org/10.1126/science.1224352
85 Barthelme, D. & Sauer, R. T. Bipartite determinants mediate an evolutionarily conserved interaction between Cdc48 and the 20S peptidase. *Proc Natl Acad Sci U S A* **110**, 3327–3332 (2013). https://doi.org/10.1073/pnas.1300408110
86 Shi, Y. A glimpse of structural biology through X-ray crystallography. *Cell* **159**, 995–1014 (2014). https://doi.org/10.1016/j.cell.2014.10.051
87 Cheng, Y. Single-Particle Cryo-EM at Crystallographic Resolution. *Cell* **161**, 450–457 (2015). https://doi.org/10.1016/j.cell.2015.03.049
88 Komander, D., Clague, M. J. & Urbe, S. Breaking the chains: structure and function of the deubiquitinases. *Nat Rev Mol Cell Biol* **10**, 550–563 (2009). https://doi.org/10.1038/nrm2731

Summary (English)

The transition of life from water to land represents one of the most profound evolutionary events in Earth's history. Around 600 million years ago, the ancestors of modern land plants colonized terrestrial habitats that were initially hostile and largely uninhabitable. Successfully colonizing terrestrial habitats required early plants to evolve novel developmental mechanisms to cope with new environmental stresses. Meeting these challenges required increasingly complex multicellular body plans, which in turn necessitated sophisticated regulatory networks capable of coordinating growth, cell differentiation, and environmental responsiveness.

Central to developmental regulation is the phytohormone auxin, a signaling molecule that controls a wide range of processes in plants including embryogenesis, organ formation, regeneration, and environmental adaptation. Auxin acts as a positional signal that guides tissue patterning, cellular identity, and developmental decision-making. Despite being a chemically simple molecule, auxin coordinates highly diverse developmental outcomes across the plant life cycle, and as such, understanding how auxin generates these complex outputs is a central question in plant biology.

Auxin signaling in land plants is primarily mediated through the Nuclear Auxin Pathway (NAP), a transcriptional system that translates changes in intracellular auxin concentrations into specific gene expression changes. Crucial components of the NAP are the AUXIN RESPONSE FACTOR (ARF) transcription factors, which bind to DNA elements and regulate transcription of auxin-responsive genes. Their activity is affected by Aux/IAA repressor proteins, which inhibit ARFs in the absence of auxin. When auxin levels increase, auxin promotes interaction between Aux/IAA proteins and the TIR1/AFB receptor complex, resulting in Aux/IAA degradation by the 26S proteasome. Removal of the inhibitory Aux/IAAs releases ARFs from repression, enabling activation of auxin-responsive gene expression.

Although this canonical model forms a highly robust framework for understanding auxin signaling and has remained mostly unchanged over the course of three decades, it largely treats ARF transcription factors as static NAP components whose abundance is primarily determined by gene expression. The activity of a transcription factor is significantly influenced by its abundance, and this abundance can be influenced by altering synthesis rates, for example through transcriptional regulation. However, transcriptional regulation alone does not allow rapid reduction of protein levels. There-

fore, other regulatory systems are required. Emerging evidence, much of which is presented in this thesis, suggests that ARF proteins themselves are also regulated through proteasome-mediated degradation. How ARF degradation is regulated at the molecular level, what its biological functions are, and how these mechanisms evolved remain largely unresolved questions.

In this thesis I investigate the mechanisms, functions, and evolutionary origins of ARF degradation. To address these questions, I exploit the liverwort model *Marchantia polymorpha*. *Marchantia* represents the minimal, yet fully complete, auxin signaling network and therefore is a powerful system for studying fundamental regulatory mechanisms which may be obscured by genetic redundancy in flowering plant models. Through a combination of genetic, biochemical, and evolutionary approaches, I demonstrate in this thesis that proteasome-mediated degradation of ARF transcription factors is an integral regulatory mechanism shaping auxin responses.

In **Chapter 1**, I introduce auxin, its role in plant development, and its mode of action. I close this chapter with a synopsis of the themes and research questions addressed in each chapter. **Chapter 2** provides a conceptual and historical framework for the thesis. In this chapter I review the discovery of auxin and the chronological identification of the Nuclear Auxin Pathway model, with a particular focus on the role of the ubiquitin–proteasome system in auxin signaling. The chapter also highlights emerging evidence suggesting that ARF proteins themselves are regulated by degradation and outlines key unanswered questions in the field. In **Chapter 3** we establish a set of experimental tools to study auxin signaling dynamics *in vivo*. Using homologous recombination, fluorescent knock-in lines are generated in *Marchantia* to visualize auxin signaling components expressed from their native genomic loci. These experiments expose dynamic accumulation patterns of ARF proteins and demonstrate that proteasome-mediated degradation rapidly alters ARF stoichiometry during development. These observations pose new questions regarding the mechanisms influencing this degradation which I address in subsequent chapters. In **Chapter 4** I investigate the molecular basis of ARF degradation. Sequence analyses identify a conserved motif within the DNA-binding domain of ARF proteins that acts as a degradation signal. Functional experiments demonstrate that this motif is required for ARF turnover and reveal that similar mechanisms operate across diverse plant species. We also show that interference with this degradation signal will impair degradation, with severe negative consequences for development. In **Chapter 5** I explore the developmental con-

sequences of perturbing ARF stability in more detail. By generating inducible stabilized ARF variants, mutant complementation assays, and a thorough analysis of concomitant mutant phenotypes, this chapter demonstrates that regulated ARF degradation is essential for normal development and is required throughout almost all *Marchantia* life stages. Additionally, the results presented in this chapter reveal functional differences between A- and B-class ARFs in their reliance on proteolytic regulation. In **Chapter 6** and **Chapter 7** I aim to identify components which regulate ARF degradation, using different, complementary strategies. In **Chapter 6**, I report on a forward genetic screen in the moss *Physcomitrium patens* to identify regulators of ARF degradation. I isolate mutants in which ARF stability is increased, and mapping the putative causative mutations lead to the identification of a set of candidate genetic components. Follow up experiments revealed that it is unlikely that any of these candidates are direct regulators of ARF degradation**. Chapter 7** employs TurboID-based proximity labeling to identify proteins associated with unstable ARFs. This approach led to a selection of candidate interaction partners that may participate in ARF degradation complexes. These partners proved refractory to mutagenesis, preventing functional assessment at present. We provide alternative strategies to test their involvement in ARF degradation. In **Chapter 8** I integrate the findings of the thesis, speculate on their biological roles, and discuss their broader implications for auxin biology, plant development, and evolutionary biology. The chapter highlights unresolved questions and outlines future research directions aimed at identifying the molecular machinery responsible for ARF proteolysis.

The work I presented in this thesis establishes proteasome-mediated degradation of ARF transcription factors as a central regulatory mechanism in auxin signaling and plant development, with deep evolutionary roots.

Summary (Dutch)

De overgang van het leven in water naar land vormt een van de meest ingrijpende evolutionaire gebeurtenissen in de geschiedenis van de aarde. Ongeveer 600 miljoen jaar geleden koloniseerden de voorouders van de huidige landplanten terrestrische habitats die aanvankelijk vijandig en grotendeels onbewoonbaar waren. Het succesvol koloniseren van deze leefomgevingen vereiste dat deze vroege planten nieuwe ontwikkelingsmechanismen evolueerden om met nieuwe omgevingsfactoren om te gaan. Het overwinnen van deze uitdagingen vereiste steeds complexere meercellige lichaamsstructuren, wat op zijn beurt de ontwikkeling van geavanceerde regulatoire netwerken noodzakelijk maakte die groei, cel differentiatie en reactie op omgevingssignalen konden coördineren.

Centraal in de regulatie van plantontwikkeling staat het fytohormoon auxine, een signaalmolecuul dat een breed scala aan processen in planten aanstuurt, waaronder embryogenese, orgaanvorming, regeneratie en aanpassing aan de omgeving. Auxine fungeert als een positioneel signaal dat patroonvorming in weefsels, cellulaire identiteit en de timing van ontwikkelingsprocessen stuurt. Ondanks dat het chemisch gezien een relatief eenvoudig molecuul is, coördineert auxine een grote diversiteit aan ontwikkelingsprocessen gedurende de volledige levenscyclus van planten. Begrijpen hoe auxine deze complexe ontwikkelingsprocessen aanstuurt vormt daarom een grote, centrale vraag binnen de plantenbiologie.

Auxinesignalering in landplanten wordt voornamelijk gemedieerd via de Nuclear Auxin Pathway (NAP), een transcriptioneel moleculair systeem dat veranderingen in intracellulaire auxineconcentraties vertaalt naar specifieke veranderingen in genexpressie. Cruciale componenten van de NAP zijn de AUXIN RESPONSE FACTOR (ARF) transcriptiefactoren, die binden aan DNA-elementen en reguleren daardoor de transcriptie van auxine-responsieve genen. Hun activiteit wordt beïnvloed door Aux/IAA remmer-eiwitten, die ARF-activiteit remmen in afwezigheid van auxine. Wanneer auxineniveaus toenemen, stimuleert auxine de interactie tussen Aux/IAA-proteïnen en het TIR1/AFB-receptorcomplex, wat leidt tot afbraak van Aux/IAA-proteïnen via het 26S proteasoom. Het verwijderen van deze remmende Aux/IAA-proteïnen heft de repressie van ARF-transcriptiefactoren op, waardoor activatie van auxine-responsieve genexpressie mogelijk wordt.

Hoewel dit canonieke model een robuust kader vormt voor het begrijpen van auxinesignalering, en gedurende de afgelopen

drie decennia grotendeels onveranderd is gebleven, beschouwt het ARF transcriptiefactoren grotendeels als statische componenten van de NAP waarvan de hoeveelheid voornamelijk wordt bepaald door genexpressie. De activiteit van een transcriptiefactor wordt echter sterk beïnvloed door zijn abundantie, en deze kan bijvoorbeeld worden gereguleerd via transcriptie van het corresponderende gen. Transcriptieregulatie op zichzelf maakt echter geen snelle verlaging van eiwitniveaus mogelijk. Daarvoor zijn aanvullende regulatoire mechanismen noodzakelijk. Toenemend bewijs, waarvan een groot deel in dit proefschrift wordt gepresenteerd, suggereert dat ARF-proteïnen zelf eveneens worden gereguleerd via proteasoom-gemedieerde afbraak. Hoe deze afbraak op moleculair niveau wordt gereguleerd, wat de biologische functies ervan zijn en hoe deze mechanismen zich evolutionair hebben ontwikkeld, zijn echter grotendeels onbeantwoorde vragen.

In dit proefschrift onderzoek ik de mechanismen, functies en de evolutionaire oorsprong van ARF-afbraak. Om deze vragen te beantwoorden maak ik gebruik van het levermos model *Marchantia polymorpha*. *Marchantia* bezit een minimaal, maar toch volledig, auxine signaleringsnetwerk en vormt daardoor een krachtig modelsysteem om fundamentele regulatoire mechanismen te bestuderen die in vaatplanten mogelijk verborgen blijven door genetische redundantie. Met een combinatie van genetische, biochemische en evolutionaire benaderingen toon ik in dit proefschrift aan dat afbraak van ARF transcriptiefactoren via het proteasoom een essentieel regulatiemechanisme vormt dat auxineresponsen vormgeeft.

In **Hoofdstuk 1** introduceer ik auxine, haar rol in plantontwikkeling en het mechanisme van auxinesignalering. Dit hoofdstuk sluit af met een overzicht van de centrale thema's en onderzoeksvragen die in de daaropvolgende hoofdstukken worden behandeld. **Hoofdstuk 2** biedt een conceptueel en historisch kader voor het proefschrift. Hierin bespreek ik de ontdekking van auxine en de chronologische ontrafeling van het Nuclear Auxin Pathway-model, met bijzondere aandacht voor de rol van het ubiquitine-proteasoomsysteem binnen auxinesignalering. Daarnaast bespreekt dit hoofdstuk aanwijzingen dat ARF-proteïnen zelf mogelijk door afbraak worden gereguleerd en worden belangrijke openstaande vragen in het veld gedefinieerd en uiteengezet. In **Hoofdstuk 3** ontwikkelen we experimentele hulpmiddelen om de dynamiek van auxinesignalering *in vivo* te bestuderen. Met behulp van homologe recombinatie worden fluorescent gelabelde knockin lijnen gegenereerd in *Marchantia* waarmee auxinesignaleringscomponenten vanuit hun endogene genomische loci kunnen worden gevisualiseerd. Deze

experimenten leggen dynamische accumulatiepatronen van ARF-proteïnen bloot en laten zien dat proteasoom-gemedieerde afbraak de stoichiometrie van ARF-proteïnen tijdens de ontwikkeling snel kan veranderen. Deze observaties roepen nieuwe vragen op over de mechanismen die deze afbraak reguleren, die ik in de daaropvolgende hoofdstukken heb onderzocht. In **Hoofdstuk 4** onderzoek ik de moleculaire basis van ARF-afbraak. Via analyses van eiwitsequenties identificeren we een geconserveerd motief in het DNA-bindingsdomein van ARF-proteïnen dat fungeert als een afbraaksignaal. Functionele experimenten tonen aan dat dit motief noodzakelijk is voor ARF-afbraak en laten zien dat vergelijkbare mechanismen aanwezig zijn in diverse plantensoorten. Daarnaast laten we zien dat verstoring van dit afbraaksignaal de afbraak van ARF-proteïnen belemmert, met ernstige gevolgen voor de ontwikkeling. In **Hoofdstuk 5** onderzoek ik de ontwikkelingsbiologische gevolgen van verstoring van ARF-stabiliteit in meer detail. Door het genereren van induceerbare gestabiliseerde ARF-varianten, het complementeren van mutanten en een uitgebreide analyse van bijbehorende mutantfenotypes laat dit hoofdstuk zien dat gereguleerde ARF-afbraak essentieel is voor normale ontwikkeling en voor vrijwel alle levensstadia van *Marchantia* noodzakelijk is. Bovendien tonen de resultaten aan dat de A- en B-klasse ARF-proteïnen verschillen in hun afhankelijkheid van proteolytische regulatie. In **Hoofdstuk 6** en **Hoofdstuk 7** richt ik me op het identificeren van componenten die betrokken zijn bij ARF-afbraak, waarbij verschillende maar complementaire strategieën worden gebruikt. In **Hoofdstuk 6** rapporteer ik een forward genetische screen in het mos *Physcomitrium patens* om regulators van ARF-afbraak te identificeren. Ik isoleer hier mutanten waarin de stabiliteit van ARF-proteïnen verhoogd is, en breng de causale mutaties in kaart. Vervolgens identificeren we de genetische componenten die hiervoor mogelijk verantwoordelijk zijn. De experimenten die hier weer op volgen suggereren echter dat onze kandidaten waarschijnlijk geen directe rol spelen binnen het proces van ARF-afbraak. **Hoofdstuk 7** maakt gebruik van TurboID-gebaseerde "proximity labeling" om eiwitten te identificeren die geassocieerd zijn met instabiele ARF-eiwitten. Deze benadering leverde een reeks kandidaat-interactiepartners op die mogelijk deel uitmaken van ARF-afbraakcomplexen. Deze genen bleken echter moeilijk te muteren, waardoor functionele analyse momenteel niet mogelijk is. Daarom worden alternatieve strategieën voorgesteld om hun mogelijke rol in ARF-afbraak te testen. In **Hoofdstuk 8** integreer ik de bevindingen van dit proefschrift, bespreekt hun biologische betekenis en plaatst ze in een bredere context van auxinebiologie, plantontwikkeling en evolutie. Daarnaast worden openstaan-

de vragen uiteengezet en toekomstige onderzoekslijnen geschetst die gericht zijn op het identificeren van de moleculaire machinerie die verantwoordelijk is voor ARF-proteolyse.

Het werk dat ik in dit proefschrift presenteer laat zien dat afbraak van ARF-transcriptiefactoren via het proteasoom een centraal regulatiemechanisme omvat in auxinesignalering en plantontwikkeling, met diepe evolutionaire wortels.

Authorship statement

Chapter 1 The idea for his PhD project naturally arose from work I carried out during my mSc thesis. I conceptualized and wrote the contents of this chapter myself.

Chapter 2 Together with my promoter (D.W.) we decided to write a review article with focus on protein degradation in auxin response. I produced the figures and the initial draft after which I received feedback by J.W.B. and D.W. I then revised the manuscript following back-and-forth discourse with my promoter and the reviewers.

Chapter 3 S.D. generated the genomic knock-in lines essential for this work. Much of the imaging presented in this chapter was carried out by both of us, whereas the quantitative data analysis was carried out by me. We performed the RNA-seq experiments together, and data analysis was performed by me, with input from S.M.. Most of the phenotyping was performed by S.D., and the modelling was done by E.F. and S.B.. W.K. measured native auxin concentrations on samples prepared by S.D. and me. S.D., J.W.B. and D.W. carried most weight when writing the manuscript, with input from me. S.D. and I produced and revised the figures.

Chapter 4 All the data in this chapter has been generated by me, with exception of the phylogenetic analysis, which was carried out by J.H.G.. I produced all figures and wrote the first draft with input and feedback from J.H.G. and D.W.. During the publication process, D.W. and I responded to reviewers and adjusted the manuscript.

Chapter 5 All the data in this chapter has been generated by me with assistance by E.H., with exception of the charge conservation analysis and phenotypic analysis of rhizoid initial cell size and formation, which was carried out by J.L.. I produced all figures and wrote the first draft with feedback from my promotor. During the publication process, D.W. and I responded to reviewers and adjusted the manuscript.

Chapter 6 Most of the data presented in this chapter was generated by me, often in close collaboration with M.P.. I performed the mutagenesis, mutant selection, mutant screening, and mutant sequencing. D.S.P. performed the bioinformatics to map the putative causative mutations, and subsequent candidate selection was carried out by me with input from all authors. M.P. generated the CRISPR-Cas9 mutants after which I performed the follow-up experiments. I wrote the chapter and produced the figures, with feedback from my promoter.

Chapter 7 Most of the data presented in this chapter was generated by me. I performed most cloning, generation of transgenic plants, selection of lines, confocal microscopy, and phenotyping. M.R. supported me during the protein purification and performed LC-MS/MS, whereas C.A. aided in plant transformation and genotyping. C.H. helped during the cloning of the gRNA constructs. J.H.G. provided the vector backbones for me to use as templates. I wrote the chapter and produced the figures, with minimum feedback from my promoter.

Chapter 8 Contains my ideas, and I wrote this chapter with no feedback.

Acknowledgments

Somehow my PhD journey has led me to put the final touches on this thesis in a coffeeshop in Đà Nẵng, Vietnam. To state that completing this PhD thesis has been tumultuous, would be a tremendous euphemism. While writing this, I realize that there is not a single person that could have convinced me at the commencement of my project ~4 years ago, that this is where I would finish it. I think at the time, I believed that obtaining a PhD would be an individual endeavor. Now, while I am at the finish line, there is absolutely no doubt in my mind that it would have been impossible without unwavering support, both professional and personal, from many people around me. To everyone who has helped me along the way: thank you. There are too many of you to thank personally, but I would like to extend my gratitude to the people most closely involved, in no particular order.

Dolf, at the risk of sounding dramatic, you have been, in many ways, one of my greatest sources of inspiration. I vividly remember you giving a guest lecture during one of my MSc courses, which was my first encounter with you, as a defining moment in my scientific career. You presented the beautiful tale of the SOSEKI discovery, and you did that in such an impressive and elegant way, that for the first time in my life, I viewed science as something close to an art form (and a worthwhile pursuit). Not only that, but your clarity of thought, eloquence, and intelligence left me deeply impressed. After working with you for half a decade, I learned that my initial impression of you was, if anything, an underestimation. Learning from you was a true privilege.

To **JW**, you are a kind and generous man with a big heart. I would like to thank you for your trust in me, and basically granting me an almost limitless, scientific carte blanche. I think I can speak on behalf of the entire group that we all benefit, and continue to do so, from having someone as kindhearted and cheerful as you are around. Thank you for your efforts to make my scientific and personal journey lighter, I genuinely appreciate this.

Joris, you have had a profoundly positive impact on many facets of my life. I hope you take no offense when I say that, in many ways, our psyches are wired in a similar manner. Because of this, and because of your intelligence, you have been able to see and understand the architecture of my mind and guide me in ways few people could. Seeing how you navigate life the way you do has been deeply inspirational.

Jorge you are irreplicable. I've said this many times, and I will say it again; I think you are one of the very few people truly born to be a scientist. Your mind is both very sharp and has an enormous bandwidth, and I benefited from that. You have taught me how to methodically approach problems, improve my writing, and how to become a more critical scientist. You taught me these skills, in your way, at a time in my project where I needed them most. There is a reason why you are either a coauthor or in the acknowledgements in almost all my chapters; you have been integral to my development. Similarly, **Cathy**, **Shubhajit**, **Jiashu**, and **Vera** have always taken the time to give me their advice (Cathy has been doing this for 5 years already!) and feedback, even when they themselves were carrying the weight of enormously demanding projects. **Mark** and **Michael**, thank you for your hospitality and welcoming me into your lab at UCSD. Thanks to you I have had an amazing introduction to fish tacos and the beautiful state of California. My stay with you was an experience that I will never forget. Thank you all so much for your expertise, pragmatism, time, effort, kindness, and most of all, patience.

Sjoerd and **Juriaan** you have been slightly ahead of me in terms of your careers, but somehow always managed to give me very grounded and sensible (I realize that this is an outrageous statement to intimates, but I fully believe it) perspectives and advice on all matters scientific and personal. Both of you are great guys, friends, and scientists. I am happy that we overlapped as much as we did. It has been a pleasure. Also thanks to **Anne** and Sjoerd for letting me play with **Wikke**, and for Wikkes help in reorganizing my bookshelves. **Jasper**, speaking of lab mates, you have made the lab and office a much more enjoyable place. After you joined us, I always had someone to talk to regarding our animal observations, niche hobbies, science, careers, and "het vuur". I am continuously impressed by you managing to juggle family life, a career taking flight, and your countless hobbies. I had a lot of fun involving you in one of my papers, and I'm sure we could work together like that for our entire careers. Please relay to your family that I am sorry for stealing you sometimes so we could be freezing cold, sitting in October storms for hours. You and I know why we do it though.

To the Hispanic ladies at BIC: **Mariana**, **Polet**, **Cecilia,** and **Melissa**. First of all, I am sorry for pretending to speak Spanish, I just wanted to fit in with the cool girls. Your warm presences have greatly lifted the social atmosphere. Melissa, you were a great addition to the *Marchantia* team, and I will fondly remember that fun lab weekend we organized. Mariana and Ceci, please accept my apolo-

gies for the mild bullying; I did it out of affection. Speaking of me pretending to speak languages; **Evgeniya**, I beg you to keep HR out of this. It was nice to share the office together and thank you for always helping me carry out my weird little projects. **Mark**, you too are a fellow linguistic mastermind. Thanks for helping me out in the lab, your availability, and speedy analyses. **Simon**, thanks for your technical help and terrible jokes. **Lisette**, thank you for your organizational skills, kindness, and flexibility. Also, thanks to **Sumanth** and **Danilo** for not only helping me by carrying out analyses but also taking the time to teach me about bioinformatics. **Susan**, your calmness and empathetic attunement have greatly helped me, and have also saved me on many occasions when I forgot to register or submit something before a deadline. A second hero in this respect, is **Laura**. Laura shows up in the acknowledgements of all my colleagues, and not without reason. I think it's unlikely that I will ever work anywhere with someone as organized, calm and skilled in charge of administrative tasks, as you. Somehow you seem to possess an infinite source of patience, even when I forgot to do something for the millionth time. I am very grateful to you.

Anna and **Clint**, my paranymphs, it is very cute that I can refer to you in this compounded way now. Anna thank you for your reliability, listening ear, advice, and patience. I wholeheartedly recognize that you as well, have shielded me from trouble on many occasions. Also, the drawings for the cover you made are amazing! I will never forget your kindness. Also thank you for being so open minded as to let me aggressively flirt with Clint as much as I did. Clint, your unique combination of professionalism and humor has and will remain to positively impact the lab, not only in terms of vibes but also organizational. **Maarten**, we have similar names and ended up sharing an almost identical PhD trajectory too. It was comforting that we submitted our papers almost simultaneous, wrote rebuttals at the same time, and even finished our theses at the same time. This gave us ample fuel to complain to each other. I feel we understood each other very well, also thank you for not absolutely demolishing me at tennis. **Aaron**, I've always felt we were on a very similar wavelength resulting in some good conversations and inside jokes between us. I hope we may continue to try and enjoy good, exotic, foods together at conferences in the future. Also thank you for being my ever-available cultural guide. Speaking of travel, **Patrick**, you're a super relaxed and fun person to be around, and I really liked our time in Spain. **Feras**, the same goes for you. **Ana**, thanks for your thoughtful conversations, fashion advice, and rants. **Daan**, you're a great person and I am happy to see that your

science is doing so well. **Patricia** and **Anna**, thank you for organizing many fun social activities, I appreciate the effort you put into that. **Bas**, **Lisa**, and **Jente**, thank you for your unique personalities and I will dearly miss continuously asking you how the writing is going and most of all, your subsequent dramatic responses. We could consider another PhD so we can continue this. To all other **BIC lab members**: thank you.

Jaimy, luckily my sister put us in touch when we were teenagers because of our common passion for animals and the outdoors. Since then, we have shared countless adventures, drunken nights, fishing trips, and naturalist expeditions, with our recent journeys abroad as some of my personal highlights. Thanks for letting me greatly benefit from your calmness and passion, and thanks for always saving and showing me funny videos. **Steven**, **Harald**, and **Tanweer** do you realize we started our studies together more than a decade ago (at the time of writing), and have known each other for that long? Since then, we have all grown personally (and physically due to our highly disciplined fitness regimes). I am grateful for your support during this PhD and us sharing so many experiences together. **Michiel** and **Jesse**, you have both been inspiring to me in your own ways. Michiel, you're an amazingly kind, smart and energizing person to hang out with. Remember when we got second place in that rowing match? It is still one of my most glorious achievements. Come sleep on my couch anytime. Jesse, your unique humor and unpredictable, mysterious course of life continue to fascinate me, I am glad to see you are doing well. **Mees** and **Rick**, with both of you I feel completely at ease and understood in a very unique way, and I hope you realize how much I appreciate that. You have had a profound influence on who I am today, and I value that deeply. I want to hang out with you forever, so please, both of you, get some more sleep so we can prolong that. **Eva** and **Jonne** thanks for your maturity (Eva) and kindness (both). Thank you **Benjamin** for your snake drawing!

Ronald, I am deeply grateful for your masterful guidance. You have had a lasting impact on how I see both myself and the world. I am considering myself extremely lucky for the opportunity to talk to you as much as I have. **Casper**, you are the best of the best, thank you for your infinite patience, incredibly good nature, and professionalism. **Marie-José**, thank you for your kindness and help, you too are a master at work.

To **Tobias**, **Willem**, and **Tijs**, we have been friends since early high school and to this date you remain among my closest

mates. I genuinely mean it when I say that being, and remaining, friends with you is one of the most important sources of happiness in my life. Without your limitless support, advice, and high levels of tolerance for my nonsense, I would not have completed this PhD. What unites you as some of my favorite people in this world is your moral integrity, open mindedness, intellect and your unprecedented abilities in de bal overkoppen in het zwembad. Keep developing the way you are, and I sincerely hope I will be a part of that for the rest of our lives; I am proud of you.

To my **mom**, **dad** and **sisters**: thank you for your unconditional support and patience. Now, more than ever do I see that I can always rely on you being there when I need you. Also, please feel free to get more dogs, I believe there is a strong correlation between dog availability and my professional and personal success.

Esmée, thank you for your intelligence, sensitivity, warmth, kindness, and support during the final stages of my PhD. You have provided me with a sense of calm and stability I find difficult to achieve on my own, and I am deeply grateful for these things.

Sophie, I am struggling to put into words how important you have been throughout these years. You stood by my side for most of this PhD and your care, humor, patience and unwavering support have meant more to me, and continues to, than I can properly express. I will forever carry on bringing you pens, notebooks and yellow items, to show my gratitude. You have taught me things that no one else could have ever taught me.

About the author



Martijn de Roij was born on the 29th of November 1996 in Haarlem (The Netherlands). From a young age he showed a broad interest in many and varied topics, alongside a strong intrinsic curiosity for the natural world and biological phenomena. He was particularly fascinated by wildlife. After completing his high school education at Hageveld (Heemstede), he went on to study for a bachelor's in Biology at Wageningen University in 2016. There, he pursued a double major in Cellular biology & Molecular interactions and Ecology & Biodiversity, reflecting his wide-ranging scientific interests. He continued with a master's degree in Molecular & Cellular biology, completing two theses at the chair groups Molecular Biology and Biochemistry, part of Wageningen University. He obtained his master's *cum laude* in early 2022.

Following the completion of his degrees, he joined the Biochemistry chair group at his alma mater as a PhD candidate and was funded by an NWO M-1 grant obtained by Jan Willem Borst and Dolf Weijers. While the project was initially aimed at studying quantitative auxin response protein dynamics, it quickly evolved into a broader investigation of post-translational regulatory mechanisms of auxin response factor proteins. This work resulted in the identification and characterization of novel regulatory mechanisms, forming the core of this thesis.

During his PhD, Martijn established himself as a meticulous and detail-oriented researcher. His work led to multiple collaborations, a research stay at the University of California San Diego, and the publication of several articles in leading scientific journals. In addition to his research, he contributed to education by teaching courses and supervising students. He will continue working in science as a postdoc at the Gregor Mendel Institute of Molecular Plant Biology in Vienna, Austria.

Beyond academia, Martijn maintains a passion for nature, wildlife, literature, photography, diving, and travel. These interests reflect his curiosity and openness to new perspectives, which continue to shape both his scientific and personal development.

List of publications

Hernández-García, J., Dipp-Alvarez, M., **de Roij, M.**, Guillem-Bernal, M., Roosjen, M., Baltaci, Z., Smith, H., dos Santos Pereira, D., Borst, J.W., Holehouse, A., Lee, H. & Weijers, D. Subnuclear cofactor partitioning underlies auxin-dependent transcriptional regulation. *Cell* (2026). In review

Chu, J., Ang, A., **de Roij, M.**, Strader, L., Xu, T. & Weijers, D. Auxin signaling. *Cell* **189**, 4531-4547 (2026). https://doi.org/10.1016/j.cell.2026.06.024

Arfman, K., Janssen, B., Romein, R., van den Boom, S., Woude, M., Jansen, L., Rademaker, M., Hernández-García, J., Ramalho, J., Alvarez, M., **de Roij, M.**, Lamers, J., Hohlbein, J., Borst, J.W., Weijers, D., van Mierlo, C. & Sprakel, J. Nanoclustering of plant transcription factor enables strong yet specific DNA binding. *Science Advances* **12**, (2026). https://doi.org/10.1126/sciadv.aed7904

De Roij, M., Heijdra, E., Lamers, J., Nishihama, R., Borst, J.W. & Weijers, D. Diversification of functional requirements for proteolysis of Auxin Response Factors. *Nature Communications* **17**, (2026). https://10.1038/s41467-026-70440-0

De Roij, M., Hernández-García, J., Das, S., Borst, J.W. & Weijers, D. ARF degradation defines a deeply conserved step in auxin response. *Nature Plants* **11**, (2025). https://doi.org/10.1038/s41477-025-01975-1

Rienstra, J., Carrillo-Carrasco, P., **de Roij, M.**, Hernández-García, J. & Weijers, D. A conserved ARF-DNA interface underlies auxin-triggered transcriptional response. *Proceedings of the National Academy of Sciences* **122**, (2025). https://doi.org/10.1073/pnas.2501915122

Hernández-García, J., Carrillo-Carrasco, V.P., Rienstra, J., Tanaka, K., **de Roij, M.**, Dipp-Alvarez, M., Freire-Rios, A., Crespo, I., Boer, R., van den Berg, W., Lindhoud, S. & Weijers, D. Evolutionary origins and functional diversification of Auxin Response Factors. *Nature Communications* **15**, 10909 (2024). https://doi.org/10.1038/s41467-024-55278-8

De Roij, M., Borst, J.W. & Weijers, D. Protein degradation in auxin response. *The Plant Cell* **36**, 3025-3035 (2024). https://doi.org/10.1093/plcell/koae125

Das, S., **de Roij, M.**, Bellows, S., Dipp Alvarez, M., Mutte, S., Kohlen, W., Farcot, E., Weijers, D. & Borst, J.W. Quantitative imaging reveals the role of MpARF proteasomal degradation during gemma germination. *Plant Communications* **5**, (2024). https://doi.org/10..1016/j.xplc.2024.101039

Schmitz, L., Yan, Z., Schneijderberg, M., **de Roij, M.**, Pijnenburg, R., Zheng, Q., Franken, C., Dechesne, A., Trindade, L., Velzen, R., Bisseling, T., Geurts, R. & Cheng, X. Synthetic bacterial community derived from a desert rhizosphere confers salt stress resilience to tomato in the presence of a soil microbiome. *The ISME Journal* ***16***, 1907-1920 (2022). https://doi.org/10.1038/s41396-022-01238-3

The research presented in this thesis was performed at the Laboratory of Biochemistry, Wageningen University & Research, and was financially supported by a grant from NWO (NWO; OCENW.M20.031).

Financial support from the Laboratory of Biochemistry for printing this thesis is gratefully acknowledged.

Cover design
Anna Daamen

Layout
Martijn de Roij

Printed by ProefschriftMaken on FCS-certified paper.

